



UNIVERSITY OF
BIRMINGHAM

Improving response to neoadjuvant chemoradiotherapy in locally advanced rectal cancer

A thesis presented to the University of Birmingham for the degree of
Doctor of Philosophy

By

Kasun Shalitha Wanigasooriya

Institute of Cancer and Genomics Sciences

College of Medical and Dental Science

University of Birmingham

October 2022

UNIVERSITY OF
BIRMINGHAM

University of Birmingham Research Archive

e-theses repository

This unpublished thesis/dissertation is copyright of the author and/or third parties. The intellectual property rights of the author or third parties in respect of this work are as defined by The Copyright Designs and Patents Act 1988 or as modified by any successor legislation.

Any use made of information contained in this thesis/dissertation must be in accordance with that legislation and must be properly acknowledged. Further distribution or reproduction in any format is prohibited without the permission of the copyright holder.

Abstract

Introduction: Response to neoadjuvant chemoradiotherapy (NCRT) for locally advanced rectal cancer (LARC) varies considerably. There is a need to unravel the elusive biological mechanisms behind treatment resistance in LARC and discover radiosensitising treatments using the latest experiment models.

Methods: Next generation sequencing (NGS) was performed on archival specimens from 23 LARC patients (retrospective cohort) to identify differentially expressed genes associated with NCRT response. Six patient derived organoid (PDO) models were derived (prospective cohort) from colorectal cancer (CRC) patients; genetically and immunohistochemically characterised. *In vitro* viability assays were conducted to determine PDO response to radiotherapy. NGS was performed on PDOs pre- and post-irradiation. Chemoradiotherapy viability assays using targeted pathway inhibitors were performed using HCT116 CRC cell line and PDOs. AKT phosphorylation following chemoradiotherapy was assessed using western blots.

Results: The first 6 out of 16 CRC PDO lines successfully derived in the laboratory were characterised through genomics and immunohistochemistry. Several genes and biological pathways of interest in radiotherapy response (sensitivity or resistance) were identified on differential expression analyses and Gene Set Enrichment Analysis of the retrospective FFPE sample and prospective organoid sample transcriptomes. The PI3K/AKT/mTOR pathway upregulation was associated

with radiotherapy resistance in retrospective and prospective cohort sample transcriptomic analyses. Radiotherapy was associated with significantly increased AKT phosphorylation in HCT116. The use of PI3K and mTOR dual inhibitors apitolisib and dactolisib radiosensitised HCT116 and PDOs *in vitro* and led to inhibition of radiation induced AKT phosphorylation. These drugs radiosensitised radioresistant PDO lines and HCT116 with maximal inhibitory concentration levels within previously published ranges for humans. Dual inhibitors may also possess chemotherapy sensitising properties in the absence of radiotherapy.

Conclusion: The PI3K/AKT/mTOR pathway upregulation is associated with NCRT resistance. The role of dual PI3K and mTOR inhibitors as radiosensitisers in LARC patients warrants further preclinical and clinical research.

Dedication

“I dedicate this thesis to my wife Priyanka, my parents Keerthi and Nalini; without whose help, understanding and support none of this work would have been possible.”

Acknowledgements

I would like to acknowledge my supervisors, Professor Andrew Beggs and Mr Tariq Ismail; whose support and guidance throughout this research was exemplary. I am grateful for the funding provided for this research by Cancer Research UK as well as The Wellcome Trust, through my supervisor and principal investigator, Professor Andrew Beggs. I would especially like to thank Dr Joao D Barros-Silva for providing his expertise, guidance and support with this research as well as his help with data analysis and interpretation. Mr Mohammed Elsarag, Dr Lennard Lee and Mr Thomas Starkey assisted with statistics and bioinformatics analyses. I would also like to extend my gratitude to other members of the team at our research laboratory, Dr Joanne Stockton, Dr Valerie Somani, Ms Clare Bryer, Ms. Celina Whalley, Ms. Rachel Hoare and Mr Konstantinos Kagiopoulos for all their help with this research. I would also like to extend my gratitude to my colleagues, Dr Helen Bermingham, Dr Oliver J. Pickles, Dr Robert Tyler, Dr Tortieju Sillo and Dr Agata Stodolna for their support. I also extend my gratitude to staff at the University Hospitals Birmingham NHS Foundation Trust, Queen Elizabeth Hospital colorectal surgery department, including the consultant body, operating theatre staff and pathology department staff for their assistance with patient recruitment and sample retrieval. I would also like to thank the team at Human Biomaterials Resource Centre in Birmingham for their support with tissue and data retrieval. I would also like to thank all the patients who donated their tissue for this research.

Publications

Peer reviewed articles:

1. **Wanigasooriya K**, Tyler R, Barros-Silva JD, Sinha Y, Ismail T and Beggs AD. Radiosensitising Cancer Using Phosphatidylinositol-3-Kinase (PI3K), Protein Kinase B (AKT) or Mammalian Target of Rapamycin (mTOR) Inhibitors (Review article). *Cancers*. 2020 May;12(5):1278-1307. doi: <https://doi.org/10.3390/cancers12051278>
2. **Wanigasooriya K, Barros-Silva JD**, Tee L, El-Asrag ME, Stodolna A, Pickles OJ, Stockton J, Bryer C, Hoare R, Whalley CM, Tyler R, Sillo T, Yau C, Ismail T and Beggs AD. Patient derived organoids reveal that PI3K/AKT signaling is an escape pathway for radioresistance and a target for therapy in rectal cancer (Original research). *Frontiers in Oncology* (2022): 2875. doi: <https://doi.org/10.3389/fonc.2022.920444>

Published abstracts:

1. **Wanigasooriya K**, Barros-Silva JD, Stodolna A, Pickles O, Sinha Y, Wheat R, Ismail T, Beggs AD. A colorectal cancer patient derived organoid (PDO) model to determine radiotherapy response and resistance *in vitro*. *Colorectal disease*, 2020

2. **Wanigasooriya K**, Barros-Silva JD, Pestinger V, Tee L, Sinha Y, Pickles O, Ismail T, Beggs AD. Gene expression profiles of radiotherapy responsive versus non-responsive colorectal cancer patient derived organoid lines. Colorectal disease, 2020

3. **Wanigasooriya K**, Barros-Silva JD, Whalley C, Bryer C, Kagiopoulos K et al. Tumour gene expression profiles of locally advanced rectal cancer patients who completely respond versus non-responders following neo-adjuvant long course chemoradiotherapy; P232. Colorectal Disease 2019; 21(s3):75

4. Barros-Silva JD, **Wanigasooriya K**, Bermingham H, Patel S, Hoare R et al 90P Patient-derived organoid models of metastatic colorectal cancer to study response to PIK3CA inhibitors. Annals of Oncology 2019, 30(s7): mdz413. 094

Contents

Abstract	2
Dedication	4
Acknowledgements	5
Publications	6
Contents	8
List of Tables	21
List of Figures	26
List of Abbreviations	31
Chapter 1: Global Introduction	35
1.1 Epidemiology of colorectal cancer	35
1.2 Anatomy and embryological origins of the colon and rectum	37
1.3 Histology of the colon and rectum	39
1.4 Colorectal cancer biology	41
1.4.1 The adenoma – carcinoma sequence	41
1.4.2 Colorectal cancer genetics	42
1.4.2.1 DNA mismatch repair protein genes	43
1.4.2.2 APC gene	45

1.4.2.3	MutYH gene	46
1.4.2.4	P53 gene	47
1.4.2.5	KRAS gene	47
1.4.2.6	PIK3CA gene.....	48
1.4.2.7	BRAF gene.....	49
1.4.2.8	Genes encoding the EGFR family of proteins	49
1.4.2.9	DNA methylation	50
1.4.2.10	Single nucleotide polymorphisms (SNPs)	51
1.4.2.11	Long non-coding RNA and micro RNA.....	51
1.4.3	Molecular classification of CRC	52
1.4.4	Intracellular pathways implicated in CRC pathogenesis	54
1.4.4.1	Wnt signalling pathway.....	55
1.4.4.2	MAPK pathway.....	55
1.4.4.3	PI3K/AKT/mTOR pathway.....	56
1.4.4.4	TGF β and SMAD pathway.....	57
1.4.5	The tumour microenvironment in CRC.....	57
1.4.5.1	Immunoscore.....	57
1.4.5.2	Cancer associated fibroblasts and tumour associated macrophages	58
1.4.5.3	The microbiome.....	58
1.5	Investigating and staging colorectal cancer	59
1.6	Rectal cancer versus colon cancer	61

1.7 Treatment of non-metastatic colorectal cancer	62
1.8 Treatment of locally advanced rectal cancer	63
1.8.1 Neoadjuvant treatment in rectal cancer	64
1.8.1.1 The mechanisms of action	65
1.8.1.2 Assessment of neoadjuvant treatment response.....	65
1.8.1.3 Factors associated with chemoradiotherapy response.....	68
1.8.2 Advancements in rectal cancer neoadjuvant treatments.....	69
1.8.2.1 Personalised treatment	69
1.8.2.2 Therapeutic targets to improve NCRT response in rectal cancer	70
1.8.2.3 Preclinical research	72
1.8.2.4 Clinical research.....	72
1.9 Treatment of metastatic colorectal cancer	73
1.10 Treatment of recurrent colorectal cancer	75
1.11 The prognosis	76
1.12 Patient derived organoid models in cancer research	77
1.13 Aims and objectives	78
1.14 Hypotheses	79
Chapter 2: Materials and Methods	80
2.1 Ethical approval.....	80
2.2 Patient recruitment.....	80
2.2.1 Retrospective samples.....	80

2.2.2	Prospective samples.....	81
2.3	Cell line methodology.....	81
2.3.1	Cell culture and passage	81
2.3.2	Cell line experiments.....	82
2.3.2.1	Cell retrieval for experiments and cell counting	82
2.3.2.2	HCT116 - drug +/- radiotherapy screens.....	83
2.3.2.3	HCT116 experiments for PI3K/AKT/mTOR pathway analysis.....	92
2.4	Patient derived organoid methodology.....	95
2.4.1	Primary culture of human patient-derived organoid lines	95
2.4.2	Human patient-derived organoid passage	97
2.4.3	Human patient-derived organoid freezing protocol	98
2.4.4	Human patient-derived organoid thawing protocol.....	99
2.4.5	Human PDO experiments	99
2.4.5.1	PDO experiment preparation and viability assessment	99
2.4.5.2	Determining the optimum cell count within PDOs for experiments ..	104
2.4.5.3	Radiotherapy (only) experiments.....	104
2.4.5.4	Drug screens	106
2.5	Genomic methodology	110
2.5.1	Extracting DNA and RNA.....	110
2.5.1.1	From formalin fixed paraffin-embedded tissue	110
2.5.1.2	Extracting DNA and RNA from patient derived organoids	113

2.5.2	Quantification and quality control	114
2.5.2.1	DNA and RNA quantification using Qubit™	114
2.5.2.2	Quality control	114
2.5.3	Library preparation and sequencing.....	115
2.5.3.1	Three prime RNA sequencing	115
2.5.3.2	Total RNA sequencing	121
2.5.3.3	Custom targeted colorectal gene panel.....	127
2.5.4	Bioinformatics	136
2.5.4.1	Partek Flow®: Raw gene counts from 3' RNA sequencing	136
2.5.4.2	Partek Flow®: Raw gene counts from Total RNA sequencing	137
2.5.4.3	Partek Flow®: Normalisation, principal component analysis and differential gene expression analysis	137
2.5.4.4	DEBrowser: Normalisation, principal component analysis and DESeq2 differential expression analysis.	138
2.5.4.5	Gene Set Enrichment Analysis (GSEA)	140
2.5.4.6	Custom targeted DNA panel (QIASeq®) sequencing data analysis	141
2.5.4.7	Visual representation of bioinformatics results	141
2.6	Proteomics methodology.....	142
2.6.1	Protein lysis and extraction	142
2.6.2	Protein sonication	142
2.6.3	Protein quantification	143
2.6.4	Western blots.....	144

2.6.4.1	Preparing the solutions required in subsequent steps.....	144
2.6.4.2	Running the gel	145
2.6.4.3	The transfer.....	146
2.6.4.4	Primary antibody	146
2.6.4.5	Secondary antibody.....	147
2.6.4.6	Chemiluminescence	148
2.6.4.7	Membrane stripping.....	148
2.6.4.8	Image analysis and densitometry	149
2.7	Immunohistochemistry methodology.....	149
2.7.1	Patient derived organoids	149
2.7.1.1	Fixing patient derived organoids.....	149
2.7.1.2	Paraffin embedding	150
2.7.1.3	Obtaining sections.....	151
2.7.2	Staining FFPE sections (Common procedure PDO and fresh tissue sections).....	151
2.7.2.1	Haematoxylin and Eosin.....	151
2.7.2.2	Pan-Cytokeratin and CDX-2 staining.....	152
2.8	Other laboratory methods	153
2.8.1	Optical microscopy.....	153
2.8.2	Mycoplasma testing	154
2.9	A list of all reagents and kits used.....	155
2.10A	A list of equipment and consumables used.....	160

Chapter 3: A Literature Review of Factors Predicting Chemoradiotherapy Response in Locally Advanced Rectal Cancer Patients.....	162
3.1 Introduction	162
3.2 Methods	163
3.3 Predictive Factors	163
3.3.1 Clinical factors.....	163
3.3.1.1 Clinicopathological factors.....	163
3.3.1.2 Radiological factors	164
3.3.2 Blood-based markers.....	165
3.3.2.1 Routine blood tests.....	165
3.3.2.2 Tumour markers	165
3.3.2.3 Circulating tumour DNA.....	166
3.3.3 Markers within tumour tissue	167
3.3.3.1 DNA mutations	167
3.3.3.2 Single nucleotide polymorphisms	168
3.3.3.3 DNA methylation	169
3.3.3.4 RNA expression	170
3.3.3.5 Protein expression.....	174
3.3.3.6 Microenvironment.....	176
3.3.3.7 Microbiome.....	176
3.4 Discussion.....	177
3.5 Conclusion	179

Chapter 4: Identifying Biomarkers and Biological Pathways Associated with Chemoradiotherapy Response in a Retrospective Cohort of Locally Advanced Rectal Cancer Patients.....	180
4.1 Introduction	180
4.2 Aims	182
4.3 Methods	182
4.4 Results	183
4.4.1 Patient demographics and clinicopathological data	183
4.4.2 Transcriptomic analysis of FFPE patient samples	186
4.4.2.1 Sample purity analysis	187
4.4.3 Gene expression in pre-NCRT rectal cancer biopsies was associated with NCRT response status.....	190
4.4.3.1 Upregulated genes in pre-NCRT biopsies of non-responders.....	192
4.4.3.2 Downregulated genes in pre-NCRT biopsies of non-responders	193
4.4.3.3 GSEA – pre-NCRT FFPE biopsy samples	195
4.4.4 Gene expression in post-NCRT (tumour resection specimen FFPE samples) versus pre-NCRT (biopsy FFPE samples) in non-responding LARC patients	198
4.4.4.1 Upregulated genes in post-NCRT non-responder FFPE samples...	201
4.4.4.2 Downregulated genes in post-NCRT non-responder FFPE samples	202
4.4.4.3 GSEA – non-responder FFPE samples (post-NCRT tumour versus pre-NCRT biopsy)	203

4.4.5	NGS of FFPE sample RNA from LARC patients reveal biological pathways of interest in NCRT resistance	208
4.4.5.1	The PI3K/AKT/mTOR pathway.....	208
4.4.5.2	P53 pathway.....	212
4.4.5.3	Oxidative phosphorylation and hypoxia signalling	213
4.4.5.4	Notch signalling pathway.....	213
4.4.5.5	The MAPK pathway.....	214
4.4.5.6	Epithelial Mesenchymal Transition pathway.....	214
4.4.5.7	The TGF β pathway.....	215
4.4.5.8	The NF κ B pathway.....	215
4.5	Discussion.....	216
4.6	Conclusion	219
Chapter 5: Patient derived organoid models to simulate radiotherapy treatment <i>in vitro</i> and transcriptomic analysis		
		220
5.1	Introduction	220
5.2	Aims.....	221
5.3	Methods	222
5.4	Results.....	223
5.4.1	Establishing and characterising PDO lines	223
5.4.1.1	Clinicopathological characteristics.....	223
5.4.1.2	Microscopic characterisations of PDO models	225
5.4.1.3	Genomic characterisation.....	227

5.4.2	PDO response to radiotherapy	230
5.4.3	Mutations identified in radioresistant versus radiosensitive PDO lines ..	233
5.4.4	Pre-irradiation PDO transcriptomic analysis	235
5.4.5	Pre-irradiation 3' RNA sequencing of PDOs	236
5.4.5.1	Upregulated genes in radioresistant PDOs	239
5.4.5.2	Downregulated genes in radioresistant PDOs.....	240
5.4.5.3	Gene clusters identified through hierarchical clustering	242
5.4.5.4	GSEA of pre-irradiation PDO lines	244
5.4.6	Pre-irradiation total RNA sequencing of PDOs	247
5.4.6.1	Upregulated genes in pre-irradiated radioresistant PDO lines	249
5.4.6.2	Downregulated genes in pre-irradiation radioresistant PDO lines ...	252
5.4.7	Gene enrichment analysis	253
5.4.8	Pre- and post-irradiation 3' RNA sequencing of PDOs	255
5.4.8.1	Upregulated genes in post-irradiated radioresistant PDO lines.....	258
5.4.8.2	Downregulated genes in post-irradiated radioresistant PDO lines ..	259
5.4.8.3	Upregulated genes in post-irradiated radiosensitive PDO lines	260
5.4.8.4	Downregulated genes in post-irradiated radiosensitive PDO lines..	262
5.4.8.5	GSEA of PDO lines, pre- versus post-irradiation.....	263
5.5	Discussion.....	264
5.6	Conclusion	267
Chapter 6: Does the PI3K AKT mTOR pathway inhibition enhance radiotherapy response?		268

6.1	Introduction	268
6.1.1	Targeted inhibition of the PI3K/AKT/mTOR pathway	271
6.1.2	Literature review: The PI3K/AKT/mTOR pathway as a target in colorectal cancer treatment	273
6.1.3	The chosen radiosensitising drugs.....	275
6.1.3.1	5FU	276
6.1.3.2	Apitolisib.....	276
6.1.3.3	Dactolisib.....	277
6.2	Methods	278
6.3	Results	279
6.3.1	CRC cell line chemoradiotherapy assays	279
6.3.1.1	Optimum seeding density	279
6.3.1.2	Improving CRC cell line response to radiation.....	280
6.3.1.3	Optimum radiotherapy dose and time point for protein extraction to detect pAKT in a CRC cell line following irradiation	283
6.3.1.4	Radiation induced AKT phosphorylation is inhibited by dual PI3K and mTOR blockers in irradiated HCT116 cells	285
6.3.2	PDO in vitro chemoradiotherapy assays.....	288
6.3.2.1	Determining the optimal PDO seeding density	288
6.3.2.2	Pilot experiments reveal feasibility of in vitro PDO drug and radiotherapy assays using dual PI3K and mTOR inhibitors	289

6.3.2.3	Dual PI3K and mTOR inhibitors radiosensitise radioresistant PDO lines	293
6.3.2.4	In vitro PDO drug assays using dual PI3K and mTOR inhibitors.....	297
6.4	Discussion.....	300
6.5	Conclusion	304
Chapter 7: General Discussion		306
Chapter 8: Future Work.....		313
8.1	Laboratory research	313
8.1.1	Additional genomic, transcriptomic and immunohistochemistry work	313
8.1.2	Downstream PI3K/AKT/mTOR pathway component analysis.....	315
8.1.3	Additional in vitro chemoradiotherapy assays	316
8.1.4	Patient derived xenografts models.....	317
8.2	Clinical research.....	318
Thesis Conclusion		322
References.....		325
Appendices		360
A)	Consent form.....	360
B)	PDO count estimation example.....	361
C)	List of genes and mutations covered by the QIASeq® Custom Targeted DNA sequencing panel	362
D)	Parameters used within the Lexogen QuantSeq data analysis pipeline on Partek Flow®.....	373

E) Parameters used within the Illumina® Total RNA Sequencing data analysis pipeline on Partek Flow®	378
F) R Script: GSEA using cluster profiler and DESeq2 Reproduced with permission from Dr Joao D. Barros-Silva, University of Birmingham.....	381
G) R Script: EnhancedVolcano	388
H) Hierarchical clustering settings on Partek Flow®	391
I) ComplexHeatMap OncoPrint R Script.....	392
J) Western blots: protein quantification and normalisation calculations, an example and formulas used.....	396
K) KEGG enrichment: All upregulated gene sets in non-responder post-NCRT surgical resection FFPE specimens	397
L) Sample mycoplasma test result	399
M) List of mutations identified on PDO lines – QIASeq Targeted DNA Panel1	400
N) HCT116 drug only versus drug and radiotherapy: Welch’s two sample t-test .	404
O) Western blots: Raw images	405
P) Western blots: Image densitometry analysis	408
Q) PDO drug only versus drug and radiotherapy: Welch’s two sample t-test.....	409

List of Tables

Table 1-1: Consensus molecular subtype classification of CRC.	52
Table 1-2: Colorectal cancer intrinsic subtypes classification system.....	53
Table 1-3: TNM version 8 and Dukes staging of colorectal adenocarcinoma	60
Table 1-4: Scoring systems used to measure tumour regression and response to NCRT in rectal cancer.....	66
Table 1-5: Emerging targeted therapies with the potential to improve NCRT response in rectal cancer.....	71
Table 2-1: Drug preparation – Initial drug stock dissolved in 100% DMSO	87
Table 2-2: Drug preparation - diluted stocks of the drugs in 100% DMSO	88
Table 2-3: Drug preparation - 5FU dilutions	89
Table 2-4: Drug preparation - apitolisib dilutions	90
Table 2-5: Drug preparation - dactolisib dilution.....	91
Table 2-6: Drug preparation – 5FU, apitolisib (API.), dactolisib (DACTO.) and in combination.....	108
Table 2-7: Tissue Lysis Buffer / Protein K Solution mix (initial mix).....	111
Table 2-8: E220 Focused Ultrasonicator settings.....	112
Table 2-9: Thermocycler settings and reagents used for library generation.....	117
Table 2-10: Thermocycler settings and reagents used for indexing and library amplification stage.....	118
Table 2-11: Thermocycler settings used for QPCR add-on stage	119
Table 2-12: Thermocycler settings for probe hybridization	122

Table 2-13: Thermocycler settings for first strand cDNA synthesis	124
Table 2-14: Thermocycler settings for cDNA library end prep.....	125
Table 2-15: Thermocycler settings for PCR enrichment of adapter ligated cDNA..	126
Table 2-16: List of genes included in the targeted QIAseq® targeted DNA panel..	128
Table 2-17: Reaction mix for fragmentation, end-repair and A-addition – QIAseq® targeted DNA panel.....	130
Table 2-18: Thermocycler settings for DNA fragmentation, end-repair and A-addition – QIAseq® targeted DNA panel	131
Table 2-19: The master mix for adapter ligation.....	131
Table 2-20: The master mix for target enrichment	132
Table 2-21: Thermocycler settings for target enrichment (1500-12,000 primers/tube) – QIAseq® Targeted Panel	133
Table 2-22: Thermocycler settings for Universal PCR – QIAseq® targeted DNA panel	134
Table 2-23: Primary antibodies used in western blots.....	147
Table 2-24: Primary antibodies used for immunohistochemistry	153
Table 2-25: Thermocycler settings for EZ-PCR Test Kit Mycoplasma DNA expansion	154
Table 2-26: A table listing all reagents and reagent kits used	155
Table 2-27: A table listing all consumables and equipment used.....	160
Table 3-1: mRNA and miRNA as biomarkers for NCRT response in LARC.....	172
Table 4-1: Demographics and clinicopathological characteristics of patient FFPE biopsy and tumour samples.	184

Table 4-2: Genes upregulated in pre-NCRT FFPE biopsy samples from non-responders	193
Table 4-3: Genes downregulated in pre-NCRT FFPE biopsy samples from non-responders	194
Table 4-4: Hallmark enrichment: Upregulated gene sets in the pre-NCRT, non-responder FFPE biopsy samples	195
Table 4-5: KEGG enrichment: Upregulated gene sets in pre-NCRT, non-responder FFPE biopsy samples	197
Table 4-6: Oncogenic Signatures enrichment: Upregulated gene sets in pre-NCRT, non-responder FFPE biopsy samples	198
Table 4-7: Upregulated genes in post-NCRT FFPE tumour samples of non-responders	201
Table 4-8: Downregulated genes in post-NCRT FFPE tumour samples of non-responders	202
Table 4-9: Hallmark enrichment: Upregulated gene in post-NCRT surgical resection FFPE specimens of non-responders	203
Table 4-10: KEGG enrichment: Gene sets upregulated in post-NCRT surgical resection FFPE specimens of non-responders	205
Table 4-11: Oncogenic Signatures enrichment: Upregulated genes in post-NCRT surgical resection FFPE specimens of non-responders.	206
Table 5-1: Patient clinicopathological characteristics	224
Table 5-2: PDO DNA quantification and quality control data	227

Table 5-3: Frequency of pathological mutations of commonly affected genes in CRC, identified amongst radiosensitive (responder) versus radioresistant (non responder) PDO lines	235
Table 5-4: PDO RNA quantification and quality control data	236
Table 5-5: Upregulated genes pre-irradiation non-responder PDO lines (653 and 557) on 3' RNA sequencing	240
Table 5-6: Downregulated genes pre-irradiation non-responder PDO lines (653 and 557) on 3' RNA sequencing	242
Table 5-7: Hallmark enrichment: Upregulated gene sets in non-responder PDOs (pre-irradiation).....	244
Table 5-8: Oncogenic Signatures enrichment: Upregulated gene sets in non-responder PDOs (pre-irradiation)	246
Table 5-9: Upregulated genes in non-responder PDO lines (653 and 557) - total RNA sequencing of pre-irradiated PDOs	250
Table 5-10: Downregulated genes in non-responder PDO lines (653 and 557) - total RNA sequencing of pre-irradiated PDOs.....	253
Table 5-11: Upregulated genes in post-irradiated radioresistant PDO lines.....	258
Table 5-12: Downregulated genes in post-irradiated radioresistant PDO lines	260
Table 5-13: Upregulated genes in post-irradiated radiosensitive PDO lines	262
Table 5-14: Downregulated genes in post-irradiated radiosensitive PDO lines.....	263
Table 6-1: In vitro and in vivo CRC research utilising PI3K/ AKT / mTOR pathway inhibitors as radiosensitisers	274
Table 6-2: Clinical trials evaluating the radiosensitising potential of PI3K/AKT/mTOR pathway inhibitors in locally advanced rectal cancer patients	275

Table 6-3: HCT116 half maximum inhibitory concentrations (IC50) after treatment with 5FU, apitolisib or dactolisib with or without radiotherapy	282
Table 6-4: IC50 values following treatment of radioresistant PDO lines with 5FU, apitolisib or dactolisib with or without radiotherapy.	297
Table 6-5: A summary of half maximum inhibitory concentration (IC50) results for the six PDO lines following treatment with 5FU, apitolisib or dactolisib.....	300

List of Figures

Figure 1-1: Distribution of CRC within the different anatomical regions of the lower gastrointestinal tract	37
Figure 1-2: Layers of the colon and rectum.....	40
Figure 1-3: The adenoma-carcinoma sequence in CRC (73).....	42
Figure 1-4: Intracellular pathways dysregulated in CRC pathogenesis (159).....	54
Figure 2-1: The 96-well plate configuration used for HCT116 seeding density experiments.....	84
Figure 2-2: The 96-well plate configuration used for HCT116 with drug(s) and radiotherapy experiments.....	86
Figure 2-3: HCT116, 2 radiotherapy doses and different protein extraction times experiment (re-pathway analysis)	93
Figure 2-4: HCT116 drug(s) and radiotherapy experiment for protein extraction (re-pathway analysis).....	94
Figure 2-5: A pictographic representation of the human PDO culture method	97
Figure 2-6: Graphical representation of the method used to estimate live cells within PDOsThe diagram above is a graphical representation of the method used to estimate PDO count for experiments. See Appendix B for a working example using this method.....	102
Figure 2-7: The 96-well plate configuration used for PDO and radiotherapy experiment	105

Figure 2-8: The 96-well plate configuration used for PDO with single drug dose and radiotherapy experiments.....	106
Figure 2-9: Workflow using truXTRAC® FFPE total NA Kit – Column, (Covaris, USA) to extract RNA.....	110
Figure 2-10: Schematic representation of double stranded cDNA library generation from RNA using Lexogen Quant-Seq library preparation kit.....	117
Figure 2-11: Final double stranded cDNA library structure prior to sequencing	118
Figure 2-12: The formula used for library molarity estimation	120
Figure 2-13: QIAseq® targeted DNA sequencing panel workflow	129
Figure 2-14: Lexogen QuantSeq data analysis pipeline on Partek Flow®	136
Figure 2-15: Illumina® Total RNA Sequencing data analysis pipeline on Partek Flow®.....	137
Figure 2-16: Workflow for normalisation, principal component analysis and differential expression analysis on Partek Flow®	138
Figure 4-1: Sample purity analysis: pre-NCRT biopsy non-responder versus complete responder samples	188
Figure 4-2: Sample purity analysis: non-responder pre-NCRT (biopsy) versus post-NCRT (tumour) samples	189
Figure 4-3: Principal component analysis of rectal cancer pre-NCRT biopsy gene expression between complete responders and non-responders	190
Figure 4-4: Volcano plot representing upregulated and downregulated genes in pre-NCRT FFPE biopsy samples from non-responders	191
Figure 4-5: Principal component analysis of gene expression between post-NCRT (tumour) and pre-NCRT (biopsy) non-responder FFPE rectal cancer samples.....	199

Figure 4-6: Volcano plot representing upregulated and downregulated genes in non-responder post-NCRT FFPE tumour samples.....	200
Figure 4-7: Hallmark MTORC1 Signalling gene set enriched in pre-NCRT, non-responder FFPE biopsy samples	209
Figure 4-8: GSEA enrichment plots and heat maps of differentially expressed genes of PI3K/AKT/mTOR pathway related gene sets	211
Figure 5-1: Optical microscopy and immunohistochemistry of 6 patient derived organoid lines	226
Figure 5-2: Heatmap demonstrating QIAseq™ targeted DNA panel sequencing data	228
Figure 5-3: An in vitro model to assess PDO radiotherapy response	231
Figure 5-4: Variations in response to radiotherapy in six PDO lines	232
Figure 5-5: Principal component analysis of PDO gene expression between non-responder and responder lines.....	237
Figure 5-6: Volcano plot representing upregulated and downregulated genes in non-responder PDO lines	238
Figure 5-7: Heatmap generated through hierarchical clustering.....	243
Figure 5-8: Principal component analysis following Total RNA Sequencing of PDO lines (pre-irradiation)	248
Figure 5-9: Volcano plot representing upregulated and downregulated genes in non-responder PDO lines.	249
Figure 5-10: Gene sets upregulated in non-responder PDOs	254
Figure 5-11: Principal component analysis of pre- and post- irradiation PDO lines	256

Figure 5-12: Volcano plots depicting significantly up and down regulated genes post-irradiation	257
Figure 6-1: The PI3K/AKT/mTOR pathway activation leads to cell growth, increased protein synthesis, inhibited apoptosis, cell cycle progression and proliferation.	270
Figure 6-2: Drugs for targeted inhibition of the PI3K/AKT/mTOR pathway.....	272
Figure 6-3: Chemical structure of 5FU (591)	276
Figure 6-4: The chemical structure of apitolisib (592).....	277
Figure 6-5: The chemical structure of dactolisib (614).....	278
Figure 6-6: HCT116 optimum seeding density experiment	279
Figure 6-7: HCT116 cell viability and half maximum inhibitory concentrations (IC50) after treatment with 5FU, apitolisib or dactolisib with or without radiotherapy	281
Figure 6-8: AKT phosphorylation in HCT116 cells over time following a single 5 Gy or 10 Gy radiotherapy fraction.	283
Figure 6-9: AKT phosphorylation following treatment with 5FU, apitolisib, dactolisib and irradiation.	287
Figure 6-10: The effect of high dose 5FU on different seeding densities of two PDO lines.....	288
Figure 6-11: Six PDO lines treated with 5FU with or without radiotherapy.....	290
Figure 6-12: Six PDO lines treated with apitolisib with or without radiotherapy.....	291
Figure 6-13: Six PDO lines treated with 5FU and apitolisib with or without radiotherapy.	291
Figure 6-14: Six PDO lines treated with dactolisib with or without radiotherapy.	292
Figure 6-15: Six PDO lines treated with 5FU and dactolisib with or without radiotherapy.	293

Figure 6-16: Schematic representation of PDO chemoradiotherapy assays	294
Figure 6-17: Radiotherapy resistant PDO lines 557 and 653 treated with 5FU, apitolisib and dactolisib with or without radiotherapy.....	295
Figure 6-18: Dose response curves and IC50 values following treatment of radiosensitive PDO lines with 5FU, apitolisib or dactolisib	298
Figure 8-1: Proposed phase II double blinded clinical trial to evaluate the safety and efficacy of dual PI3K and mTOR inhibitor dactolisib (with or without capecitabine) and radiotherapy versus current standard treatment in LARC patients	319

List of Abbreviations

3D	Three-dimensional
5FU	5-fluorouracil
AKT	Protein Kinase B
APC	Adenomatous polyposis coli
API	Apitolisib
ATR	Ataxia telangiectasia and rad3 related protein
BAD	B-cell lymphoma 2 associated agonist of cell death
BCL	B cell CLL/lymphoma
BCL-2	B-cell lymphoma 2
Cafs	Cancer associated fibroblasts
cCR	Complete clinical remission
CDK	Cyclin Dependent Kinase
cDNA	Complementary DNA
CDX2	Caudal related homebox - 2
CIMP	Change in methylator phenotype
CIN	Chromosomal instability
CMS	Consensus molecular subtype
CRC	Colorectal cancer
CRIS	CRC intrinsic subtypes
ctDNA	Circulating tumour DNA
DACTO	Dactolisib

DIN	DNA integrity number
dMMR	DNA mismatch repair
DNA	Deoxyribose nucleic acid
DNA-PK	DNA-dependent protein kinase
DSB	Double strand break
EGFR	Epidermal growth factor
ES	Enrichment score
F	Female
FAP	Familial adenomatous polyposis
FDA	Food and drug administration
FDR	False discovery rate
FFPE	Formalin fixed paraffin embedded
FOX	Forkhead family
GBM	Glioblastoma multiform
GSA	Gene specific analysis
GSEA	Gene set enrichment analysis
H&E	Haematoxylin and eosin
H&N	Head and neck
HER	Human epidermal growth factor receptor
KRAS	Kirsten rat sarcoma virus
LARC	Locally advanced rectal cancer
M	Male
MAPK	Mitogen activated protein kinase
MDM	Mouse double minute
MEK	Mitogen activated protein kinase-kinase

MGMT	O6-methylguanine–DNA methyltransferase
miRNA	Micro RNA
MSI	Microsatellite instability
MSigDB	Molecular Signatures Database
MSS	Microsatellite stable
MTOR	Mammalian target of rapamycin
Mut	Mutant
NAR	Neoadjuvant rectal (score)
NCRT	Neoadjuvant chemoradiotherapy
NF κ B	Nuclear factor kappa-light-chain-enhancer of activated B cells
NGS	Next generation sequencing
NSCLC	Non-small cell lung cancer
Nx	Neoadjuvant treatment
pAKT	Phosphorylated protein kinase B
PCK	Pancytokeratin
pCR	Pathological complete response
PCR	Polymerase chain reaction
PDO	Patient derived organoids
PDX	Patient derived xenografts
PI3K	Phosphoinositide 3-kinase
PIP2	Protein phosphatidylinositol-4,5-bisphosphate
PIP3	Phosphatidylinositol-3,4,5-bisphosphate
PTEN	Phosphatase and tensin homologue
QPCR	Quantitative real-time PCR
RAF	Rapidly accelerated fibrosarcoma

RIN	RNA integrity number
RNA	Ribonucleic acid
RT	Radiotherapy
SCRT	Short course radiotherapy
siRNA	Small interfering RNA
TAMS	Tumour associated macrophages
TGF β	Transforming growth factor beta
TRG	Tumour regression grade
UK	United Kingdom
USA	United States of America
V	Version
VEGF	Vascular endothelial growth factor
Wnt	Wingless / integrated
WT	Wild-type
XIAP	X-linked inhibitor of apoptosis protein
YAP	Yes-associated protein 1 (YAP)

Chapter 1: Global Introduction

1.1 Epidemiology of colorectal cancer

Colorectal cancer (CRC) is the third most commonly diagnosed cancer in men and women in the United Kingdom (UK) (1). Rectal cancer accounts for a third of all CRC (2). The current lifetime risk of developing CRC in the UK is 1 in 15 for males and 1 in 18 for females (3). It is also the third most common cause of cancer-related death in men and women in the UK (4). The cost to the UK economy from CRC has been estimated at £1.6 billion (5). Even though traditionally CRC was a disease of industrialised nations; rising incidence is observed in emerging economies (6-8). The global burden is expected to rise with an estimated 60% increase in new diagnoses and deaths from the disease by the end of the next decade (9).

The rise in incidence of CRC in the UK and other developed nations may have stabilised over the last few decades (8). Better preventative measures, greater awareness, early diagnosis through screening programmes, significant investment in research and consequent advancements in treatment have played a significant role (8, 10, 11). The median age at diagnosis for CRC is between 60-70 (12). The highest incidence is observed amongst 70 to 80 year-olds with over 60% of diagnoses being made in patients over the age of 70 (1, 13). However, the incidence of CRC is rising amongst younger people (14, 15).

Risk factors for CRC are inherited or acquired (16). Approximately 5% of patients have inherited conditions such as Familial Adenomatous Polyposis (FAP), Hereditary Non-Polyposis Colon Cancer (also known as Lynch Syndrome), Peutz-Jegher Syndrome, *MutYH* associated polyposis and juvenile polyposis syndrome which significantly increases their risk of developing CRC (17). Acquired risk factors for developing CRC include smoking, excess alcohol consumption, obesity, excess processed and red meat consumption (18, 19). Patients with inflammatory bowel disease (e.g., Crohn's disease, ulcerative colitis), primary sclerosing cholangitis and those on immunosuppressant medication after organ transplantation also have a higher acquired risk of developing CRC (20-22).

The commonest symptoms at presentation include a change in bowel habit or rectal bleeding (23). Abdominal pain, distension, vomiting, weight loss and tenesmus are often late symptoms (24). CRC patients may also present with iron deficiency anaemia (25). Around 20-25% of patients have metastatic disease at the time of diagnosis (26, 27). Approximately 15-33% will present as a surgical emergency due to complications (e.g. bowel obstruction or perforation) (28, 29). However, following the implementation of bowel cancer screening programmes amongst the asymptomatic population more patients with early stage disease are being diagnosed (30).

1.2 Anatomy and embryological origins of the colon and rectum

The large bowel can be subdivided into ten anatomical regions. From proximal to distal, these include: 1. Appendix, 2. Caecum, 3. Ascending colon, 4. Hepatic flexure, 5. Transverse colon, 6. Splenic flexure, 7. Descending colon, 8. Sigmoid colon, 9. Rectosigmoid junction and 8. Rectum (Figure 1-1) (31). Regions 1 to 4 and the proximal half of the transverse colon are often referred to as the right colon. The rest is classed as the left colon (32). A third of CRC originates in the rectum (33). The rectum is the most common site of carcinoma origin within the lower gastrointestinal tract (Figure 1-1). Overall, CRC is detected more frequently on the left side of the colon including the rectum compared to the right colon (34).

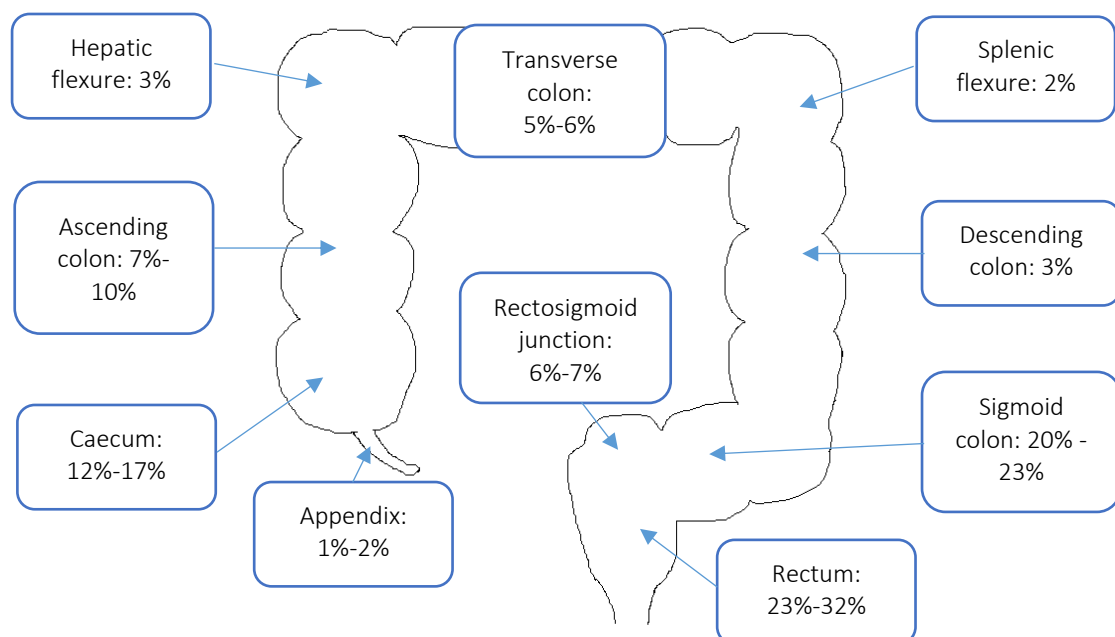


Figure 1-1: Distribution of CRC within the different anatomical regions of the lower gastrointestinal tract

The distribution of CRC varies throughout the colon and rectum. A third of CRC occurs in the rectum, followed by the sigmoid colon, caecum, right colon and transverse colon and left colon. Data source: Cancer Research UK (33)

The rectum can be further subdivided into thirds as the upper, middle and lower rectum (35). The rectum extends vertically from the anal verge up to a length of 15-20cm (31, 36, 37). Longitudinal folds of adipose tissue called taenia coli run the entire length of the serosal surface of the colon (38). Taenia coli are absent on the rectum (39). The convergence of taenia coli marks the transition between the sigmoid colon and rectum (40). Anatomists define the origin of the rectum at the sacral vertebral level S3 (37). Whilst there is some debate as to the exact definition of the superior border of the rectum, the widely accepted definitions include the point of convergence of the taeniae coli or the level of the sacral promontory (37, 41). Over a third of the rectum is above the peritoneal reflection and encapsulated by the visceral peritoneum on the anterior and lateral surfaces (31). The middle third of the rectum is lined by the visceral peritoneum anteriorly and the lower third is wholly extraperitoneal (37). Below the peritoneal reflection, the rectum is enclosed posteriorly by the mesorectal fascia comprising of lymph nodes, lymphatic channels, end arterioles, venules and capillary networks (35, 42). Distal to the rectum lies the anal canal which is the distal-most part of the alimentary tract. The length of the adult human anal canal ranges from 5-8cm (43).

The colon, rectum and proximal anal canal are derived entirely from the embryological endoderm (44). The endodermic midgut derives the right colon and the proximal two-thirds of the transverse colon (32, 45). The arterial supply for midgut structures is from branches of the superior mesenteric artery (46). Venous drainage is via the branches of the superior mesenteric vein (47). The distal third of the transverse colon, left colon, the rectum and anal canal up to the dentate line is derived from the endodermic hindgut (44). The arterial supply to the hindgut

structures is from the inferior mesenteric artery and venous drainage from the inferior mesenteric vein (46). Colonic and rectal lymphatic drainage follows the arterial supply (48). The anal canal distal to the dentate line and the external anal sphincter complex originates from the ectoderm (49). The middle, lower rectal arteries and veins, supplying and draining the latter structures are terminal branches of the internal iliac vessels (50). Lymphatic drainage is through inguinal, iliac and para-aortic lymph nodes, which run in parallel to the arterial supply (35).

The arterial supply, venous and lymphatic drainage of the human alimentary tract originating from the latter embryological differentiations; maintain these distinct distributions throughout adult life. These remain crucial in the pathophysiology of CRC, the anatomical basis for local and distant metastasis (51). Commonest sites for CRC metastasis include the liver, lungs and peritoneum (52). Rarer sites include the central nervous system, ovaries, superficial inguinal lymph nodes and the axial skeleton (53). The blood supply to the colon and rectum also determines the type of operation offered to CRC patients undergoing surgical management (54).

1.3 Histology of the colon and rectum

The wall of the colon and rectum comprise of four layers (55). Deep to superficial, these include the mucosa (epithelium, lamina propria and muscularis mucosa), submucosa, muscularis propria (circular and longitudinal smooth muscle layers), and serosa (Figure 1-2). The colonic, rectal and proximal anal canal mucosa is formed of simple columnar epithelial cells, goblet cells, Paneth cells and stem cells (56). A stratified squamous epithelium lines the distal anal canal (57). The dentate line

(pectinate line) marks the transition zone between the stratified squamous epithelium of the distal anal canal and the simple columnar epithelium of the proximal anal canal (49). The human intestinal epithelium comprises of crypts containing different cell types (58). Scattered within these crypts are goblet cells and enteroendocrine cells with secretory functions, and LGR5 stem cells with restorative functions, and Paneth cells with bactericidal functions (58). The enteric nervous system comprising of the submucosal and myenteric plexus traverses the submucosa and muscularis mucosa respectively (59). End arterioles dispersed within the submucosa feed the capillaries lining the epithelium. These drain into venules and lymph channels also lying within the submucosa.

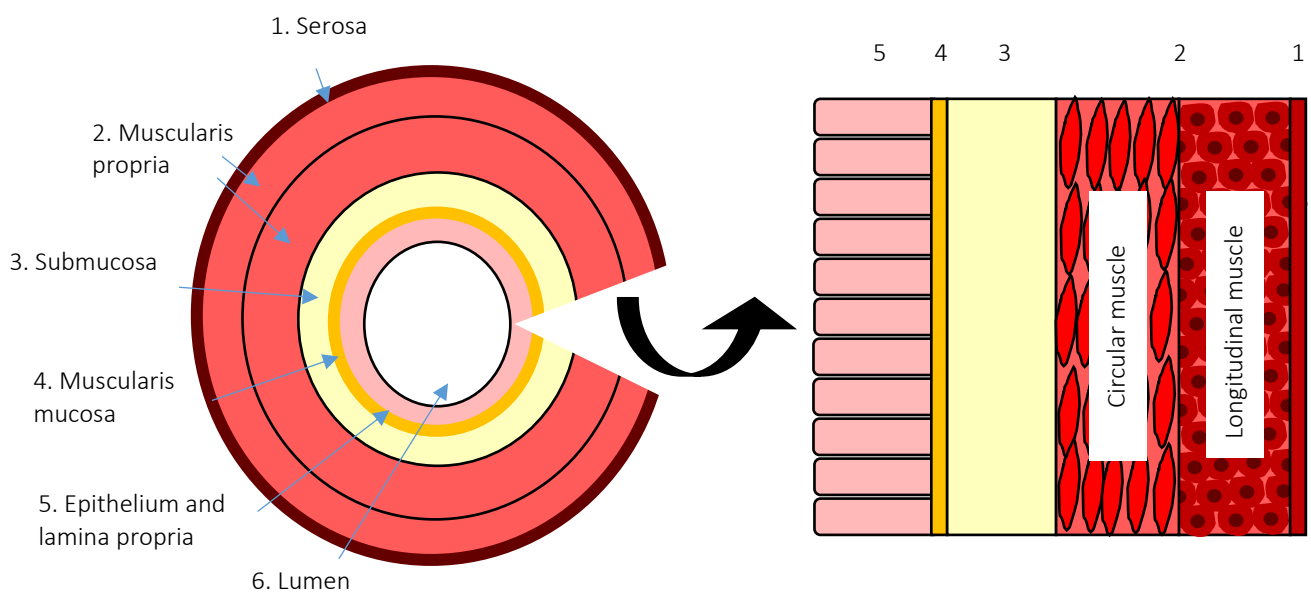


Figure 1-2: Layers of the colon and rectum

The image depicts the layers of the colon and rectum. From superficial to deep includes (1)-serosa, (2)-muscularis propria, (3)-submucosa, (4)-muscularis mucosa, (5)-epithelium and lamina propria and (6)-the lumen.

The majority (>90%) of CRC is adenocarcinoma, which originate from the simple columnar epithelial cells of the colon or rectum (60). Rare histological subtypes include mucinous adenocarcinoma, signet-ring cell carcinoma, neuroendocrine tumours, spindle cell carcinomas and undifferentiated tumours (27, 61). Squamous cell carcinoma originating within the squamous epithelium of the anal canal is the commonest type of anal cancer; with rarer subtypes including melanomas, lymphomas and adenocarcinoma of the anal canal (62). The term CRC in this thesis refers to adenocarcinoma of the colon and rectum. Colon cancer refers to adenocarcinoma of the colon and rectal cancer refers to adenocarcinoma of the rectum.

1.4 Colorectal cancer biology

1.4.1 The adenoma – carcinoma sequence

The adenoma to carcinoma transformation sequence is well established in the pathogenesis of CRC (63, 64). The majority of CRC originates from conventional adenomas (65); the remainder, perhaps originate from sessile serrated or traditional serrated lesions (66). Only 5% of adenomatous polyps may progress to colorectal adenocarcinoma (67). Endoscopic polypectomy and polyp surveillance programmes have been demonstrated to significantly reduce the risk of CRC (68-70). Figure 1-3 highlights the adenoma - carcinoma sequence; where the cumulative inherited or acquired genetic mutation burden over time within colorectal epithelial cells leads to adenoma formation subsequently leading to invasive carcinoma (64). CRC is a Wntless/Integrated (Wnt) pathway driven tumour (71). Adenoma formation begins with dysregulated Wnt signalling due to any of the following: APC gene mutation,

RSPO2/3 fusion, *RNF43* mutation or *CTNNB1* mutation. Mutations within genes such as *KRAS*, *BRAF*, *TP53*, *PIK3CA* oncogenes act as modifiers and contribute to the downstream transformation of benign adenomas to malignant CRC (72).

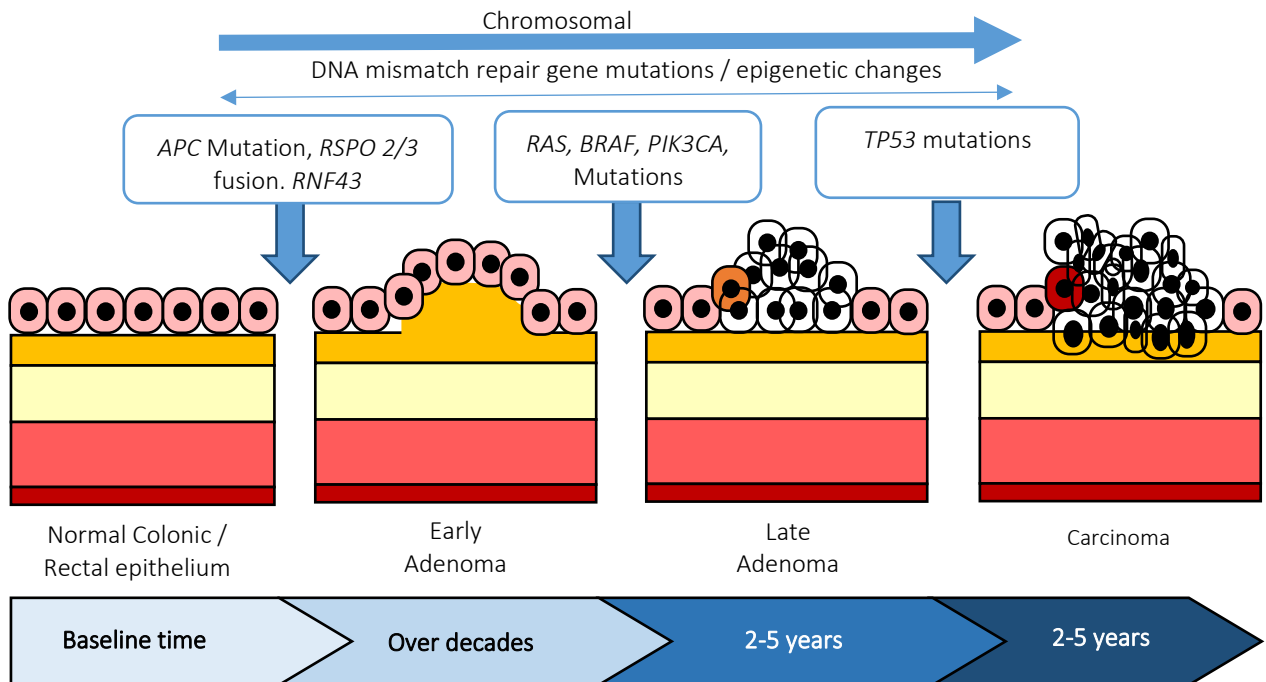


Figure 1-3: The adenoma-carcinoma sequence in CRC (73)

Disrupted WNT signalling and *APC* gene mutations in colonic crypt epithelial cells lead to adenoma formation. Subsequent *RAS*, *BRAF*, *PIK3CA*, *TP53* or DNA mismatch repair gene mutations result in the transition to high grade dysplasia or carcinoma. This process may take several years to decades.

1.4.2 Colorectal cancer genetics

Approximately a third of CRC is inherited and the rest are sporadic (74, 75).

However, only 5% of inherited CRC is associated with a known syndrome (17).

There are several inherited germline and somatic driver mutations of CRC (76).

Germline or somatic mutations in CRC may lead to the following distinct phenotypes:

Chromosomal instability (CIN), microsatellite instability (MSI) and CpG island methylator (CIMP) phenotypes (77). The majority (85%) of CRC demonstrates CIN or CIMP phenotypes (78). The remaining 15% of CRC tumours demonstrate MSI (79). More than one phenotype can be detected within a given tumour amongst the heterogeneous population of cells within that tumour (80). The common genetic and epigenetic variants associated with CRC and their clinicopathological significance has been described below.

1.4.2.1 DNA mismatch repair protein genes

Mutations in *MLH1* (3p21), *MSH2* (2p16), *MSH6* (2p16) and/or *PMS-2* (7p22) can lead to the loss of expression of DNA mismatch repair (dMMR) proteins encoded by these genes leading to hypermutation. (81). Microsatellites are regions of short 1-6bp repeating short tandem sequences, which account for approximately 3% of the human genome and are also susceptible to higher rates of mutations (82). The dMMR system ensures genomic stability during cellular replication and DNA repair by preventing and repairing base mismatches particularly within areas of high microsatellite prevalence (83).

Amongst the 15% of CRC patients with MSI, 3% are due to germline inherited mutations and 12% due to somatic mutations of dMMR protein genes (79). MSI tumours frequently originate in the proximal colon with only about 2% of RCs demonstrating MSI (84). Tumours with \geq 30% of markers of microsatellite region defects are referred to as MSI high (MSI-H). Those without any such defects are referred to as Microsatellite Stable (MSS). There is a third category of tumour with

some evidence of unstable microsatellite regions but does not meet the criteria for MSI-H. The latter group referred to as MSI low (MSI-L). MSI-L and MSS tumours, are similar in terms of pathogenesis, prognosis and response to treatment (85). MSI-H tumours have a better prognosis compared to MSS tumours but respond poorly to 5-fluorouracil (5FU) based chemotherapy (86).

Germline mutations of the dMMR genes lead to Lynch syndrome. The condition is characterised by early onset CRC (under the age of 50), at least two first degree relatives with CRC and a scattered family history of CRC (Amsterdam Criteria) (17). Patients with Lynch syndrome are also at risk of developing endometrial, gastric, ovarian, small intestine and urinary tract cancer (87). *MLH1* and *MHS2* mutations account for over 90% of all patients with Lynch Syndrome and 7-10% have *MSH6*, and 5% have *PMS2* mutations (88, 89). Deletions within the terminal exons of the *EPCAM* gene account for approximately 1-3% of Lynch syndrome patients, and is thought to be due to its silencing effects of *MSH2* (89).

The majority of sporadic MSI-H tumours do not express MutL Homolog 1 (*MLH1*) and PMS1 Homolog2 (*PMS2*) (86). The most frequent genetic defect (>90%) in sporadic MSI-H CRC is *MLH1* silencing by promoter hypermethylation and *BRAF* (*V600E*) mutation leading to a CIMP phenotype (90). UK NICE guidance mandates that all primary tumour from CRC patients are assessed for dMMR protein expression using immunohistochemistry given the significance of MSI status on subsequent management (91). The loss of *MLH1* and *PMS2* is therefore, correlated with the presence of *MLH1* promoter hypermethylation or *BRAF* (*V600E*) mutation

which would indicate a sporadic mutation. Therefore, germline testing or screening is not required. In contrast, lack of expression of MSH2, MSH6 or lack of *MLH1* promoter hypermethylation or *BRAF (V600E)* mutation would warrant further investigations including genetic counselling, germline testing and appropriate screening for the patient and at-risk family members.

1.4.2.2 *APC gene*

The *APC* gene is a tumour suppressor gene located at chromosome 5q21 (66). The gene encodes the intracellular adenomatous polyposis coli (APC) protein which has several functions (72). APC binds to β -catenin to enable phosphorylation of the latter and inhibits β -catenin mediated transcription. Therefore, APC regulates the β -catenin levels within the cell and β -catenin mediated transcription. Pooling of β -catenin is noted in cells with *APC* mutations (92). The protein also plays an essential role in cell migration, adhesion, proliferation (microtubular assembly, chromosomal segmentation) (72).

APC mutations can be found in over 70% of CRC (93, 94). The commonest site for germline as well as somatic mutations is along exon 15 also known as the mutation cluster region (95). Germline mutations of this gene causes FAP; an autosomal dominantly inherited condition which gives rise to numerous polyps (several thousand) within the colonic epithelium of affected patients (96). Their age onset of CRC is typically between the 2nd to 4th decade of life. Regular surveillance colonoscopies and prophylactic panproctocolectomy are used in the management of these patients. Patients with FAP may also develop upper gastrointestinal polyps

and rarely benign hepatobiliary, adrenal, thyroid tumours (97). A variant of FAP includes Gardner's syndrome where numerous colonic polyps occur alongside extra-colonic pathology such as benign osteoid tumours and epidermoid skin cysts (98). In addition to the germline *APC* mutation, CRC tumours from FAP patients also harbour other somatic mutations and allele loss (loss of heterozygosity) (99). The condition typically has near 100% penetrance but the significant variation in phenotypic expression could be partly attributed to the severity and frequency of this "second hit" mutation (99, 100).

Somatic mutations within the *APC* gene have been found in over 80% of sporadic CRC tumours (100). Whilst *APC* mutations occur relatively early within the pathogenesis of CRC, it is often preceded by a dysregulated Wnt signalling pathway (101). Approximately two thirds of somatic *APC* mutations occur within a small mutation cluster region on exon 15 between codons 1286 and 1513 (102). Epigenetic modification of the *APC* promoter region 1A by hypermethylation is commonly detected in CRC than in adenomas (103). *APC* hypermethylation which suppresses *APC* expression significantly impedes downstream APC mediated β -catenin phosphorylation leading to β -catenin pooling.

1.4.2.3 *MutYH* gene

The *MutYH* gene encodes a DNA glycosylase which prevents Adenine to Thymine transversion and facilitates DNA base-excision repair (104). Damages to single DNA bases through oxidation, deamination or alkylation without significant disruption of the DNA double helix may be repaired through DNA base excision repair (105).

Mutations in *MutYH* may result in impaired DNA repair leading to oncogenesis. The *MutYH* oncogene is located on chromosome 1p34 and sporadic mutations of this gene are rare (106). Inherited germline mutations within this gene causes the rare MutYH associated polyposis syndrome; the clinical presentation of which is very similar to FAP.

1.4.2.4 *P53* gene

The *p53* gene on chromosome 17p13 encodes the P53 tumour suppressor protein (107). P53 induces cell cycle arrest in response to irreparable DNA damage (108). Activated P53 regulates *P21* expression and P21 binds to cyclin dependent kinase (CDK) leading to cell cycle arrest at G1 or G2/M phase (109, 110). P53 also upregulates pro-apoptotic protein expression and downregulates pro-survival proteins (111). *P53* mutations have been detected in 40-50% of colorectal tumours (112, 113). Abnormal *p53* mutations have been associated with increased risk of death in CRC particularly amongst those patients with a lower baseline clinicopathological risk (114). Accumulation of this mutation within a sporadic tumour can result in the progression of a colorectal adenoma to a carcinoma (Figure 1-3).

1.4.2.5 *KRAS* gene

Mutations within the *KRAS* oncogene have been found in up to 30-40% of primary colorectal tumours (115). Located on chromosome 12p12.1 (116), this gene encodes the Kirsten rat sarcoma virus (KRAS) protein which is an isoform of the RAS family of proteins which also include NRAS and HRAS. Mutations within the *KRAS* gene accounts for over 86% of RAS mutations (117). The RAS protein is activated in

response to activation of a G-Protein Coupled Receptor leading to downstream activation of pathways such as the phosphatidylinositol-3-kinase (PI3K), protein kinase B (AKT) and mammalian target of Rapamycin (mTOR) pathway, and rapidly accelerated fibrosarcoma (RAF), mitogen activated protein kinase-kinase (MEK), mitogen activated protein kinase (MAPK) and extracellular signal regulated kinase (ERK) pathway (118). *KRAS* mutations are associated with a poor prognosis and increased tumour aggressiveness in CRC, independent of other clinicopathological features (119). Approximately 35-45% of metastatic CRC tumours are *KRAS* mutant (120, 121). Furthermore, anti-EGFR treatment (e.g. cetuximab) used in the treatment of metastatic CRC is ineffective against *KRAS* mutant tumours (122). Therefore, *KRAS* mutation status is frequently assessed in biopsies and tumour resection specimens from CRC patients using next generation sequencing (NGS).

1.4.2.6 *PIK3CA* gene

The *PIK3CA* gene located on chromosome 3q26, encodes the p110 α subunit of the PI3K protein (123). PI3K is an intracellular membrane bound oncoprotein comprising of two classes. Class1a is formed of 3 protein catalytic subunits p110 α , p110 β , p110 δ and Class1b which is made up of the single unit, p110 γ . PI3K activation leads to activation of the PI3K/AKT/mTOR pathway (see 1.4.4.3). *PIK3CA* oncogene mutations have been reported in 15-30% of primary CRC (124, 125). *PIK3CA* mutations have been associated with poor survival as well as resistance to first line chemotherapy (126, 127). *PIK3CA* mutations also lead to resistance to anti-EGFR therapies (128). In rectal cancer, *PIK3CA* mutations were associated with an increased risk of local recurrence (129). Mutations within genes coding for the other

catalytic subunits (e.g., *PIK3CB* and *PIK3CD*) and Class1b PI3K are less frequently reported (130).

1.4.2.7 *BRAF* gene

BRAF is an oncogene located on chromosome 7q34 and encodes the B-RAF protein which is part of the MAPK pathway (131). *BRAF* mutations were detected in various malignancies, with approximately 10-20% of primary CRC reported to contain *BRAF* mutations (132). Most *BRAF* mutations occur in codon 600 (mutation hotspot region) and leads to hyperactivation of its kinase domain (133). Furthermore, 10% of metastatic colorectal tumours may harbour *BRAF* mutations and have been associated with a poor response to chemotherapy, and worse prognosis independent of other clinicopathological features (134). Nearly 90% of *BRAF* mutations were shown to be present in *MLH1* promoter hypermethylated, sporadic colorectal tumours indicating a strong association between the two (135). Where immunohistochemistry demonstrates loss of *MLH1* or *PMS2* expression, NGS is routinely performed to check for a *BRAF* (*V600E*) mutation and *MLH1* promoter hypermethylation in order to exclude Lynch Syndrome (136).

1.4.2.8 *Genes encoding the EGFR family of proteins*

HER1, *HER2*, *HER3* and *HER4* belong to the *EGFR* family of tyrosine kinase receptor proteins (137). Approximately, 5% of primary colorectal tumours contain *ERBB2* mutations (138, 139). Mutations within the genes encoding the other three receptors are rare in CRC. *ERBB2* oncogene is located on chromosome 17q12 and encodes *HER2* receptor (140). *HER2* is a transmembrane tyrosine kinase receptor.

Expression of HER2 (HER2 positive) is detected in up to 90% of breast adenocarcinoma and is a significant marker of poor prognosis and recurrence in breast cancer patients (141). Similarly, HER2 expression can be detected in up to 50% of colorectal tumours and is a marker of poor prognosis in CRC patients (142, 143). *ERBB2* mutations are associated with poor prognosis particularly amongst those patients receiving anti-EGFR therapies (144). Studies have also shown that MSI and *PIK3CA* mutations frequently co-exist with *ERBB2* mutations (145). Research is underway to evaluate the role of HER-2 inhibitors as targeted precision therapy in CRC patients with HER-2 expression (146).

1.4.2.9 DNA methylation

Hyper- or hypomethylation of the CpG islands in the promoter region of a gene can lead to gene silencing. Epigenetic silencing of tumour suppressor genes such as *MLH1*, *APC*, *p53* and *PTEN* is frequently detected in CRC (147). Certain differentially methylated regions in CRC may serve as markers of therapeutic response and prognosis in CRC. DNA hypermethylation also leads to the CIMP phenotype. The CIMP phenotype is associated with a significantly worse prognosis in CRC patients (148). However, a meta-analysis by Kokelaar et al. from 2018 identified no significant prognostic predictive value of the CIMP phenotype amongst rectal cancer patients (149). More research is needed to evaluate the significance of various differentially methylated regions on CRC pathogenesis, treatment response and prognosis.

1.4.2.10 Single nucleotide polymorphisms (SNPs)

SNPs are variations in the genetic sequence of a particular gene characterised by the substitution of one nucleotide occurring at a frequency of 1% or higher in a given population (150). Research exploring the significance of SNPs in CRC is still in its infancy. A meta-analysis by Wen et al. of 5114 publications identified 1788 germline SNPs associated with CRC susceptibility (151). The authors identified 15 high quality SNPs with biomarker potential. Several SNPs have been linked to treatment response and prognosis in CRC. Polymorphisms in *MGMT* (-535G/T), *GSTP1* (Ile105Val), *MTHFR* (677C/T) and *MTHFR* (1298A/C) were associated with poor response to 5FU based treatment and longer survival in advanced CRC (152). Conversely, *CCND1* (rs9344 A/A) and *WNT5B* SNP rs2010851 were associated with shorter time to tumour recurrence in CRC (153, 154). SNPs have also been associated with *DPYD* gene regulation and fluoropyrimidine-based chemotherapy toxicity and efficacy (155). *DPYD* encodes the dihydropyrimidine dehydrogenase (DPD) enzyme which catabolises thiamine and uracil, thus a key determinant of pharmacokinetics of fluoropyrimidine-based chemotherapy agents such as 5FU or Capecitabine(156). Approximately 5% of patients treated with latter agents may experience the effects DPYD deficiency and related severe toxicity (157).

1.4.2.11 Long non-coding RNA and micro RNA

Several micro RNA (miRNA) and long non-coding RNA (lncRNA) have been linked to the pathogenesis of CRC (158, 159). The clinicopathological and prognostic significance of miRNA and lncRNA are unclear. However, Carter et al. demonstrated through a systematic review and meta-analysis that miRNA could distinguish CRC patients from healthy controls (160). Furthermore, the authors concluded that

specific miRNA could be used as a non-invasive biomarker to diagnose CRC in the future.

1.4.3 Molecular classification of CRC

The consortium for CRC subtyping classified CRC into four distinct molecular phenotypes based on RNA expression. The consensus molecular subtype (CMS) classification comprises of four categories with several distinct genetic and epigenetic characteristics (Table 1-1). Tumours within each category may also differ in their microenvironment, transcriptomic pathways and clinicopathological features (161).

Table 1-1: Consensus molecular subtype classification of CRC.

CMS	Characteristics	% CRC
CMS-1	Microsatellite instability: Unstable microsatellite regions, are hypermutated and have strong immune response	14%
CMS-2	Canonical: Wnt and MYC signalling epithelial tumours	37%
CMS-3	Metabolic: Epithelial tumour, metabolic dysfunction	13%
CMS-4	Mesenchymal: Stromal invasion with angiogenesis, growth factor-b activation	23%
Mixed	Mixture of the above – due to tumour heterogeneity	13%

The CRC intrinsic subtypes (CRIS) classification system is a novel molecular classifier. Its five subgroups focus on CRC cell intrinsic pathways and minimises confounders related to heterogeneity associated with the tumour microenvironment (Table 1-2). The different subgroups also demonstrated varying response to

chemotherapy agents such as cetuximab (162). More research is needed to determine the frequency of each subgroup within the CRC patient population and their prognosis.

Table 1-2: Colorectal cancer intrinsic subtypes classification system.

CRIS	Characteristics
CRIS-A	KRAS mutant, glycolytic, hypoxic tumours
CRIS-B	TGF β and epithelial mesenchymal transition
CRIS-C	Elevated EGFR signalling (ERBB1 /3) and moderate Wnt
CRIS-D	High Wnt signalling, positive LGR5 signature, IGF amplification
CRIS-E	Paneth cell like phenotype, TP53 mutation, high Wnt signalling

1.4.4 Intracellular pathways implicated in CRC pathogenesis

One or more intracellular pathways are dysregulated in colorectal tumours (Figure 1-4). These pathway disruptions are linked to the genetic defects described in section 1.4.2.

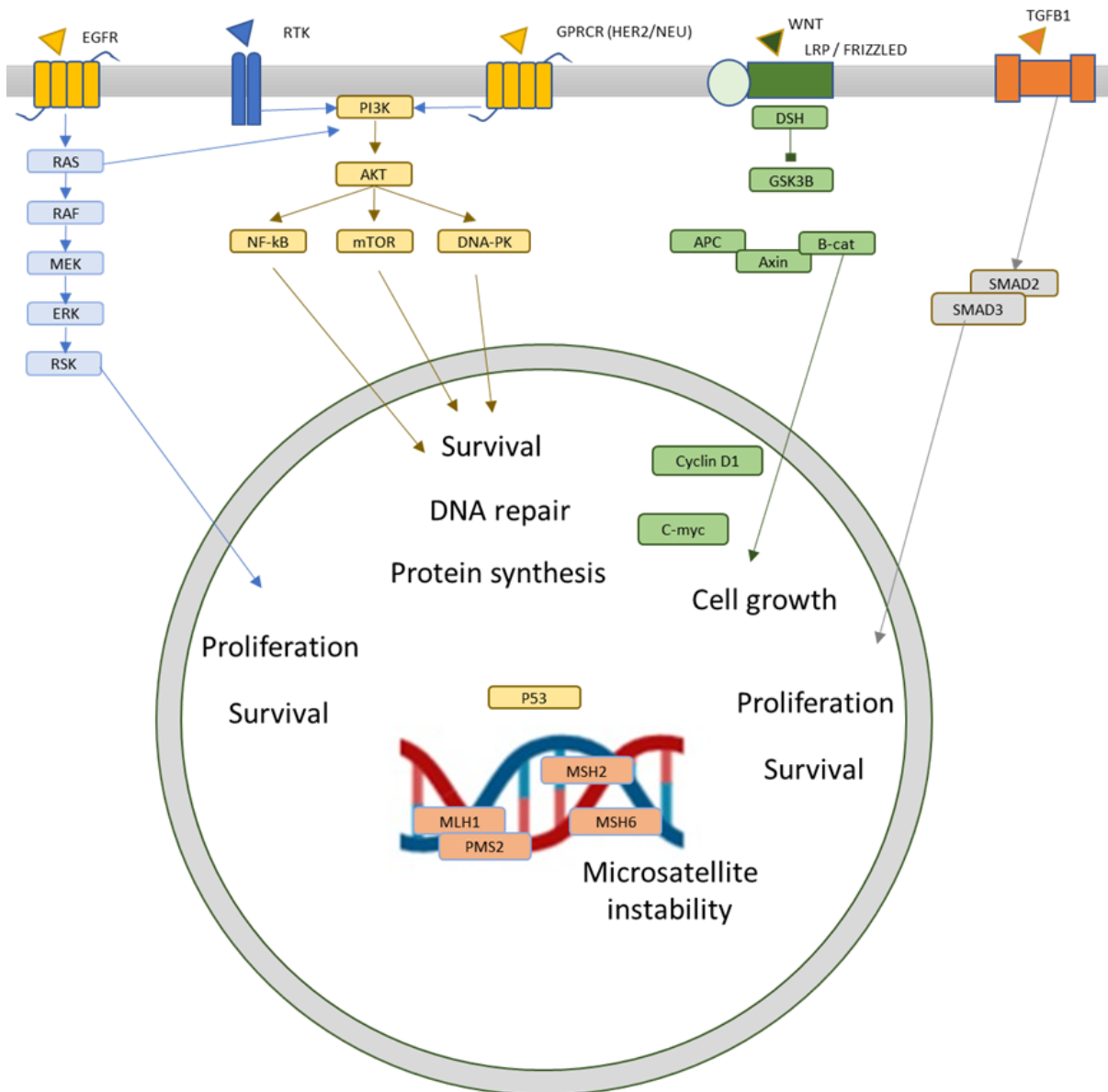


Figure 1-4: Intracellular pathways dysregulated in CRC pathogenesis (159)
 A diagram depicting the most common intracellular pathways implicated in the pathogenesis of CRC. From left to right the MAP kinase pathway, PI3K/AKT/mTOR pathway, Wnt signalling pathway and TGFβ/SMAD4 pathway and their downstream effects have been summarised. The P53 and dMMR systems are also implicated in CRC pathogenesis.

1.4.4.1 *Wnt signalling pathway*

Wnt activates transmembrane receptors of the frizzled family which are coupled with a low density lipoprotein related receptor (LRP) (163). In the presence of Wnt, β -catenin degradation is inhibited by Dishevelled (DSH) by inhibiting glycogen synthase kinase 3 β (GSK3 β) (Figure 1-4). β -catenin promotes transcription of Wnt target genes responsible for cell growth, differentiation and migration (164). APC phosphorylates β -catenin and inhibits downstream β -catenin mediated transcription and is a negative regulator of the Wnt signalling pathway. Dysregulation of this pathway leading to an accumulation of β -catenin is one of the initial steps in the pathogenesis of colorectal adenomas and consequently carcinoma (Figure 1-3). *APC* mutations are frequently responsible for the disruption of this pathway (93, 94). Mutations in genes encoding other proteins along this pathway are rare in CRC. However, altered expression of Wnt ligands, Frizzled receptors may contribute to the pathogenesis and invasiveness (165). Pathway activation has also been associated with chemoradiotherapy resistance in breast cancer and neuroblastoma (163, 166). Several Wnt/ β -catenin pathway blocking drugs have been tested *in vitro* as cancer treatment with varying efficacy (71).

1.4.4.2 *MAPK pathway*

This pathway is activated following the activation of RAS by EGFR. It includes several intracellular proteins which are sequentially activated as well as numerous downstream effectors. The EGFR / RAS / RAF / MEK / MAPK / ERK pathway contains several proteins which are encoded by genes which are often mutated early

in the pathogenesis of CRC (167). These include *KRAS* which can be mutated in over a third to two fifths of CRC (115); *BRAF (V600E)* which is associated with MSI and CIMP (168). Activated RAS and RAF can also activate the PI3K/AKT/mTOR pathway (169). Downstream MEK and MAPK activation leads to the transcription of genes responsible for cell proliferation and prevents apoptosis (170). ERK activation promotes mitosis as well as cell differentiation (171). Several pathway inhibitors such as BRAF inhibitors, MEK inhibitors and EGFR inhibitors have been explored as novel therapeutic targets in CRC treatment (172).

1.4.4.3 *PI3K/AKT/mTOR pathway*

This pathway is activated in response to stressful stimuli and growth factors through the activation of Class1 transmembrane PI3K proteins (173, 174). Pathway activation leads to the activation of AKT, mTORC1 and mTORC2 by phosphorylation leading to the activation downstream effectors resulting in cell growth, survival, anti-apoptosis, proliferation and migration (175). The PI3K/AKT/mTOR pathway is often dysregulated in malignancy (176). Mutations within the *PIK3CA* (found in 15%-30% of CRC) and *AKTE17K* (found in 6% of CRC) genes, which encode the p110 α catalytic subunit of PI3K and AKT respectively, are frequently detected in CRC (177). Mutations in *PIK3CB*, *PIK3R1*, *AKT2*, *PDK1* and *PTEN* are rare in CRC (130). Whilst mutations of *PTEN* are uncommon, epigenetic silencing and loss of heterozygosity has been detected in 19% of MSI-H CRC and 23-35% of sporadic CRC (178). *KRAS* mutations and *EGFR* overexpression which are also frequently detected in CRC leads to the indirect activation of this pathway through crosstalk with the MAPK pathway (169). Research has also demonstrated that the activation of this pathway is crucial in chemoradiotherapy resistance amongst various cancers (173, 179-182).

Therefore, the benefits of targeted inhibition of this pathways components in the treatment of various cancers has been extensively researched (183, 184).

1.4.4.4 TGF β and SMAD pathway

The TGF β pathway is activated by ligands binding to transmembrane TGF β receptors. This leads to downstream activation of transcription factors SMAD2, SMAD3 and SMAD4. The pathway also has a role in controlling cell proliferation, apoptosis, differentiation and migration (185). The pathway has been shown to be dysregulated in various cancers including CRC, TGF β signalling also plays a significant role in regulating the cellular microenvironment and stromal cells in CRC (186). Furthermore, there is crosstalk between this pathway and the PI3K/AKT/mTOR pathway. Several drugs targeting this pathway components in the treatment of CRC is currently underway (187, 188).

1.4.5 The tumour microenvironment in CRC

1.4.5.1 Immunoscore

The tumour-immune system interaction in CRC has been explored in depth. This has led to the development of the Immunoscore which is a histopathological scoring system derived by measuring the CD3+ and CD8 T-cell densities within a resected tumour specimen. Pagès et al. demonstrated a significant lower risk of recurrence of CRC in patients with a high immunoscore compared to a low immunoscore (HR 0.2 [95% CI 0.10–0.38]; $p < 0.0001$) (189). The score was an independent and more reliable prognosticator over clinicopathological staging, tumour differentiation, MSI and lymphovascular invasion (190).

1.4.5.2 *Cancer associated fibroblasts and tumour associated macrophages*

Various other cell types are also found in the tumour microenvironment. Cancer associated fibroblasts (Cafs) are found in large numbers in the tumour microenvironment and secrete cytokines (e.g. IL-6) and play a vital role in tumour growth, migration and angiogenesis (191). Cafs have also been associated with poor prognosis (192) and metastasis (193) in CRC. Cafs closely interact with tumour associated macrophages (TAMS) which are another type of stromal cell found in abundance in colorectal tumours. TAMS in combination with cafs have the ability to regulate natural killer cells in colorectal tumours thus masking the tumour cells from the immune system (191). Most common phenotype of TAM detected in tumours is the M2 type. TAMs not only promote tumour migration, angiogenesis but play a crucial role in regulating the antitumour immune response (194). TAM derived cytokines also demonstrate chemoresistance *in vitro* (195).

1.4.5.3 *The microbiome*

Variations within the gut microbiome has been observed in patients with CRC (196). Several organism such as *Fusobacterium*, *Porphyromanas*, *Peptostreptococcus* and *Clostridium* species are detected in high numbers within the microbiome of CRC patients compared to those that do not have CRC (196, 197). Whilst there is an association between the microbiome and CRC pathogenesis the exact aetiology is unknown. Studies have also demonstrated an association between the microbiome variations and therapy response in CRC patients (198). Whilst, NGS has revolutionised and changed the pace of research into microbiomes of various tissues

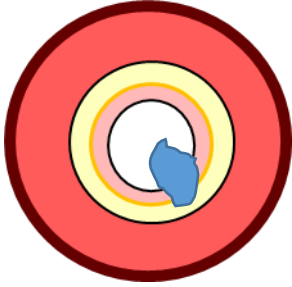

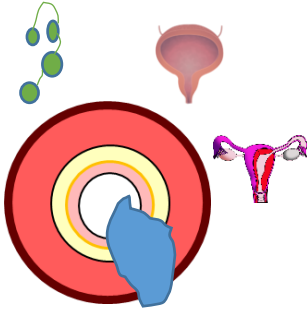
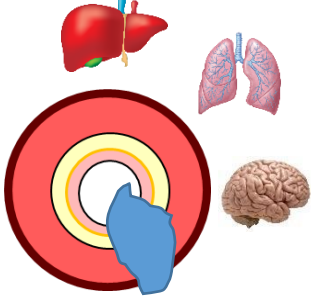
and their association with pathology, much remains unknown regarding the significance of the microbiome in the pathophysiology of CRC and impact on treatment.

1.5 Investigating and staging colorectal cancer

The gold standard investigation for CRC is direct visualisation through lower gastrointestinal tract endoscopy (optical colonoscopy or flexible sigmoidoscopy) (199). Biopsies are obtained through endoscopy for histological confirmation of diagnosis, tumour subtyping and risk stratification. The CRC miss rate for optical colonoscopy is around 1.5%-3.5% (200, 201). Alternative investigations include computed tomographic virtual colonoscopy (CTVC) or standard computed tomographic (CT) scan with intravenous contrast (199, 202). Both these imaging modalities carry a CRC miss rate of approximately 7% and 9%, respectively (201).. Faecal occult blood testing was routinely being used to screen the asymptomatic population for CRC in the UK (203). However, faecal immunochemical testing has emerged as a superior diagnostic and potential screening tool in asymptomatic individuals, with greater sensitivity (98%-100% compared to 92%-94% in faecal occult blood tests) and specificity of 95.3% (204). Two yearly faecal immunochemical testing is used to screen the general population for CRC from the age of 60-74 in England, Wales and Northern Ireland, and between 50-74 in Scotland (203, 205). Additional one-off screening with flexible sigmoidoscopy is being rolled out in the UK and is offered at the age of 56 to patients in England (205). Management, as well as prognosis, depends on the stage of the tumour (Table 1-3). The TNM (tumour-node-

metastasis) and Dukes classification systems are widely used in the staging of CRC (206).

Table 1-3: TNM version 8 and Dukes staging of colorectal adenocarcinoma

Dukes A	Dukes B	Dukes C	Dukes D
			
Limited to submucosa	Transmural extension	Lymph node / adjacent organ involvement	Distant metastases
A – T1 N0 M0	B1 – T2 N0 M0 Limited to muscularis propria	C1 – T2 with enlarged regional lymph nodes	D – Any T stage with distant metastasis
	B2 – T3 N0 M0 Transmural extension	C2 – T3 with enlarged distant lymph nodes or T4 – Invasion of adjacent organs	
Stage-I	Stage-II	Stage-III	Stage-IV

Over half of patients with CRC present with Stage-II/III disease and approximately 25% still present with metastatic disease (1). Staging of the disease is performed using computed tomography (CT) cross sectional imaging of the thorax, abdomen and pelvis (207). Local staging is further performed in rectal cancer using magnetic resonance imaging (MRI) scan of the pelvis or less frequently using endorectal

ultrasound scan (208, 209). A multi-disciplinary team approach is recommended in the management of CRC, which has been shown to improve prognosis (208, 210).

1.6 Rectal cancer versus colon cancer

Whilst there are numerous similarities between colon cancer and rectal cancer as far as tumour biology, response to treatment and prognosis are concerned, emerging data from clinical and biological research identified the need for these two conditions to be considered as two distinct disease entities (211, 212). Whilst the risk factors, cellular origin, pathogenesis and type of genetic mutations are similar across colonic and rectal tumours, differences have been observed in the frequency of certain mutations, the microenvironment and the microbiomes of tumours that originate in the rectum. For example, rectal tumours comprise of predominantly CMS-2 tumours and MSI-H is uncommon (161, 213). Nevertheless, insufficient evidence is available to assess the significance of these variations on clinicopathological outcomes between colon cancer and rectal cancer patients.

The management of rectal cancer also varies significantly to colon cancer (214). The various stages of rectal cancer are also treated very differently with multiple different treatment modalities being considered (see 1.7). However, many of these differences are owing to the anatomical location of rectal cancer as opposed to significant biological differences between colonic and rectal tumours. Early stage, small rectal cancer can be treated with localised resection. Locally advanced disease requires NCRT followed by surgery. Whilst, neoadjuvant chemotherapy is being trialled in locally advanced colon cancer, radiotherapy is not used in the treatment of

colon cancer due to associated toxicity to surrounding organs. The use of radiotherapy in the treatment of rectal cancer introduces a new dimension to treatment challenges, related to radiotherapy resistance. The prognosis between colon cancer and rectal cancer patients are similar for a given tumour stage. However, sub-groups of rectal cancer patients who completely respond to neoadjuvant therapy benefit from a better prognosis. Given colon cancers vastly outnumber rectal cancer cases more research has been conducted in colon cancer and using colonic tumours or colon cancer cell lines or three-dimensional (3D) tissue cultures derived from colon cancer. Therefore, most clinical and laboratory research continues to class colon cancer and rectal cancer as one disease entity (i.e., CRC).

1.7 Treatment of non-metastatic colorectal cancer

Non-metastatic primary adenocarcinoma of the colon is managed with surgery to resect the anatomical segment of the colon containing the tumour. Adjuvant chemotherapy is administered to patients with a postoperative staging of Dukes C or higher, or in those with a high-risk Dukes A or B tumour. High-risk groups include those patients with threatened resection margin (R1 or R2), extramural vascular invasion and poorly differentiated tumours. Preliminary data from clinical trials show that neoadjuvant chemotherapy may also play a role in the treatment of locally advanced colon cancer (215). Upper rectal cancer of any stage, located at or above the peritoneal reflection and localised, early stage rectal cancer elsewhere in the rectum, is treated in the same way as colon cancer. This involves surgery followed by adjuvant therapy based on post-operative staging and histopathological risk stratification. Smaller malignant rectal lesions (pT1 or pT2) which are close to the

anal verge or cancers occurring within polyps can be treated with local resection techniques (e.g. Trans anal endoscopic microsurgery or endoscopic mucosal resection) (208). Some CRC patients may undergo emergency surgery to remove the tumour if presenting with an obstruction or perforation. Adjuvant chemotherapy will be considered based on subsequent histology and risk stratification pending recovery from the emergency admission. Treatment of other rarer types of tumours within the colon, rectum and anal canal (e.g., neuroendocrine tumours, lymphomas) also differs considerably and will not be covered in this thesis.

1.8 Treatment of locally advanced rectal cancer

In the UK, approximately 10-15% of patients have locally advanced rectal cancer (LARC) at diagnosis (216). Approximately a third of patients in the United States of America (USA) had LARC at diagnosis (19). LARC is defined as all T3c, T3d, T4 tumours of any N stage and M0; tumours of any T stage and M0 with N1 lymph node stage or above, or tumours with mesorectal fascia involvement, or genitourinary structure involvement (seminal vesicles, uterovaginal wall or bladder) (208, 217, 218). The National Institute of Health Care Excellence (NICE) in the UK also stratifies rectal cancer as low, moderate and high risk for local recurrence using similar criteria (208, 218). Neoadjuvant treatment is offered to downstage the disease in LARC patients, which decreases the risk of local recurrence and significantly improves the rates of sphincter-sparing surgery (208, 219). The seminal German rectal cancer trial (CAO/ARO/AIO-94) demonstrated the superior efficacy of a pre-operative (neoadjuvant) long-course chemoradiotherapy over the same treatment administered post-operatively (adjuvant chemoradiotherapy) in LARC

patients (220). Consequently, NCRT followed by surgery with TME has become the widely accepted standard of treatment for patients with LARC (208, 217, 220, 221).

1.8.1 Neoadjuvant treatment in rectal cancer

The two main types of neoadjuvant treatment used in LARC include long-course NCRT and short-course preoperative radiotherapy (SCRT) (219, 222). NCRT is administered pre-operatively using intravenous 5FU (bolus regimen or continuous infusion) or regular oral Capecitabine (an orally available prodrug of 5FU); in conjunction with 45 – 50.4 Gray (Gy) radiotherapy administered in 1.8 – 2.0 Gy doses, five days a week over a five-week period (223, 224). Short course radiotherapy (SCRT) is administered in 5 Gy/day doses for 5 days (225, 226). The latter is often limited to patients who cannot tolerate chemotherapy or a longer treatment course (227). The debate on NCRT versus SCRT as the superior form of neoadjuvant treatment in LARC is ongoing (228). Therefore the decision regarding which neoadjuvant treatment option to choose for LARC patients is currently subject to multidisciplinary clinician team discretion, patient factors and patient-choice (229). Furthermore, limited current evidence being available on one treatment regimen over the other has led to significant geographical variation in choice of SCRT / NCRT with many European centres advocating SCRT with the USA, UK and Japan advocating NCRT in LARC (222, 229). The duration from neoadjuvant treatment to surgery can be short or long. Following SCRT surgery can be performed sooner after just one week (225, 230). Surgery may only be performed within 6-14 weeks after NCRT and is preceded by restaging with MRI and CT (231-234).

1.8.1.1 The mechanisms of action

Radiotherapy utilises X-Rays to cause direct and indirect cell damage. Direct effects are due to ionizing radiation energy of X-ray photons whilst indirect effects are through free radicals and oxidative stress. Both mechanisms lead to DNA base damage, single strand breaks and double strand breaks (DSB) within the nucleus of cells (235). This leads to the activation of intracellular pathways geared at DNA repair. The two main mechanisms of DNA DSB repair are homology directed repair (HDR) and non-homologous end join repair (NHEJ) (236, 237). The former uses a donor DNA template from a sister chromatid to repair the damaged DNA strand, resulting in a more accurate final repair. With NHEJ repair the two broken ends of the DNA strands are joined end-to-end resulting in deletions within the DNA sequence. Such a deletion within an exon may result in a pathological mutation. When DNA repair is impossible the cell will undergo apoptosis or autophagy (238, 239). Radiotherapy can lead to significant changes within the tumour microenvironment (240). The immune system also plays an important role in eliminating damaged or dying cells following radiotherapy through the dispersion of immune system stimulating tumour antigens (241). 5FU is an analogue of uracil which is a thymidylate synthase inhibitor. It is routinely used as a radiosensitising agent. The drug works by impairing nucleotide synthesis and consequently inhibiting DNA repair and RNA synthesis (242).

1.8.1.2 Assessment of neoadjuvant treatment response

Numerous validated scoring systems are available to histologically stratify the degree of response following neoadjuvant treatment (243). The Mandard five-tier

grading system (Tumour regression grade – TRG), the four-tier Tumour regression score (TRS) and Dworak / Rödel five-tier grading system are also widely used clinically (Table 1-4).

Table 1-4: Scoring systems used to measure tumour regression and response to NCRT in rectal cancer.

Mandard system (244)		Tumour regression score (245)		Dworak grading system (246)	
TRG - 1	Complete response	TRS -0	Complete response - no viable cancer cells	Grade -0	No response
TRG -2	Scattered isolated cells	TRS -1	Near-complete response - single cells or rare small groups of cancer cells	Grade -1	Minimal response - dominant tumour minimal fibrosis
TRG -3	More scattered isolated cells but fibrosis predominant	TRS -2	Partial response – More single cells/groups	Grade -2	Moderate response - dominant fibrosis but easy to find tumour cells/groups
TRG -4	Residual cancer outgrowing fibrosis	TRS -3	Poor or no response – No tumour regression	Grade -3	Near complete response – difficult to find tumour cells, more fibrotic tissue
TRG -5	Absence of regressive changes			Grade -4	Complete response – no tumour cells, fibrotic mass

Other scoring systems such as the Japanese Society for the Cancer of Colon and Rectum (JSCCR) system, American Joint Committee on Cancer (AJCC) system, the Becker three-tier system, the Memorial Sloan Kettering Cancer Center (MSKCC) three-tier system and the Mandard three-tier system have been used predominantly within the context of research (247). To overcome the significant variability in the reporting methodology across the different tumour response grading systems and the lack of consensus in research, the neoadjuvant rectal (NAR) score was proposed by Valentini et al. (248). It aims to serve as a standardised surrogate endpoint for rectal cancer research and is better predictor of overall survival than pCR in rectal cancer (249).

1.8.1.2.1 Complete response

Post-operative histopathological analysis of tumour specimens from post- NCRT patients reveal that approximately 10-30% have a complete pathological response (pCR); where no residual malignant cells would be seen at microscopy (250, 251). Rates of pCR up to 2-6% have been observed in patients undergoing SCRT (252). pCR is associated with significantly reduced risk of local recurrence and decreased risk of distant recurrence (metastatic disease) (253-256). The commonest cause of death from rectal cancer is from recurrent metastatic disease (257). Therefore, in patients achieving pCR there is improved overall and disease free survival (250, 258). Patients who achieve a complete response (complete clinical remission or cCR) on repeat staging imaging following NCRT, can be managed using a “watch and wait” strategy without the need for major surgery (259). Eligible patients must be appropriately counselled on the risks, benefits and alternatives to the “watch and wait” strategy.

1.8.1.2.2 Poor response (treatment resistance)

Approximately 30-40% of rectal cancer patients receiving long course NCRT are complete non-responders and have worse outcomes; the remaining partial responders receive no appreciable benefit from NCRT (260, 261). The latter groups (the non-responders and partial responders) are subjected to a prolonged course of treatment which delays their surgery but also exposes patients to potentially unfavourable side effects such as bladder and sexual dysfunction (262, 263). Hence, the need to better predict patients who are likely to respond and those who will not respond to NCRT.

1.8.1.3 Factors associated with chemoradiotherapy response

Numerous clinicopathological, radiological factors and biomarkers have been linked to chemoradiotherapy response ("response" refers to sensitivity or resistance) in LARC (264). Recent focus has been directed towards biomarkers which can predict response as well as patient outcomes following NCRT (264, 265). Biomarkers can be detected in the blood of patients (blood-based) or in tumour tissue (tissue-based). Blood-based markers may include tumour markers such as CEA and CA19-9 which have been associated with LARC response to NCRT (266-282). Various circulating-tumour DNA (ctDNA) markers might play a role in predicting NCRT response (283-285). Association between common DNA mutations and NCRT response has also been extensively researched. However, research has failed to conclusively support an association between NCRT response and mutations in *APC*, *BRAF*, *KRAS*, *p53*, *PIK3CA*, *SMAD4* and genes encoding dMMR proteins, all of which are frequently encountered in CRC (286-290). Preliminary research has demonstrated an association between several SNPs and NCRT response in LARC (264, 291-297).

Associations have also been found between hypermethylated promoter regions of genes such as *MGMT*, *TFAP2E*, *KLHL34*, *CRBP1* and *TIMP3* and NCRT response (298-303). However, there was no association between CIMP and NCRT response (304, 305). The vast majority of evidence pertaining to genomic predictors of NCRT response in LARC comes from RNA expression studies (306-312) and gene signatures (264, 313-318). The expression status of various oncoproteins (288, 319-322), the tumour microenvironment (323-325) and the microbiome (326-329) may also influence NCRT response in LARC. Chapter 3 elaborates further on the current evidence pertaining to predictors of NCRT response.

1.8.2 Advancements in rectal cancer neoadjuvant treatments

1.8.2.1 Personalised treatment

Resistance to oncological therapies is a significant challenge in treatment of cancers. The “one size fits all” approach used in the management cancer patients likely contributes to therapy resistance. Recent advances in genomics have led to a better understanding of the biological basis of treatment resistance and this has led to personalised targeted treatments in cancer patients. The use of OncotypeDX (Exact Sciences, USA), a targeted DNA panel to identify common mutation with clinical significance, used as standard of care in the treatment of breast cancer patients is an example of personalised genomic medicine being utilised in cancer treatment (330). Routine MMR status assessment through immunohistochemistry, assessing for *MLH1* promoter hypermethylation and *BRAF (V600E)* mutation status where there is loss of *MLH1*, *PMS2* expression and routine assessment of *KRAS* mutation status are steps in the right direction for personalised treatment in CRC (136).

1.8.2.2 Therapeutic targets to improve NCRT response in rectal cancer

Several factors contributing to neoadjuvant treatment resistance in rectal cancer have been identified in the literature. The majority relate to radiotherapy resistance. Resistance might be due to specific tumour genotypes and their resulting treatment resisting phenotypes. Buckley et al. suggested that the radioresistant phenotype of gastrointestinal tract cancers demonstrate the capability to evade apoptosis, repopulate through cancer stem cells, tolerate hypoxia, contain diverse subclones, enhance DNA damage response, alter metabolism, inflammation and immune invasion (331). Several biological pathways such as the PI3K/AKT/mTOR pathway, VEGF pathway, EGFR and KRAS signalling have been associated with NCRT resistance (264, 331). Since the seminal German rectal cancer trial demonstrated superior effects of 5FU as a radiosensitiser in LARC at reducing local recurrence rates, several novel therapeutic targets have been identified (Table 1-5) (220, 331). Spitzner et al. evaluated gene expression profiles of 12 colorectal cancer cell lines and identified that the Wnt and insulin signalling pathways, as well as *STAT3*, *RASSF1*, *DOK3*, and *ERBB2* as potential therapeutic targets to improve chemo radiosensitivity (332). Buckley et al. summarised the most promising targets and drugs of interest in radiosensitising gastrointestinal tract cancer (331). Whilst many of the drugs identified in their review remain in preclinical stages some have entered early clinical trials (Table 1-5).

Table 1-5: Emerging targeted therapies with the potential to improve NCRT response in rectal cancer

Class of drug	Examples	Research stage
Cellular energetics:		
Medication for diabetes	Metformin	<i>In vivo</i> xenograft Phase II clinical trial – terminated (low recruitment)
DNA repair:		
CHK1 / CHK2 inhibitors	AZD7762	<i>In vitro</i> cell lines
PARP inhibitors	Olaparib	<i>In vitro</i> cell lines
MEK1/2 Inhibitors	Trametinib	Phase II clinical trial
ATR inhibitor	VE-821	<i>In vitro</i> cell lines
ATM inhibitor	Quercetin	<i>In vivo</i> xenograft
Toporomase I inhibitors	CRLX101	Phase Ib/II clinical trial
Proteosome inhibitor	Bortezomib	Phase I clinical trial
Other	YU238259	<i>In vitro</i> cell lines
Mediating host immunity:		
CTLA4 blockade	Anti-CTLA4 antibodies	<i>In vivo</i> xenograft
PD-1 blockade	Durvalumab	Phase ii clinical trial – in progress
TGFβ R1 blockade	Galunisertib	Phase II clinical trial
Growth Signal Disruption:		
EGFR inhibitors	Nitromidazole Cetuximab Panitumumab	<i>In vitro</i> cell lines Phase I/II clinical trials
PI3K, AKT and mTOR pathway inhibitors	BI-69A11 Dactolisib PI-103 Everolimus and rapamycin	<i>In vitro</i> cell lines <i>In vivo</i> xenografts Phase II clinical trials
Targeting angiogenesis:		
VEGF signalling inhibitors	Monoclonal antibodies	<i>In vivo</i> xenograft
Disrupting telomeres:		
Telomerase inhibitors	Bipartite vector to disrupt <i>HTERT</i>	<i>In vitro</i> cell lines

Summary of results from reviews by Buckley et al. and Wanigasooriya et al. (184, 331).

1.8.2.3 *Preclinical research*

Several laboratory and clinical studies evaluating the efficacy of these targets using targeted inhibitors have also been conducted (184, 331). Traditionally, CRC cell lines have been widely used to research targeted treatments to improve NCRT response in rectal cancer (173, 333). Many *in vitro* and *in vivo* research drug assays utilising CRC cell lines and murine xenografts have been conducted, aimed at improving NCRT response in LARC with some evaluating specific pathway blocking drugs (e.g. PI3K/AKT/mTOR inhibitors) (184). However, 3D patient derived organoid (PDO) models have also recently been used for *in vitro* research evaluating radiotherapy effects on rectal cancer (334, 335). Most *in vitro* research in this field remains significantly heterogenous and is difficult to interpret and translate to the clinical setting.

1.8.2.4 *Clinical research*

There were very few clinical trials available evaluating novel radiosensitisers in LARC. MTOR inhibitors rapamycin and everolimus have been safely used in phase II clinical trials in rectal cancer patients (336, 337). However, both drugs failed to demonstrate clinically significant pCR rates in these trials. A phase II clinical trial evaluating the effects of metformin in combination with capecitabine and radiotherapy in LARC was terminated due to failure to meet endpoint and another trial is currently underway (331). EGFR inhibitors cetuximab and panitumumab have been tested in phase I/II clinical trials and failed to show significant increase in pCR rates (338-340). Drugs targeting the NF- κ B pathway have also been utilised as radiosensitisers in LARC. Examples include the proteasome inhibitor Bortezomib

and Topoisomerase I inhibitor CRLX101 have also both completed early phase clinical trial safely in humans (341, 342). A recent phase II clinical trial combining traditional NCRT with galunisertib, a TGF β receptor 1 inhibitor demonstrated pCR rates of up to 32% (343). The PRIME-RT trial is a phase II randomised trial being conducted in the UK evaluating the role of PD-1 immune checkpoint inhibitor durvalumab in radiosensitising LARC (344)

1.9 Treatment of metastatic colorectal cancer

Of the 20-25% of CRC patients who present with metastatic disease at the time of initial diagnosis (stage IV disease) (26, 27). Approximately 10% will have synchronous liver metastases (only) (345). Where the metastatic disease burden is resectable and the patient is clinically fit, neoadjuvant chemotherapy, followed by surgery to perform a non-anatomical resection of the liver or a hemi hepatectomy may be performed (346). The surgery to remove the primary colorectal tumour is performed several weeks later. Whilst the “liver-first” approach is the preferred treatment strategy for resectable, synchronous metastatic CRC, simultaneous resection of primary CRC tumour and liver metastases may also be performed (347). Rarely, CRC patients may undergo colorectal surgery first if presenting with an obstruction or perforation. Adjuvant chemotherapy may also be administered based on subsequent histology and risk stratification. In the former group of patients it recommended where possible to consider conservative management of the primary tumour initially (e.g. colonic stenting or formation of a defunctioning stoma) to still allow treatment of the liver metastasis(es) (348). The CAIRO4, a large multicentre randomized controlled trial demonstrated higher mortality amongst patients

undergoing primary tumour resection before systemic chemotherapy or treatment of liver metastases (349). Patients with LARC presenting with resectable liver metastases will be treated in a similar fashion to CRC presenting with synchronous liver metastasis(es); but a short course of radiotherapy to the rectum prior to surgery may also be considered in those who demonstrate features of locally advanced disease (214).

Infrequently, CRC patients may also present with pulmonary metastases (1.1%) (345). Where the disease is resectable a pulmonary resection is performed usually after surgery to remove the primary colorectal cancer. Approximately 3% of patients present with liver and pulmonary metastases at diagnosis (345). Most of these patients will not have curable disease, but a very small minority have resectable disease at all three sites from the outset or respond well to their palliative chemotherapy, and could therefore, be treated with a curative intent. The treatment pathway for these patients often involves neoadjuvant chemotherapy, surgery to remove liver metastases, followed by the primary colorectal tumour and finally the pulmonary metastases. The patients will then go on to receive further adjuvant chemotherapy. Chemotherapy regimens used include FOLFOX (5FU and oxaliplatin) and FOLFIRI (5FU, oxaliplatin and irinotecan), as well as monoclonal antibody therapies such as cetuximab and panitumumab (latter two anti-EGFR) and bevacizumab (anti-VEGF), (350).

Approximately 5% of CRC patients may present with peritoneal metastasis (345). In a highly selected cohort of patients within this group, surgery to remove the primary

tumour, resectable liver metastases may be performed with cytoreductive surgery and heated intraperitoneal chemotherapy (351). This high risk surgery is reserved for patients who are young and clinically fit. Unfortunately, a vast majority of patients who present with metastatic CRC do not have curable disease. These also include a very small group of patients presenting with cerebral metastases (345). These patients will be managed with a palliative approach with palliative chemotherapy, symptom control interventions – e.g. palliative surgery, colonic stenting (352). Radio frequency ablation of liver or pulmonary metastases might also be considered (353, 354). Where the disease has significantly advanced, or the patient lacks fitness for palliative oncological or surgical treatment, a best patient supportive treatment approach which focuses on patient symptom control and wellbeing is utilised (355).

1.10 Treatment of recurrent colorectal cancer

CRC recurrence may be a primary recurrence at the site where the tumour was previously resected in approximately 21% of cases or as a metachronous tumour elsewhere in the lower gastrointestinal tract (356). Where the recurrence is a primary colonic recurrence and the disease is resectable, treatment will involve surgery and adjuvant chemotherapy if indicated. Recurrent rectal cancer localised to the rectum will be treated in the same way as a first presentation of rectal cancer. However, radiotherapy will only be administered to treatment naïve patients. Locally advanced pelvic recurrence of rectal cancer (i.e. a regional recurrence) is difficult to treat and may require neoadjuvant therapy and pelvic exenteration surgery, which is associated with significant morbidity (357). CRC patients may also present with a recurrence as metastatic disease either in the liver (33%), lungs (22%), other intra-

abdominal sites (18%), retroperitoneal (10%) and peripheral lymph nodes (4%) (356). Where the disease is amenable to resection, their treatment will include surgery followed by adjuvant chemotherapy (26). Where the disease is not resectable either due to disease burden, anatomical location or poor patient fitness, this will result in palliative treatment strategies.

1.11 The prognosis

The overall five and ten-year life expectancy of patients with CRC in the UK is 59%, 56% for males, 57% for females respectively (358). Several patient-related and tumour-related (i.e., clinicopathological factors) as well as biological prognostic factors of CRC exist. A key determinant of survival in CRC includes tumour stage at presentation, presence of lymph node involvement or metastases (359).

Presentation with bowel obstruction or tumour perforation are associated with lower overall survival in CRC patients (360). Poorly differentiated tumours, lymphovascular invasion, perineural invasion and threatened resection margins are also associated with poor outcomes (359). Large scale population studies have shown that there is no significant difference in overall survival between colonic and rectal cancer patients at any given tumour stage following treatment, except amongst the small group of LARC patients who demonstrate pCR following NCRT (361).

1.12 Patient derived organoid models in cancer research

Organoid models have been derived from a range of different biological tissues in the last decade since Sato and Cleavers et al. first demonstrated the *in vitro* expansion of intestinal epithelial cells as 3D organoid cultures through the regulation of Wnt and LGR5 signalling (362). Organoid models have been derived using healthy as well as pathological tissue from the gastrointestinal tract, liver, lung, prostate, kidneys and brain tissue from humans and animals (363). Organoids maintain their cellular heterogeneity and genetic stability despite multiple passages rendering them a powerful, highly adaptable and flexible tool in cancer research (364). Recent research has focused on the use of PDO models for cancer research (349, 358). Within the context of CRC several studies have emerged utilising PDO models to evaluate pathogenesis and treatment response. Vlachogiannis et al. demonstrated that *in vitro* PDOs accurately recapitulated patient response to treatment using PDO models derived from CRC liver metastases. The authors reported an overall sensitivity of 100%, specificity of 93%, positive and negative predictive values of 88% and 100% for PDOs forecasting patient response to chemotherapy (365). Ganesh et al. demonstrated that PDO models derived from pre-treatment rectal cancer models can be grafted to mice, generating patient derived xenograft (PDX) models (334). The authors derived over 60 PDO models *in vitro* and dozens of PDX models to successfully test NCRT response *ex vivo*. Yao et al. observed a broad range of intrinsic PDO responses to conventional chemoradiation (335). Research utilising PDO models co-cultured with immune system cells have also been conducted in recent years to study the

microenvironment effects on tumour progression and treatment response.

Schnalzger et al. co-cultured natural killer cells with CRC organoids (366). Dijkstra et al. successfully co-cultured T-cells with CRC organoids (367). Furthermore, genome editing of intestinal organoids with CRISP-CAS9 technology has also been successfully performed (368). Functional validation of driver genes of CRC has also been possible using gene editing of CRC organoids (369).

1.13 Aims and objectives

The aims of this research included the identification of genomic markers and intracellular pathways of significance in neoadjuvant radiotherapy response in LARC from formalin fixed and paraffin embedded (FFPE) tissue from pre-treatment biopsies and post resection tumour specimens. This research aimed to establish an *in vitro* experimental model to determine radiotherapy response and resistance of PDO cultures. DNA and RNA extracts pre and post radiotherapy treatment will be used to evaluate differences in baseline as well as post-treatment variation in gene expression. The research aimed to generate hypotheses relating to biological pathways of interest in radiotherapy response through gene expression analyses. The research aimed to assess the role of PI3K/AKT/mTOR pathway dual inhibition in radiosensitisation of CRC cell lines and PDOs *in vitro*.

1.14 Hypotheses

1. Differential gene expression and differentially expressed pathways can be detected between radioresistant versus radiosensitive archived FFPE samples and PDO samples pre-irradiation.
2. The PI3K/AKT/mTOR pathway genes are significantly differentially expressed in pre-operative tumour biopsies in completely responsive versus completely non-responsive LARC patients to NCRT.
3. Primary CRC derived PDO models can be used to simulate radiotherapy response *in vitro*.
4. Significantly differentially expressed genes of the PI3K/AKT/mTOR pathway can be identified between the radiotherapy responsive versus non-responsive PDO lines.
5. The use of dual PI3K and mTOR inhibitors led to PI3K/AKT/mTOR pathway inhibition by inhibiting AKT phosphorylation.
6. Targeted dual PI3K and mTOR inhibitors radiosensitise CRC cell line and PDO lines *in vitro*.

Chapter 2: Materials and Methods

2.1 Ethical approval

Ethical approval for the procurement of all human biomaterials (including fresh tissue, blood or archived tissue), as well as anonymised clinical data required for this project was obtained from consenting patients, under the project approval code 17-287 from the Human Biomaterials Resource Centre (HBRC), Birmingham (Biobank); which has ethical approval from North West - Haydock Research Ethics Committee (Reference: 15/NW/0079).

2.2 Patient recruitment

2.2.1 *Retrospective samples*

A retrospective cohort of locally advanced rectal cancer (LARC) who underwent neoadjuvant chemoradiotherapy (NCRT) was identified using a prospectively maintained radiotherapy database. Patients with pre-NCRT biopsy and post-NCRT formalin-fixed paraffin-embedded (FFPE) blocks were identified. Tumour only containing blocks as specified by the reporting pathologist were selected.

Approximately 3-6 blocks per patient were selected. 4 x 8 μ m scrolls were obtained per block from the HBRC.

2.2.2 *Prospective samples*

Fresh tissue was sampled for *in vitro* PDO models from patients undergoing surgery for colonic resection for colorectal adenocarcinoma. Patients were recruited prospectively between November 2017 and October 2019 at a UK tertiary centre hospital. The patients were identified from operating theatre lists. Patients consented under the HBRC ethics using HBRC and hospital approved consent forms (Appendix A). Fresh normal and paired colorectal tumour tissue was obtained from the resection specimens, sampled by a pathologist. Samples were transferred to media containing Dulbecco's Modified Eagle's Medium (DMEM, Gibco, USA) or Roswell Park Memorial Institute (RPMI) 1640 Medium (Gibco, USA). The samples were retrieved, catalogued and anonymised by the local Biobank team. These samples were subsequently received in our laboratory on the same day as the patient's surgery and immediately stored at 4°C.

2.3 Cell line methodology

2.3.1 *Cell culture and passage*

HCT116 *KRAS* +/- (#HD 104-008, Horizon Discovery, UK) CRC cell line was used in these experiments. Cells were cultured in T75 flasks (Corning, USA) in McCoy's 5a Medium (Gibco, USA) with 10% fetal bovine serum (FBS, Gibco, USA), and 100 units/ml penicillin and 100 µg/ml streptomycin (Gibco, USA), which from this point onwards will be referred to as HCT116 media within this thesis. Cells were passaged when they reached approximately 70% confluence. The cell passage protocol was as follows. The media was removed with a pipette from the flask and 7-10ml Phosphate Buffered Saline (PBS) was added to the flask to gently wash away the

media. 2mls of pre-warmed TrypLE™ Express (Gibco, USA) was added to the flask containing the cells and incubated for 5 minutes at 37°C for cell detachment.

Subsequently, the TrypLE™ Express was inactivated by adding 6-8mls of HCT116 media. The cells were centrifuged at 200 x g, for 5 minutes at room temperature. The supernatant was discarded without disturbing the cell pellet. The pellet was dissolved in 1-2ml of HCT116 media. The cells were plated in the required dilution in a new T75 flask. The flask was topped up to 15ml of media and incubated at 37°C, 5% CO₂ in a New Brunswick Galaxy 170 (Eppendorf, Germany) incubator.

2.3.2 Cell line experiments

2.3.2.1 Cell retrieval for experiments and cell counting

HCT116 cells were retrieved from T75 flasks when they were at 70-80% confluence. Media was removed and a gentle wash performed with 7-10ml PBS and removed. This was immediately followed with 2-3ml TrypLE™ Express treatment at 37°C for 5 minutes for cell detachment. Subsequently, 6-8ml of PBS was added to flask to inactivate the TrypLE. The cells in solution were aspirated and transferred to a 15ml falcon tube and centrifuged for 5 minutes, 200 x g at room temperature. The supernatant was discarded without disturbing the pellet. The pellet was dissolved in 5ml of HCT116 media and dissolved thoroughly and proceeded to cell counting. Ten microlitres of the cells in solution were added to 10µl of Trypan Blue Solution (Sigma-Aldrich, USA) in an Eppendorf tube. After mixing several times with a pipette, 10µl was placed into each chamber of a transparent cell counting slide (Bio-Rad, USA). A TC20™ automated cell counter (Bio-Rad, USA) was used, set at default settings (auto-gate) to obtain a live cell count from each chamber of the slide. The

average of the two readings was considered the final cell count in 1ml. This was multiplied by 5ml (volume of media the cell pellet was dissolved in) to estimate the cell count in the original solution.

2.3.2.2 *HCT116 - drug +/- radiotherapy screens*

2.3.2.2.1 Stage 1: Determining optimum HCT116 seeding density

Different cell densities ranging from 500, 1000, 1500 and 2000 cells per well (cell/well) were chosen for this experiment. Cell counting was performed as described in section 2.3.2.1. Cell dilution was performed by initially obtaining a total cell count in each volume from cell extracted from culture plate. The volume of the latter solution required to obtain the total specific cell count for the experiment wells (allowing for at least 10 spare wells) was calculated and diluted in the total volume of media required. Four replicates were plated for each one of the former cell counts, with the cells contained in 100 μ l of HCT116 media per well, in a 96-well flat clear bottom sterile microplate (Corning, USA). An additional 100 μ l of HCT116 media was added to each experimental well resulting in a final volume of 200 μ l per well. All remaining empty wells on the plate were filled with 200 μ l PBS to reduce evaporation losses. Plates were incubated at 37°C, 5% CO₂ in the incubator. In total three such plates were seeded with cells to serve as the three experiment conditions: 1 Gray (Gy) for 5 days, 5 Gy for 5 days and control plate (Figure 2-1). Radiotherapy was commenced the day after cell plating and was administered for five days using a CellRad (Faxitron, USA) irradiator (129.8keV, 5mA, 0.625 Gy/min). On the sixth day the cell viability was assessed as described below (see 2.3.2.2.2).

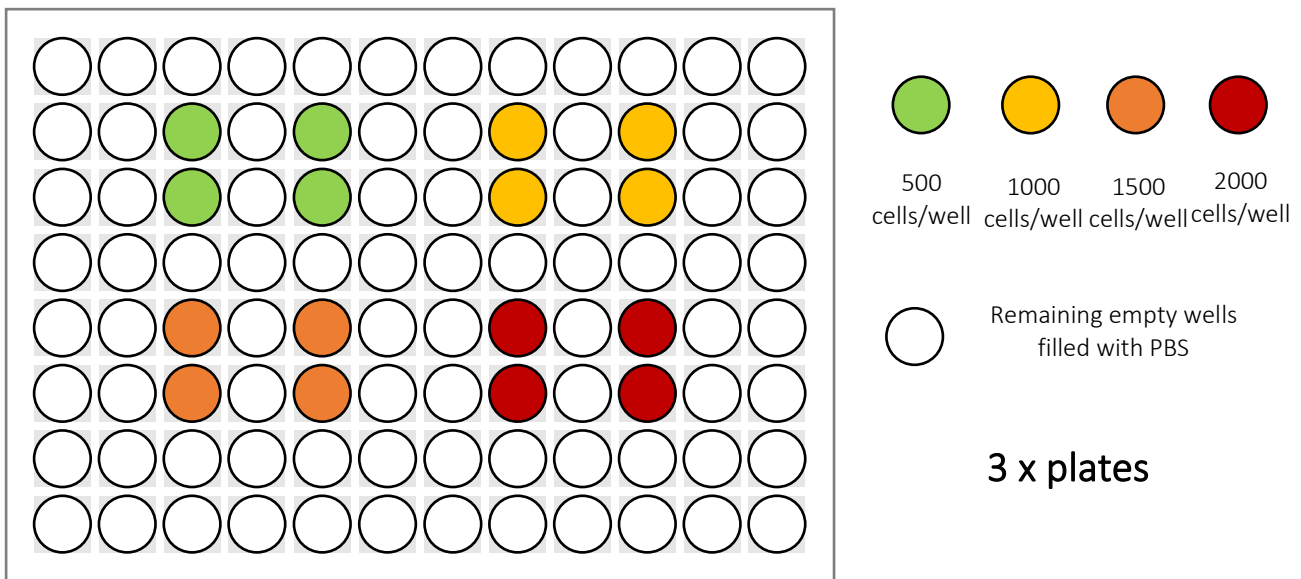


Figure 2-1: The 96-well plate configuration used for HCT116 seeding density experiments

The shaded regions represent the experiment wells. The different colours represent the different cell counts.

2.3.2.2.2 Stage 2: Assessing cell viability at experiment endpoint

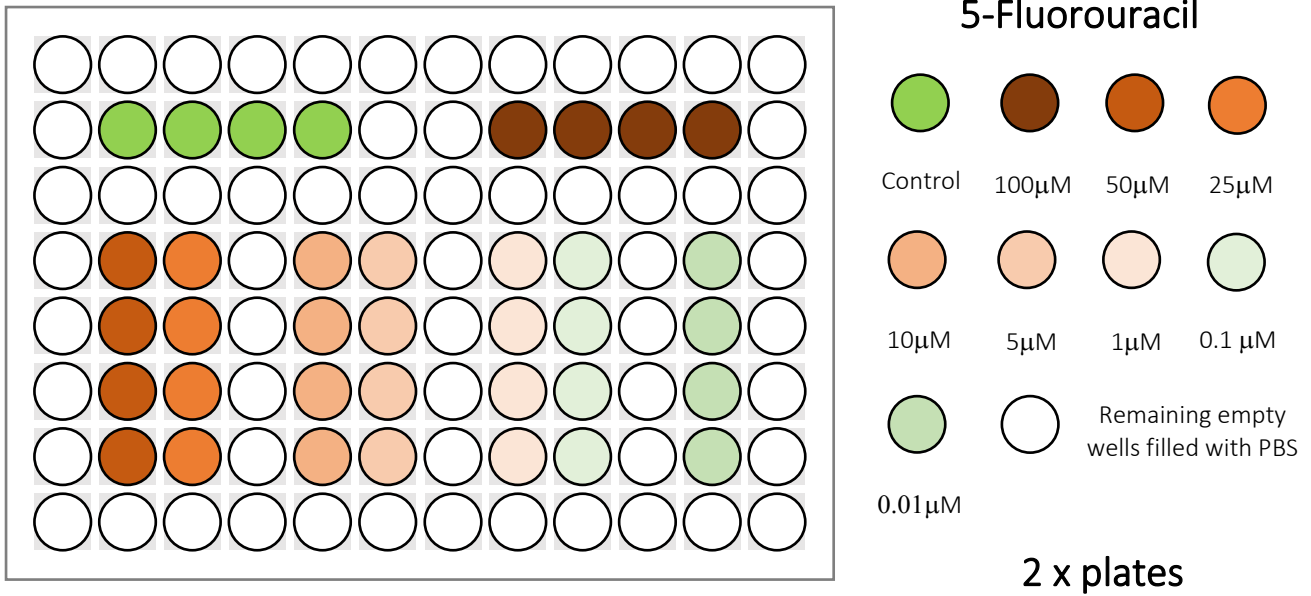
Cell viability assessment through chemiluminescence was chosen as the objective outcome measure at the end of chemoradiotherapy experiments instead of clonogenic assays. The former was compatible with organoids and cell lines. It was cheap and generated reliable, reproducible and consistent results across multiple repeat experiments. A total of 100µl of media was removed from each experiment well and 100µl of CellTiter-Glo® 2.0 Assay (Promega, USA) thawed to room temperature was added to each well. The assay was light sensitive. Therefore, the plate was covered in aluminium foil to prevent direct exposure to light. The cells were exposed to this cyto-toxic endpoint assay for 30 minutes. During this time, each plate was also placed on an orbital shaker for 5 minutes, set to the lowest speed.

Subsequently, the cell viability was assessed using the EnSpire® luminescence plate reader (Perkin Elmer Life Science, USA). Data were collated and normalised relative to the average of endpoint viability of untreated control replicates from each experiment using Excel (Microsoft, USA), and were analysed using Prism V8 (GraphPad, USA). Dose-response graphs were generated on Prism V8 using the log (inhibitor) vs. response equation and half maximal inhibitory concentrations (IC₅₀) with 95% confidence interval (CI) were determined using nonlinear regression. Welch's two sample t-tests were performed using Excel to assess significance in efficacy of drug treatment with or without radiotherapy on the cell line.

2.3.2.2.3 Stage 3: Plating cells for experiment

Based on the results from the experiment above a cell count of 1000 cells/well was the optimum seeding density for this experiment. HCT116 was treated with radiotherapy alone, with 5FU (PanReac AppliChem, USA), GDC-0980 (apitolisib, Aduro Bioscience, USA) and BEZ235 (dactolisib, Selleckchem, USA) alone or latter drugs in combination with radiotherapy during this stage of the experiment. The experiment drug concentration range for 5FU was 0.1 µM to 100 µM (Table 2-3), whilst the concentration range for apitolisib and dactolisib was 0.001 µM to 5 mM (Table 2-4 and Table 2-5). These concentrations were selected based on preliminary experiments conducted within our laboratory and taking into consideration previously published *in vitro* studies which utilised these drugs. Cells were retrieved from culture flasks and cell counting was performed (see section 2.3.2.1). Cells were plated 1000 cells/well across six, 96-well flat clear bottom sterile microplates as illustrated in Figure 2-2. Four replicates were plated for each drug concentration as well as the control. All remaining empty wells on the plate were filled with 200 µl PBS

to minimise evaporation losses. Plates were incubated at 37°C, 5% CO₂ in an incubator.



All controls and experiment conditions were in HCT-116 media with a final DMSO concentration of 0.1%

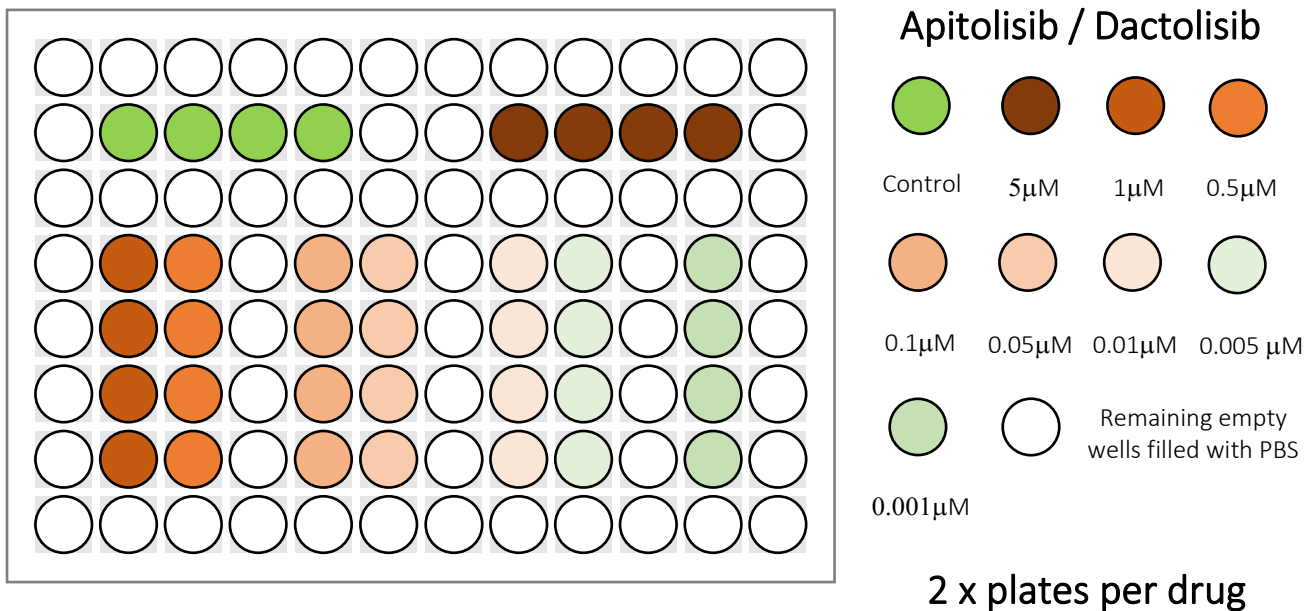


Figure 2-2: The 96-well plate configuration used for HCT116 with drug(s) and radiotherapy experiments

The coloured circles represent the experiment wells of the 96-well plate. The different colours represent the different doses.

2.3.2.2.4 Stage 4: Preparing the drugs

The three drugs were dissolved in 100% dimethyl sulfoxide (DMSO, Cell Signalling Technology, USA) (Table 2-1).

Table 2-1: Drug preparation – Initial drug stock dissolved in 100% DMSO

	5FU	Apitolisib	Dactolisib
Mass	14mg	6.5mg	5.5mg
Molar mass	130.077Da	498.6Da	469.548Da
Volume	1ml	2ml	2ml
Molarity of initial stock	107.63mM	6.52mM	5.86mM

Further dilutions in 100% DMSO were performed to obtain a range of stock concentrations (Table 2-2). From these stock concentrations the desired drug concentrations were prepared at a final 0.2% DMSO concentration in HCT116 media (Table 2-3, Table 2-4 and Table 2-5). The drugs were prepared at twice the final desired experiment concentration (e.g., for a final concentration of 100 μ M in HCT116 media with 0.1% DMSO a preparation was made for 200 μ M in HCT116 media with 0.2% DMSO). A final DMSO concentration of 0.1% was deemed safe and inert for live cells, in keeping with previously published research using DMSO as a vehicle for drug delivery *in vitro*.

Table 2-2: Drug preparation - diluted stocks of the drugs in 100% DMSO

	10,000μM	1,000μM	100μM	10μM	1μM
<u>5FU</u>					
Stock taken from	Initial stock	Initial stock	10,000 μ M	1,000 μ M	Not
Volume of above stock	92.91 μ l	9.29 μ l	100 μ l	100 μ l	required
Volume of DMSO	907.09 μ l	990.71 μ l	900 μ l	900 μ l	
<u>Apitolisib</u>					
Stock taken from	Not possible	Initial stock	1,000 μ M	100 μ M	10 μ M
Volume of above stock		153.42 μ l	100 μ l	100 μ l	100 μ l
Volume of DMSO		846.58 μ l	900 μ l	900 μ l	900 μ l
<u>Dactolisib</u>					
Stock taken from	Not possible	Initial stock	1,000 μ M	100 μ M	10 μ M
Volume of above stock		170.74 μ l	100 μ l	100 μ l	100 μ l
Volume of DMSO		829.26 μ l	900 μ l	900 μ l	900 μ l

Table 2-3: Drug preparation - 5FU dilutions

	Concentration (μM) or volume (μl)								
Desired concentration (X)	Control	100 μM	50 μM	25 μM	10 μM	5 μM	1 μM	0.5 μM	0.1 μM
Prepared concentration (2X)	Control	200 μM	100 μM	50 μM	20 μM	10 μM	2 μM	1 μM	0.2 μM
Total Volume	6ml	3ml	3ml	3ml	3ml	3ml	3ml	3ml	3ml
Maximum DMSO volume (0.2%)	12 μl	6 μl	6 μl	6 μl	6 μl	6 μl	6 μl	6 μl	6 μl
Volume of media	5988 μl	2994 μl	2994 μl	2994 μl	2994 μl	2994 μl	2994 μl	2994 μl	2994 μl
Concentration of stock used	-	107,628.6 μM	107,628.6 μM	107,628.6 μM	10,000 μM	10,000 μM	1,000 μM	1,000 μM	100 μM
Volume of above stock for 2X	-	5.57 μl	2.79 μl	1.39 μl	6 μl	3 μl	6 μl	3 μl	6 μl
Volume of neat DMSO for 0.2%	12 μl	0.43 μl	3.21 μl	4.61 μl	-	3 μl	-	3 μl	-

Table 2-4: Drug preparation - apitolisib dilutions

	Concentration (μM) or volume (μl)								
Desired concentration (X)	Control	5 μM	1 μM	0.5 μM	0.1 μM	0.05 μM	0.01 μM	0.005 μM	0.001 μM
Prepared concentration (2X)	Control	10 μM	2 μM	1 μM	0.2 μM	0.1 μM	0.02 μM	0.01 μM	0.002 μM
Total Volume	6ml	3ml	3ml	3ml	3ml	3ml	3ml	3ml	3ml
Maximum DMSO volume (0.2%)	12 μl	6 μl	6 μl	6 μl	6 μl	6 μl	6 μl	6 μl	6 μl
Volume of media	5988 μl	2994 μl	2994 μl	2994 μl	2994 μl	2994 μl	2994 μl	2994 μl	2994 μl
Concentration of stock used	-	6518.2 μM	1000 μM	1000 μM	100 μM	100 μM	10 μM	10 μM	1 μM
Volume of above stock for 2X	-	4.60 μl	6 μl	3 μl	6 μl	3 μl	6 μl	3 μl	6 μl
Volume of neat DMSO for 0.2%	12 μl	1.40 μl	-	3 μl	-	3 μl	-	3 μl	-

Table 2-5: Drug preparation - dactolisib dilution

	Concentration (μM) or volume (μl)								
Desired concentration (X)	Control	5 μM	1 μM	0.5 μM	0.1 μM	0.05 μM	0.01 μM	0.005 μM	0.001 μM
Prepared concentration (2X)	Control	10 μM	2 μM	1 μM	0.2 μM	0.1 μM	0.02 μM	0.01 μM	0.002 μM
Total Volume	6ml	3ml	3ml	3ml	3ml	3ml	3ml	3ml	3ml
Maximum DMSO volume (0.2%)	12 μl	6 μl	6 μl	6 μl	6 μl	6 μl	6 μl	6 μl	6 μl
Volume of media	5988 μl	2994 μl	2994 μl	2994 μl	2994 μl	2994 μl	2994 μl	2994 μl	2994 μl
Concentration of stock used	-	5856.7 μM	1,000 μM	1,000 μM	100 μM	100 μM	10 μM	10 μM	1 μM
Volume of above stock for 2X	-	5.12 μl	6 μl	3 μl	6 μl	3 μl	6 μl	3 μl	6 μl
Volume of neat DMSO for 0.2%	12 μl	0.88 μl	-	3 μl	-	3 μl	-	3 μl	-

2.3.2.2.5 Stage 5: The experiment, endpoint assay and data collection

The drugs were added the 6-8 hours after plating the cells as this allowed adequate time for the cells to adhere to the culture plate. Radiotherapy was commenced the following day for logistical reasons and this also prevented over-confluence of cells within the small experiment plate wells towards the end of the experiment.

Radiotherapy was administered 1 Gy per day for 5 consecutive days. On day six the experiment was terminated with assessment of cell viability, data collection and analysis as per the steps described in 2.3.2.2.2. The entire process was repeated to obtain three independent replicates using different cultures and passages at different time points.

2.3.2.3 *HCT116 experiments for PI3K/AKT/mTOR pathway analysis*

2.3.2.3.1 Identifying the optimum radiotherapy dose and protein collection time for pAKT detection following radiotherapy

HCT116 cells were retrieved and counted as described in 2.3.2.1. Cells were plated at 200,000 cell/well in 1ml of HCT116 media and topped up with a further 1ml of media resulting in a final volume of 2ml in 4 of the 6 wells of a 3 x 2 (Corning, USA) cell culture plate. A configuration of 2 such plates for the two experiment conditions and 1 plate with cells occupying 1 well was used as the control (see Figure 2-3). The cells were incubated in an incubator at 37°C, 5% CO₂ for a further three days to ensure adequate confluence (60%+). On the 4th day the experiment plates were administered a single dose of either 5 Gy or 10 Gy radiotherapy using a CellRad irradiator. Protein was extracted at 30 minutes, 60 minutes, 120 minutes and 24 hours following irradiation, and processed, quantified and stored using the steps

described in section 2.6 below. Western blots were performed using the technique described in 2.6.4.

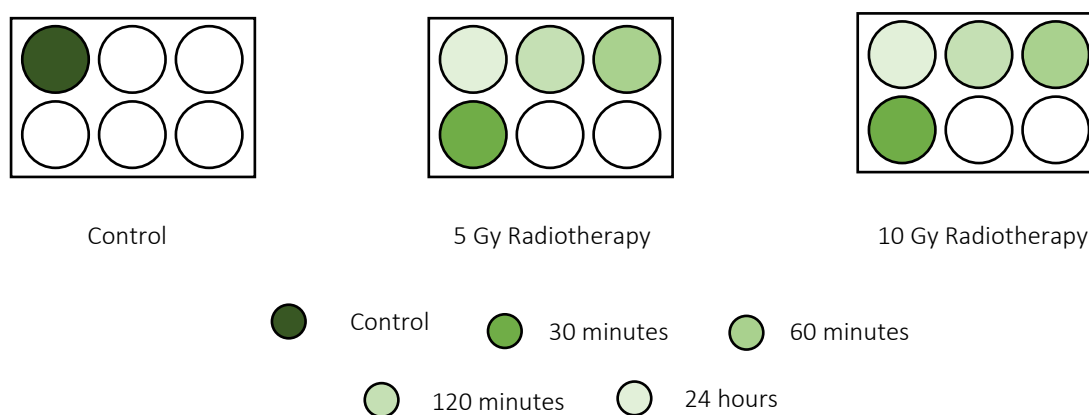
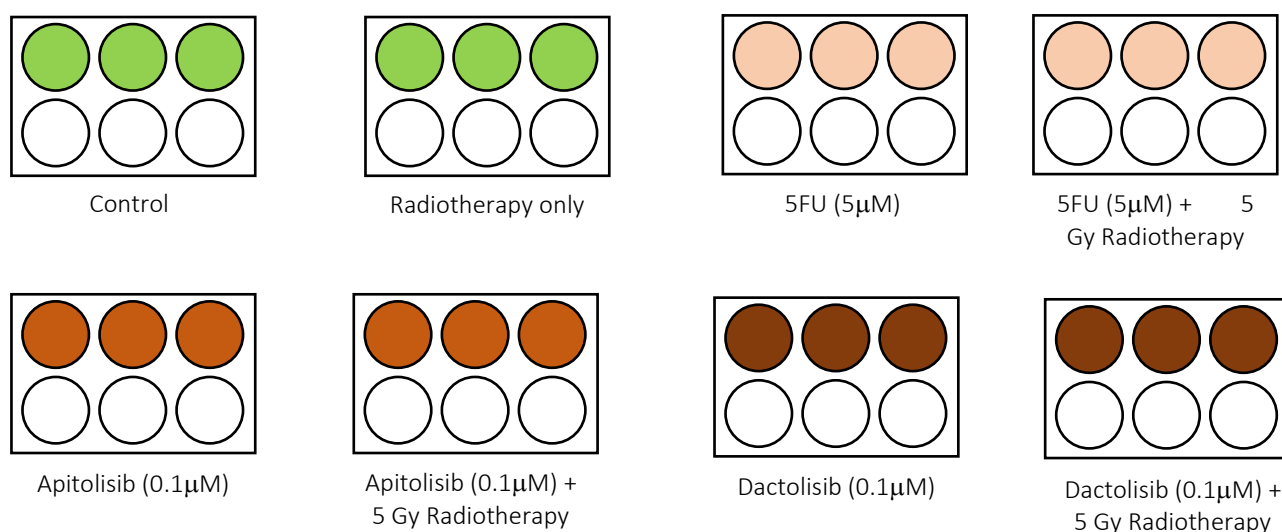


Figure 2-3: HCT116, 2 radiotherapy doses and different protein extraction times experiment (re-pathway analysis)

Coloured circles represent plated wells and different shades of green represent different extraction time points. Three 2x3 cell culture plates were used for each experiment repeat.

2.3.2.3.2 Pathway response to drugs

HCT116 cells were retrieved and counted as described in 2.3.2.1. Cells were plated in 3 wells (i.e., 3 replicates) of 3 x 2 cell culture plates at 200,000 cell/well in 1 ml of HCT116 media. Eight such plates were prepared (see Figure 2-4). The cells were kept at 37°C, 5% CO₂ in an incubator overnight to adhere and expand. The following day the three drugs were added to 6 of the plates at a volume of 1ml per well in HCT116 media at 2X concentrations (10 μ M and 0.2 μ M) for a final concentration of 5 μ M and 0.1 μ M, for 5FU and apitolisib as well as dactolisib, respectively. Drugs were diluted and prepared using a similar method to Table 2-3, Table 2-4 and Table 2-5 but for a final volume of 9ml per each concentration instead of 3ml.



All controls and experiment conditions were in HCT-116 media with a final DMSO concentration of 0.1%

Figure 2-4: HCT116 drug(s) and radiotherapy experiment for protein extraction (re-pathway analysis)

The circles represent wells plated with cells in 2 x 3 cell culture plates. Each coloured circle in the experiment plates represents an independent replicate. The different colours represent a different drug treatment. Eight plates were used for each experiment repeat.

The cells were incubated in experiment conditions for 72 hours. A single 5 Gy dose of radiotherapy was administered on day-4 using a CellRad irradiator. Protein extraction was commenced 2 hours after treatment (based on the results from the experiment described in 2.3.2.3.1) for irradiated plates, and 1 hour before the former for the non-irradiated plates for logistical reasons to ensure all protein was extracted at approximately same time. Protein extraction, processing and western blots were performed (see section 2.6).

2.4 Patient derived organoid methodology

2.4.1 *Primary culture of human patient-derived organoid lines*

A protocol derived from Clevers et al. was used for 3D PDO culture (Figure 2-5) (362). Fresh tissue samples from prospectively recruited patients undergoing surgery (as described in section 2.2.2) were retrieved via the Biobank, the same day as their surgery. The samples were stored overnight at 4°C in DMEM and 0.1 mg/ml Primocin™ (Invivogen, USA) at a concentration of 0.2%. The latter is an antibacterial as well as a fungicidal agent. The sample was processed the following day. Thorough washout of the sample was performed using Dulbecco's Phosphate Buffered Saline (DPBS) modified without calcium chloride and magnesium chloride (PBS0, Sigma-Aldrich, USA) with 0.2% Primocin™. The normal sample as well as a small proportion (up to 30mg) of the tumour was snap-frozen in liquid nitrogen. The tissue was stored in 1.8ml CryoTube vials (Thermo Fisher Scientific, USA) at -80°C. These samples were archived for future germline genomic work which outside the scope of this thesis.

The remaining tumour tissue was dissected using a scalpel to approximately 3mm x 3mm smaller pieces. The tumour was transferred to a small container with 3-4ml of digestion buffer. The digestion buffer comprised of 2.5% FBS; 75 U/ml Collagenase (Sigma-Aldrich, USA); 125 ug/ml Dispase (Fisher Scientific, USA); 0.2% Primocin™ in Advanced DMEM/F12 (ADMEM/F12, Gibco, USA). The tumour was mechanically dissected using micro-scissors until macroscopically fragmented or for at least 15 minutes. The sample was then incubated at 37°C for one hour for the first digestion

with intermittent mixing of the sample every 15-20 minutes with a Pasteur pipette. The digestant was transferred to a 50ml falcon through a 70µm cell strainer (EASYstrainer™, Greiner, Austria). The strainer was washed with 5-10ml of cold PBS0 + 0.2% Primocin™. Remnant tissue on the strainer was transferred back to the small digesting container with a further 2-3ml of digestion buffer and incubated at 37°C for another half an hour as part of the second digestion. The 50ml falcon containing single cells from the first digestion was kept on ice during this period. At the end of the second digestion, the digestant was once again filtered through a 70µm cell strainer to the same 50ml container and the strainer was washed through with a further 5-10ml of cold PBS0 + 0.2% Primocin™. The resulting solution containing single cells was centrifuged at 400 x g for 4 minutes at 4°C. The supernatant was discarded ensuring and the pellet was not disturbed. The pellet was dissolved in 2ml of cold PBS0 + 0.2% Primocin™ and transferred to a 15ml falcon tube. The 50ml falcon was washed with a further 2-3mls of cold PBS0 + 0.2% Primocin™ and all fluid transferred to the 15ml falcon tube. The resulting suspension was centrifuged at 400 x g for 4 minutes at 4°C. The supernatant was removed without disturbing the pellet and the falcon tube containing pellet was transferred to ice. On ice, the pellet was gently dissolved in the desired total volume of 10.0-12.1mg/ml Matrigel® (Corning, USA). The single cells immersed in Matrigel® were plated, 50µl per well on a 24-well Co-Star plate (Corning, USA). The plate was transferred to a New Brunswick Galaxy 170 incubator and left at 37°C for 30 minutes to allow for the Matrigel® to polymerise. 500µl of PDO culture media, Human Intesticult™ Component A and B (Stemcell Technologies Inc, Canada) was added per well and incubated at 37°C, 5% CO₂. Media was refreshed every 72-96 hours.

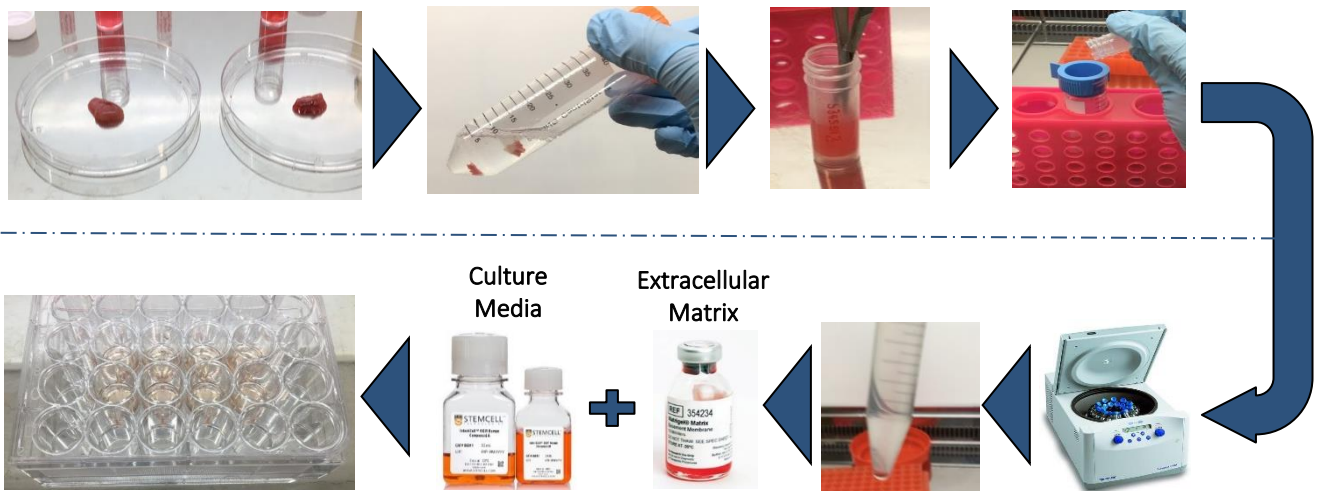


Figure 2-5: A pictographic representation of the human PDO culture method. Fresh tumour tissue was sampled from patients, washed in PBSO containing antibiotics, mechanically and chemically digested. The single cells were filtered, centrifuged, embedded in Matrigel® and maintained in culture media.



Copyright of STEMCELL Technologies (Canada). Image used with permission.

Source: <https://www.stemcell.com/cell-separation/immunomagnetic>



Copyright 2020 Corning Incorporated. Image used with permission.

2.4.2 Human patient-derived organoid passage

Adequately confluent PDOs were extracted from wells of 24-well culture plates, with 1ml of cold Cultrex® Organoid Harvesting Solution (OHS, Trevigen, USA) containing 0.2% Primocin™; per each well. Matrigel® was scraped and transferred to a 15ml falcon tube using a Pasteur pipette. The solution was thoroughly mixed using a Pasteur pipette and left on ice for 30-45 minutes for the Matrigel® to dissolve. Intermittent mixing was performed with a Pasteur pipette to ensure that the Matrigel® dissolved faster. Subsequently, the solution was centrifuged for 4 minutes at 400 x g,

4°C. The supernatant was carefully removed without disturbing the pellet. The pellet was dissolved in 1ml of pre-warmed (37°C) TrypLE™ Express and mixed using a Pasteur pipette. Mechanical splitting of PDOs was performed using a 1000µl pipette tip attached to 10µl non-filter pipette tip aspirating up and down for up to 2-3 times maximum. The total digestion period was not exceeded beyond a maximum of 3 minutes. At the end of the 3 minutes, the TrypLE™ Express was inactivated using 5ml of cold PBS0 + 0.2% Primocin™. The solution was centrifuged at 400 x g, for 4 minutes at 4°C. The supernatant was removed without disturbing the pellet and the falcon tube containing pellet transferred to ice. On ice the pellet was gently dissolved in the desired total volume of Matrigel®. The passaged PDOs immersed in Matrigel® were plated, 50µl per well on a 24-well Co-Star plate. The Matrigel® was allowed 30 minutes to polymerise in an incubator at 37°C and 500µl of PDO culture media, Human Intesticult™ Component A and B, were added to each well and maintained at 37°C, 5% CO₂ in an incubator.

2.4.3 Human patient-derived organoid freezing protocol

PDO freezing buffer solution was prepared at 2X concentration, comprising of 20% DMSO, 80% FBS, 0.4% Primocin™ and 0.2% ROCK inhibitor (Strattech Scientific LTD, UK) and kept on ice. PDOs were gently extracted in OHS + 0.2% Primocin™ from the 24-well culture plate using the exact same methodology used for PDO passage as described above. PDOs in solution were incubated for up to 30 minutes on ice until the Matrigel® had completely dissolved. The solution was centrifuged for 4 minutes at 400 x g, 4°C. The supernatant was carefully removed without disturbing the pellet. The pellet was dissolved in 1ml of cold ADMEM/F-12. 1ml of freezing

buffer was added drop by drop to the solution containing PDOs over 30 seconds. The solution was gently mixed and transferred to a 1.8ml CryoTube, and immediately transferred to a Freezing Container (Nalgene, USA) and stored at -80°C for 24 hours. The samples were stored long term in liquid nitrogen at -210°C.

2.4.4 Human patient-derived organoid thawing protocol

Frozen PDOs were transferred to the laboratory from liquid nitrogen storage on dry ice. The sample was thawed in a water bath set at 37°C until defrosted and was immediately transferred to 5ml of pre-warmed ADMEM/F12 at 37°C, and was mixed gently with a Pasteur pipette. The solution was centrifuged for 3 minutes at 200 x g at room temperature. The supernatant was carefully discarded without disturbing the pellet. The pellet was dissolved in the desired volume of Matrigel®. The thawed PDOs were plated, 50µl per well on a 24-well Co-Star plate. A 30-minute incubation at 37°C allowed the Matrigel® to polymerise. 500µl of PDO culture media, Human Intesticult™ Component A and B, was added per well and incubated at 37°C, 5% CO₂.

2.4.5 Human PDO experiments

2.4.5.1 PDO experiment preparation and viability assessment

2.4.5.1.1 PDO extraction from culture plates

PDOs were extracted from 24 well culture plates approximately 4-5 days after a passage in OHS with 2% Primocin™ (1ml per well, approximately 10-12 wells) in a 15 ml falcon tube. The PDOs in solution were left for 30-40 minutes on ice for the

Matrigel® to be completely dissolved. The solution was subsequently centrifuged for 4 minutes at 400 x g in 4°C. The supernatant was discarded without disturbing the pellet.

2.4.5.1.2 Estimating the live cell count within a solution containing established patient derived organoids

The experiments required plating PDOs already organised into 3D structures. The experiments also required similar counts to be plated across the different experiments. Therefore, a sample of PDOs in solution of a given volume was obtained, digested to single cells and a live cell count was obtained from this sample. This count was extrapolated to obtain an estimate of live cells present within the original sample. This method was validated through multiple repeat preliminary experiments (data not shown). The PDOs were of comparable in size, confluence and appearance when inspected under optical microscopy at the start of each experiment. This method provided consistent results with narrow confidence intervals across repeat experiments using different PDO lines (see Chapter 6). This process is illustrated in Figure 2-6 and explained in more detail below. The pellet from section 2.4.5.1.1 was dissolved in 4ml of ice-cold Human Intesticult™ Component A and B media and gently dissolved with a 1ml pipette. One millilitre of this solution containing PDOs was transferred to a fresh 15ml falcon tube. The remaining 3ml was kept on ice for later use. The 1ml sample was topped up with 4-5ml of ice-cold PBS0 and centrifuged for 4 minutes at 400 x g, 4°C. The supernatant was carefully discarded without disturbing the pellet. The pellet was dissolved in 1 ml of TrypLE™ Express pre-warmed to 37°C. The pellet was dissolved with a 1ml filtered tip pipette. The PDOs were mechanically digested whilst in TrypLE™ Express using a 1ml filtered tip attached to a 10µl non-filtered tip by mixing with

pipette (fully aspirating and releasing the pipette) up to 10 times. Subsequently, the PDOs were incubated at 37°C in an incubator for 20 minutes with intermitting stirring to prevent cell clumping. Following the incubation, 6-8ml of ice-cold PBS0 was added to the falcon tube to inactivate the TrypLE™ Express. The suspension of single cells was centrifuged at 200 x g for 5 mins in a centrifuge set to 4°C. The supernatant was discarded without disturbing the pellet.

The single cell pellet was dissolved in 1ml of Human Intesticult™ Component A and B media. A 100µl sample from this solution was aliquoted into an Eppendorf tube and mixed with 100µl of Trypan blue. Two dual chamber transparent cell counting slides were prepared by placing 10µl of the latter mixture to each chamber of the two slides. A live cell count was obtained for each chamber using a TC20™ automated cell counter set at default settings (auto-gate). The average of the four results was an estimate of the live cell count in 1 ml of the original PDO sample. This was multiplied by 3 (given that the remaining volume was 3 ml) from the original sample to obtain an estimate of the live cell count available for plating for experiments. Using the latter count and the desired estimated cell count required for each experiment conditions, calculations were carried out to determine the volume of the original solution required, containing formed PDOs. This method of estimation and live cell counts in PDOs generated consistent, reliable and reproducible results.

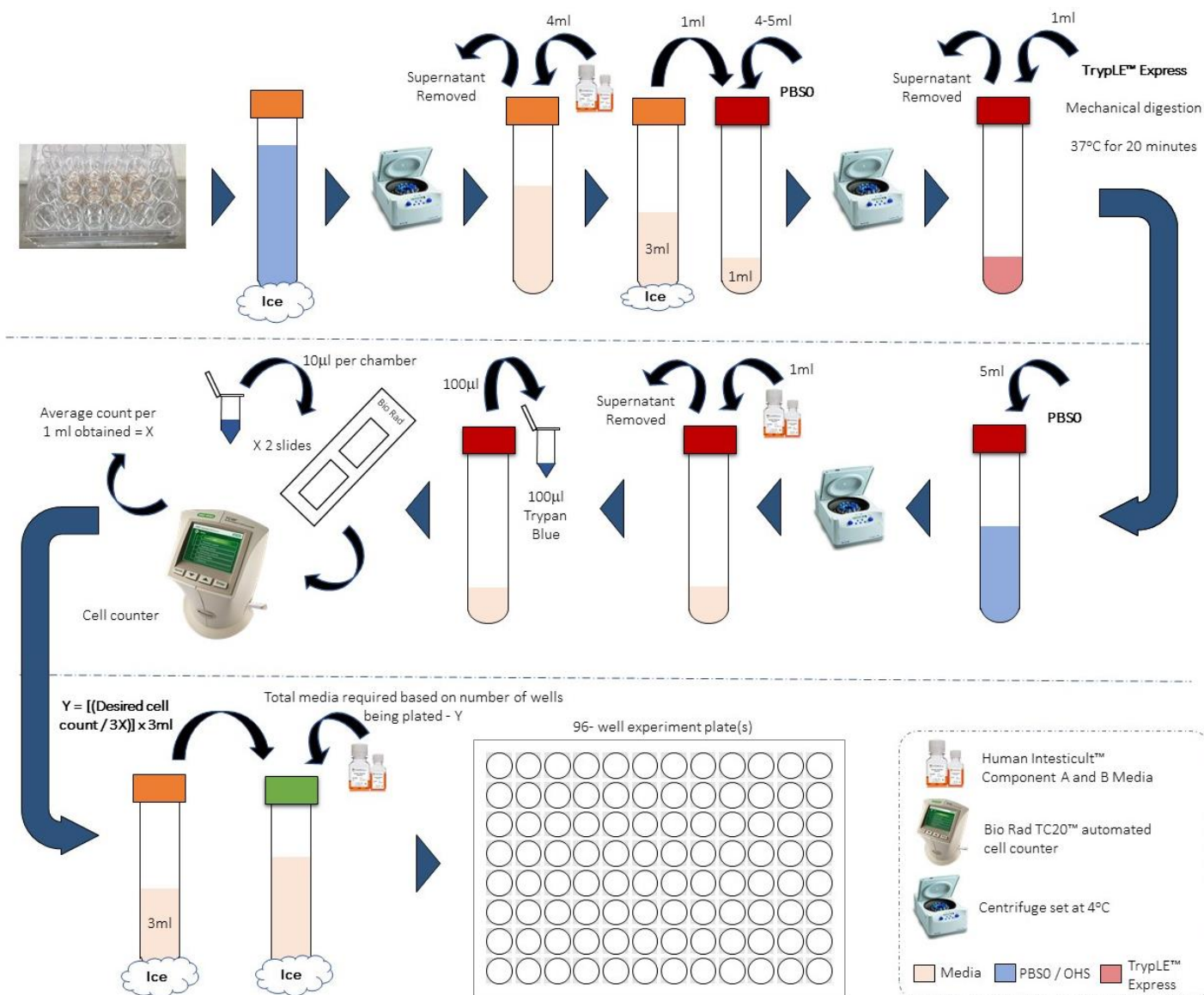




Figure 2-6: Graphical representation of the method used to estimate live cells within PDOs. The diagram above is a graphical representation of the method used to estimate PDO count for experiments. See Appendix B for a working example using this method

 Copyright of STEMCELL Technologies (Canada). Image used with permission.
Source: <https://www.stemcell.com/cell-separation/immunomagnetic>

 Copyright of Bio-Rad (USA). Image used with permission. Source: http://biorad-ads.com/green/system-tour/TC20/1_2-whats-new.html

2.4.5.1.3 Plating PDOs for experiments

PDOs were plated in 96-well flat clear bottom sterile microplates for the experiments described below. The plates were pre warmed in an incubator at 37°C.

Approximately 55µl of Matrigel® was added to the base of each well. The plate was left in an incubator for at least 30 minutes for the Matrigel® to polymerise. PDOs in solution were added at the desired count to each well in a volume of 100µl of Human Intesticult™ Component A and B media, such that the PDOs would adhere to the surface of the Matrigel® base in each plate. Each well was topped up with a further 100µl of PDO media. All residual empty wells on the plate were filled with PBS to minimise evaporation losses. The plated PDOs were left for at least 72 hours in a 37°C, 5% CO₂ incubator prior to commencing any treatment.

2.4.5.1.4 Patient derived organoid viability assessment at experiment endpoint

Experiment outcomes were assessed by measuring relative cell viability using an ATP based, cyto-toxic (endpoint) chemiluminescence assay- CellTiter-Glo® 3D Cell Viability Assay Solution (Promega, USA). The solution was thawed at 4°C overnight and was left at room temperature for at least 1 hour before use. At the end of a PDO experiment, 100µl of media was carefully removed from each plate and 100µl of CellTiter-Glo® 3D Cell Viability Assay Solution was added. The assay was light sensitive. Therefore, the plate was covered in aluminium foil and was incubated for 30 minutes at room temperature. During this time, each plate was placed on an orbital shaker set to the lowest speed for 5 minutes. Subsequently, the cell viability was assessed using the EnSpire® luminescence plate reader. Data were collated and normalised using Excel and analysed using Prism V8. Normalisation was performed relative to the average endpoint viability of untreated control replicates

from each experiment run. Dose-response graphs were generated on Prism V8 using the log (inhibitor) vs. response equation. IC50 values with 95% confidence interval (CI) were determined using nonlinear regression. Welch's two sample t-tests were performed using Excel to assess significance in efficacy of drug treatment with or without radiotherapy on the cell line.

2.4.5.2 Determining the optimum cell count within PDOs for experiments

PDOs were plated in different counts measured using the methodology described above. PDOs were plated at 10,000 cells/well, 5000 cells/well and 2500 cells/well, counted using the method described in Figure 2-6. On the third day after plating 100µl of media was removed from each well. The PDOs were treated with 25µM 5FU in 0.1% DMSO in Human Intesticult™ Component A and B. The drug was prepared at double the desired final concentration (50µM in 0.2% DMSO) and was added in a 100µl volume to each well. The drugs were prepared using the formula described in Table 2-3. There were four replicates for each experiment condition. The PDOs were incubated in drug for 5 days. The experiment was terminated on day 6 by assessing PDO viability using the methodology described in 2.4.5.1.4.

2.4.5.3 Radiotherapy (only) experiments

PDOs were plated in eight replicates at 5000 cells/well by following the methods described in section 2.4.5.1. The plate configuration used is illustrated in Figure 2-7. Six such plates were prepared. Radiotherapy treatment was commenced on the third

day. Media was changed; 100µl removed and 100µl fresh Human Intesticult™ Component A and B was added to each well, prior to starting treatment. The media was changed every 72 hours till the end of the experiment. One of the six plates was the control plate and did not receive any radiotherapy. The remainder were treated with 2 Gy, 5 Gy, 10 Gy, 20 Gy or 40 Gy per day for five days using a CellRad irradiator. This wide range was chosen to clearly distinguish between predominantly radiosensitive and predominantly radioresistant PDO lines. The plates were left in the incubator for a further 5 days to allow time for radiotherapy related cell damage and death to occur. The experiment was terminated with an endpoint cell viability assessment using the method described in section 2.4.5.1.4.

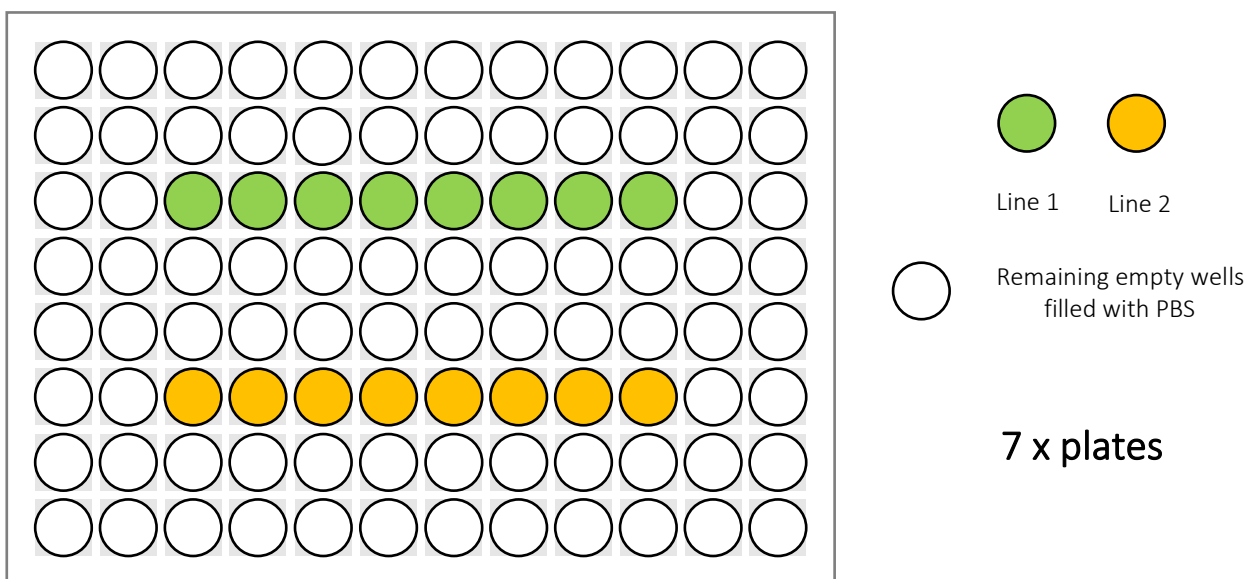


Figure 2-7: The 96-well plate configuration used for PDO and radiotherapy experiment

The coloured wells in the figure above represent wells containing PDOs in culture on a Matrigel® base and media.

2.4.5.4 Drug screens

2.4.5.4.1 Single drug dose (on its own or combined) +/- radiotherapy experiments

Six PDO lines were plated at 5000 cells/well in 4 replicates per line, per experiment condition using the PDO plating methodology described section 2.4.5.1. The plate configuration used is illustrated in Figure 2-8. A single dose of each of the three drugs (5FU, apitolisib or dactolisib) were tested on their own, with radiotherapy and in combination (5FU + apitolisib or 5FU + dactolisib) with or without radiotherapy were tested. The drugs concentrations tested were 25 μ M (5FU), 1 μ M (Apitolisib) and 1 μ M (dactolisib), in a final 0.1% DMSO, in Human Intesticult™ Component A and B media. The drugs were prepared at double the value of the desired final concentration. Table 2-6 highlights the formulae and stock concentrations used to prepare these drugs.

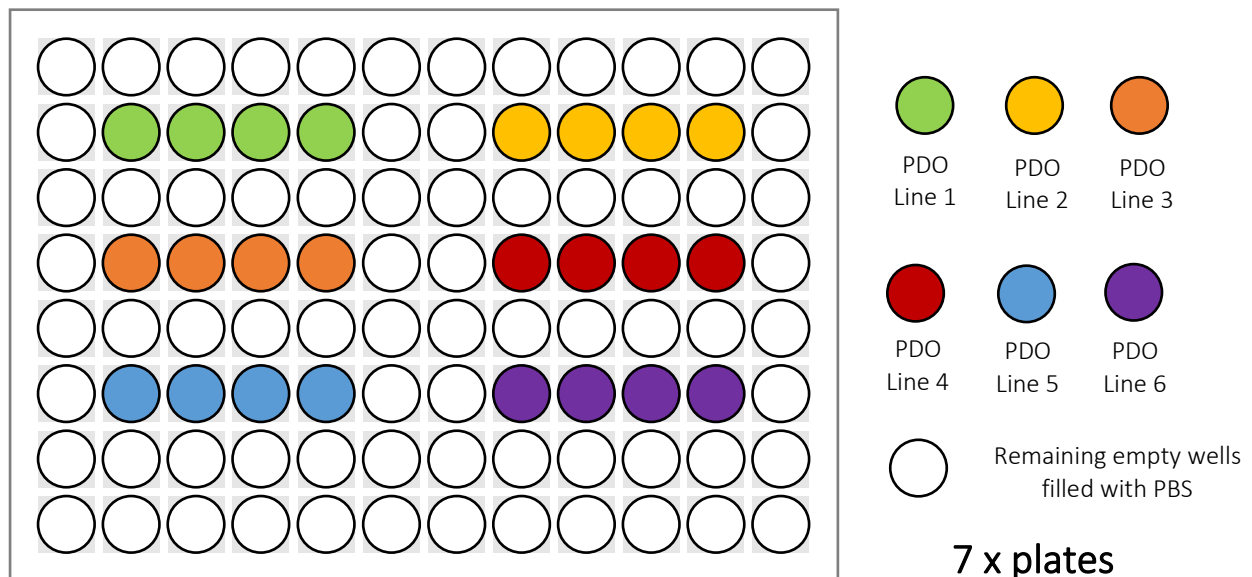


Figure 2-8: The 96-well plate configuration used for PDO with single drug dose and radiotherapy experiments

The coloured wells in the figure above represent wells containing PDOs in culture on a Matrigel® base and media (+- drug)

One hundred microlitres of media were removed from each experiment well and 100µl of the prepared double strength drug was added to each experiment well. The drugs were added on the second day after plating to six of the seven plates. The remaining plate was the control plate containing only media with 0.1% DMSO. Radiotherapy was administered from day 3 using a CellRad irradiator at 5 Gy a day for three of the plates. The drugs and media were replenished on the 5th day after plating, by removing 100µl of drug and adding the drug in 100µl Human Intesticult™ Component A and B, at a single strength concentration to each well. The media in the control plate wells were also similarly replenished. Radiotherapy was administered daily for five days (to simulate a SCRT regimen) and treatment was completed on day 7. Media was changed twice on day 8; 100µl was removed at a time from each plate. This ensured adequate removal of drug from those plates treated with 5FU, apitolisib or dactolisib. From day 9 to day 12 the PDOs were maintained in the incubator with a 100µl media change on the 10th day. This additional incubation time following treatment allowed for any radiotherapy and drug induced cell death to take place. The experiment was terminated on day 13, and PDO viability was assessed using the methodology described in section 2.4.5.1.4.

Table 2-6: Drug preparation – 5FU, apitolisib (API.), dactolisib (DACTO.) and in combination

	Control	5FU	API.	DACTO.	5FU + API	5FU + DACTO
Desired concentration (X)	-	25mM	1mM	1mM	25mM / 1mM	25mM / 1mM
Prepared concentration (2X)	-	50mM	2mM	2mM	50mM / 2mM	50mM / 2mM
Total Volume (Vol)	6ml	6ml	6ml	6ml	6ml	6ml
Max. DMSO vol. (0.2%)	12ml	12ml	12ml	12ml	12ml	12ml
Vol. of media (ml)	5988	5988	5988	5988	5988	5988
Stock conc. Used (μ M)	-	46126.5	6016.8	3194.6	46126.5/ 6016.8	46126.5 / 3194.6
Vol. of stock for 2X	-	6.50 μ l	1.99 μ l	3.76 μ l	6.50 μ l / 1.99 μ l	6.50 μ l / 3.76 μ l
Vol. of DMSO for 0.2%	12 μ l	5.50 μ l	10.01 μ l	8.24 μ l	3.50 μ l	1.74 μ l

2.4.5.4.2 Drugs and radiotherapy (combined) dose - response experiments

PDO lines were treated with different concentrations of 5FU, apitolisib and dactolisib with or without radiotherapy. PDOs were plated at 5000 cells/well using the plating and counting methodology described in section 2.4.5.1. The plate configuration used, is illustrated in Figure 2-2. The drugs were added on the 2nd day after plating the experiments. The drugs were prepared at double strength concentration using the formulae and methods described in Table 2-3, Table 2-4 and Table 2-5, and the range of different drug concentrations used for each of the three drugs can also be

found in the latter tables. The drugs were added in a volume of 100µl of Human Intesticult™ Component A and B in 0.1% DMSO, to each well.

Radiotherapy treatment was commenced on the third day. Radiotherapy was administered using a CellRad irradiator at a dose of 5 Gy a day for five consecutive days. The media and drug were replenished on day 5 in a similar manner to the previous experiment (2.4.5.4.3). On day 8, 100µl of media was removed from each well and replenished with 100µl of fresh Human Intesticult™ Component A and B. The process was repeated on the same day to ensure adequate dilution of drugs in all the treated wells. A further 100µl media change was performed on day 10. PDO viability was assessed day 12 (see 2.4.5.1.4). The experiment was repeated three times in total for each PDO line.

2.4.5.4.3 Drug (only) dose - response experiments

Six PDO lines were treated with 5FU, apitolisib and dactolisib at different drug concentrations. Four replicates for each experimental condition were used. The plate configuration used was the same as the one used in HCT-116 cell line dose response experiments as illustrated in Figure 2-2 and three such plates were prepared per line. The PDOs were extracted and plated at 5000 cells/well as per the methodology described in 2.4.5.1. The drugs were prepared at double the final desired concentration as per the formulae described in Table 2-3, Table 2-4, Table 2-5, and were added in a volume of 100µl of Human Intesticult™ Component A and B in 0.1% DMSO, to each well. The drugs were added on the second day after plating the PDOs. One hundred microlitres of media were removed from each well and 100µl of drugs at double strength concentration were added to each well. The

drug (or media with DMSO for control plates) were replenished on day 5, where 100µl of media was removed from each and the drugs were added at a single strength concentration to each well. On day 8, 100µl of media was removed from each well and replenished with 100µl of fresh Human Intesticult™ Component A and B. The process was repeated on the same day to ensure adequate dilution of drugs in all treated wells. A further 100µl media change was performed on day 10. PDO viability assays were performed on day 12 (see 2.4.5.1.4). The experiment was repeated twice in total for each PDO line.

2.5 Genomic methodology

2.5.1 *Extracting DNA and RNA*

2.5.1.1 *From formalin fixed paraffin-embedded tissue*

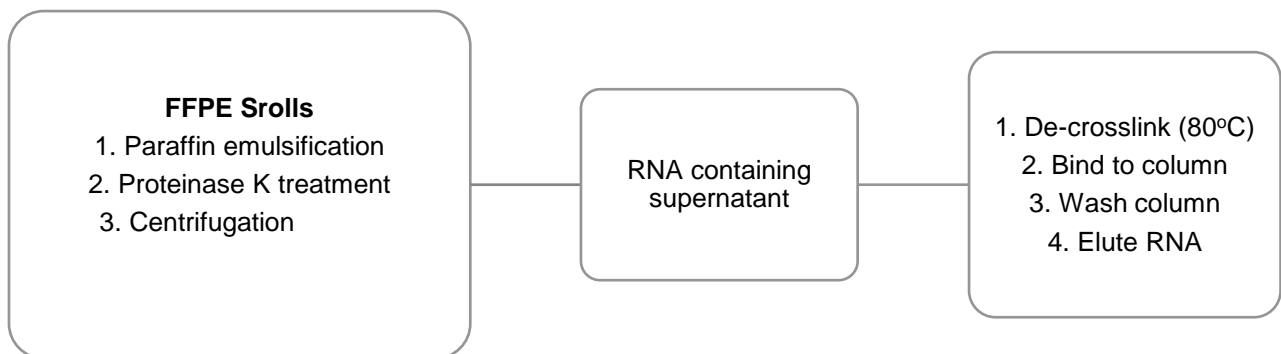


Figure 2-9: Workflow using truXTRAC® FFPE total NA Kit – Column, (Covaris, USA) to extract RNA

RNA was extracted from FFPE scrolls using an E220 Focused Ultrasonicator (Covaris, USA) and truXTRAC® FFPE total NA Kit – Column (Covaris, USA), as per

the manufacturer's protocol (370). The kit contained all the necessary reagents, spin columns and screw capped micro-TUBE-130 sonication tubes. The workflow using this kit has been summarised in Figure 2-9.

2.5.1.1.1 Relevant equipment and preparation

The ultrasonicator was prepared several hours in advance. The water bath was filled with deionized H₂O (diH₂O) up to the manufacturer recommended level (Level 10) as specified on the protocol. The water was cooled to 18°C and degassed, ensuring that a Rack 24 Place microTUBE Screw Cap, Plate and heat block adapters (included with device) were available. Heat blocks set to 56°C and 80°C. Sixty five percent isopropanol (VWR Chemicals, USA) and 100% ethanol (VWR Chemicals, USA) were aliquoted.

2.5.1.1.2 Paraffin emulsification and tissue hydration

The microTUBE-130 Screw-Capped tubes were labelled and preheated in heat block adapters on the 56°C heat block. Tissue Lysis Buffer (TLB) and Proteinase K Solution (PKS) were prepared in a master mix as illustrated in Table 2-7. One to two 8µm FFPE scrolls were gently placed within the microTUBES using forceps and the 132µl of the TLB and PKS master mix was added to each microTUBE.

Table 2-7: Tissue Lysis Buffer / Protein K Solution mix (initial mix)

Reagent	Volume for one sample	Volume for N samples
Tissue Lysis Buffer	121µl	121µl x N
Proteinase K Solution	11µl	11µl x N

The sample was processed in the ultrasonicator as per the manufacturer's specifications as illustrated in Table 2-8 to emulsify and rehydrate tissue. The microTUBEs were removed from the ultrasonicator and were placed on a 56°C heat block for 30 minutes (Proteinase K treatment). At the end of the incubation, they were cooled down to room temperature. The microTUBEs were centrifuged at 5000G for 15 minutes in a microcentrifuge. One hundred microlitres of the resulting supernatant was transferred into a 1.5ml Eppendorf tube and immediately proceeded to RNA purification (see 2.5.1.1.3).

Table 2-8: E220 Focused Ultrasonicator settings

	Setting
Peak Incident Power	175 Watts
Duty Factor	10%
Cycles per Burst	200
Temperature (Instrument)	20°C
Emulsification Treatment Time	300 seconds

2.5.1.1.3 RNA purification

The supernatant, which contained RNA collected in 2.5.1.1.2 was incubated on the 80°C heat block for 20 minutes for de-crosslinking and was subsequently cooled down to room temperature for three minutes. RNA purification was performed using manufacturer supplied buffers (B1, RNA Wash Buffer, RNA elution buffer), 65% Isopropanol and RNA purification spin columns, by following the steps on page-14 and 15 of the manufacturer's protocol (370). The eluted RNA was treated in-column during the extraction using TURBO DNA-free™ Kit (Invitrogen, USA)) to remove

remnant DNA, using the directions specified on page-21 of this protocol (370, 371). Approximately 30-50µl of eluted RNA could be obtained per sample using this protocol. The RNA was immediately quantified, subjected to quality control procedures (see 2.5.1.1.4) and stored at -80°C.

2.5.1.1.4 Quantification, quality control and storage

Quantification and quality control of the extracted DNA and RNA was performed (see 2.5.2 below). DNA and RNA were stored in DNA Lo Bind tubes (Eppendorf, Germany) at -20°C and -80°C respectively.

2.5.1.2 Extracting DNA and RNA from patient derived organoids

PDOs were extracted in OHS using the same method described in the PDO passage section (see 2.4.2). The sample containing PDOs in OHS was incubated for 30 minutes on ice to ensure that the Matrigel® was fully dissolved. The solution was centrifuged for 4 minutes, 400 x g at 4°C. The supernatant was discarded without disturbing the pellet. The pellet was dissolved in 350-600µl (depending on the total number of PDO wells extracted) of manufacturer supplied RLT Plus buffer containing 1% β-mercaptoethanol and mixed thoroughly using 1000µl filtered tip pipette for up to 2 minutes on ice. The lysate was used for immediate DNA and RNA extraction.

AllPrep DNA/RNA Mini Kit (Qiagen, Germany) was used to extract DNA and RNA from fresh tissue and PDOs. RNA followed by DNA extraction performed using spin columns and reagents provided in the kit as per the manufacturer's protocol (Quick-Start Protocol 2016, AllPrep DNA/RNA Mini Kit, Part 1 and Part 2) (372, 373). In

solution routine DNase treatment of the RNA was performed using the TURBO DNA-free™ Kit according to page-3 of the manufacturer's protocol (371). Quantification and quality control of the extracted DNA and RNA was performed (see below). DNA and RNA were stored in DNA Lo Bind Eppendorf tubes at -20°C and -80°C respectively.

2.5.2 Quantification and quality control

2.5.2.1 DNA and RNA quantification using Qubit™

DNA and RNA quantification were performed using Qubit™ RNA Broad Range Assay Kit (Invitrogen, USA), Qubit™ DNA High Sensitivity Assay Kit (Invitrogen, USA). Qubit™ DNA or RNA buffer-dye reagent mix prepared at 200:1 concentration. 2µl sample added to 198µl buffer dye reagent mix and concentration checked using digital luminescence assay reader (Qubit™ 3.0 Fluorometer, Invitrogen, USA) and value compared between two manufacturer supplied standards (Standard 1 and Standard 2) which contained a set concentration of DNA or RNA to allow for calibration of the device, to obtain a concentration of nucleic acid in ng/µl within our samples.

2.5.2.2 Quality control

Quality control was performed using Genomic DNA and RNA High Sensitivity ScreenTapes® (Agilent, USA) on TapeStation® 2200 (Agilent, USA) as per the manufacturer's protocols reagents for genomic DNA and RNA (Genomic DNA ScreenTape® protocol (374); RNA High Sensitivity ScreenTape® protocol (375)).

For quantification of DNA or complementary DNA (cDNA) following library preparation, D1000 High Sensitivity ScreenTapes® were used as per the manufacturer's protocol and reagents (376). The TapeStation® Analysis software, Version A.02.02 (SR1) (Agilent, USA) was used to obtain DNA integrity number (DIN) and RNA integrity number values (RIN) as well as estimate average base pair length following library preparation. For genomic DNA and RNA samples with DIN or RIN values under 8 were excluded ensuring all genomic material used for downstream analyses were of high quality and with minimal degradation.

2.5.3 Library preparation and sequencing

2.5.3.1 Three prime RNA sequencing

Quant-Seq FWD (Lexogen, Austria) was used to prepare cDNA libraries from FFPE RNA and PDO RNA extracted at baseline or following radiotherapy for NGS. The process generated a single fragment per transcript which was an accurate reflection of gene expression. Three prime (3') sequencing is both cost-effective and quick to generate results. The library manufacturer recommended a total RNA input in the range of 10ng-2µg. However, they have approved the use of the kit for use with degraded RNA (e.g., extracted from FFPE) and at inputs below 10ng by following specific additional steps within the manufacturer's protocol (377). The protocol also allows total RNA input and therefore ribosomal RNA (rRNA) depletion or poly(A) enrichment was not needed. The manufacturer advised against paired-end sequencing using of a reverse strand using this library preparation kit and method.

2.5.3.1.1 RNA normalisation

For RNA extracted from FFPE as well as PDOs were normalised based on the available RNA concentration and volume of RNA available in the weakest sample. Normalisation was performed by adding nuclease free sterile H₂O (Invitrogen, USA) either manually by hand or through automation with the aid of the Microlab STAR automated liquid handling platform (Hamilton, USA).

2.5.3.1.2 Library Generation

The RNA input for library preparation was 5ng for PDOs as well as FFPE RNA. The library generation process began with two complementary cDNA strands being synthesised sequentially. The first strand was synthesised from the 3', poly(A)-tail end of the RNA transcripts in each sample (reverse transcription). The RNA was subsequently degraded and removed. This step was immediately followed by the synthesis of the second strand. This was a complementary cDNA strand synthesised from random priming by DNA polymerase using the cDNA strands generated in the former reverse transcription step as a template. The resulting cDNA strand contained the same sequence as the original RNA transcripts. The forward read (Read 1 primer) linker sequence was also introduced at this stage. Therefore, NGS would sequence this synthesised second strand from the Read 1 end towards the 3', poly(A) tail yielding the exact same sequence as the original RNA transcript (Figure 2-10). Read 2 primer for reverse read was also attached to the 5' end. However, as per the manufacturer's recommendation reverse reads were not performed during sequencing. Linker sequences for Illumina (USA) NGS devices were also introduced at this stage. Table 2-9 summarises the specifications for the C1000 Touch™ (Bio-Rad, USA) thermocycler used in the different stages of library generation process. Subsequently, the library was purified through bead and ethanol wash by following

the manufacturer's protocol. By the end of this stage a double-stranded cDNA library, complete with NGS linker sequences and forward read primer (Read 1) attachments had been generated from the RNA.

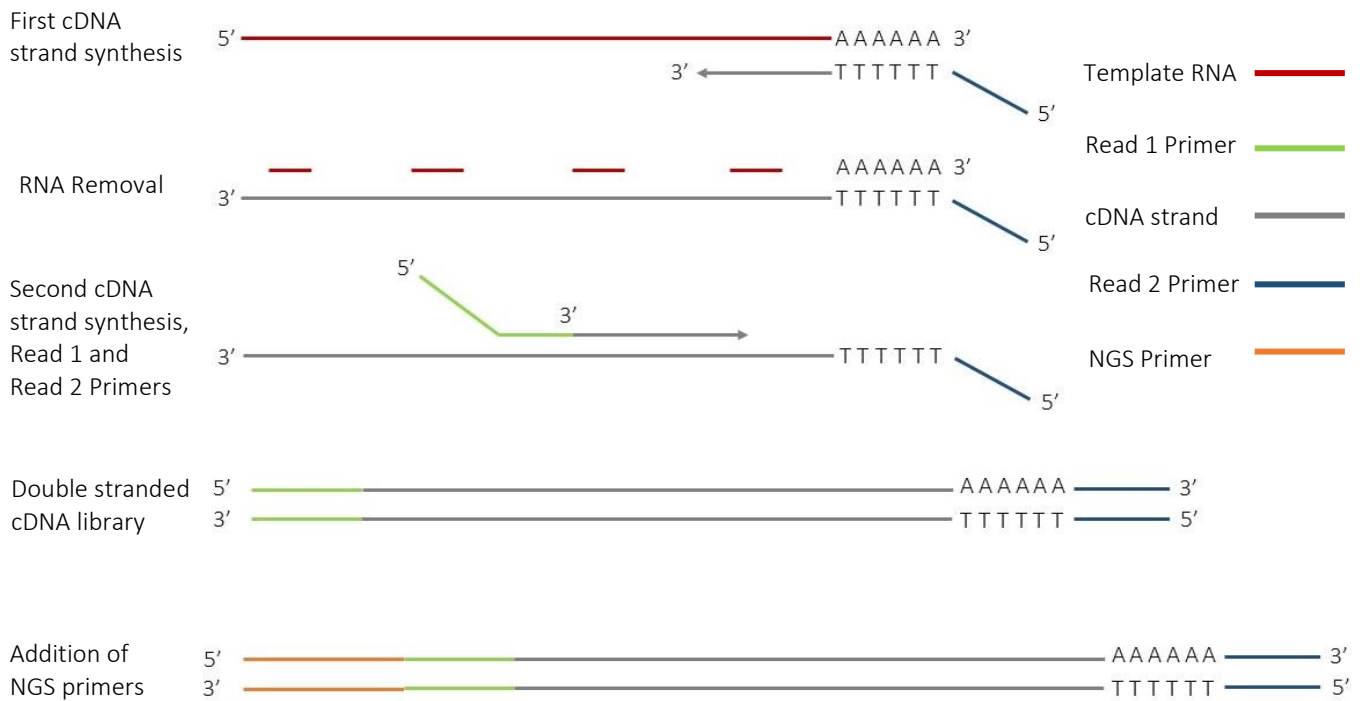


Figure 2-10: Schematic representation of double stranded cDNA library generation from RNA using Lexogen Quant-Seq library preparation kit

Table 2-9: Thermocycler settings and reagents used for library generation

First cDNA strand synthesis	RNA Removal	Second Strand Synthesis
Reagents FS1, FS2 and E1	Reagent RS O	Reagents PB, PS, EB, SS1
85°C 3 minutes	95°C 10 minutes	98°C 1 minute
(Omit step for FFPE RNA)		
42°C 15 minutes	25°C Infinite hold	25°C (0.5°C/sec)
		25°C 30minutes
		Reagents SS2 / E2
		25°C 15 minutes

2.5.3.1.3 Library indexing and Amplification

The cDNA library was indexed by sample using the manufacturer provided unique i7 indices. These would link to each strand of the complementary cDNA strands at the opposite end to the NGS adapters and forward Read1 primer. The library was amplified by PCR on a thermocycler. The number of PCR cycles was as per the manufacturer's recommendation; for 5ng RNA input this equated to 19 PCR cycles (Table 2-10). For FFPE samples containing degraded RNA an additional quantitative PCR (QPCR) step was introduced prior to PCR to determine the number of PCR cycles (see 2.5.3.1.4). The library was subsequently purified with a bead wash, quantified using Qubit™ (see 2.5.2.1) and tested for quality using D1000 ScreenTapes® on the TapeStation® 2200 (see 2.5.2.2). At the end of the library preparation, final purification and quality control the cDNA library volume was approximately 15-17µl. The cDNA library was stored at -20°C until sequencing.

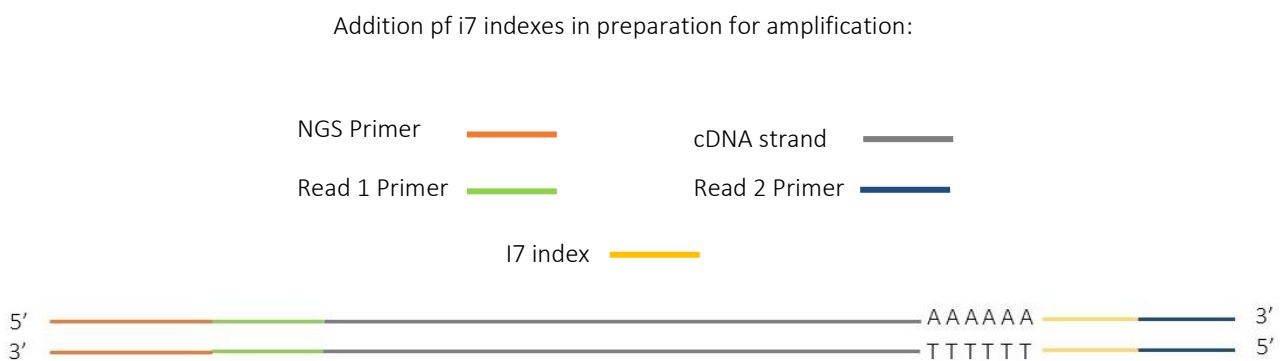


Figure 2-11: Final double stranded cDNA library structure prior to sequencing

Table 2-10: Thermocycler settings and reagents used for indexing and library amplification stage

Step	First cDNA strand synthesis	
	Reagents	PCR, E3 and i7
1	98°C	30 seconds
2	98°C	10 seconds
Cycle number - 12-26*	65°C	20 seconds
	72°C	30 seconds
3	72°C	1 minute
4	10°C	Infinite hold

* As per the manufacturer guidance based on input RNA amount or for FFPE RNA based on QPCR result described in 2.5.3.1.4. A heated lid on the thermocycler was used in this stage.

2.5.3.1.4 Optional QPCR step for FFPE RNA

An optional QPCR step was introduced prior to the form library amplification step to obtain the number of cycles required for PCR for FFPE RNA using the PCR Add-on Kit for Illumina (Lexogen, Austria) (378). A master mix was prepared using containing kit reagents (buffer PCR, E, 7000) and SYBR® Green (Thermo Fisher Scientific, USA) and added to 1.5-1.7µl (1/10th) of the library generated in 6.3.1.2. PCR was conducted as per the program in Table 2-11 using a QuantStudio™ 3 Real-Time PCR System (Thermo Fisher Scientific, USA). Using the Thermo Fisher Connect™ analysis software the fluorescence value at which the plateau was reached was determined. The number of cycles at which 50% fluorescence was reached was calculated. Given the original sample contained ten times more cDNA the final cycle number of PCR cycles chosen was 3 minus the latter cycle number.

Table 2-11: Thermocycler settings used for QPCR add-on stage

Step	Temperature	Duration
1	98°C	30 seconds
2	98°C	10 seconds
(45 cycles)	65°C	20 seconds
	72°C	30 seconds
3	72°C	1 minute
4	10°C	Infinite hold

A heated lid on the thermocycler was used in this stage.

2.5.3.1.5 Library normalisation and pooling

TapeStation® Analysis software, Version A.02.02 (SR1) was used to estimate the average basepair length for each sample. The formula below was used to estimate the molarity (nM) for each library (Figure 2-12). Subsequently, the libraries were pooled manually or using the Microlab® STAR automated liquid handling platform at 4nM. Pooled library quality control was performed using D1000 High Sensitivity ScreenTapes® and TapeStation® 2200 (see 2.5.2.2).

$$\text{Library Molarity (nM)} = \frac{\text{Library concentration (ng/}\mu\text{l)}}{\left(\frac{\text{Average base pair length}}{\text{Constant 1}} \right) + \text{Constant 2}} \times 10^6$$

Constant 1 = 607.4
Constant 2 = 157.9

Figure 2-12: The formula used for library molarity estimation

2.5.3.1.6 Sequencing

The pooled library was denatured in 20% sodium hydroxide (NaOH) and Trizma® hydrochloride (Sigma-Aldrich, USA). The denatured library was further diluted in HT1 (Hybridization Buffer) yielding a 20pM denatured library. A PhiX sequencing control was also used when sequencing. A 10nM PhiX stock was thawed and diluted to 4nM in Resuspension Buffer. The PhiX was denatured using 20% NaOH and Trizma® hydrochloride. For high output kits the library and PhiX were both diluted to 1.8pM in HT1. The corresponding figure for mid output kits was 1.5pM. In both cases, PhiX was combined with the library at a concentration of 1% of the final solution and loaded on to the sequencing cartridge. Single-ended sequencing was performed using NextSeq™ (Illumina, USA) flow cells and NextSeq™ 500 NGS platform. For FFPE a NextSeq™ HIGH 75 output flow cells (Illumina, USA) with 400 million read capacity (400 million reads per sample) were used. For PDO RNA a NextSeq™ MID or HIGH 150 output flow cells (Illumina, USA) with 130 or 400 million read capacity (130 or 400 million reads per sample) were used for sequencing. The data were directly uploaded to and securely stored in BaseSpace® (Illumina, USA) cloud-based computer servers until downstream bioinformatics analysis.

2.5.3.2 *Total RNA sequencing*

The previously quantified and quality checked RNA samples were diluted to 12.5ng/μl by hand. The RNA input was at 150ng per sample. A ribosomal RNA (rRNA) Depletion Kit (Human/Mouse/Rat) (New England BioLabs [NEB, USA]) was used as per the manufacturer's protocol for rRNA depletion (379). Library

preparation was performed by hand using NEBNext® Ultra™ II RNA Library Prep Kit for Illumina (NEB, USA) as per the manufacturer's instructions (380).

2.5.3.2.1 Probe hybridization

The normalised, diluted and ribo-depleted RNA was transferred to a 96-well PCR plate and kept on ice. The RNA/Probe master mix was prepared using the NEBNext® rRNA Depletion Solution and Probe Hybridization Buffer. The master mix was added to each sample and was mixed thoroughly with a multichannel pipette. The plate was sealed with an Adhesive PCR Film and pulse centrifuged. The samples were placed in a thermocycler set to the following settings (Table 2-12). The plate was removed from the thermocycler, pulse centrifuged and kept on ice, and immediately proceeded to the next step.

Table 2-12: Thermocycler settings for probe hybridization

Step	Temperature	Duration
1	95°C	2 minutes
2	22°C	0.1°C / second
3	10°C	Infinite hold

2.5.3.2.2 RNase H digestion

The RNase H master mix was prepared using NEBNext® RNase H, NEBNext® RNase H Reaction Buffer and nuclease-free water, on ice as per the manufacturer's protocol (380). This was added to each sample and mixed using multichannel pipette. The plate was sealed, then pulse centrifuged. The plate was transferred to a thermocycler set at 37°C with the lid set to 40°C. Following this incubation, the plate

was removed from the thermocycler, pulse centrifuged, left on ice and immediately proceeded to the next step.

2.5.3.2.3 DNase I digestion

The DNase I master mix was prepared using DNase I Reaction Buffer, DNase I and nuclease-free water, on ice, using manufacturer specified volumes and was added to each sample and mixed thoroughly with a pipette (380). The plate was sealed and incubated in a thermocycler using the same settings in 2.5.3.2.2). The plate was pulse centrifuged following the incubation, kept on ice, and immediately proceeded to purification using an ethanol and bead wash step by following the instructions in the manufacturer's protocol (380). Approximately 5ml eluted RNA was collected in a fresh PCR plate and was kept on ice.

2.5.3.2.4 RNA fragmentation and priming

A master mix was prepared using manufacturer supplied NEBNext® First Strand Synthesis Reaction Buffer and Random Primers using manufacturer specified volumes (380). The master mix was added to each sample and mixed thoroughly with a pipette. The plate was sealed with an Adhesive PCR Film and transferred to a thermocycler set 94°C for 15 minutes. The plate was pulse centrifuged and kept on ice.

2.5.3.2.5 Synthesis of the first strand cDNA

The first stand synthesis reaction was assembled by adding Nuclease-free water and NEBNext® First Strand Synthesis Enzyme Mix, on ice, as per the manufacturer's instruction using manufacturer specified volumes, and was added to each sample of fragmented RNA from 2.5.3.2.4 (380). The reagents were mixed thoroughly with a multichannel pipette. The plate was sealed, pulse centrifuged and was incubated in a

thermocycler programmed to the settings in Table 2-13. The plate was removed from the thermocycler kept on ice and immediately proceeded to second strand synthesis.

Table 2-13: Thermocycler settings for first strand cDNA synthesis

Step	Temperature	Duration
1	25°C	10 minutes
2	42°C	15 minutes
3	70°C	15 minutes
4	4°C	Infinite hold

2.5.3.2.6 Synthesis of the second strand cDNA

The second strand synthesis reaction mix was prepared using NEBNext® Second Strand Synthesis Reaction Buffer (10X), NEBNext® Second Strand Synthesis Enzyme Mix and nuclease-free water to the first strand synthesis product from 2.5.3.2.5. The reagents were added on ice and mixed thoroughly by pipetting. The plate was sealed and pulse centrifuged. The samples were incubated for 1 hour at 16°C with the heated lid set at 40°C. The plate was removed from the thermocycler, pulse centrifuged and immediately proceeded to purification with another bead and ethanol wash. Approximately 50ml of cDNA library was eluted at the end of purification and was transferred to a fresh PCR plate and was kept on ice.

2.5.3.2.7 cDNA library end prep

The reaction mix for this stage was assembled as a master mix using NEBNext® Ultra II End Prep Reaction Buffer and Enzyme Mix, and were added to the second strand synthesis product from the previous step. The reagents were mixed

thoroughly with the samples. The plate was sealed, pulse centrifuged and was transferred to a thermocycler set to the following programme. The plate was removed from the thermocycler, pulse centrifuged, kept on ice and immediately proceeded to adapter ligation.

Table 2-14: Thermocycler settings for cDNA library end prep

Step	Temperature	Duration
1	20°C	30 minutes
2	65°C	30 minutes
3	4°C	Infinite hold

2.5.3.2.8 Adaptor ligation

The NEBNext® Adaptor was diluted at a 5-fold dilution in ice-cold Adaptor Dilution Buffer and was kept on ice. The adaptor ligation reaction mix was prepared by adding NEBNext® Ligation Enhancer, NEBNext® Ultra II Ligation Master Mix and Diluted Adaptor to the end prepped cDNA from 2.5.3.2.7, on ice. The reagents were mixed thoroughly using a multichannel pipette. The plate was sealed with an Adhesive PCR Film and pulse centrifuged. The samples were incubated for 15 minutes at 20°C in a thermocycler. Following incubation, 3ml of USER Enzyme was added to the ligation mixture and was mixed well with a multichannel pipette. The plate was sealed, pulse centrifuged and incubated in a thermocycler for 15 minutes at 37°C with a heated lid set to 4°C. The latter incubation was followed by another purification step using beads and ethanol washes. Following purification, approximately 15ml of cDNA was eluted and transferred to a fresh PCR plate.

2.5.3.2.9 PCR enrichment of adaptor ligated cDNA

In this step the library was indexed and amplified by PCR. The reaction mix was prepared by adding NEBNext® Ultra II Q5 Master Mix and Index Primer Mix to the adaptor ligated cDNA from the previous step. NEBNext® oligos containing unique i7 indices were added to each sample and mixed thoroughly with a multichannel pipette. The plate was sealed, pulse centrifuged and transferred to a thermocycler with a heated lid set to 105°C and programmed to the following settings.

Table 2-15: Thermocycler settings for PCR enrichment of adapter ligated cDNA

Step	Temperature	Duration
1	98°C	30 seconds
2	98°C	10 seconds
(*10 cycles)	65°C	75 seconds
3	4°C	Infinite hold

**As per the manufacturer's recommendation for 100ng+ initial RNA input*

Immediately following PCR amplification and indexing the library was purified with a bead and ethanol washing step. Approximately 20µl cDNA library was eluted by adding 0.1X TE buffer provided with the kit and was transferred to a fresh PCR plate. The library was quantified using Qubit™ (see 2.5.2.1) and tested for quality using D1000 ScreenTapes® on the TapeStation® 2200 (see 2.5.2.2). By the end of library preparation, final purification step, quantification and quality control the cDNA library volume was approximately 17µl. The library was stored at -20°C until sequencing.

2.5.3.2.10 Sequencing

The methodology for library normalisation and pooling was the same as the one used for 3' RNA sequencing, described earlier. The libraries were pooled at 300nM. Following the manufacturer's instructions, the library was diluted and was loaded to the sequencing cartridge at a final concentration of 1.8pM. Sequencing was performed using NextSeq™ HIGH 150 flow cell (Illumina, USA) on the NextSeq™ 500 NGS platform (Illumina, USA). A PHIX control was prepared and used as per the manufacturer's direction. The data were stored in BaseSpace® until downstream bioinformatics analysis.

2.5.3.3 *Custom targeted colorectal gene panel*

The QIAseq® (Qiagen, Germany) custom targeted DNA panel was used to genomically characterise PDO models. The custom panel contained 30 colorectal cancer candidate genes including those that have been shown to demonstrate a role in radiotherapy sensitivity and CRC prognosis. Table 2-16 below and Appendix C lists the candidate genes and more information about the panel. The panel was designed to cover all +/- 10bp of coding exons of these genes as well as within 1000bp of the transcription start site (TSS) and featured 8bp unique molecular identifiers (UMI), allowed detection down to 0.1% variant allele frequency. The library preparation included the following stages: DNA fragmentation, library construction with unique molecular index (UMI) with sample indexing, target enrichment by single primer extension, sample indexing and amplification. The procedure for library preparation has been highlighted in Figure 2-13 below to generate a NGS ready library. All reagents required for the library preparation was supplied by the

manufacturer. The comprehensive [manufacturer's protocol](#) can be found on the Qiagen website (381).

Table 2-16: List of genes included in the targeted QIAseq® targeted DNA panel

Gene	Chromosome	Base pair region of interest (ROI)
<i>MSH6</i>	2	4183
<i>BRAF</i>	7	2660
<i>TCF7L2</i>	10	2425
<i>BCL9L</i>	11	4580
<i>TP53</i>	17	1383
<i>B2M</i>	15	413
<i>TGIF1</i>	18	1365
<i>NRAS</i>	1	610
<i>PIK3CA</i>	3	3407
<i>GNAS</i>	20	4186
<i>SMAD4</i>	18	1769
<i>BMPR2</i>	2	3247
<i>PTEN</i>	10	1302
<i>RPL22</i>	1	619
<i>SMAD2</i>	18	1504
<i>ATM</i>	11	9791
<i>POLE</i>	12	7351
<i>ARID1A</i>	1	7058
<i>FBXW7</i>	4	2758
<i>RNF43</i>	17	2442
<i>MLH1</i>	3	2461
<i>MSH2</i>	2	3107
<i>KRAS</i>	11	737
<i>ELF3</i>	1	1256
<i>POLD1</i>	19	3662
<i>CTNNB1</i>	3	2486
<i>ZFP36L2</i>	2	1505
<i>APC</i>	5	8857
<i>SOX9</i>	17	1560
<i>ACVR2A</i>	2	1652

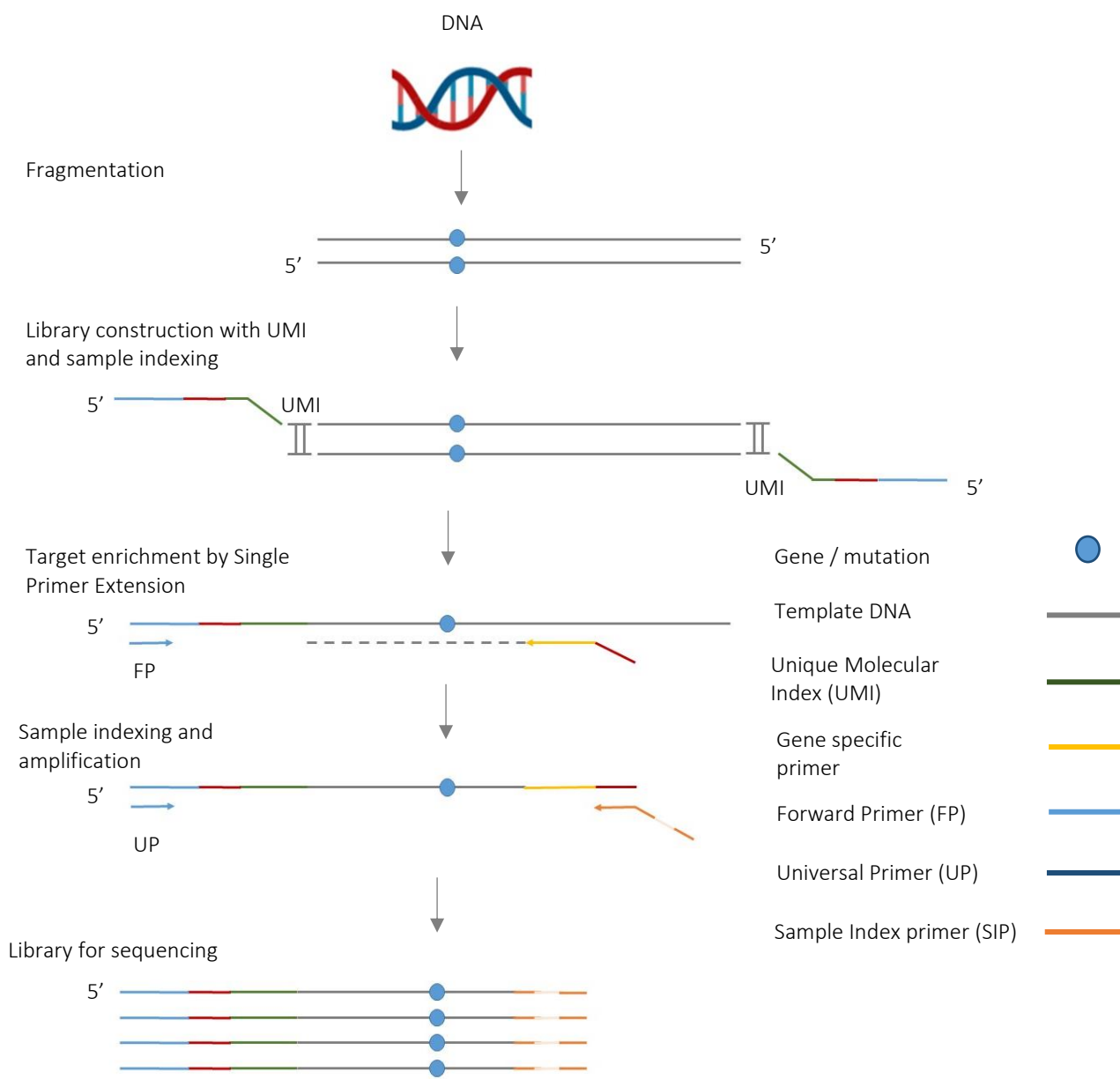


Figure 2-13: QIAseq® targeted DNA sequencing panel workflow

2.5.3.3.1 DNA fragmentation

Forty nanograms of DNA from each of the 6 CRC PDOs were used in this library preparation protocol (manufacturer recommended range 10-40ng). DNA was kept on

ice during the preparation stage and added to nuclease-free H₂O on a 96-well PCR plate (Bio-Rad, USA) at the volumes specified in Table 2-17 below.

Table 2-17: Reaction mix for fragmentation, end-repair and A-addition – QIAseq® targeted DNA panel

Sample	Conc.	DNA vol. (for 40ng)	Fragmentation Buffer, 10x	FERA Solution	Nuclease-free H₂O	Total vol.
884	15.00	2.67µl	2.5µl	0.75µl	14.08µl	20µl
411	13.5	2.96µl	2.5µl	0.75 µl	13.79µl	20µl
653	8.35	4.79µl	2.5µl	0.75 µl	11.96µl	20µl
389	14.25	2.81µl	2.5µl	0.75 µl	13.94µl	20µl
064	13.25	3.02µl	2.5µl	0.75 µl	13.73µl	20µl
557	12.03	3.33µl	2.5µl	0.75 µl	13.42µl	20µl

Conc. - concentration, vol. – volume

A master mix was prepared containing Fragmentation Buffer 10x and FERA solution for n+2 reactions where n was the number of samples. A 3.25µl volume of this master mix was added to each sample as well as 5µl of Fragmentation Enzyme mix to each reaction and mixed with pipette. The plate was sealed with an Adhesive PCR Film (Scientific Laboratory Supplies, UK) and left on a thermocycler prepared as per the settings displayed on Table 2-18.

Table 2-18: Thermocycler settings for DNA fragmentation, end-repair and A-addition – QIAseq® targeted DNA panel

Step	Temperature	Time
0	4°C	Pre-cool step
1	4°C	1 minute
2	32°C	24 minutes
3	72°C	30 minutes
4	4°C	Infinite hold

A heated lid on the thermocycler was used in this stage.

2.5.3.3.2 Adapter ligation

The plate was removed from the thermocycler and transferred on to ice. The following steps were all completed on ice until the next thermocycler step. The adapter ligation master mix was prepared according using the reagents and volumes specified on Table 2-19, and 15µl was added to each reaction containing the fragmented DNA from the previous stage and mixed with a multichannel pipette. A unique IL-N7 adapter (2.8µl) was added to each reaction. The highly viscous Ligation solution (7.2µl) was added to each reaction and gently mixed with a multichannel pipette.

Table 2-19: The master mix for adapter ligation

Component	Volume / reaction	Master mix for n+2 samples
Ligation buffer 5x	10µl	80µl
DNA Ligase	5µl	40µl

The plate was sealed with an Adhesive PCR Film and pulse centrifuged to ensure the liquid collected at the bottom of wells. The plate was transferred to a thermocycler set at 20°C (without a heated lid) for 15 minutes. Subsequently, an ethanol and bead wash was performed as per the manufacturer's directions to clean up the DNA after adapter ligation.

2.5.3.3.3 Target enrichment

The target enrichment master mix was prepared as described in Table 2-20.

Table 2-20: The master mix for target enrichment

Component	Volume / reaction	Master mix for n+2 samples
TEPCR buffer, 5x	4µl	28µl
QIAseq® targeted DNA panel	5µl	40µl
IL-Forward primer	0.8µl	6.4µl

The master mix (9.8µl) followed by 0.8µl of HotStarTaq® DNA Polymerase was added to each reaction on the PCR plate and were mixed several times using a multichannel pipette. The plate was sealed with an Adhesive PCR Film, pulse centrifuged and transferred to a thermocycler at the settings as described on Table 2-21.

Table 2-21: Thermocycler settings for target enrichment (1500-12,000 primers/tube)
– QIAseq® Targeted Panel

Step	Temperature	Time
0	95°C	Pre-heat step
1	95°C	13 minutes
2	98°C	2 minutes
3	98°C	15 seconds
(6 cycles)	65°C	15 minutes
4	72°C	5 minutes
5	4°C	5 minutes
6	4°C	Infinite hold

The plate was removed from the thermocycler, pulse centrifuged and immediately proceeded to an ethanol and bead wash step, following the steps as detailed in the [manufacturer's protocol](#) (381). The library preparation was paused at the end of this stage and the library was stored at -21°C in the PCR plate overnight at this point.

2.5.3.3.4 Universal PCR

The next day, the library was thawed on ice and pulse centrifuged. 1.6µl of nuclease free H₂O was added to each sample. Approximately 10µl of the library was transferred to a unique adapter row on the IL-S5 adapter plate. The library was mixed with the adapter in the plate and retransferred to the PCR plate.

Subsequently, 5µl of UPCR Buffer, 5x and 1µl of HotStarTaq® DNA Polymerase was added to each reaction. The reactions were mixed several times with a multichannel pipette. The plate was sealed with an Adhesive PCR Film, pulse centrifuged and transferred to a thermocycler at the settings as described on Table 2-22.

Table 2-22: Thermocycler settings for Universal PCR – QIAseq® targeted DNA panel

Step	Temperature	Time
0	95°C	Pre-heat step
1	95°C	13 minutes
2	98°C	2 minutes
3	98°C	15 seconds
(21 cycles)*	60°C	15 minutes
4	72°C	5 minutes
5	4°C	5 minutes
6	4°C	Infinite hold

**Given the presence of 1500-3072 primers per pool 21 cycles was chosen as per the manufacturer's guidance*

Following the reaction in the thermocycler, the plate was pulse centrifuged and was cleaned up using an ethanol and bead wash by following the steps in the [manufacturer's protocol](#) (381). The library was quantified using Qubit™ (see 2.5.2.1) and tested for quality using D1000 ScreenTapes® on the TapeStation® 2200 (see 2.5.2.2). At the end of this library preparation, final purification step, quantification and quality control the DNA library volume was approximately 25µl. The library was stored at -20°C until sequencing.

2.5.3.3.5 Sequencing

The libraries were normalised and diluted to 4nM using nuclease free H₂O and equal volumes of the libraries were pooled at 4nM to ensure uniform coverage across the libraries. A quality control step of the pooled library was performed using D1000 High

Sensitivity ScreenTapes® and TapeStation® 2200 (see 2.5.2.2). The library was denatured and diluted in 20% NaOH yielding a 20pM denatured library in 1 mM NaOH. The library was further diluted in pre-chilled HT1 (Hybridization Buffer) to obtain a final library input concentration of 12pM. QIAseq® A Read 1 primer was diluted in HT1 to obtain a final concentration of 0.5µM and 18µl of which was also loaded on to the sequencing cartridge. Manufacturer provided Read 1 primer was used instead of PhiX sequencing control. Sequencing was performed on a MiSeq™ (Illumina, USA) NGS platform using MiSeq™ v2, 300 cycle flow cell paired-end at 500X coverage. The data were stored in BaseSpace® until downstream bioinformatics analysis (see 2.5.4.6).

2.5.4 Bioinformatics

2.5.4.1 Partek Flow®: Raw gene counts from 3' RNA sequencing

The NGS output FASTQ files stored in BaseSpace® were downloaded to a local computer and uploaded to Partek Flow® (Figure 2-14). A pipeline developed by Partek for Lexogen QuantSeq data analysis was used to obtain raw gene counts. The assembly used was Homo sapiens (human) – hg19 and aligner index was Whole genome (Administrator). Gene/feature annotation was set to Ensembl

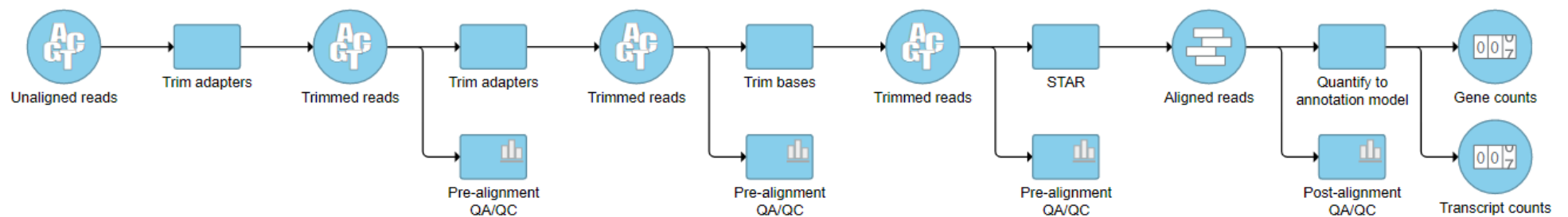


Figure 2-14: Lexogen QuantSeq data analysis pipeline on Partek Flow®

Adapters were trimmed from the 3'prime end using manufacturer provided adapter sequences. Spliced Transcripts Alignment to a Reference (STAR) was performed followed by quantification to an annotation model to obtain raw gene and transcript count. Detailed parameters used in the first, second trim adapter stages, trim bases stage, STAR stage and quantify to annotation model stage can be found in Appendix D. Quality assurance - QA and quality control - QC analyses were performed after each step.

2.5.4.2 Partek Flow®: Raw gene counts from Total RNA sequencing

The NGS output FASTQ files stored in BaseSpace® were downloaded to a local computer and uploaded to Partek Flow® (Figure 2-15). A pipeline developed by Partek Flow® for Illumina Total RNA sequencing data analysis was used to obtain raw gene counts. The assembly used was Homo sapiens (human) – hg19 and aligner index was Whole genome (Administrator). Gene/feature annotation was set to Ensembl Transcripts release 75 (Administrator). The noise reduction filter was set to exclude features where maximum ≤ 1.0 .



Figure 2-15: Illumina® Total RNA Sequencing data analysis pipeline on Partek Flow®

Spliced Transcripts Alignment to a Reference (STAR) was performed followed by quantification to an annotation model to obtain raw gene counts. Detailed parameters used in each of these stages can be found in Appendix E.

2.5.4.3 Partek Flow®: Normalisation, principal component analysis and differential gene expression analysis

The gene counts were normalised by adding 0.0001 to each count in each sample following for 3' RNA sequencing and 1.00 was added following total RNA sequencing. Exploratory analysis was performed using principal component analysis (PCA) function with the number of principal components set to "All" and features contribute set to "equally." Differential expression analysis was performed using

Gene Specific Analysis (GSA) pipeline on Partek Flow®. This method uses a log-normal with shrinkage model (382). It has been previously published as a valid method for differential expression analysis using RNA sequencing data (383), and is recommended for use by the manufacturer (Lexogen) of the 3' RNA sequencing library preparation kit used in these experiments (384). The differentially expressed genes with their corresponding fold change, nominal p -value and false discover rate (FDR) corrected q -values using FDR step-up method by Benjamini-Hochberg (385), were obtained. The results were filtered to display excluding samples with a FOLD CHANGE between -1.5 to 1.5 and a nominal p -value of less than 0.05 was assigned as the level of statistical significance. The differentially expressed gene data were downloaded as CSV files and securely stored. The workflow has been summarised below (Figure 2-16).

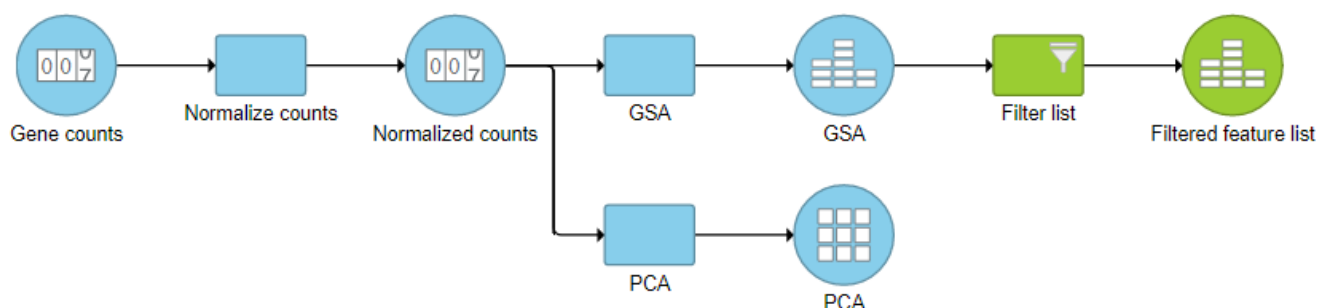


Figure 2-16: Workflow for normalisation, principal component analysis and differential expression analysis on Partek Flow®

GSA – Gene specific analysis, PCA – principal component analysis

2.5.4.4 DEBrowser: Normalisation, principal component analysis and DESeq2 differential expression analysis.

Raw gene counts following RNA sequencing were obtained using Partek Flow® (see 2.5.4.1 or 2.5.4.2). The gene counts were downloaded as comma separated values

(CSV) files with features on rows. One CSV file was prepared containing the gene names (rows) and gene counts for all the sample (in columns) and another containing sample metadata. RStudio Desktop V1.3 (RStudio, USA) running R V4.0.2 (r-project.org, USA) was launched. Bioconductor V3.13 was installed using the following script found at <https://www.bioconductor.org/install/>.

```
if (!requireNamespace("BiocManager", quietly = TRUE))
  install.packages("BiocManager")
BiocManager::install(version = "3.13")
```

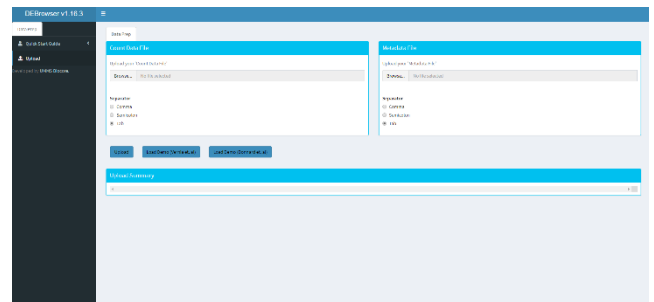
DEBrowser V.1.16.3 was installed using launched using the following code found at [https://bioinfo.umassmed.edu/pub/debrowser/debrowser-](https://bioinfo.umassmed.edu/pub/debrowser/debrowser-docs/docs/build/html/local/local.html)

[docs/docs/build/html/local/local.html](https://bioinfo.umassmed.edu/pub/debrowser/debrowser-docs/docs/build/html/local/local.html).

```
source("https://www.bioconductor.org/biocLite.R")
biocLite("debrowser")

library(debrowser)

startDEBrowser()
```



The CSV files were uploaded using the DEBrowser interface. Within DEBrowser, normalisation was performed and principal component analysis was performed. Differential expression analysis was also performed within DEBrowser typically using DESeq2 (386). DeSeq2 was installed earlier on R using the following script found at <https://bioconductor.org/packages/release/bioc/html/DESeq2.html>

```
BiocManager::install("DESeq2")
```

Fold-change and adjusted q-value cut-offs were used to filter the data. Upregulated and downregulated genes were downloaded separately as CSV files.

2.5.4.5 Gene Set Enrichment Analysis (GSEA)

2.5.4.5.1 GSEA using Broad Institute software

Raw RNA sequencing gene count data were downloaded from Partek Flow® with features on rows. The file was imported on to Excel and transformed into the format required for GSEA and saved as .gct file (387). A .cls format file was created with the phenotype data using Notepad text following in the instructions published by Kuehn et al (388). The GSEA software (Broad Institute, USA) was downloaded (source: <http://www.gsea-msigdb.org/gsea/downloads.jsp>) and installed on to a desktop computer running Windows 64-bit (Microsoft Corporation, USA). The GSEA software was launched and the “Load Data” option was selected to link expression data (.gct file) and phenotype data (.cls file) onto the software. Run GSEA analysis option was selected and largely the default options were chosen. The gene sets were chosen from the Gene Matrix (from website) tab. Analyses were run against Hallmarks, KEGG and Oncogenic Signatures gene sets. The collapse / remap to gene symbols option was set to “No_Collapse.” Metric for ranking genes was chosen as Signal2Noise where sample size included at least three per analysed group and difference_of_classes where less than three samples per group. Plot graphs for the top 30 gene sets was selected. Run command option generated GSEA results in the pre-set target directory.

2.5.4.5.2 RStudio: MSigDB and Clusterprofiler – Gene Set Enrichment Analysis

The raw gene counts were obtained from PartekFlow®. The data files were formatted within R into the desired format. DESeq2 package on R was used for differential expression analysis. ENSEMBL gene name and EntrezID was added to the result. GSEA was performed using Hallmark, KEGG and Oncogenic Signatures

collections using MSigDbr and Clusterprofiler packages on R. Pathview and GGPUBR packages were used to design dot plots representing enriched pathways. The complete R Script can be found in Appendix F.

2.5.4.6 Custom targeted DNA panel (QIASeq®) sequencing data analysis

Data analysis was performed using the Biomedical Genomics Workbench (Qiagen, Germany) bioinformatics software and manufacturer designed custom workflow. The custom workflow was installed as per the manufacturer's instructions. Data stored on BaseSpace® was downloaded to a local computer and imported to BGW. The primer metadata were uploaded and Human hg19 reference sequence was used. The step by step software wizard was used to run the analysis to generate an excel file containing a list of genes with variants passing filters for each sample. The mutations were compared individually to identify potential pathological mutations by using GeneGlobe (Qiagen, Germany) and ClinVar (<https://www.ncbi.nlm.nih.gov/clinvar/>, National Library of Medicine, USA)

2.5.4.7 Visual representation of bioinformatics results

Volcano plots generated either using Partek Flow® or using EnhancedVolcano package (Appendix G) on RStudio. Partek Flow® was also used for hierarchical clustering and to generate heatmaps following 3' RNA sequencing data analysis. Samples and features were clustered with average linkage as clustering distance metric and Euclidean set as point distance metric (Appendix H). ComplexHeatmap

and Oncoprint packages on RStudio was used to generate heatmaps from QIASeq® data analysis (Appendix I).

2.6 Proteomics methodology

2.6.1 Protein lysis and extraction

Media was removed from the 6 x 6 Corning cell culture plate containing the experimented cells. Each well was gently washed with 1-2ml PBS (Life Technologies, UK) and all fluid removed without disturbing the cells. Up to 100µl of Pierce® RIPA cell lysis buffer (Thermo Fisher Scientific, USA) and Protease/Phosphatase Inhibitor Cocktail (100X) (Cell Signalling Technology, USA) kept at a temperature of 4°C, was added in a final concentration of 1 in 100, to each well of the experiment plate. Cells were extracted from the plate on ice using a cell scraper and pipetted into autoclaved 1ml Eppendorf tubes. The extracted cells were boiled to 100°C in a heat block for 5 minutes. The tubes containing protein was immediately transferred on to ice and stored at -80°C.

2.6.2 Protein sonication

The protein was thawed on ice. Protein sonication was performed using Soniprep 150 (Sanyo, Japan) sonication device at maximum sonication frequency for a total of 20 seconds for each Eppendorf tube containing protein, in 10 second intervals with a gap on ice to prevent overheating of the tubes. Following sonication, the samples were centrifuged at maximum speed at 4°C for five-minutes using a micro-centrifuge.

The supernatant was transferred to fresh tubes without disturbing the pellet and kept on ice.

2.6.3 Protein quantification

Quantification was performed immediately after the sonication process described above. Pierce© BCA Protein Assay Kit (Thermo Fisher Scientific, USA) was used for the quantification as per the manufacturer's protocol

[https://assets.thermofisher.com/TFS-](https://assets.thermofisher.com/TFS-Assets/LSG/manuals/MAN0011430_Pierce_BCA_Protein_Asy_UG.pdf)

[Assets/LSG/manuals/MAN0011430_Pierce_BCA_Protein_Asy_UG.pdf](https://assets.thermofisher.com/TFS-Assets/LSG/manuals/MAN0011430_Pierce_BCA_Protein_Asy_UG.pdf) using a luminescence reading from samples and standards on a protein assay standard curve. The Working Reagent (WR) was combined with BCA reagent A in a concentration of 50 to 1 (e.g., 120µl of BCA Reagent A to 6mls of WR). This was added to each sample or standard in a concentration of 1:20 (e.g. 190µl of WR and 10µl of sample or standard). The standards had been previously prepared as per the manufacturer's guidance from supplied neat album and diluted to concentrations ranging from 2000µg/ml to 25µg/ml in Pierce© RIPA cell lysis buffer, the same buffer used in protein extraction. A 0µg/ml standard containing wholly of RIPA buffer was used to determine background luminescence reading. The samples and standards were added to a WR reagent in a 96-well flat round bottom plate and incubated for 37°C for 30mins. A reading was obtained per each standard and sample using the PIERCE450 protocol on the EnSpire® luminescence plate reader. A standard curve was generated using the manufacturer's guidance

<https://assets.thermofisher.com/TFS-Assets/LSG/Application-Notes/TR0057-Read-std-curves.pdf> on Excel (Microsoft, USA) and protein concentrations calculated in

ug/ml. A working example can be found in Appendix J. Quantified protein was either stored at -80°C or proceeded to western blots.

2.6.4 Western blots

The protocols followed in the Western Blot technique were as per those available on the Abcam (Cambridge, UK) website (<https://www.abcam.com>). Widely used solutions in western blots such as concentrated Tris-buffered saline (TBS), TBS (0.1%) with Tween 20- commonly known as TBST and mild stripping buffer were prepared according to the recipes available on the Abcam website (<https://www.abcam.com/protocols/buffer-and-stock-solutions-for-western-blot#TBS-10x>).

2.6.4.1 *Preparing the solutions required in subsequent steps*

2.6.4.1.1 Concentrated TBS 10x

Concentrated TBS 10x was prepared by adding 24g of Trizma® hydrochloride, 5.6 g Trizma® base (Sigma-Aldrich, USA) and 88 g sodium chloride (Thermo Fisher Scientific, USA) to 900 ml diH₂O. The reagents were allowed time to fully dissolve on a magnetic stirrer. The pH was adjusted to 7.6 with real-time pH monitoring using a digital pH meter and adding hydrochloric acid (HCL, J.T. Baker®, USA) as required. The final solution volume was brought up to 1L by adding further diH₂O.

2.6.4.1.2 TBST

TBS (0.1%) with Tween 20 was prepared by adding 100ml of TBS 10x prepared above was added to 900ml of diH₂O and 1ml of Tween 20 (Scientific Laboratory Supplies, UK) in a final volume of 1L. The final solution pH was checked using a digital pH meter.

2.6.4.1.3 Mild stripping buffer

Mild stripping buffer was prepared by adding 15g of Glycine (Sigma-Aldrich, USA), 1g of Sodium dodecyl sulphate (Sigma-Aldrich, USA) and 10mL Tween 20 to 800mL of diH₂O. Reagents allowed time to dissolve on a magnetic stirrer. The pH was adjusted to 2.2 by adding HCL acid with real time pH monitoring using a digital pH meter. The final volume brought up to 1L by adding further diH₂O.

2.6.4.2 *Running the gel*

Ten well, 30µl 10% Mini-PROTEAN TGX Precast Protein Gels (Bio-Rad, USA) were submerged in running buffer comprising of 900ml diH₂O and 100ml 10x Tris/Glycine/SDS buffer (Bio-Rad, USA) in a Mini Trans-Blot® Cell (Bio-Rad, USA). The protein was loaded at a concentration of 20µg in 20% lane marker reducing buffer (Thermo Fisher Scientific, USA) and nuclease free sterile H₂O in a final total volume of up to 20-30µl per sample. The samples were prepared in strip tubes and boiled for 5 minutes in a thermocycler preheated to 100°C under a heated lid. Precision Plus Protein Western C Standards (Bio-Rad, USA) protein ladder and a phospho-AKT positive control (AKT control cell extracts – 9273S, Cell Signalling Technology, USA) were added to 2 of the 10 wells in each gel. Subsequently, the samples were carefully loaded on to each of the wells of the gel with a pipette

ensuring - no carry-over. A voltage generator was used to run the gel initially for 10 minutes at 80 Volts (V) followed by 140V for a further 40-45 minutes.

2.6.4.3 The transfer

The transfer buffer was prepared with 100ml Tris/Glycine 10x buffer (Bio-Rad, USA), 200ml of 100% methanol (VWR Chemicals, USA) and 700ml diH₂O. The run-gel was carefully removed from the precast plastic cartridge into the transfer buffer. A 0.45µm Amersham™ Hybond™ PVDF blotting membrane (GE Healthcare, USA) was used for the transfer, cut to the necessary dimensions. The membrane was initially submerged in 100% methanol for approximately 1-2 minutes to activate the membrane. The gel was carefully placed on the membrane between 6 layers of filter paper and 2 x wire mesh in a transfer cassette. The transfer was performed using a Mini Trans-Blot® Cell device at 4°C with the application of 90V over a 90-minute period using a voltage generator.

2.6.4.4 Primary antibody

Immediately following the transfer, the membrane was carefully extracted from the transfer apparatus by holding the edge with forceps and transferred to 50ml of 5% Bovine Serum Albumin (BSA, Roche, Switzerland) in TBST for phospho-proteins; 5% milk (Marvel, UK) in TBST for non-phospho-proteins; to facilitate non-specific binding site blockade. The membrane was left in the blocking reagents on a gentle shaker for up to 1 hour at room temperature. Subsequently, the membrane was transferred to a 50ml Falcon tube containing the primary antibody diluted in TBST or

milk as illustrated in Table 2-23. The membrane was exposed to the primary antibody for at least 12 hours at 4°C on a gentle roller.

Table 2-23: Primary antibodies used in western blots

Antibody Target	Manufacturer (ID)	Source	Concentration	Diluent
Phospho-AKT (Ser473)	Cell Signalling Technology (4060S)	Rabbit	1:1000	5% BSA in TBST
AKT	Cell Signalling Technology (9272S)	Rabbit	1:1000	5% BSA in TBST
GAPDH (D16H11)	Cell Signalling Technology (5174S)	Rabbit	1:1000	5% milk in TBST

2.6.4.5 Secondary antibody

The following were all performed at room temperature. The membrane was removed from the primary antibody and transferred to TBST for 5 minutes on a gentle shaker to wash off any residual antibody. The TBST was discarded at the end of the five minutes. The wash-step was repeated twice (total three times). Whilst the wash was underway the secondary antibody was prepared in 5% milk in TBST (approximately 30ml volume). Peroxidase-AffiniPure Goat Anti-Rabbit IgG (H+L) (Jackson ImmunoResearch Laboratories INC, USA) at a concentration of 1:1000 was the secondary antibody of choice. Precision Protein™ StrepTactin-HRP Conjugate 1:3000 was added to detect the protein ladder. The latter step was only performed following the first primary antibody exposure of the membrane. This step was not repeated in any subsequent secondary antibody steps for a given membrane

undergoing western blotting. The membrane was exposed to the secondary antibody for up to 1 hour at room temperature on a gentle shaker. After the 1-hour the secondary antibody with diluent was discarded and the membrane was washed in TBST for three five-minute cycles.

2.6.4.6 Chemiluminescence

The following were all performed at room temperature. The Pierce™ ECL Western Blotting Substrate reagents (Thermo Fisher Scientific, USA) was used for chemiluminescence detection. Equal parts of reagent 1 and 2 were mixed in a 15ml Falcon tube and pipetted on to membrane (approximately 1ml per 12cm² surface area of membrane). ChemiDoc™ MP Imaging System (Bio-Rad, USA) was used for chemiluminescence blot (647SP, No Light, Manual, 2x2). Exposure times included either 60 seconds or 3 minutes for blots. Care was taken to ensure the membrane does not dry out during this time by ensuring adequate coverage of the membrane by reagents 1 and 2.

2.6.4.7 Membrane stripping

The following were all performed at room temperature. Following chemiluminescence the membrane was transferred to a volume of mild stripping buffer in a flat container and left on a shaker for 15-25minutes. The membrane was washed once with PBS and then kept in PBS on a shaker for 5 minutes. The membrane was subsequently washed with TBST and kept in TBST on a shaker for a further 5 minutes. The membrane was now ready for re-blocking and primary antibody once more and therefore, proceeded to section 2.6.4.4. A maximum of 3

such cycles were performed per membrane given the highly sensitive nature of the targets probed.

2.6.4.8 Image analysis and densitometry

Images were stored on Windows (Microsoft, USA) as .tiff files and processed for presentation using PowerPoint (Microsoft, USA) and Word (Microsoft, USA). Image J software (<https://imagej.nih.gov/ij/>, National Institute of Health, USA) was used for image densitometry analysis. Data were collated and a student t-test was performed using Excel (Microsoft, USA).

2.7 Immunohistochemistry methodology

2.7.1 Patient derived organoids

2.7.1.1 Fixing patient derived organoids

PDOs were cultured in 24-well plates for up to 5 days. The PDOs were extracted from a minimum of 4-6 wells of a 24-well plate. The Matrigel® was dissolved in OHS by following the same protocol as per PDO passage as described in section 2.4.2. Following centrifuge, the supernatant was discarded, and the pellet was gently dissolved in 1 ml of 4% Pierce™ 16% Formaldehyde (Thermo Fisher Scientific, USA) and left for 1 hour at room temperature for fixation. At the end of the 1-hour 10mls of PBS was added to inactivate the formalin. The solution was centrifuged at 400 x g for 4mins at room temperature. The supernatant was discarded. A further PBS wash was performed with 10mls of PBS and centrifuged under the same parameters as before. Following the second centrifuge the pellet was dissolved in

1ml of PBS and transferred to an Eppendorf tube. The Eppendorf tube was centrifuged at 200 x g for 5 minutes in a microcentrifuge. The supernatant was discarded. 2% Agarose (Sigma-Aldrich, USA) was prepared and kept in Eppendorf tubes on a heat block at 65°C. The pellet was dissolved in 150µl of 2% Agarose and left to set. The fixed PDOs in agarose pellet was carefully removed from the Eppendorf tube and transferred to a cassette for fixing. The cassette was stored in PBS at 4°C and paraffin embedding performed within a day or two.

2.7.1.2 Paraffin embedding

The cassette containing the PDO pellet in agarose was dehydrated in 70% ethanol for 1 hour, 90% ethanol for 1 hour and 100% ethanol for 1 hour. The cassette was immersed in HistoClear (Geneflow, UK) for a total of 2 hours with two further changes of the HistoClear solution during this time. The paraffin embedding was performed on a HistoStar paraffin embedding station (Thermo Fisher Scientific, USA). The oven was set to 58°C and pellet in agarose was immersed in molten paraffin in a stainless-steel mould for a total of 2 hours. The cassette was then immersed in molten paraffin and attached to the top of the stainless-steel mould. The block was cooled for several hours. Once solidified the block containing the PDOs in agarose embedded to cassette was removed from the stainless-steel mould, labelled, and stored at room temperature wrapped in foil for future use.

2.7.1.3 Obtaining sections

Sections were obtained from the FFPE PDOs in agarose gel using a microtome. Sections were examined under optical microscopy to identify area containing the PDO pellet. The sections were placed on glass slides and proceeded to staining.

2.7.2 Staining FFPE sections (Common procedure PDO and fresh tissue sections)

2.7.2.1 Haematoxylin and Eosin

The primary tumour section tissues and PDO tissue on slides were washed in Histoclear, 100%, 90% and 70% ethanol consecutively in this order for 5 minutes for each reagent. The sections were transferred to diH₂O for 2 minutes. Staining with Haematoxylin (Sigma Aldrich, USA) for 30 seconds was performed. The duration was increased up to 10 minutes if stronger stain was required. Following the Haematoxylin stain the sections were run under tap water till clear. A swift wash in 1% acid alcohol (12ml 5M HCL and 488ml of 70% ethanol was performed and washed under tap water for 5 minutes. Subsequently, Eosin (Sigma Aldrich, USA) staining was performed for 3 minutes. The slide was washed with diH₂O for 5 seconds. Washes were performed with 70%, 90%, 100% ethanol and Histoclear consecutively in this specified order for 1 minute for each reagent. The cover slip was mounted with DPX and the stained sections on slides were visualised under light microscopy.

2.7.2.2 Pan-Cytokeratin and CDX-2 staining

The DAKO EnVision™+ System (Agilent, USA) with Peroxidase (DAKO EnVision™+ System, HRP) kits and all manufacturer supplied reagents were used. Primary pan-Cytokeratin (ab27988, Abcam PLC, UK) and CDX2 (ab157524, Abcam PLC, UK) antibodies were used to detect antigens in sections from FFPE PDO and primary tissue sections under light microscopy. The protocol used was as follows: The slides were placed in an oven overnight at 60°C. The following day the slides were dewaxed with a HistoClear wash for five minutes and dehydrated using 100%, 90% and 70% ethanol washes, sequentially in this order with 5 minutes for each wash. The slides were washed in diH₂O for 3 minutes. The slides were placed in pre-heated antigen retrieval solution (Abcam PLC, UK) in a pressure cooker for 10 minutes at full pressure. Following this incubation slides were left to cool down to room temperature (up to 10 minutes) and the pressure was released. The pressure cooker was further cooled down for 20-30mins under tap water.

The slides were removed from the pressure cooker and rinsed with PBS twice. Using a PAP pen (Abcam PLC, UK) the area of staining required was drawn on the slides. The slides were incubated in the DAKO peroxidase block for 10mins in a humidified chamber. The slides were removed and washed three times in PBS (3 minutes per wash). The serum block was applied (~100ul/slide) and incubated for 30 mins in a humidified chamber. Any excess was cleared by blotting with tissue paper. The slides were subsequently stained with primary antibody for 1 hour. The antibody dilution and preparation are described in Table 2-24.

Table 2-24: Primary antibodies used for immunohistochemistry

Antibody Target	Manufacturer (ID)	Source	Concentration	Diluent
Pan-Cytokeratin	Abcam PLC (ab27988)	Goat	1:500	DAKO antibody diluent
CDX2	Abcam PLC (9272S)	Goat	1:100	DAKO antibody diluent

Following the primary antibody stain the slides were washed in PBS four times (3-minutes per wash). The slides were incubated in DAKO labelled polymer for 30 minutes in a humidified chamber. After another PBS wash, DAKO DAB was applied for 5 to 10 minutes. Subsequently the slides were washed with diH₂O. The slides were counterstained in haematoxylin for approximately 30 seconds. The slides were rinsed in tap water. They were quickly immersed in acid alcohol and removed. The slides were washed again with diH₂O for a further 5 minutes. The slides were rehydrated with 70%, 90%, 100% ethanol and HistoClear washes sequentially in this order (1 minute per wash). The cover slip was mounted with DPX and the stained sections on slides were visualised under light microscopy.

2.8 Other laboratory methods

2.8.1 Optical microscopy

Optimal microscopy was performed using EVOS™ XL Core microscope and imaging system (Thermo Fisher Scientific, USA). Cell and PDO cultures were visualised at

10x magnification under bright field microscopy. High resolution images were captured using the system and were stored as .jpg files.

2.8.2 Mycoplasma testing

The EZ-PCR™ Mycoplasma Test Kit (Biological Industries, Israel) was used for mycoplasma testing of all PDO lines and cell line used for experiments. The media was collected from culture plate or flasks in separate tubes for each line. A sample of 1ml was taken per line and was processed as per the manufacturer's protocol (389). Amplification of any mycoplasma DNA was performed by PCR amplification on a thermocycler using the following settings (Table 2-25).

Table 2-25: Thermocycler settings for EZ-PCR Test Kit Mycoplasma DNA expansion

Step	Temperature	Time
0	4°C	Pre-cool step
1	4°C	1 minute
2	32°C	24 minutes
3	72°C	30 minutes
4	4°C	Infinite hold

The amplified products were analysed using gel electrophoresis in 2% agarose gel and a voltage generator. A positive control was also used. The gel was imaged using a U:Genius³ (Syngene, India) gel imaging system. The lack of a band at the level of the positive control across any of the lanes that had contained media from samples was classed as a negative mycoplasma test.

2.9 A list of all reagents and kits used

Table 2-26: A table listing all reagents and reagent kits used

Name	Catalogue / Product Number	Manufacturer	Headquarters
10% Mini-PROTEAN TGX Precast Protein Gels, 10-well, 30 Microlitre	4561033	Bio Rad	USA
5-fluorouracil	A7686,005	Appllichem Panreac	USA
Advanced DMEM/F12	12491-023	GIBCO	USA
Agarose	A7174-10G	Sigma Aldrich	USA
AKT antibody	9272S	Cell Signalling Technology	USA
AllPrep DNA/RNA Mini Kit (50)	80204	Qiagen	Germany
Apitolisib (GDC-0980)	A11023	Adooq Bioscience	USA
Bovine Serum Albumin (BSA) FRACTION V, 100G	10 735 086 001	Roche	Switzerland
CellTiter-Glo 2.0 Assay - 1 x 100ml bottle	G9242	Promega	USA
CellTiter-Glo® 3D Cell Viability Assay, 10 x 10ml	G9682	Promega	USA
Collagenase		Sigma-Aldrich	USA
Dactolisib (BEZ 235)	S1009	Selleckchem	USA

Dako antibody diluent with background reducing components	S3022	Agilent	USA
Dako EnVision Dual Link System-HRP mouse/rabbit:	#K4063	Agilent	USA
Dako Liquid DAB+ substrate chromogen system	#K3467	Agilent	USA
DAKO peroxidase block	#S2023	Agilent	USA
Dako Target Retrieval Solution (pH6)	#S1700	Agilent	USA
Dimethyl sulfoxide (DMSO)	12611P	Cell Signalling Technology	USA
Dispase		Thermo Fisher Scientific	USA
DMEM	41965-039	GIBCO	USA
DPX	06522	Sigma Aldrich	USA
Dried skimmed milk powder	5 000183 932780	Marvel	UK
Dulbecco's Phosphate Buffered Saline, M0 (PBS0)	D8537	Sigma-Aldrich	USA
Eosin	HT110116	Sigma Aldrich	USA
Ethanol	MFCD00003568	VWR Chemicals	USA
EZ-PCR™ Mycoplasma Test Kit	20-700-20	Biological Industries	Israel
Fetal Bovine Serum (FBS)	-	GIBCO	USA
16% Formaldehyde Solution		Thermo Fisher Scientific	USA

GAPDH (D16H11) antibody	5174S	Cell Signalling Technology	USA
Glycine	G8898	Sigma Aldrich	USA
Goat serum	S-1000	VectorLabs	USA
Haematoxylin	HHS32	Sigma Aldrich	USA
Histoclear	A2-0101	Geneflow	UK
Human Instesticult™ Component A and B	06010	Stem Cell Technologies	Canada
Hydrochloric acid	-	J.T. Baker®	USA
Isopropanol	MFC00011674	VWR Chemicals	USA
Lane marker reducing sample buffer	39000	Thermo Fisher Scientific	USA
Matrigel®		Corning	USA
Matrigel® - Growth Factor Reduced GFR Basement Membrane Matrix, Phenol Red-Free, LDEV-Free, 10mL	356231	Corning	USA
McCoy's 5a Medium	26600	GIBCO	USA
Methanol	20847.307	VWR Chemicals	USA
MiSeq™ v2, 300 cycle flow cell	MS-102-2002	Illumina	USA
NEBNext® Ultra™ II RNA Library Prep Kit for Illumina® E7770 and rRNA Depletion Kit (Human/Mouse/Rat)	E6310	New England Biolabs	USA

NEBNext® Ultra™ II RNA Library Prep Kit for Illumina	E7770S	New England Bio Labs	USA
NextSeq™ High 150 cycle flow cell	20024904	Illumina	USA
NextSeq™ HIGH 75 cycle flow cell	20024906	Illumina	USA
Nuclease free water	AM9915G	Invitrogen	USA
Organoid Harvesting Solution	3700-100-01 20-700-20	Trevigen	USA
Pencillin and Steptomycin	P4333	Sigma Aldrich	USA
Peroxidase-AffiniPure Goat Anti-Rabbit IgG (H+L)	111-035-003	Jackson ImmunoResearch Laboratories INC	USA
Phospho-AKT (Ser473) antibody	4060S	Cell Signalling Technology	USA
Phosphpate Buffered Saline Tablets	18912-014	Gibco	USA
Precision Protein™ StrepTactin-HRP Conjugate 1:3000	1610381	Bio Rad	USA
Primocin™	ant-pm-2	Invivogen	USA
Protease/Phosphatase Inhibitor Cocktail (100X)	5871S	Cell Signalling Technology	USA
QIASeq® custom targeted DNA panel	CDHS-14542Z-1197	Qiagen	Germany
QuantSeq 3'mRNA-seq libr prep kit (FWD), 96 preps	015.96	Lexogen	Austria

RIPA Buffer	89900	Thermo Fisher Scientific	USA
ROCK inhibitor	Y27632	Strattech Scientific LTD	UK
Sodium chloride	A12313	Alfa Aesar, Thermo Fisher Scientific	USA
Sodium dodecyl sulfate	L3771	Sigma Aldrich	USA
Tris/Glycine 10x buffer (Bio- Rad, USA),	1610771	Bio Rad	USA
Tris/Glycine/SDS buffer (Bio- Rad, USA)	1610772	Bio Rad	USA
Trizma® base	T6066	Sigma-Aldrich	USA
Trizma® hydrochloride		Sigma-Aldrich	USA
truXTRAC FFPE total NA Kit - Column	520220	Covaris	USA
Trypan Blue Solution	T8154	Sigma Aldrich	USA
TrypLE™ Express	12605-028	GIBCO	USA
Turbo DNA-free™ Kit	AM1907	Invitrogen	USA
TWEEN 20	che3852	Scientific Laboratories Supplies	UK

2.10 A list of equipment and consumables used

Table 2-27: A table listing all consumables and equipment used

Name	Manufacturer / Supplier	Headquarters
24-well cell culture plates	Corning	USA
3ml Graduated Plastic Pasteur Pipettes	Appleton Woods	UK
6-well cell culture plates	Corning	USA
96-well assay plates	Corning	USA
96-well cell culture plates	Corning	USA
96-well PCR plates	Corning	USA
Amersham™ Hybond™ PVDF Blotting Membrane	Sigma Aldrich	USA
C1000 Touch Thermal Cycle	BioRad	USA
Cole-Palmer™ Stuart™ Orbital Shaker	Thermo Fisher Scientific	USA
Centrifuge tubes (50ml, 15ml)	Corning	USA
ChemiDoc™ MP Imaging System	BioRad	USA
CryoTube™ vials	Thermo Fisher Scientific	USA
DNA LoBind Tube	Eppendorf	Germany
E220 Focused Ultrasonicator	Covaris	USA
EASYstrainer™ 70mm	Greiner	Austria
EnSpire® luminescence plate reader	Perkin Elmer Life Science	USA
EVOS XL Core optical microscope	Thermo Scientific	USA

Faxitron Irradiator	CellRad	USA
Hanna® Edge digital pH monitor	HANNA	USA
Megafuge 16R Centrifuge	Thermo Scientific	USA
Micro pipettes and tips	Start Labs	USA
Microcentrifuge	BioRad	USA
Mini Trans Blot® Cell	BioRad	USA
MiSeq™	Illumina	USA
Multichannel pipettes and tips	Rainin	USA
NALGENE™ 1°C Freezing Container	Nalgene	USA
New Brunswick Galaxy 17 incubators	Eppendorf	Germany
NEXTSeq™ 500	Illumina	USA
PCR Film Lid (Adhesive Sealing Sheets)	Thermo Fisher Scientific	USA
Petri Dishes	SLS laboratory supplies	UK
Qubit™ 3.0 Fluorometer	Invitrogen	USA
Scalpel	Swan-Morton	
ScreenTapes® (Genomic DNA and RNA High Sensitivity, D1000)	Agilent	USA
Soniprep 150 MSE	Sanyo	Japan
StarTub Reagent Reservoir	Star Labs	USA
Stripettes and aspirator	ERGOne	Not known
TapeStation® 2200	Agilent	USA
TC20™ Automated Cell Counter	BioRad	USA
Monmouth Guardian MSCT1200 Tissue Culture Hoods	Monmouth Scientific	UK
Warer Bath	Not known	Not known

Chapter 3: A Literature Review of Factors Predicting Chemoradiotherapy Response in Locally Advanced Rectal Cancer Patients

3.1 Introduction

There is significant inter-patient variability to NCRT response in LARC, with approximately 30-40% of LARC patients demonstrating resistance to NCRT (260, 261). These patients undergo NCRT enduring side-effects and complications of NCRT, delaying their surgery, which also makes subsequent surgery challenging (262, 263). Consequently, research has focused on identifying factors which could potentially predict NCRT response or resistance in LARC. Such research has also identified potential biological targets to improve NCRT response. Various clinicopathological and biological predictive factors may be associated with NCRT response in LARC. A systematic review by Ryan et al. in 2016, on biomarkers predictive of NCRT response in LARC found that molecular profiling perhaps holds the greatest potential to accurately predict NCRT response (264). However, the significance of many such predictors remains untested in the clinical environment. A

further review of the latest evidence on factors predicting NCRT response in LARC was undertaken to summarise latest developments in this area of research.

3.2 Methods

Published literature on biomarkers associated with NCRT response was reviewed. Google Scholar®, PubMed, MEDLINE, EMBASE and Cochrane databases were searched using the key words “rectal cancer,” “chemoradiotherapy,” “radiotherapy,” “neoadjuvant,” “biomarkers,” “pathological complete response,” “response,” “resistance” using and/or parameters in various combinations. Published abstracts and peer-reviewed full text articles were reviewed to identify relevant literature published after the year 1990, in the English language. Studies involving patients or patient samples were included. The reference lists of any identified studies were explored to detect any further relevant studies. *In vitro* and *in vivo* studies were excluded in this review. Studies reporting on The data were collated and presented in clinically and biologically relevant categories.

3.3 Predictive Factors

3.3.1 *Clinical factors*

3.3.1.1 *Clinicopathological factors*

Examples of clinicopathological features which predict pCR in patients undergoing NCRT for LARC include non-smoking status (272), smaller pre-NCRT tumour size (272, 390, 391), greater distance from the anal verge (392-394), well differentiated tumours (272) and lower tumour stage (e.g. T, N stage) (272, 395). Poor tumour

differentiation (396, 397) and mucinous adenocarcinoma (398) may be associated with a poor response to treatment. The post-treatment, duration to surgery also impacts NCRT response status (395, 399).

3.3.1.2 *Radiological factors*

Several radiological predictors of NCRT response have also been described. A systematic review of 10 studies and a total of 302 patients, conducted by Maffione et al. found that positron emission tomography (PET) / CT demonstrated reasonable sensitivity (79%) and specificity (78%) at detecting early response during NCRT (400). The authors found that the percentage decrease in SUV (referred to as the response index) was associated with higher mean sensitivity and pooled specificity (82% and 85% respectively) for treatment response. With a sensitivity of 100%, a pre-NCRT tumour SUVmax of less than 27 on PET / CT scans may identify those who are unlikely to achieve pCR (401). A systematic review of five studies amounting to 330 patients by Krug et al. found that complete metabolic response compared to partial or no response detected on PET / CT, was associated with a pooled hazard ratio of 0.39 (95% CI 0.18–0.86; $p=0.02$) for overall survival and 0.70 (95% CI 0.16–3.14; $P = 0.64$) for disease free survival (402). Other imaging modalities have also been considered as NCRT response predictors. Diffusion weighted MRI imaging could play a role in predicting response to NCRT in LARC, but the findings from individual studies remain contradictor (264, 403). However, MRI detected extramural vascular invasion may predict poor response to NCRT in some patients (404).

3.3.2 Blood-based markers

3.3.2.1 *Routine blood tests*

Routine widely performed blood tests such as the full blood count may contain markers which could ascertain NCRT response. Kim et al. demonstrated that a pre-NCRT, high blood neutrophil / lymphocyte ratio (NLR ≥ 3) was associated with poor response (i.e., absence of pCR) in 102 LARC patients receiving NCRT (405). The authors found no significant association between an elevated post-NCRT NLR and poor response. Caputo et al. demonstrated that amongst 87 LARC patients undergoing NCRT, elevated NLR before and after treatment was associated with poor response (TRG ≥ 4) (406). Several studies have also demonstrated that an elevated pre- or post-NCRT NLR as an independent predictor of poor survival amongst patients undergoing NCRT for LARC (405, 407-409). However, a study of 202 LARC patients failed to demonstrate a statistically significant association between pre-NCRT NLR ≥ 3 and tumour regression grade, pCR or survival (410).

3.3.2.2 *Tumour markers*

Tumour markers such as pre-NCRT chorionic embryonic antigen (CEA), post-treatment CEA and CA19-9 have been associated with NCRT responsiveness in LARC. A pre-NCRT CEA of less than 5 $\mu\text{g/l}$ was associated with at least 2 to 3 times higher odds of pCR (266-275). An immediate post-operative CEA of less than five demonstrated approximately twice as greater odds of pCR (276, 277). A pre or post-operative CEA of less than five have also been associated with improved overall survival and disease free survival, following NCRT for LARC (278-282). Several

studies have also demonstrated an association between tumour downstaging or pCR and low pre-operative carbohydrate antigen 19-9 (CA19-9) (411, 412).

3.3.2.3 *Circulating tumour DNA*

The role of ctDNA, also known as cell free DNA (cfDNA) as a biomarker predictive of NCRT response is under investigation. Carpinetti et al. demonstrated that a personalised liquid biopsy, in the form of ctDNA assessment of targets identified through whole genome sequencing (WGS) of the parent tumour, at different time points (pre-NCRT, during treatment and following NCRT) could predict treatment response and recurrence in LARC (413). Two groups have also reported that a net reduction of blood ctDNA levels may be observed upon commencing NCRT (283, 284). However, the significance of this reduction in predicting response is uncertain. Sun et al. demonstrated that the detection of *MGMT* promoter hypermethylation in the plasma, pre-NCRT in LARC patients was significantly associated with a good response (pCR, or downstaging to yPT1,2, $p=0.04$) (285). Detection of pathological *KRAS* mutations within ctDNA, pre-NCRT was not associated with response to treatment (285, 414). There were several other studies that also did not show any significant association between various ctDNA testing methods and NCRT response. More research is needed to evaluate the significance of ctDNA detection as biomarker to predict NCRT response in LARC patients.

3.3.3 *Markers within tumour tissue*

3.3.3.1 *DNA mutations*

Several mutations identified in LARC tissue have been associated with NCRT response status. A range of different methods have been used to test for prevalent mutations in tumour suppressor genes and oncogenes (e.g., *p53* and *KRAS*), including NGS, quantitative real time polymerase chain reaction (qPCR) and gene signatures derived from DNA microarray analysis (264). A meta-analysis of 30 studies by Chen et al. reported that *p53* wild-type genotype or normal *p53* protein expression on immunohistochemistry were associated with a relative risk of 1.65 (95% CI=1.19–2.30; $p=0.003$) for pCR and 0.85 (95% CI=0.75–0.96; $p=0.007$) for a poor response, following NCRT in LARC (286). Furthermore, a lack of immunohistochemistry detected *p53* expression or qPCR detected pathological *p53* mutations in pre-NCRT biopsies were associated with a lower rate of pCR following NCRT (415-417). The significance of *KRAS* mutations on pCR, tumour downstaging and treatment resistance also remains unclear. The presence of specific *KRAS* mutations (e.g., *G13D*, *G13C*) may be associated with a poor response to NCRT (418). However, a systematic review and meta-analysis by Clancy et al. concluded that *KRAS* status was not predictive of tumour downstaging or cancer specific survival following NCRT in LARC patients (287). Garcia-Aguilar et al. demonstrated that the presence of *KRAS* and *p53* mutation is significantly likely to lead poor response (i.e., lack of pCR; $p=0.0003$) (419). The authors did not find any significant associations between *p53*, *BRAF* or *PIK3CA* mutation status in-isolation and NCRT response. Whilst Davies et al. demonstrated no association between *KRAS* or *BRAF* status and NCRT response (288), Jiang et al. demonstrated *BRAF* or *SMAD4* mutations were associated with complete non-response (resistance) following NCRT

($p=0.012$ and $p=0.020$) (420). Russo et al. found that mutations in *KRAS*, *PIK3CA*, *APC* and *p53* occurred frequently in patients who did not demonstrate pCR (290). However, this study failed to demonstrate a statistically significantly different association between pCR and tumours containing latter mutations and wild-type genes. The significance of dMMR gene mutations in NCRT has also been considered. However, a systematic review and meta-analysis by O'Connell et al. found no association between MSI and response to NCRT in LARC (289).

3.3.3.2 Single nucleotide polymorphisms

Specific SNPs could predict NCRT response in LARC (264, 291). The significance of SNPs of the *TYMS* gene in the treatment response of LARC patients has been extensively researched (264, 292). *TYMS* encodes thymidylate synthase which is the target enzyme of the chemotherapy agents 5FU and Capecitabine used in NCRT regimes. A systematic review and meta-analysis by Yang et al. concluded that *TYMS* 2R/2R or 2R/3R SNPs within LARC tissue led to a better response following NCRT (292). The authors did not find an association between *TYMS* SNPs 1494del6 and 5'UTR, and NCRT response. Lamas et al. also reported germline *TYMS* 2R/3G, 3C/3G, and 3G/3G SNPs to be predictive of better NCRT response. The authors also demonstrated a similar association between *XRCC1* G/G and improved response. *XRCC1* encodes X-ray repair cross-complementing protein 1 which predominantly functions in single strand break and base excision repair but not DSB repair (421). Several other studies have also explored the role of SNPs within genes encoding proteins involved in DNA DSB repair pathways. Páez et al. concluded that the *TYMS* genotype and the *XRCC1* Arg399Gln SNP may predict a better outcome

following NCRT in LARC (293). Grimminger et al. demonstrated an association between the *XRCC1* A399G (rs25487) SNP and improved response to NCRT (294). Sebio et al. demonstrated that *AREG* (rs11942466) region polymorphism and the C>T polymorphism in *ERCC1* (rs11615) correlated with pCR in LARC patients (295). *AREG* encodes amphiregulin which is a ligand of EGFR, frequently detected in tumour stromal and epithelial cells, and leads to the activation of downstream pathways such as the MAP kinase and PI3K/AKT/mTOR pathways (422). Furthermore, it leads to expression of programmed cell death 1 ligand which leads to the suppression of T-cell mediated immunity in the tumour microenvironment and targeting amphiregulin has been shown to promote chemo sensitisation and immunopotency *in vitro* (423). *ERCC1* encodes excision the repair cross complementation group 1 protein which is involved in nucleotide excision repair which often takes place following damage to up to 30 bases of adjacent individual nucleotides (424). SNPs of *EGFR* G/G or 61G and Sp1 -216 G/T may have a role as biomarkers capable of predicting NCRT response in LARC (296, 297). The research exploring SNPs as biomarkers predictive of NCRT response in LARC is at its infancy. The clinical significance of this research remains uncertain.

3.3.3.3 *DNA methylation*

Pre-NCRT hypermethylation of promoter regions of several genes have been linked to response in LARC (298). Sun et al. demonstrated that the hypermethylation of the promoter region of the *MGMT* gene was predictive of good response to NCRT (299). Furthermore, Jeong et al. conducted a phase I clinical trial of 22 LARC patients and treated them with Temozolomide and radiotherapy, and found a higher pCR rate in LARC patients treated with this drug (425). Pre-NCRT methylation status of promoter

regions of genes *TFAP2E* (300) and *TIMP3* (303) were predictive of a good response to NCRT in LARC in clinical and *in vitro* studies. *TFAP2E* encodes Transcription factor AP-2 epsilon regulates expression of the gene encoding the protein dickkopf homolog 4 which is an inhibitor of the Wnt signalling pathway (300, 426). *TIMP3* encodes Tissue inhibitor of metalloproteinase-3 which has several anticancer properties including the inhibition of matrix metalloproteinases essential for the breakdown of extracellular matrix which is required for cancer progression and metastasis (427). Whilst the pre-NCRT methylation status of *KLHL34* which encodes the Kelch Like Family Member 34 protein and *CRBP1* which encodes cellular retinol binding protein-1 were also predictive of a good response following NCRT, the biological mechanisms behind this remain unknown (301, 302). Tsang et al. demonstrated that pre-NCRT global methylation (assessed using immunohistochemistry) was predictive of pCR ($p=0.01$) and correlated with tumour regression as well as post-treatment T-stage (428). Two studies also used whole genome methylation arrays to identify predictors of NCRT response as well as prognosis (304, 429). These studies showed no association between CIMP and NCRT response in LARC (304, 305). CIMP caused by dMMR gene mutations or *MLH1* promoter hypermethylation is a rare phenotype in rectal cancer (430).

3.3.3.4 *RNA expression*

Several studies have analysed gene expression profiles to reveal biomarkers predictive of NCRT response in LARC. Genomic studies (microarrays, qPCR and NGS) of mRNA and miRNA have identified several biomarkers which can predict NCRT response (Table 3-1). Several miRNA transcripts have been correlated to NCRT response. The clinical as well as the biological significance of most of these

transcripts remain uncertain. Relatively higher levels of expression of genes encoding proteins involved in apoptosis (e.g., apoptosis inducers *Lumican*, *Thrombospondin 2* and *galectin-1*; *NFK β 2*, *TGF β 1*, *Caspase-1*, *BAX*) were observed in the pre-NCRT biopsies of responders (306-308). Furthermore, there were lower levels of expression of genes involved in cell growth, proliferation and hypoxia resistance (e.g., *EGFR*, *VEGF* and *HIF-1 α*) in responders (309, 310). In contrast, genes responsible for stemness (*LGR5*), growth and proliferation (*PDRG1*, *GLUT1*, *MKI67*) and apoptosis inhibition (*Cyclophilin 40*, *Glutathione Peroxidase*) were overexpressed in the pre-NCRT biopsies of non-responding tumours (306, 310, 311). Huh et al. demonstrated that CD44 mRNA expression was associated with the expression of CD44 antigen and 12 other immunohistochemistry markers on pre-NCRT biopsies (312). In this study the expression of CD44 antigen was associated with a good response to NCRT (odds ratio, 4.694 [1.155, 17.741], $p=0.030$). Saigusa et al. failed to demonstrate any association between CD44 gene expression and NCRT response (311). Whilst several individual biomarkers have been identified through transcriptomic analysis their clinical significance remains uncertain.

Table 3-1: mRNA and miRNA as biomarkers for NCRT response in LARC

Author	N	Method	Genomics	TRG	Biomarkers
mRNA					
Garajová et al (2008) (431)	17	Fresh biopsy	Microarrays	Not specified	<i>RB1, RBBP4, HYOU1, JUNB, MDM4, CANX, MMP2, TCF7L2</i>
Ghadimi et al (2005) (314)	30	Not specified	Microarray	Not specified	<i>REGL, ACVR2B, SMARCC1, and ZNF134</i>
Huh et al (2014) (312)	123	Fresh biopsy	qPCR	Not specified	<i>CD44</i>
Millino et al (2016) (316)	59	Fresh biopsy	Microarray	Mandard	<i>TMEM188, ITGA2, NRG, TRAM1, BCL2L13, MYO1B, KLF7, GTSE1, mir-630</i>
Nishioka et al (2011) (308)	17	Fresh biopsy	Microarray	Not specified	<i>MMP, NFKB2, TGFB1, TOP1, ITGB1, MMP7</i>
Palma et al (2014) (432)	26	Fresh biopsy	Microarray and qPCR	Mandard	<i>Gng4, c-MYC, polA1, and RRM1</i>
Rimkus et al (2007) (307)	43	Fresh biopsy	qPCR	Mandard	<i>ETS2, SLC35E1, Caspase -1</i>
Saigusa et al (2012) (310)	64	FFPE biopsy	qPCR	Various	<i>BAX, LRG5, PDRG1, GLUT1</i>
Saigusa et al (2012) (311)	52	FFPE biopsy	qPCR	Various	<i>LRG5, CD44</i>
Toiyama et al (2010) (309)	40	Fresh biopsy	qPCR	Not specified	<i>VEGF, HIF-1, EGFR</i>

Watanabe et al (2006) (306)	52	Fresh biopsy	Microarray	Mandard	<i>Lumican, thrombospondin 2, galectin-1, Cyclophilin 40, Glutathione Peroxidase</i>
Watanabe et al (2014) (313)	46	Not specified	qPCR	Not specified	<i>LRRIQ3, FRMD3, SAMD5, and TMC7</i>

miRNA

Conde-Muiño et al (2020) (433)	45	Fresh tissue	Microarray and qPCR	Mandard	<i>miRNA-148 and miRNA-375</i>
D'angelo et al (2016) (434)	38	Fresh tissue	Microarray	Mandard	<i>miR-154, miR-409-3p, miR-127-3p, miR-214*, miR-299-5p, miR-125b</i>
D'angelo et al (2018) (435)	38	Fresh tissue	Microarray	Mandard	<i>mir-194</i>
Drebber et al (2011) (436)	40	FFPE	qPCR	Not specified	<i>miR-21, miR-143, miR-145</i>
Du et al (2018) (437)	38	Fresh tissue	Microarray	Mandard	<i>miR-548c-5p, miR-548d-5p and miR-663a</i>
Kheirelseid et al (2013) (318)	12	FFPE	Microarray and qPCR	Mandard	<i>miR-16, miR-590-5p and miR-153, miR-519c-3p, miR-561</i>
Machackova et al (2020) (438)	87	Fresh tissue	qPCR	Mandard	<i>miR-487a-3p</i>
Svoboda et al (2012) (439)	20	Fresh tissue	Microarray	Mandard	<i>let-7e, miR-196b, miR-450a, miR-450b-5p, miR-99a, miR-215, miR-190b, miR-29b-2</i>

Several gene signatures derived from this research might be able to predict response (or resistance) to NCRT (264). Watanabe et al. demonstrated sensitivity (complete response) and specificity (non-response) of a gene signature utilising 4 genes in two cohorts of LARC patients, and reported a sensitivity of 87.5% and 81.3% and specificity of 90.9% and 100% (313). Ghadimi et al. demonstrated a sensitivity of 78% and specificity of 86% using a gene signature (314). This gene signature was subsequently validated by Lopes-Ramos et al. through an independent cohort of patients yielding a sensitivity of 66.7% and specificity of 81.2% (315). The authors also validated gene signatures from four other studies and found that the specificity varied between 68.7% to 100%. However, the sensitivity was zero as these signatures were unable to predict patients with a complete response. Casado et al. also demonstrated that a 13-gene signature could predict tumour response to NCRT with 87% sensitivity and 82% specificity (440). Several gene signatures have also been developed using miRNA expression profiles (316-318). Other studies have also demonstrated association between certain long non-coding RNA and NCRT response (e.g., Lincp21-RNA which has been associated with pCR) (441, 442). The clinical significance of the above has yet to be determined. Whilst gene expression profiles and gene signatures may have the potential to predict non-response, their ability to predict pCR remains uncertain.

3.3.3.5 *Protein expression*

Testing for the expression of specific proteins using immunohistochemistry or protein assays (e.g., western blots) could serve as a biomarker predictive of NCRT response. Davies et al. demonstrated that higher pre-treatment phospho-ERK levels were associated with better response to NCRT (288). The authors also found that

increased expression of phosphorylated-AKT (pAKT) prior to treatment may be associated with a better response to NCRT in LARC which contradicted their original hypothesis. However, Farkas et al. found no significant association between pre-NCRT pAKT expression and tumour regression grade (321). All rectal cancer samples within this study expressed pAKT. Another study of 717 primary colorectal tumours by Baba et al. found that pAKT expression was associated with lower tumour stage and good prognosis (319). Whilst the mechanism behind these observations remains uncertain, the authors conclude that pAKT may therefore, serve as a potential biomarker and therapeutic target to predicting and improving NCRT response in LARC. Furthermore, there is close association with pAKT, EGFR and pAKT, with cross-talk between the PI3K/AKT/mTOR, MAPK and VEGF pathway (443). Lobe et al. demonstrated that loss of VEGF expression (Odds ratio [OR] (95% CI) =0.24 (0.08–0.69), $p=0.009$) and positive EGFR (3.82 (1.37–10.6, $p=0.01$) were predictive of pCR (320). Therefore, VEGF and EGFR status could also serve as a potential biomarker to predict NCRT response in LARC. Farkas et al. also correlated the pre-NCRT expression of GHRH-R and Hsp90 to poor response (321). RAD51 expression was evaluated by Iwata et al. The group found that pre-treatment RAD51 expression was associated with poor response amongst a cohort of 42 LARC patients receiving NCRT (322). RAD51 is an essential component in DNA DSB repair through HDR where it is actively seeks out the complementary template DNA strand and invasion of the template strand (444). Huh et al. and Saigusa et al. evaluated the role of CD44 expression as a marker of NCRT response but their results were contradictory (311, 312). CD44 is a membrane bound antigen typically detected in CRC stem cells and plays a significant role in cell proliferation and migration (445).

3.3.3.6 *Microenvironment*

The tumour microenvironment undergoes significant changes following NCRT. Kamran et al. performed whole exome sequencing (WES) and total RNA sequencing of pre-NCRT LARC biopsies and post-resection specimens (323). Whilst the authors did not find any significant changes between the pre-NCRT and post-treatment tumour genomic profiles, they found significant genomic changes within the tumour immune microenvironment. The total immune infiltrate levels were significantly higher after treatment, with non-responders containing significantly more TAMs (M2), naïve B cells, monocytes and resting mast cells were present following NCRT. However, there were more activated mast cells in the pre-NCRT biopsies of non-responders. An over-abundance of CD56 positive Natural Killer (NK) cells was observed by Alderdice et al. amongst pre-NCRT biopsies from a cohort of responders compared to non-responders (324). El Sissy et al. went on to demonstrate that the immunoscore combined with post treatment imaging was an effective discriminator of good responders following NCRT (325).

3.3.3.7 *Microbiome*

Shen et al. reported significant variations within the microbiome following NCRT in LARC (326). The authors reported the higher prevalence of *Bifidobacteriaceae* and *Firmicutes* (*Roseburia*, *Anaerostipes* and *Doreo*) within the responding group. Sun et al. also demonstrated significant changes within the gut microbiome with a marked reduction in 6 genera *Porphyromonas*, *Parvimonas*, *Peptostreptococcus*, *Fusobacterium*, *Ezakiella* and *unidentified_Clostridiales* during NCRT; measured at

three time points – pre-NCRT, during treatment and post-NCRT (327). They found that patients who were responders had a significantly higher diversity within their microbiome as measured by the Chao1 diversity index. In contrast, a higher abundance of *Fusobacterium* was reported by Toomy et al (328). Jang et al reported differences in microbial diversity amongst a cohort of patient who had pCR following NCRT compared to those that did not demonstrate pCR (329). This study reported relatively high abundance of Bacteroidales (*Bacteroidaceae*, *Rikenellaceae*, *Bacteroides*) amongst non-pCR patients. The authors found that *Duodenibacillus massiliensis* might be linked to pCR.

3.4 Discussion

Several clinical factors and biological markers associated with NCRT response in LARC were identified during this literature review. Pre-NCRT clinical factors such as tumour stage, size and distance from the anal verge were associated with NCRT response. Biomarkers predictive of NCRT response have been of interest in rectal cancer research for decades. Some of the most promising results come from studies evaluating the role of pre-treatment CEA and NCRT response. Several studies have consistently demonstrated that an elevated pre-treatment CEA levels may be associated with poor response to NCRT in LARC. The positive predictive values were increased when the cut off used for CEA was lower. Other tumour markers (e.g., CA19-9) and haematological markers (e.g., NLR) were not associated with NCRT response or yielded contradictory results. Research suggests that ctDNA could have a role in distinguishing between responders and non-responders following NCRT. However, their role is more likely a disease relapse monitoring or

early recurrence detection tool. The role of ctDNA as a pre-NCRT predictive marker of response requires additional research.

Various genomic markers were also associated with NCRT response. Several mutations within commonly encountered genes in CRC have been associated with poor response following NCRT. *KRAS*, *P53*, *BRAF* and *SMAD4* mutations may have association with NCRT resistance. In isolation, mutations within most other commonly mutated genes in CRC (e.g., *APC*, *PIK3CA*, *BRAF*, *SMAD4*, dMMR genes) showed no association with pCR or resistance following NCRT. With approximately 2% of rectal cancer harbouring dMMR gene mutations, the clinical significance of dMMR mutations and NCRT response is limited. In summary, the significance of individual genetic mutations and radiotherapy remains unclear. However, combining genetic mutation profiles could provide potential biomarker scores which may predict NCRT response.

There were several limitations encountered in this literature review. The numerous *in vitro* or *in vivo* studies that identified biomarkers predictive of NCRT response were excluded. Whilst this ensured consistency with the review focusing on research conducted only in human patients, certain potential novel targets could have been missed. Overall, the number of studies identified for each predictor of response was small and most had very small sample sizes. Significant variability across study methodology and outcome measures was also observed. There were major differences in the technology available and being utilised by different research groups to identify different biomarkers over the long period in review. The review

included studies evaluating pCR, good response and poor response. There was significant heterogeneity amongst methodology followed by researchers with different groups using different methods (e.g., TRG versus Dworak) to evaluate response. The criteria used to categorise good or poor response were also variable. Therefore, direct objective comparison across the individual studies, a systematic review or meta-analysis was not feasible. Whilst this was not a systematic review, the preferred reporting items for systematic review and meta-analyses guidelines were adhered to where feasible. This review also provides a detailed summary of some of the latest evidence on biomarkers predictive of NCRT response in LARC.

3.5 Conclusion

Significant advances have been made in the field of biomarker research evaluating predictors of response to LARC following NCRT. However, the abundance of poor quality research lacking consensus on study design, methodology and reporting leads to difficulties in drawing clinically relevant conclusions. Pre-NCRT tumour size, tumour stage and CEA remain key determinants of response following NCRT in LARC. Several tumour transcriptomic markers, gene signatures and methylations arrays may be associated with NCRT response. However, in isolation such clinicopathological and biological predictors of NCRT appear to have limited value in predicting NCRT response. The clinical significance of many such biomarkers warrants further research. Therefore, more multicentre research with large sample sizes and consensus on study design are needed to progress research in this field and to develop predictive tools capable of distinguishing between patients who are unlikely to respond to NCRT compared to those that do.

Chapter 4: Identifying Biomarkers and Biological Pathways Associated with Chemoradiotherapy Response in a Retrospective Cohort of Locally Advanced Rectal Cancer Patients

4.1 Introduction

The biological mechanisms which underpin radiotherapy response in LARC remain elusive. However, ongoing research into predictive biomarkers, continue to increase our understanding of the intra and extra cellular biological mechanisms responsible for NCRT response or resistance. Such research can identify novel drug targets which may improve radiotherapy response in rectal cancer (446). They may also lead to treatment stratification tools, which can be used in the clinical environment to direct individual patients to the most efficacious treatment for them. Similarities can be drawn to OncotypeDX in breast cancer which was the culmination of decades of research into biomarkers predicting response to oncological treatment in breast cancer (447). However, more research is needed to identify and understand clinically significant biomarkers and pathways responsible for radiotherapy response in LARC.

Several studies have already utilised microarray and NGS gene expression data to identify biomarkers such as individual genes, gene expression profiles and gene signatures of interest in predicting LARC response to NCRT (Chapter 3).

NGS techniques have led to the discovery of several novel biomarkers through differential gene expression analysis, linked to the pathogenesis or treatment response in various diseases (448). Whilst numerous methods of gene expression analysis have been reported, one powerful computational analysis widely used to analyse gene expression data is GSEA (449). GSEA is used to test pre-defined gene sets (e.g., those categorised on the basis of biological pathway or location within a chromosome) for associations with disease or treatment states (i.e. phenotype) (450). GSEA tests for significant differential expression of pre-defined gene sets within transcriptomic data and their association to a phenotype (451). This method generates an enrichment score (ES) which quantifies the extent to which a gene set is overrepresented within a ranked list of genes in test sample over a control (387). Therefore, enriched gene sets identified through GSEA are indicative of those that are upregulated in the test sample over the control. Where a gene set correlates to a biological pathway, the results may therefore, indicate upregulation of that pathway in the test sample. Parametric (signal-to-noise, t-test) and non-parametric (difference of classes) statistical tests can be used within GSEA to test for significance of differentially expressed gene sets and generates FDR corrected q-values. According to the creators of GSEA, gene sets associated with an FDR adjusted q-value of less than 0.25 (25%) are likely to generate hypotheses of biological significance (387).

4.2 Aims

The primary objective of this research was to contribute to the existing evidence on gene expression biomarkers associated with NCRT response in LARC. The secondary aims included, demonstrating feasibility of extracting genomic material, using an established technique, from archived FFPE rectal cancer biopsy and tumour samples, differential gene expression analysis and GSEA to detect biomarkers and biological pathways associated with NCRT response in LARC patients.

4.3 Methods

A retrospective cohort of patients who underwent NCRT for LARC were identified from a local radiotherapy database. Where available, archived FFPE sections of pre-NCRT biopsies and post-NCRT surgical resection specimens were obtained. Anonymised demographic and clinicopathological data were obtained using electronic patient records. RNA was extracted from archived FFPE samples from this retrospective cohort of LARC patients and 3' RNA sequencing was performed. Data were uploaded to PartekFlow® and raw gene counts were obtained using a manufacturer designed bioinformatics pipeline. ESTIMATE analysis was performed to determine sample purity (452). PCA and differential gene expression analysis was performed using GSA which utilises a log-normal with shrinkage model (382). A fold change of greater than 1.5 and less than -1.5 were considered biologically significant. An FDR adjusted q-value was also generated for differentially expressed genes using the FDR step-up method by Benjamini-Hochberg (385). A nominal or FDR adjusted q-value of less than 0.05 was assigned as the level of statistical

significance. GSEA was performed with the recommend, default option of signal-to-noise testing given that the sample size in each category exceeded three. The Hallmark, KEGG and Oncogenic Signatures collections of the MSigDB V7.4 were used to identify related genes and consequently, biological pathways of interest in non-responder pre-NCRT rectal cancer biopsy samples. An FDR adjusted q-value of less than 0.25 was used to identify gene sets of biological interest and the results were displayed in tables (387). Enrichment plots and heatmaps were generated through hierarchical clustering for each significant gene set and clinically relevant results were presented.

4.4 Results

4.4.1 *Patient demographics and clinicopathological data*

A total of 96 patients were identified as having undergone NCRT followed by surgical resection for primary LARC at the Queen Elizabeth Hospital, Birmingham, UK, between 2009 and 2016. Partial responders (M2, M3 or TRS-2) were excluded and 42 complete responder and complete non-responder (TRS-3, M4 or M5) patients were identified. Of these only 37 patients had archived, retrievable, matched FFPE pre-NCRT biopsies and post-NCRT surgical resection specimens available. Failure to extract high quality RNA with unrecordable RIN values which was deemed unsuitable for library preparation resulted in a further 14 patients (10 non-responders and 4 complete responders) being excluded. Therefore, only 23 patients were included in the final analysis (Table 4-1).

Table 4-1: Demographics and clinicopathological characteristics of patient FFPE biopsy and tumour samples.

M= male, F= female, M1/M4/M5= Mandard score 1/4/5, M- Male

Sample ID (Biopsy, Tumour)	Age	Gender	Pre-Op TNM Stage	Location	RT Duration (Days)	Radiotherapy Dose (Grey)	Chemotherapy	Tumour Regression Grade / Score
C10, D10	67	M	T3 N1 M0	Lower	35	45	Capecitabine	M4
G5, H5	67	M	T3C N1 M0	Lower	36	45	Capecitabine	M4
H7, I4	68	F	T3C N1 M1	Middle	35	45	Bevacizumab, folfirinox + cetuximab	M4
D7, E4	60	M	T3a N2 M0	Lower	37	45	5FU + oxaliplatin	M4
F, G	65	M	T3c N2 M0	Upper	32	45	Capecitabine	M4
A7, B7	44	M	T2 N1 M0	Lower	34	45	Capecitabine	M4
A9, B9	81	F	T3 N1 M1	Middle	36	45	5FU + oxaliplatin	M5
A8, B8	83	M	T3 N1 M1	Lower	35	45	Capecitabine	M4
J3, E10	62	M	T3d N2 M0	Lower	32	45	Capecitabine	M4
A10, B10	60	M	T3 N0 M0	Middle	35	45	5FU	M4
D8, K4'	56	M	T3 N0 M0	Lower	32	45	Capecitabine	M5

E3, F3	40	M	T3 N1 M0	Lower	39	50.4	Capecitabine	M5
A6, C6	70	M	T3 N2 M0	Lower	38	50.4	Capecitabine	M4
F7, G7	55	F	T3 N2 M0	Lower	37	50.4	Capecitabine	M4
G4, H4	71	M	T3 N1 M0	Lower	42	50.4	5FU	M5
N1, A13	78	F	T3 N2 M1b	Middle	32	45	Capecitabine	M5
O1, C13	78	M	T4a N2 M0	Upper	32	45	Capecitabine	M5
A11	71	M	T3b N2 M0	Upper	35	45	Capecitabine	M1
D11	80	M	T3 N2 M0	Lower	32	45	5FU	M1
F8	75	M	T3a N1 M0	Lower	35	45	5FU	M1
I5	74	F	T3 N0 M0	Lower	36	45	Capecitabine	M1
A12	78	M	T3 N2 M0	Lower	31	45	5FU	M1
D12	78	M	T4 N2 M0	Middle	38	50.4	Capecitabine	M1

The median age was 70 (interquartile range [IQR]=78-61). Seventy eight percent (n=18, 78%) were male and the rest were female. All tumours were Stage 3 (T3 and N1) or higher, pre-NCRT. Whilst 65% (n=15) were lower rectal tumours, 22% (n=5) were middle rectal tumours and the remainder (13%, n=3) were upper rectal tumours. All patients received intravenous 5FU or oral capecitabine based chemotherapy and radiotherapy totalling 45 Gy or 50.4 Gy over a median duration of 35 days (IQR=32-37 days). The tumour regression grade was assessed by trained pathologists using the Mandard scoring system. There were 6 (28%) complete responders (M1) and 17 (72%) were non-responders (M4/5).

4.4.2 *Transcriptomic analysis of FFPE patient samples*

RNA extracted from FFPE samples from pre-NCRT biopsy samples and post-NCRT surgical resection specimens were quantified and subject to quality control. RIN values ranged from 1.9-2.9 (concentration range: 5.8ng/μl – 154ng/μl) for non-responder biopsy samples; 1.8-3.2 (concentration range: 4.8ng/μl -63.4 ng/μl) for non-responder surgical resection specimens; 1.8-2.7 (concentration range 21.2 ng/μl -45.6 ng/μl) for responder biopsy samples. The extracted RNA was normalised. Library preparation was performed using Lexogen QuantSeq for 3' RNA sequencing kit. Quality control of the library was performed using TapeStation®. NGS was performed using Illumina® NextSeq™.

4.4.2.1 *Sample purity analysis*

Sample purity and stromal, immune cell contamination was assessed using the ESTIMATE score (452). The ESTIMATE R package and raw gene counts generated from PartekFlow® were used to calculate StromalScore, ImmuneScore, ESTIMATEScore and TumorPurity for each individual sample. Student t-tests were performed to test for statistically significant differences in scores across the different test categories, pre-NCRT biopsy non-responder versus complete responder and post-NCRT (tumour) versus pre-NCRT (biopsy) non-responder samples. A significant difference ($p < 0.05$) across any of the test groups would mean potentially significant differences across the level of stromal and immune system cell contamination in the two groups and downstream results must be interpreted with caution.

4.4.2.1.1 *Pre-NCRT biopsy non-responder versus complete responder*

There was no significant difference in StromalScore, ImmuneScore, ESTIMATEScore or TumorPurity between pre-NCRT non-responder versus complete responder biopsy samples ($p > 0.05$) (Figure 4-1). Therefore, no significant differences in immune system or stromal contamination were present in samples from the two groups.

	StromalScore	ImmuneScore	ESTIMATEScore	TumorPurity
Complete Response	-3.32161045	771.0676194	767.746009	0.75205125
Average - No Response	-153.126996	528.5632355	375.4362396	0.785971535
T-Test p-value	0.228852645	0.168605757	0.132652918	0.163122306

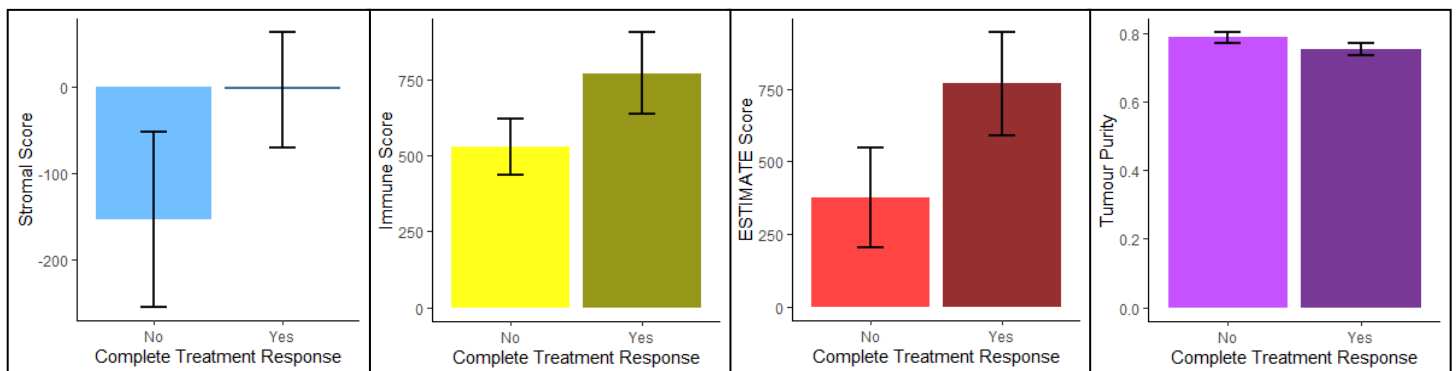


Figure 4-1: Sample purity analysis: pre-NCRT biopsy non-responder versus complete responder samples

The data analysis was performed with the assistance of Mr Thomas Starkey and Dr Lennard Lee of the University of Birmingham, Institute of Cancer and Genomic Science. The results and figures have been reproduced with their permission.

4.4.2.1.2 Non-responder pre-NCRT (biopsy) versus post-NCRT (tumour)

A statistically significant difference was observed between the StromalScore, ESTIMATEScore and TumorPurity scores from non-responder pre-NCRT (biopsy) vs post-NCRT (tumour) samples (Figure 4-2). The ImmuneScore was not statistically significantly different. Whilst the purity levels across both groups were acceptable (approximately 70% or more), the significant differences in the observed scores was likely due to the significant influx of inflammatory and immune system cells which

occurs naturally following radiotherapy. However, the results from downstream sequencing analyses using these two groups should be interpreted with caution.

	StromalScore	ImmuneScore	ESTIMATEScore	TumorPurity
Average - Biopsy	-129.0055912	600.7758958	471.7703046	0.777295171
Average - Tumour	590.1307369	711.0237836	1301.154521	0.693809153
T Test p-value	5.15674E-05	0.44127707	0.004815892	0.00274565

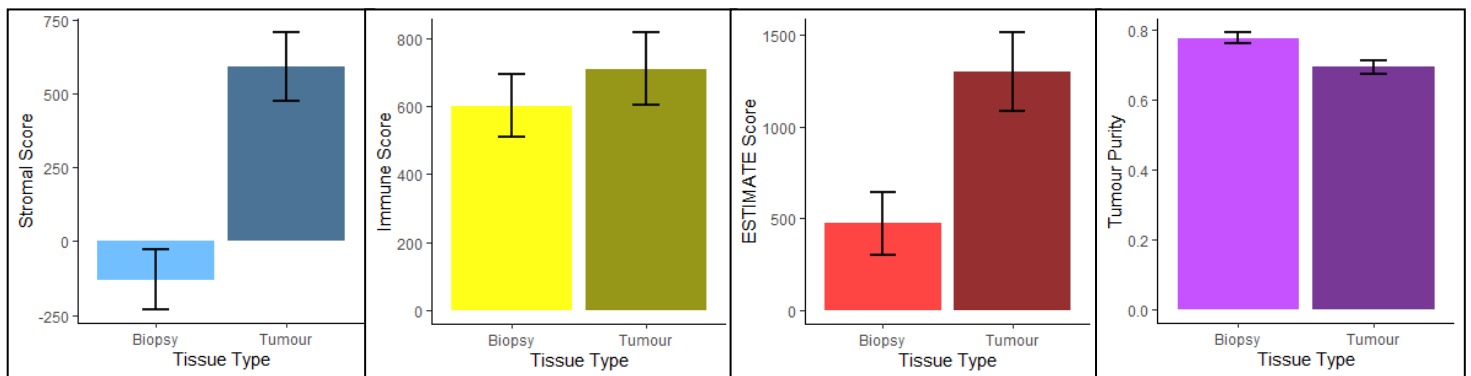


Figure 4-2: Sample purity analysis: non-responder pre-NCRT (biopsy) versus post-NCRT (tumour) samples

The data analysis was performed with the assistance of Mr Thomas Starkey and Dr Lennard Lee of the University of Birmingham, Institute of Cancer and Genomic Science. The results and figures have been reproduced with their permission.

4.4.3 Gene expression in pre-NCRT rectal cancer biopsies was associated with NCRT response status

PCA using PartekFlow® revealed no clustering between the gene expression of complete responders and non-responders (Figure 4-3). The PCA value was 22.55%. There was one outlying sample (O1) which originated from a 78 year old male patient with T4a N2 M0 patient who received capecitabine based NCRT and recorded a TRG of M5.

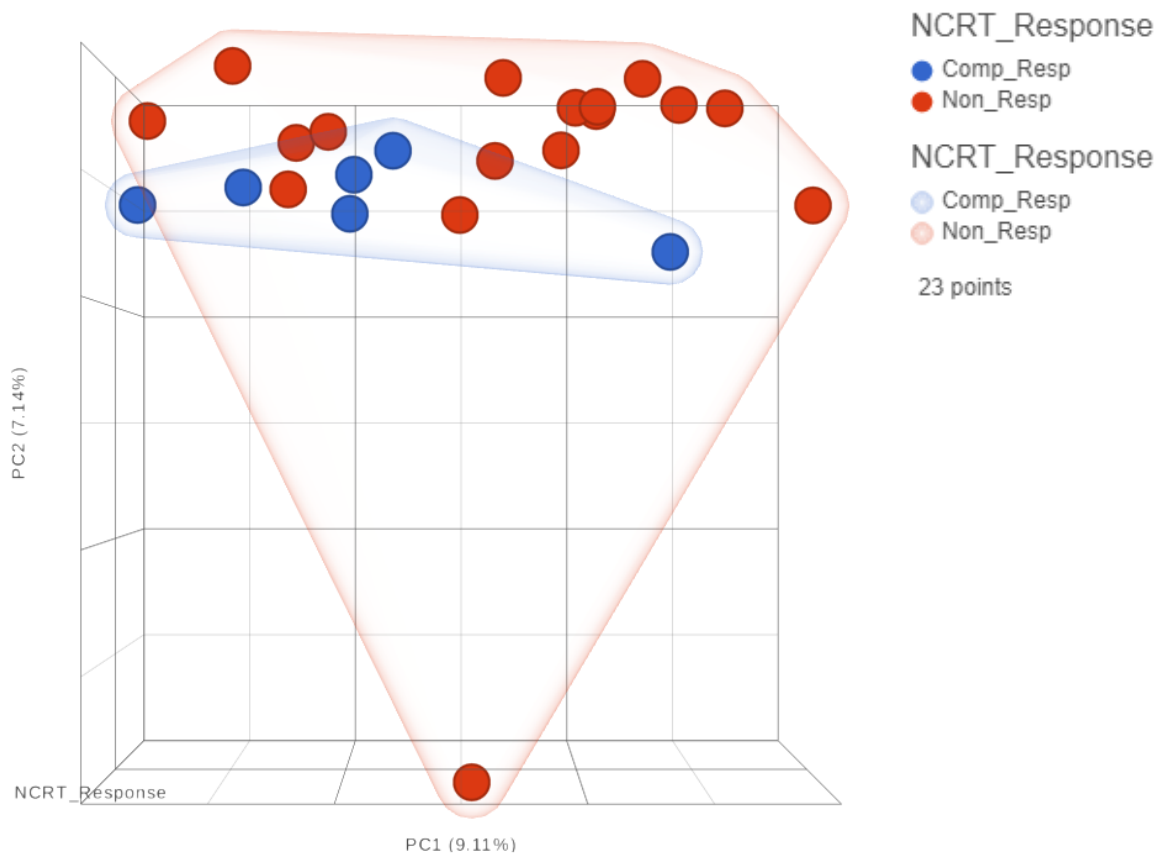


Figure 4-3: Principal component analysis of rectal cancer pre-NCRT biopsy gene expression between complete responders and non-responders
Principal component analysis was performed and plotted. Circles represent individual samples. Shaded area represents sample grouping by response status. The first principal axis along which the largest sample variance was observed was the x-axis (PC1). The y-axis

was the second most important direction in which samples showed significant variation (PC2). *Comp_Resp* = complete responder, *Non_Resp* = non-responder

Differential gene expression analysis using GSA revealed 6393 differentially expressed genes of which 518 were upregulated and 7 were downregulated in non-responders, when data were filtered by $1.5 < \text{fold change} > -1.5$ and $p < 0.05$ (Figure 4-4). A large number ($n=5868$) of genes were not statistically significantly differentially expressed.

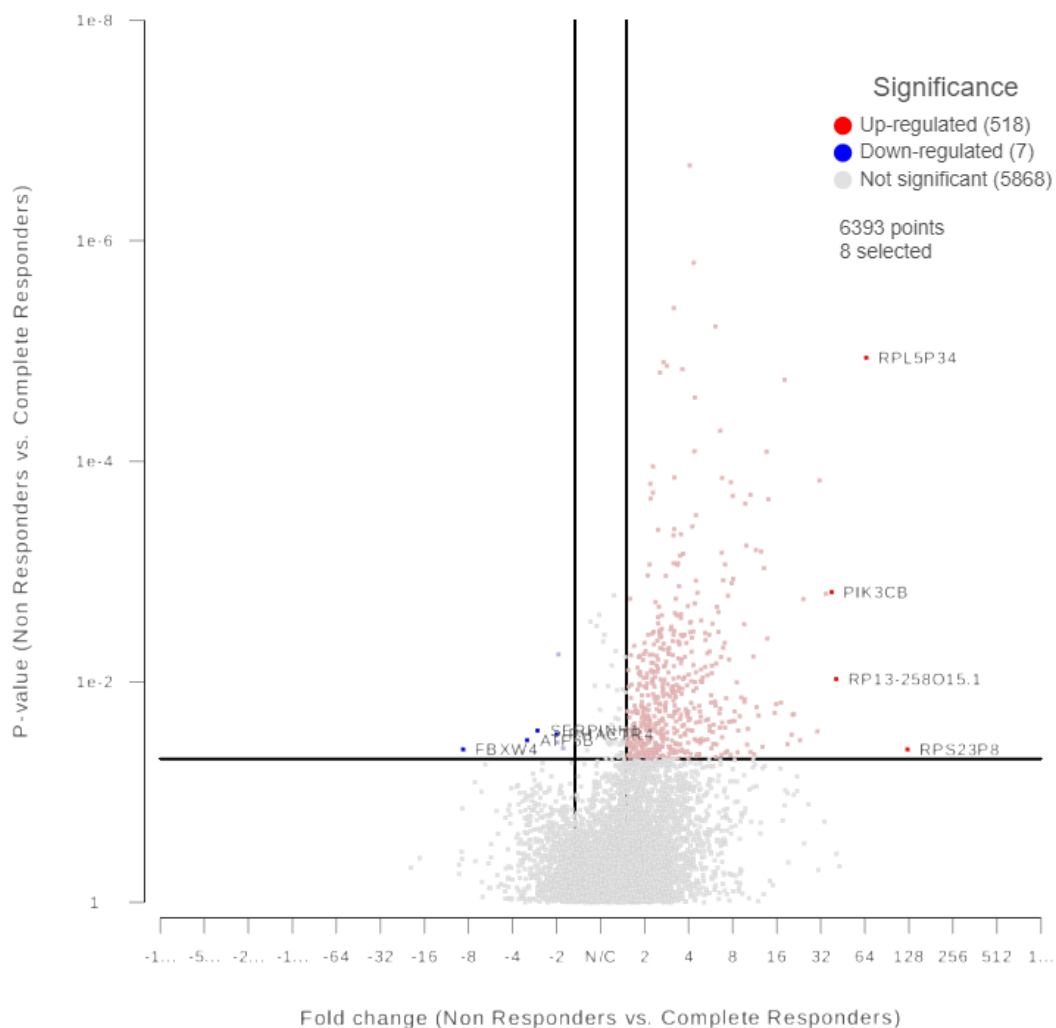


Figure 4-4: Volcano plot representing upregulated and downregulated genes in pre-NCRT FFPE biopsy samples from non-responders

The y-axis of the volcano plot represents the p-value which was plotted against the fold change on the x-axis for each of the expressed genes. The red dots represent the significantly upregulated genes, blue dots represent the significantly downregulated genes and the light grey dots represent the non-significant genes. The top four upregulated and downregulated genes have been labelled with their respective gene name. The black horizontal line represents the level of significance at 0.05. The two black vertical lines represent the fold change cut off at -1.5 and 1.5.

4.4.3.1 Upregulated genes in pre-NCRT biopsies of non-responders

The top 10 differentially upregulated genes in the pre-treatment biopsy samples of non-responders were identified and listed in descending order of fold change (Table 4-2). These included the following ribosomal protein encoding genes: *RPS23P8*, *RPL5P34*, *RP13-258O15.1* and *RPL6P27*. Their significance in NCRT response in rectal cancer is unclear. Expression of *PIK3CB* was significantly higher in non-responders (fold change=37.90; $p=0.002$). The latter encodes the PI3K β catalytic subunit of the PI3K protein of the PI3K/AKT/mTOR pathway. Yu et al. previously demonstrated that significantly higher levels of PI3K β expression in patients exhibiting poor response to NCRT (453). The activation of the PI3K/AKT/mTOR pathway in response to radiotherapy has also been well established (173, 333). *OBSL1* which encodes a cytoskeletal adaptor protein, was also upregulated in non-responders. Previous research has shown that methylation and subsequent silencing of *OBSL1* is associated with pCR in LARC patients (454). Genes *ACAD9*, *HLA2*, *C19orf77* and *AC004453.8* were also upregulated in non-responders. No prior association with radiotherapy response and these genes have previously been reported in malignancy.

Table 4-2: Genes upregulated in pre-NCRT FFPE biopsy samples from non-responders

Gene symbol	Fold change	p-value	FDR q-value
<i>RPS23P8</i>	125.00	0.041	0.532
<i>RPL5P34</i>	65.40	<0.001	0.011
<i>RP13-258O15.1</i>	40.90	0.009	0.321
<i>PIK3CB</i>	37.90	0.002	0.189
<i>RPL6P27</i>	34.50	0.002	0.189
<i>C19orf77</i>	31.30	<0.001	0.051
<i>ACAD9</i>	30.30	0.028	0.469
<i>AC004453.8</i>	24.30	0.002	0.192
<i>HHLA2</i>	23.10	0.034	0.502
<i>OBSL1</i>	21.00	0.020	0.418

4.4.3.2 Downregulated genes in pre-NCRT biopsies of non-responders

There were seven significantly differentially downregulated genes in the pre-treatment biopsy samples of non-responders (Table 4-3). These were listed in descending order of fold change and ascending order of *p*-value. The most downregulated gene was *FBXW4* (fold change=-8.71; *p*=0.041). The latter gene encodes a F-box protein 4 which targets proteins for ubiquitin mediated degradation (455). Low *FBXW4* expression is associated with poor disease free survival following NCRT in LARC patients (456). The remaining six genes (*ATF6B*, *SERPINH1*, *PHACTR4*, *YRDC*, *B2M* and *PDIA3*) did not have any published evidence of associations with radiation response in cancer patients. *ATF6B* encodes the activating transcription factor 6 beta is a expressed in response to stressful stimuli

and regulated downstream protein translation (457). *SERPINH1* encodes serpin family H member 1 which is a member of serine protease inhibitor family of proteins and is essential in collagen synthesis (458). *PHACTR4* encodes phosphatase and actin regulator 4 protein which is part of a family of proteins known to regulate the reorganisation of the actin cytoskeleton of cells (459). *YRDC* encodes yrdC N6-threonylcarbamoyltransferase domain containing protein which enables nucleotidyltransferase and transfer RNA activity (460). *B2M* encodes beta-2-microglobulin, a protein associated with the major histocompatibility protein complex (461). *PDIA3* encodes protein disulphide isomerase family A member 3, which sits on the endoplasmic reticulum and is associated with folding of newly synthesised glycoproteins (462). The biological mechanisms which underpin radioresistance following their downregulation of the above proteins remain uncertain.

Table 4-3: Genes downregulated in pre-NCRT FFPE biopsy samples from non-responders

Gene symbol	Fold change	p-value	FDR q-value
<i>FBXW4</i>	-8.71	0.041	0.532
<i>ATF6B</i>	-3.19	0.034	0.502
<i>SERPINH1</i>	-2.69	0.028	0.466
<i>PHACTR4</i>	-2.00	0.030	0.480
<i>YRDC</i>	-1.98	0.036	0.508
<i>B2M</i>	-1.94	0.006	0.266
<i>PDIA3</i>	-1.80	0.040	0.527

4.4.3.3 GSEA – pre-NCRT FFPE biopsy samples

GSEA was performed using the Hallmark, KEGG and Oncogenic Signatures gene set collections of the MSigDB V7.4 to identify biological pathways of significance in NCRT resistance.

4.4.3.3.1 Hallmark collection

GSEA revealed that 48 of 50 gene sets of the Hallmark collection were upregulated in non-responders. Seventeen of these were significant at an FDR adjusted q-value cut-off under 0.25 and could theoretically lead to biologically relevant hypotheses. Rank at max scores remained positive, demonstrating a correlation towards non-responders. Top three ES were associated with Androgen Response, NOTCH Signalling, Pancreas Beta Cells and Reactive Oxygen Species gene sets (Table 4-4). Furthermore, Cholesterol Homeostasis, Peroxisome, UV Response Down, P53 Pathway, MTORC1 signalling, HEME Metabolism, Apoptosis, Hypoxia, DNA Repair and Myogenesis gene sets were also associated with an enrichment score of at least 0.3. GSEA also revealed 2 of 50 gene sets were upregulated in the pre-NCRT, complete responder FFPE biopsy samples. Neither gene set was significant at FDR adjusted q-value under 0.25.

Table 4-4: Hallmark enrichment: Upregulated gene sets in the pre-NCRT, non-responder FFPE biopsy samples

Gene set	Size	ES	FDR q-value	Rank at max
HALLMARK_ANDROGEN_RESPONSE	95	0.41	0.218	5947
HALLMARK_NOTCH_SIGNALING	32	0.39	0.231	1053
HALLMARK_PANCREAS_BETA_CELLS	29	0.38	0.242	8747

HALLMARK_REACTIVE_OXYGEN_SPECIES_PATHWAY	46	0.38	0.244	5644
HALLMARK_CHOLESTEROL_HOMEOSTASIS	71	0.37	0.229	6857
HALLMARK_PEROXISOME	101	0.34	0.204	3286
HALLMARK_UV_RESPONSE_DN	137	0.33	0.195	4201
HALLMARK_P53_PATHWAY	189	0.33	0.215	6789
HALLMARK_MTORC1_SIGNALING	195	0.33	0.246	5527
HALLMARK_HEME_METABOLISM	174	0.31	0.228	4129
HALLMARK_APOPTOSIS	153	0.31	0.241	5646
HALLMARK_HYPOXIA	178	0.31	0.244	4725
HALLMARK_DNA_REPAIR	146	0.3	0.232	6720
HALLMARK_MYOGENESIS	168	0.3	0.242	7270
HALLMARK_GLYCOLYSIS	187	0.29	0.246	4973
HALLMARK_ESTROGEN_RESPONSE_EARLY	188	0.28	0.247	6693

Upregulated gene sets listed in descending order of enrichment score (ES) followed by ascending order of false discover rate (FDR) adjusted q-value. FDR adjusted q-value cut-off set to less than 0.25.

4.4.3.3.2 KEGG collection

Out of 172 KEGG collection gene sets, 160 were upregulated in pre-NCRT, non-responder FFPE biopsy samples (Table 4-5). The FDR adjusted q-value was less than 0.25 for ten of these gene sets (Table 4-5). Amongst these was the Oxidative Phosphorylation gene set (ES = 0.55, FDR adjusted q-value = 0.019) which belongs to a pathway closely associated with radiotherapy response (463). The analysis also revealed that 12 of 172 gene sets were upregulated in pre-NCRT, complete responder FFPE biopsy samples. However, only one of the 12 gene sets were

associated with an FDR adjusted q-value less than 0.25 and this was the Asthma gene set (ES = -0.53; FDR adjusted q-value = 23.7%).

Table 4-5: KEGG enrichment: Upregulated gene sets in pre-NCRT, non-responder FFPE biopsy samples

Gene set	Size	ES	FDR q-value	Rank at max
KEGG_STEROID_BIOSYNTHESIS	16	0.62	0.120	1354
KEGG_OXIDATIVE_PHOSPHORYLATION	106	0.55	0.019	2921
KEGG_PARKINSONS_DISEASE	106	0.53	0.015	4143
KEGG_BASAL_CELL_CARCINOMA	45	0.52	0.124	6685
KEGG_HOMOLOGOUS_RECOMBINATION	26	0.5	0.202	2330
KEGG_CARDIAC_MUSCLE_CONTRACTION	58	0.45	0.205	1389
KEGG_ALZHEIMERS_DISEASE	138	0.43	0.118	3194
KEGG_SNARE_INTERACTIONS_IN_VESICULAR_TRANSPORT	36	0.43	0.214	2585
KEGG_HUNTINGTONS_DISEASE	155	0.42	0.111	4065
KEGG_NON_SMALL_CELL_LUNG_CANCER	53	0.41	0.234	4185

Upregulated gene sets listed in descending order of enrichment score (ES) followed by ascending order of false discover rate (FDR) adjusted q-value. FDR adjusted q-value cut-off set to less than 0.25.

4.4.3.3.3 Oncogenic Signatures collection

Amongst the 187 gene sets of the Oncogenic Signatures collection, 185 were upregulated in pre-NCRT, non-responder FFPE biopsy samples (Table 4-6).

However, only one gene set (BCAT_GDS748_DN), associated with β -catenin and Wnt signalling was significant at an FDR adjusted q-value level of 13%. Furthermore,

2 of 187 gene sets of this collection were upregulated in the complete responder group. However, neither gene set was associated with an FDR adjusted q-value of less than 0.25.

Table 4-6: Oncogenic Signatures enrichment: Upregulated gene sets in pre-NCRT, non-responder FFPE biopsy samples

Gene set	Size	ES	FDR q-value	Rank at max
BCAT_GDS748_DN	40	0.44	0.13	4010

4.4.4 Gene expression in post-NCRT (tumour resection specimen FFPE samples) versus pre-NCRT (biopsy FFPE samples) in non-responding LARC patients

PCA demonstrated that pre- and post-NCRT non-responder samples were distinctly clustered. The PCA statistic was 43.31%. The pre-NCRT samples were more tightly clustered compared to the post-NCRT samples. Sample O1 was once again an outlying sample.

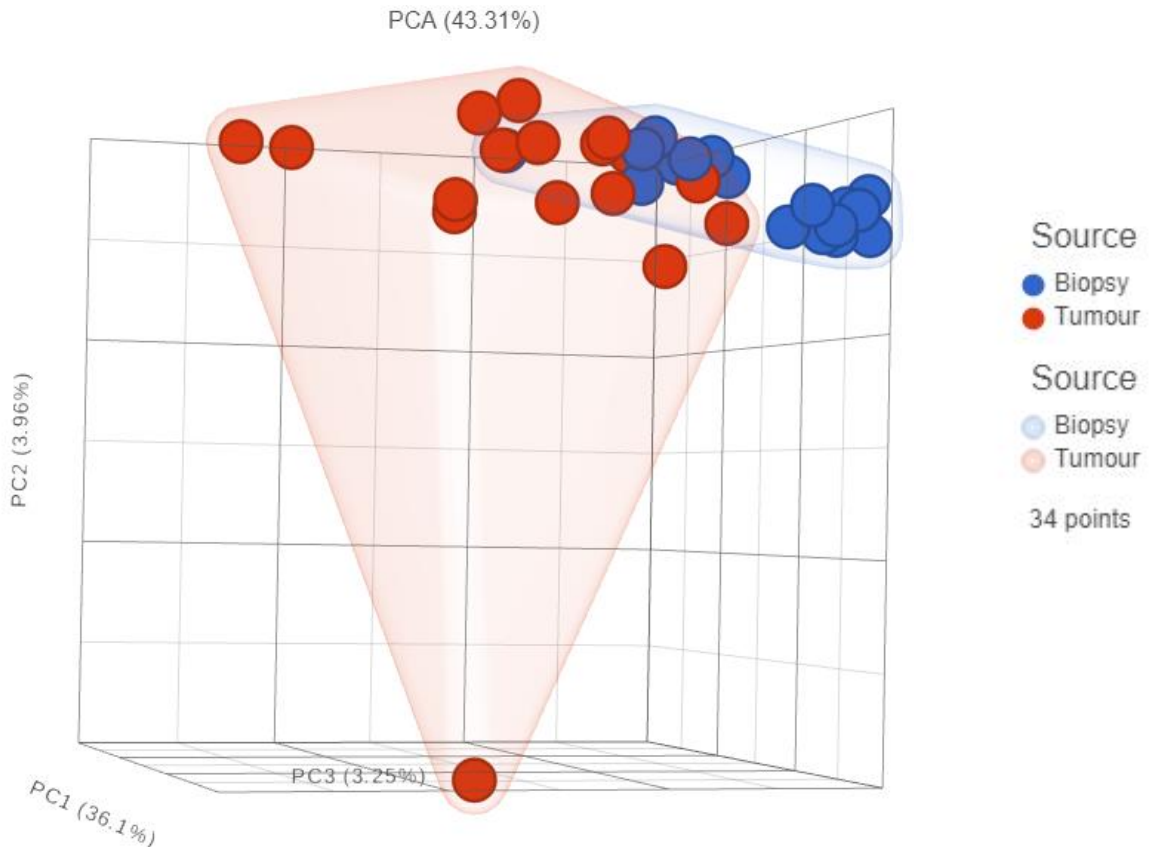


Figure 4-5: Principal component analysis of gene expression between post-NCRT (tumour) and pre-NCRT (biopsy) non-responder FFPE rectal cancer samples. Principal component analysis (PCA) was performed and plotted. Circles represent individual samples. Shaded area represents sample grouping by pre- versus post-NCRT. The first principal axis along which the largest sample variance was observed was the x-axis (PC1). The y-axis was the second most important direction in which samples showed significant variation (PC2). The third most important direction was the z-axis (PC3).

Differential expression analysis using GSA revealed 181 upregulated genes and 111 downregulated genes in post-NCRT non-responder samples, when data were filtered by $1.5 < \text{fold change} > -1.5$ and $p < 0.05$ (Figure 4-6). A large number ($n=5862$) of genes were not significantly differentially expressed.

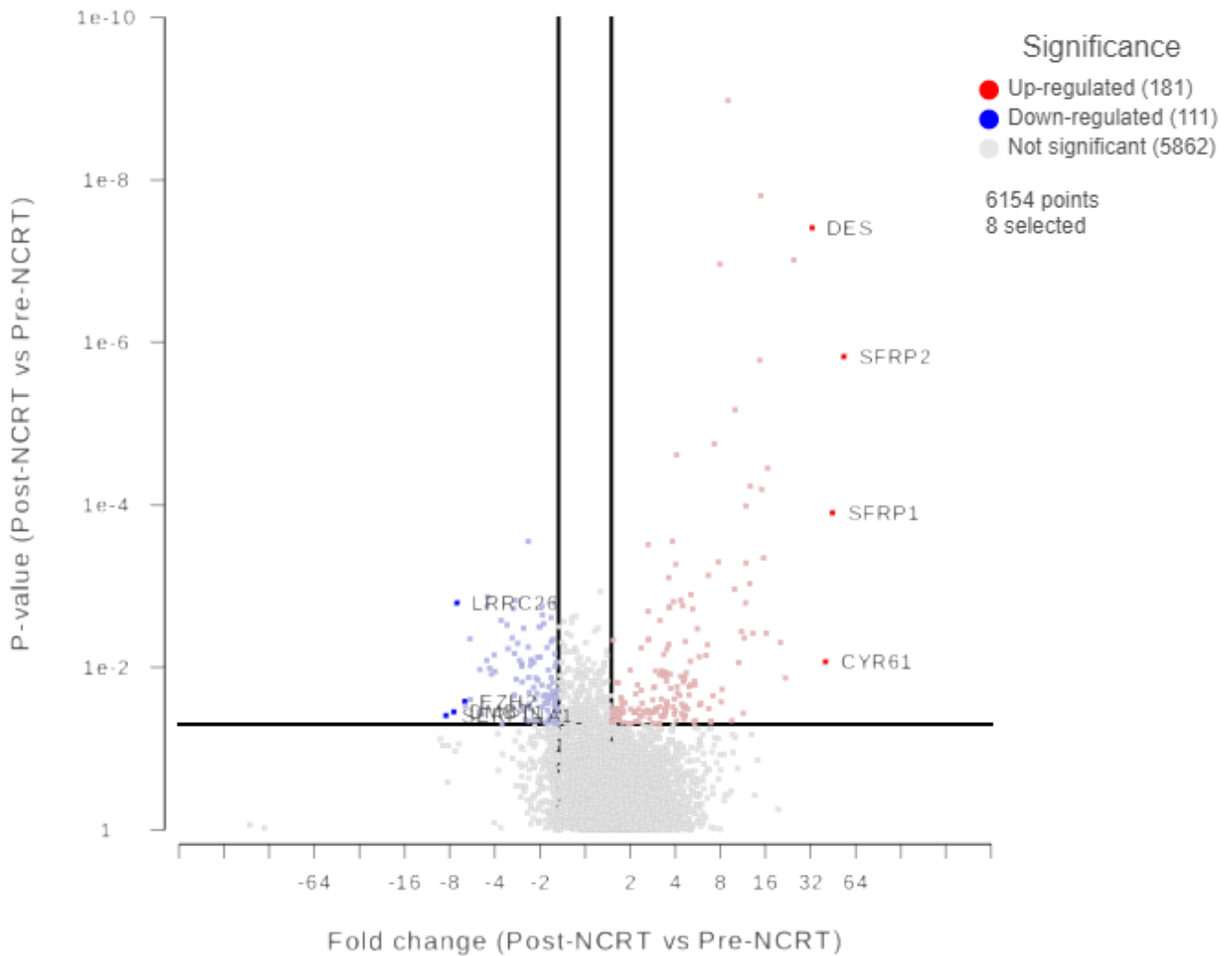


Figure 4-6: Volcano plot representing upregulated and downregulated genes in non-responder post-NCRT FFPE tumour samples

The y-axis of the volcano plot represents the p-value which was plotted against the fold change on the x-axis for each of the expressed genes. The red dots represent the significantly upregulated genes, blue dots represent the significantly downregulated genes and the light grey dots represent the non-significant genes. The top four upregulated and downregulated genes have been labelled with their respective gene name. The black horizontal line represents the level of significance at 0.05. The two black vertical lines represent the fold change cut off at -1.5 and 1.5.

4.4.4.1 *Upregulated genes in post-NCRT non-responder FFPE samples*

The top 10 of 181 differentially upregulated genes in post-NCRT non-responder FFPE tumour samples were identified and listed in descending order of fold change and ascending order of *p*-value (Table 4-7). *SFRP2* (fold change=53.28; *p*<0.001) and *SFRP1* (fold change=44.89; *p*<0.001) were the most upregulated genes in non-responders post-NCRT. These genes encode the secreted frizzled-related protein 1 and 2 respectively, and they modulate of Wnt signalling. The remaining overexpressed genes included the gene coding for long non-coding RNA *AC002398.12* (fold change=24.59; *p*<0.001). None of the genes in Table 4-7 have previously been linked to radiotherapy response in cancer. However, many of these genes belonged to pathways associated with inflammatory response in keeping with post-irradiation cellular repair.

Table 4-7: Upregulated genes in post-NCRT FFPE tumour samples of non-responders

Gene symbol	Fold change	<i>p</i>-value	<i>FDR q</i>-value
<i>SFRP2</i>	53.28	<0.001	0.001
<i>SFRP1</i>	44.89	<0.001	0.051
<i>CYR61</i>	40.27	0.008	0.465
<i>DES</i>	32.67	<0.001	<0.001
<i>AC002398.12</i>	24.59	<0.001	<0.001
<i>PSD</i>	21.74	0.013	0.489
<i>PLIN4</i>	20.07	0.005	0.394

<i>MYH11</i>	16.54	<0.001	0.020
<i>DUSP1</i>	16.11	0.004	0.365
<i>FOSB</i>	15.54	<0.001	0.146

4.4.4.2 Downregulated genes in post-NCRT non-responder FFPE samples

SERPINA1 was most downregulated gene with a fold change of -8.47 ($p=0.039$) in post NCRT non-responder samples. This gene encodes the serpin family A member 1 protein which regulates alpha-1 antitrypsin synthesis. *MMP1* was also amongst the downregulated genes in post NCRT non-responder samples (fold change=-6.28; $p=0.030$). The protein matrix metalloproteinase 1 encoded by *MMP1* promotes cell survival and migration, and MMP1 knockdown using siRNA has been shown to promote radiosensitivity in CRC cancer cells (464). The exact associations between the 111 genes found to be differentially downregulated in non-responder FFPE post-NCRT tumour samples and radiotherapy response in human cancer remains unclear. The top 10 of these 111 differentially downregulated genes can be found in Table 4-8. The remaining data not shown in this thesis.

Table 4-8: Downregulated genes in post-NCRT FFPE tumour samples of non-responders

Gene symbol	Fold change	p-value	FDR q-value
<i>SERPINA1</i>	-8.47	0.039	0.564
<i>DMBT1</i>	-7.48	0.035	0.560
<i>LRRC26</i>	-7.17	0.002	0.278

<i>EZH2</i>	-6.36	0.026	0.558
<i>MMP1</i>	-6.28	0.030	0.560
<i>CSF3R</i>	-5.88	0.004	0.393
<i>NBEAL2</i>	-5.83	0.025	0.554
<i>MFSD12</i>	-5.02	0.011	0.481
<i>COL7A1</i>	-4.89	0.037	0.563
<i>TFF1</i>	-4.53	0.008	0.465

4.4.4.3 GSEA – non-responder FFPE samples (post-NCRT tumour versus pre-NCRT biopsy)

4.4.4.3.1 Hallmark collection

GSEA using Hallmark collection revealed that 45 out of 50 gene sets were upregulated in post-NCRT, non-responder tumour resection FFPE specimens. Of these, only 13 gene sets were associated with an FDR adjusted q-value of less than 0.25. These included the Epithelial Mesenchymal Transition, Angiogenesis, Myogenesis, Downregulated in UV Response and TGF Beta Signalling gene sets, all of which recorded an ES of at least 0.5 (Table 4-9). The remaining five of the 50 gene sets of this collection were upregulated in the pre-NCRT, non-responder FFPE biopsy samples. However, none of the five were associated with an FDR adjusted q-value under 0.25.

Table 4-9: Hallmark enrichment: Upregulated gene in post-NCRT surgical resection FFPE specimens of non-responders

Gene set	Size	ES	FDR q-value	Rank at max
HALLMARK_EPITHELIAL_MESENCHYMAL_TRANSITION	193	0.61	<0.001	3395

HALLMARK_ANGIOGENESIS	35	0.56	0.003	2906
HALLMARK_MYOGENESIS	185	0.53	0.001	4006
HALLMARK_UV_RESPONSE_DN	137	0.53	0.004	3739
HALLMARK_TGF_BETA_SIGNALING	54	0.5	0.046	6365
HALLMARK_APICAL_SURFACE	39	0.46	0.012	3041
HALLMARK_HYPOXIA	182	0.44	0.007	3464
HALLMARK_TNFA_SIGNALING_VIA_NFKB	195	0.43	0.01	3397
HALLMARK_APOPTOSIS	154	0.41	0.119	3348
HALLMARK_ANDROGEN_RESPONSE	96	0.37	0.152	7785
HALLMARK_APICAL_JUNCTION	187	0.33	0.128	4192
HALLMARK_COMPLEMENT	192	0.32	0.135	4905
HALLMARK_INFLAMMATORY_RESPONSE	185	0.28	0.143	3311

Upregulated gene sets listed in descending order of enrichment score (ES) followed by ascending order of false discover rate (FDR) adjusted q-value. FDR adjusted q-value cut-off set to less than 0.25.

4.4.4.3.2 KEGG collection

GSEA using KEGG collection identified 108 out of 133 gene sets which were upregulated in non-responder, post-NCRT tumour resection specimen FFPE samples. Forty one of these were significant at an FDR adjusted q-value less than 0.25. There were several gene sets linked to pathways previously associated with radiation response. These included the P53 Signalling Pathway (ES = 0.48; FDR adjusted q-value = 0.051; Table 4-10) and MAPK Signalling Pathway (ES = 0.34; FDR adjusted q-value = 0.051; Appendix K) gene sets. The remaining twenty five gene sets of the KEGG collection were upregulated in pre-NCRT, biopsy FFPE samples of non-responders. However, the FDR adjusted q-values of all twenty five

gene sets were at least 25% and therefore, unlikely to lead to hypotheses of biological interest.

Table 4-10: KEGG enrichment: Gene sets upregulated in post-NCRT surgical resection FFPE specimens of non-responders

Gene set	Size	ES	FDR q-value	Rank at max
KEGG_VIRAL_MYOCARDITIS	61	0.51	0.046	6695
KEGG_SNARE_INTERACTIONS_IN_VESICULAR_TRANSPORT	38	0.5	0.046	6658
KEGG_ARRHYTHMOGENIC_RIGHT_VENTRICULAR_CARDIOMYOPATHY_ARVC	65	0.49	0.006	6883
KEGG_P53_SIGNALING_PATHWAY	63	0.48	0.051	3551
KEGG_ANTIGEN_PROCESSING_AND_PRESENTATION	58	0.48	0.126	6451
KEGG_ECM_RECEPTOR_INTERACTION	81	0.46	0.008	2691
KEGG_AUTOIMMUNE_THYROID_DISEASE	32	0.46	0.072	6451
KEGG_ENDOMETRIAL_CANCER	52	0.46	0.13	7327
KEGG_HYPERTROPHIC_CARDIOMYOPATHY_HCM	73	0.45	0.006	7901
KEGG_FOCAL_ADHESION	189	0.45	0.038	7952
KEGG_ADHERENS_JUNCTION	66	0.45	0.176	10639
KEGG_DILATED_CARDIOMYOPATHY	78	0.44	0.008	7901
KEGG_PRION_DISEASES	34	0.44	0.07	2662
KEGG_COLORECTAL_CANCER	60	0.43	0.121	7479
KEGG_VASCULAR_SMOOTH_MUSCLE_CONTRACTION	101	0.42	0.001	3927
KEGG_REGULATION_OF_ACTIN_CYTOSKELETON	194	0.42	0.053	8142

KEGG_MELANOMA	64	0.4	0.043	7394
KEGG_TIGHT_JUNCTION	117	0.39	0.127	7906
KEGG_LEUKOCYTE_TRANSENDOTHELIAL_MIGRATION	105	0.39	0.132	7778
KEGG_AXON_GUIDANCE	120	0.38	0.047	4198
KEGG_N_GLYCAN_BIOSYNTHESIS	44	0.38	0.249	2322

Top 25 upregulated gene sets following GSEA listed in descending order of enrichment score (ES) followed by ascending order of false discover rate (FDR) adjusted q-value. FDR adjusted q-value cut-off set to less than 0.25.

4.4.4.3.3 Oncogenic Signatures collection

Of 183 gene sets from the Oncogenic Signatures collection, 165 were upregulated in post-NCRT tumour resection specimen FFPE samples from non-responders. Ninety three of these gene sets were significant at an FDR adjusted q-value less than 0.25. Amongst these were several gene sets of interest including AKT Up V1 Down, MTOR Up V1 Down, PTEN Down V1 Up and P53 Down V1 Down (Table 4-11). The remaining 18 gene sets were upregulated in pre-NCRT FFPE biopsy samples from non-responders. However, none were associated with an FDR adjusted q-value of 25%.

Table 4-11: Oncogenic Signatures enrichment: Upregulated genes in post-NCRT surgical resection FFPE specimens of non-responders.

Gene set	Size	ES	FDR q-value	Rank at max
AKT_UP.V1_DN	170	0.43	<0.001	2488
KRAS.KIDNEY_UP.V1_UP	120	0.45	<0.001	6778

CAHOY_ASTROGLIAL	87	0.45	<0.001	3878
ATF2_UP.V1_DN	166	0.42	<0.001	3276
ATF2_S_UP.V1_DN	167	0.39	<0.001	3276
LEF1_UP.V1_UP	180	0.37	0.001	3449
ESC_V6.5_UP_EARLY.V1_DN	140	0.52	0.001	3625
RAF_UP.V1_DN	178	0.4	0.002	3830
TGFB_UP.V1_UP	170	0.37	0.002	3435
MEL18_DN.V1_DN	130	0.38	0.004	2423
BMI1_DN_MEL18_DN.V1_DN	129	0.41	0.004	2119
CSR_LATE_UP.V1_DN	137	0.38	0.005	3601
MTOR_UP.V1_DN	167	0.36	0.007	4269
CRX_DN.V1_DN	117	0.37	0.01	2817
P53_DN.V1_DN	179	0.32	0.012	1396
BMI1_DN_MEL18_DN.V1_UP	133	0.35	0.013	3449
RPS14_DN.V1_UP	175	0.38	0.014	3994
STK33_SKM_UP	240	0.36	0.017	6586
STK33_NOMO_UP	270	0.37	0.016	3857
CORDENONSI_YAP_CONSERVED_SIGNATURE	52	0.46	0.016	2877
BMI1_DN.V1_UP	137	0.35	0.017	7413
IL2_UP.V1_UP	160	0.3	0.017	3289
YAP1_UP	41	0.51	0.02	7227
STK33_UP	259	0.37	0.021	7252
RB_P107_DN.V1_UP	119	0.35	0.02	3692
PTEN_DN.V1_UP	136	0.32	0.022	4103

Top 25 upregulated gene sets listed in ascending order of FDR adjusted q-value followed by rank at max ascending order. ES= enrichment score. FDR= false discovery rate. Gene sets enriched in more than one gene set collection highlighted in bold italics.

4.4.5 NGS of FFPE sample RNA from LARC patients reveal biological pathways of interest in NCRT resistance

GSEA identified several gene sets that could lead to biologically significant hypotheses in relation to NCRT resistant in LARC. Gene sets from different collections (Hallmark, KEGG and Oncogenic Signatures) were enriched by differentially expressed genes from the pre-NCRT and post-NCRT, responder and non-responder FFPE samples. Many of these gene sets represented intracellular pathways that have been previously reported to have an association with radiotherapy response in various cancers.

4.4.5.1 The PI3K/AKT/mTOR pathway

Excluding differentially expressed ribosomal proteins, *PIK3CB* was the most upregulated gene in pre-NCRT, non-responders FFPE samples (fold change=37.90; $p=0.002$; Table 4-2). *PIK3CB* encodes the PI3K β functional subunit of the PI3K protein. The most downregulated gene in this group was *FBXW4* (fold change=-8.71; $p=0.041$). The latter encodes FBOX proteins a downstream target of mTOR associated with protein synthesis (465). GSEA using Hallmark collection revealed that gene sets associated with MTORC1 signalling were enriched by genes from pre-NCRT, non-responder FFPE biopsy samples (FDR adjusted q-value = 24.6%; Table 4-4). The enrichment plot revealed a positive enrichment score and a rank at max indicating a correlation with non-responders (Figure 4-7[A]). Hierarchical clustering and the resulting heatmap demonstrated several distinct gene groups of interest

(Figure 4-7[B]). Of 195 genes found to be significantly differentially expressed within this gene set, the top five ranking genes were *HSPA9*, *DHCR24*, *SKAP2*, *STC1* and *SQSTM1* (Figure 4-7[C]).

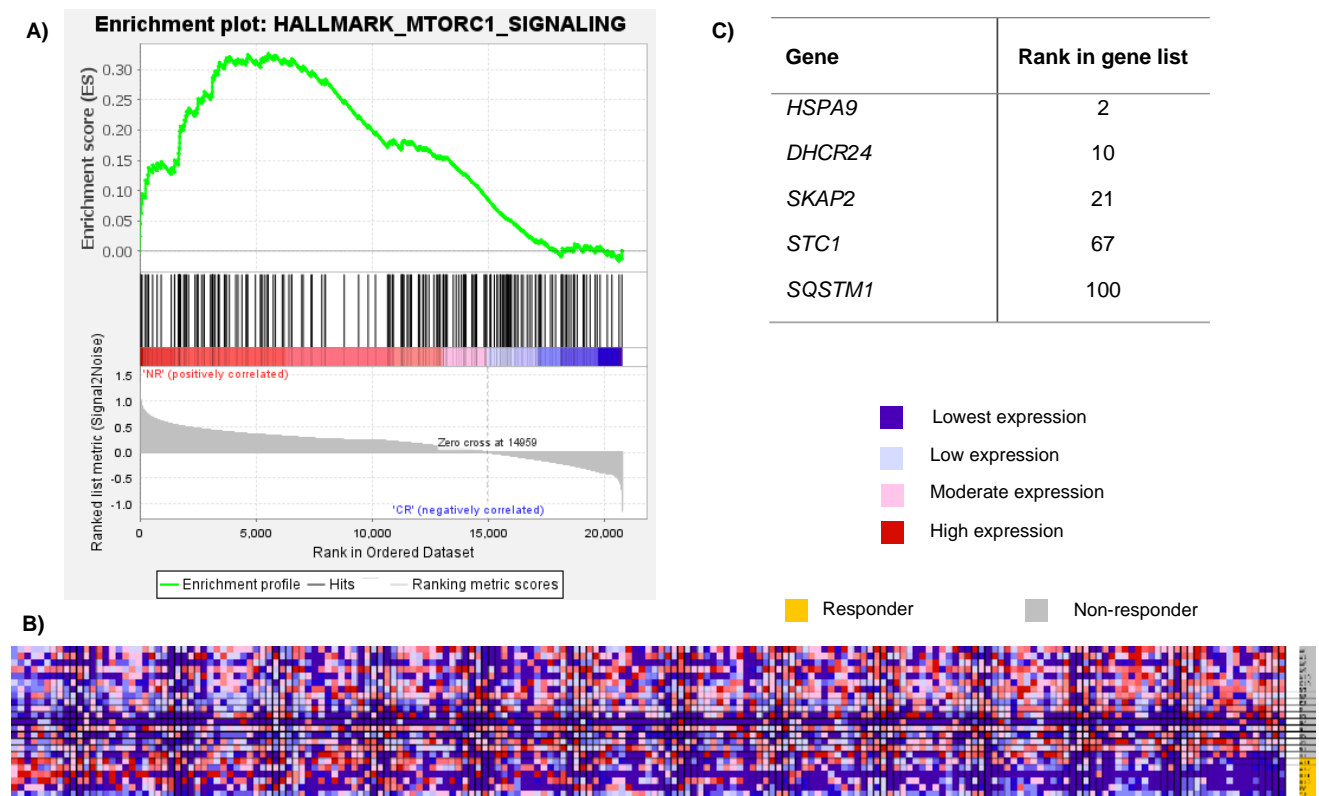
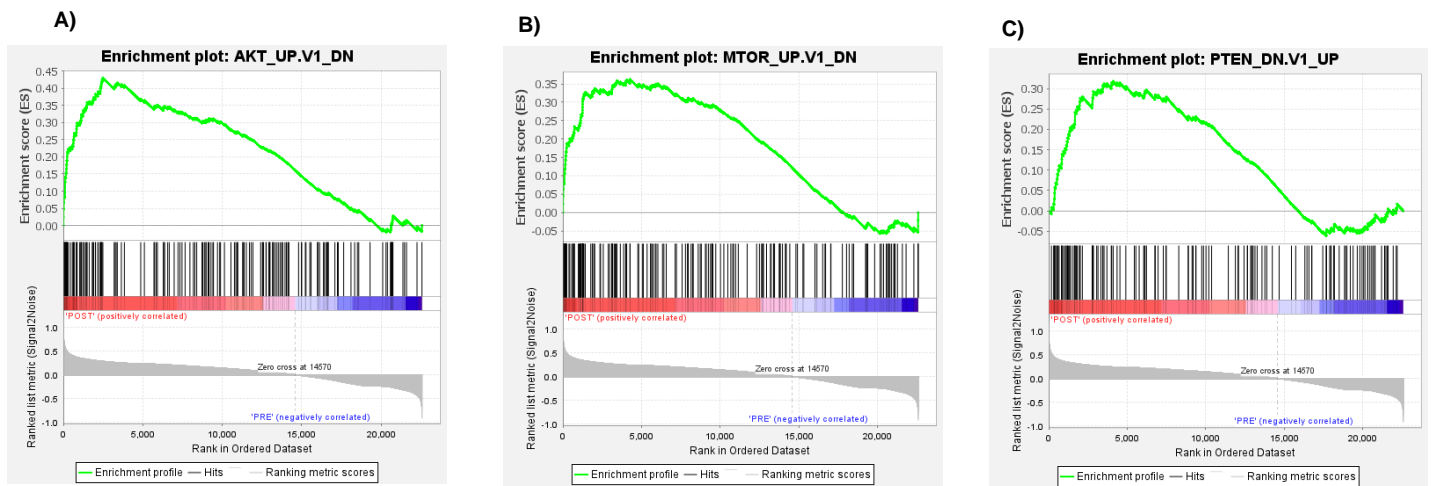


Figure 4-7: Hallmark MTORC1 Signalling gene set enriched in pre-NCRT, non-responder FFPE biopsy samples

A) Enrichment plot generated following GSEA using Hallmark collection. There was a correlation of enrichment score towards non-responders. B) A heat map generated through hierarchical clustering of differentially expressed genes of the MTORC1 Signalling gene set of the Hallmark collection. The colours dark blue, light blue, pink and red represent range of expression values lowest, low, moderate and high. Columns represent individual genes and rows represent samples. C) A list of the top five ranking genes of this gene set identified during GSEA and their rank within the gene list. Expression values are represented as colours, where the range of colours (red, pink, light blue, dark blue) shows the range of expression values (high, moderate, low, lowest).

The post-NCRT, non-responder tumour resection FFPE sample genes enriched AKT Up V1. Down (genes downregulated in mouse prostate by transgenic expression of human AKT1 gene; FDR adjusted q-value < 1%), MTOR Up V1. Down (genes downregulated by everolimus in prostate tissue; FDR adjusted q-value=0.007) and PTEN Down V1. Up (genes downregulated upon knockdown of PTEN; FDR adjusted q-value=0.022) gene sets of the Oncogenic Signatures collection (Table 4-11). The enrichment score and rank at max were positive indicating correlation with the post-NCRT phenotype (Figure 4-8 [A-C]). One hundred and seventy genes enriched the AKT Up V1 Down gene set and the top five ranking genes were *SFRP2*, *SCARA3*, *OGN*, *DPT* and *PTGIS*. Of 167 genes enriched in the MTOR Up V1 Down gene set, the top five ranking genes included *MYH11*, *SCARA3*, *DUSP1*, *AOC3* and *PPP1R14A* (Figure 4-8 [E]). Similarly, 136 genes enriched the PTEN Down V1. Up gene set and the top five ranking included *RGS2*, *EDN1*, *MAL*, *SSBP2* and *UCHL1* (Figure 4-8 [F]). Hierarchical clustering and the resulting heatmaps once again demonstrated several distinct gene clusters of interest (Figure 4-8 [G-I]). Several genes within the analysed samples demonstrated moderate or high expression within the identified gene sets associated with the PI3K/AKT/mTOR pathway. These findings led to the hypothesis that the latter pathway was associated with NCRT response. PI3K/AKT/mTOR pathway dysregulation is frequently detected in various cancers (176, 466). Preliminary research has shown inhibitors of various components of this pathway may lead to enhanced radiotherapy response in breast, CRC, prostate, lung, head and neck (H&N) cancers, and glioblastoma multiforme (GBM) (184). In CRC cell lines, pathway activation was observed in response to radiation (173).



D)

Gene	Rank in gene list
<i>SFRP2</i>	9
<i>SCARA3</i>	12
<i>OGN</i>	28
<i>DPT</i>	41
<i>PTGIS</i>	101

E)

Gene	Rank in gene list
<i>MYH11</i>	8
<i>SCARA3</i>	12
<i>DUSP1</i>	23
<i>AOC3</i>	34
<i>PPP1R14A</i>	100

F)

Gene	Rank in gene list
<i>RGS2</i>	176
<i>EDN1</i>	316
<i>MAL</i>	350
<i>SSBP2</i>	378
<i>UCHL1</i>	386

■ Pre-NCRT
 ■ Post-NCRT
 ■ Lowest expression
 ■ Low expression
 ■ Moderate expression
 ■ High expression

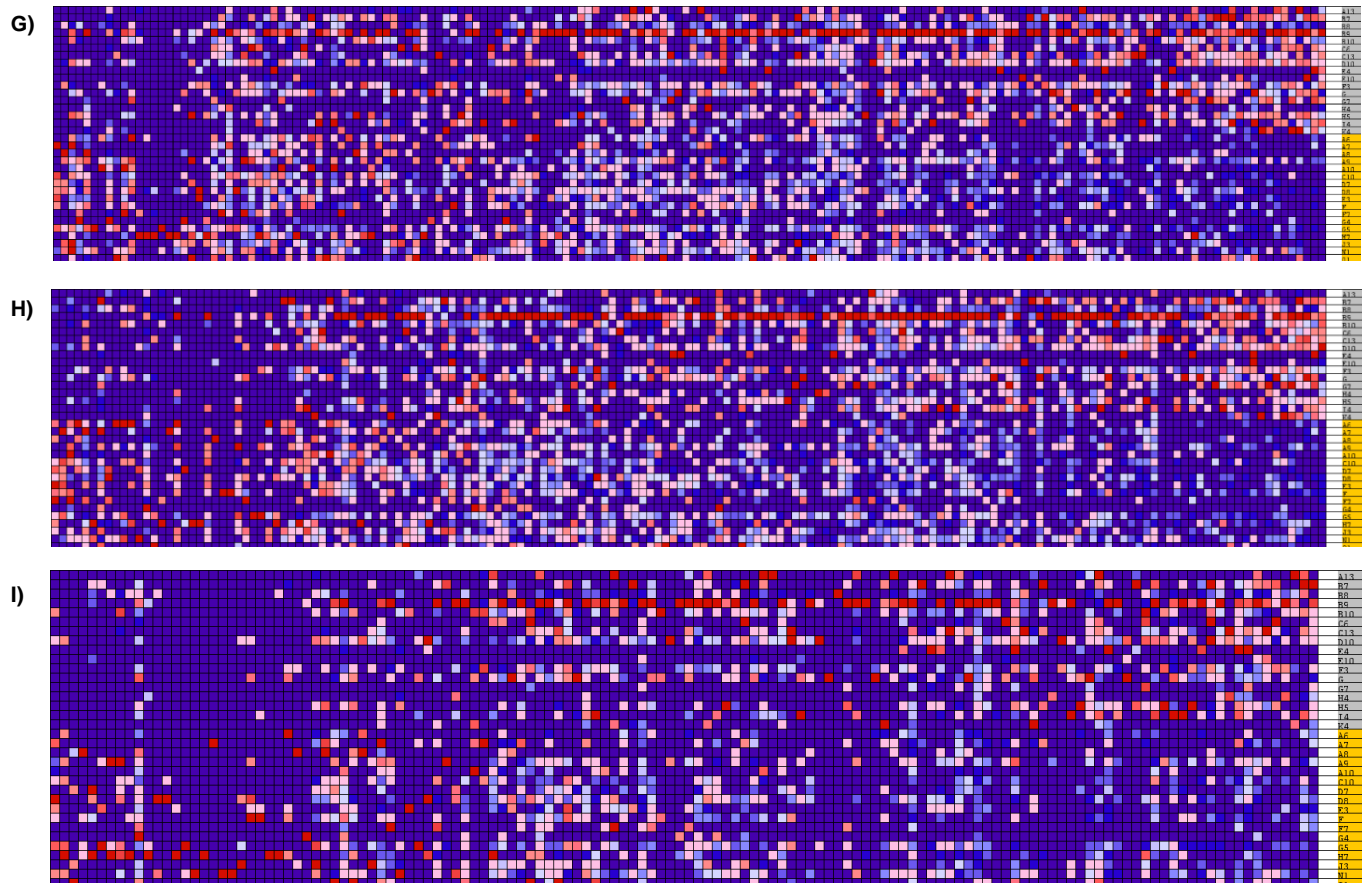


Figure 4-8: GSEA enrichment plots and heat maps of differentially expressed genes of PI3K/AKT/mTOR pathway related gene sets

A-C) Enrichment plots of gene sets associated with the PI3K/AKT/mTOR pathway, generated following GSEA using the Oncogenic Signatures collection. There was a correlation of enrichment score towards post-NCRT FFPE samples. D-F) A list of the top 5 ranking differentially expressed genes for each gene set. G-I) Heat maps generated through hierarchical clustering of differentially expressed genes of the AKT Up V1. Down (G), MTOR Up V1. Down (H) and PTEN Down V1. Up (I) gene set of the Oncogenic Signatures collection. The colours dark blue, light blue, pink and red represent range of expression values lowest, low, moderate and high. Columns represent individual genes (gene names not shown) and rows represent samples. Expression values are represented as colours, where the range of colours (red, pink, light blue, dark blue) shows the range of expression values (high, moderate, low, lowest).

4.4.5.2 P53 pathway

The pre-NCRT, non-responder FFPE biopsy sample genes enriched the P53 Pathway gene set of the Hallmark collection (FDR adjusted q-value=21.5%; Table 4-4). The top five ranked genes of 189 differentially expressed genes within this gene set included *CD81*, *SFN*, *SEC61A1*, *STEAP3* and *HINT1*. Furthermore, post-NCRT, non-responder FFPE surgical resection specimen genes enriched the P53 Signalling Pathway gene set of the KEGG collection (FDR adjusted q-value=5.1%; Table 4-10) and P53 Down V1. Down gene set (genes which were downregulated in a NCI-60 cell line panel containing TP53 mutations), of the Oncogenic Signatures collection (FDR adjusted q-value=1.2%; Table 4-11). The top five of 63 differentially expressed genes of the P53 Signalling Pathway gene set of the KEGG collection included *SERPINE1*, *ZMAT3*, *IGF1*, *GADD45B* and *CDKN1A*. The top five of 179 differentially expressed genes of the P53 Down V1. Down pathway gene set were *CRYAB*, *ACTA2*, *FBLN5*, *IL1R1* and *VIM*. P53 mutations have been associated with

radiotherapy response in lung, breast, rectal, head and neck cancers (286, 467-469). Radiotherapy leads to DNA DSB and P53 plays a crucial role in apoptosis of cells with irreparable DNA damage (470). However, tumour cells often harbour *P53* mutations and are radioresistant due to inhibited apoptosis of cells containing damaged DNA (467). In LARC, *P53* wild-type genotype has been associated with pCR in LARC (286).

4.4.5.3 *Oxidative phosphorylation and hypoxia signalling*

GSEA revealed pre-NCRT, non-responder FFPE biopsy samples enriched Oxidative Phosphorylation gene set of the KEGG collection (FDR adjusted q-value=1.9%; Table 4-5). Of the 106 genes which were differentially expressed within this gene set, the top five ranking genes included *MT-ND6*, *MT-ND6*, *COX4I1*, *MT-ND3*, *MT-CYB* and *NDUFS5*. This gene set relates to the oxidative phosphorylation pathway which is frequently upregulated in cancer cells resistant to tumour hypoxia (471, 472). Tumour hypoxia leads to chemoradiotherapy resistance and poor prognosis in various cancers (473, 474). Hypoxic tumour cells frequently express HIF1 α and VEGF promoting oxidative phosphorylation and angiogenesis promoting tumour cell survival (475, 476).

4.4.5.4 *Notch signalling pathway*

Pre-NCRT non-responder FFPE biopsy samples also enriched the Notch Signalling gene set of the Hallmark collection (FDR adjusted q-value=23.1%; Table 4-4). Of 32 genes that were differentially expressed within this gene set, the top five ranking genes in non-responders included *TCF7L2*, *PSENEN*, *FBXW11*, *HEYL* and

NOTCH3. Inhibition of notch signalling has been shown to promote radiotherapy response in glioblastoma multiforme (477), lung cancer (478), nasopharyngeal carcinoma (479) and breast cancer (480).

4.4.5.5 *The MAPK pathway*

GSEA revealed that post-NCRT non-responder tumour resection specimen genes enriched KRAS Kidney Up V1. Up (genes upregulated in epithelial kidney cancer cell lines over-expressing an oncogenic form of KRAS; FDR adjusted q-value < 1%; Table 4-11) and RAF UP V1. Down (genes downregulated in MCF-7 breast cancer cells positive for ESR1 stably over-expressing constitutively active RAF1; FDR adjusted q-value < 1%; Table 4-11) gene sets of the Oncogenic Signatures collection. The top five ranking differentially expressed genes of each gene set were *SFRP1*, *CRYAB*, *SORBS1*, *ANK2*, *CPE* and *MGP*, *MYLK*, *TSC22D3*, *FOS*, *PALLD* respectively. The significance of *KRAS* mutation status on radiotherapy response in LARC is unclear with some studies showing an association with pCR whilst others did not (287). The pathway also cross-talks with the PI3K/AKT/mTOR pathway (118).

4.4.5.6 *Epithelial Mesenchymal Transition pathway*

The epithelial mesenchymal transition pathway gene set of the Hallmark collection was enriched by post-NCRT, non-responder tumour resection specimen genes (FDR adjusted q-value <1%; Table 4-9). Of the 193 genes differentially expressed within this gene set, the top five ranking genes included *MGP*, *TAGLN*, *MYLK*, *MYL9* and *FBLN1*. Epithelial mesenchymal transition is upregulated in response to radiation and leads to radiotherapy resistance (481). The pathway also closely interacts with

the PI3K/AKT/mTOR pathway, notch signalling pathway, Wnt signalling pathway, EGFR pathway, ERK pathway. NF κ B pathway and TGF- β pathway (482).

4.4.5.7 *The TGF β pathway*

The post-NCRT, non-responder FFPE samples enriched the TGF Beta Signalling gene set of the Hallmark collection (FDR adjusted q-value= 4.5%; Table 4-9) and TGFB Up V1. Up (TGFB1 upregulated genes in a panel of epithelial cells; FDR adjusted q-value < 1%; Table 4-11) of the Oncogenic Signatures collection. Of 54 genes differentially expressed in the Hallmark gene set, the top five ranking genes included *JUNB*, *SERPINE1*, *MAP3K7*, *SKI* and *RHOA*. The top five ranking genes out of 170 differentially expressed genes of the Oncogenic Signatures set included *TAGLN*, *JUNB*, *SMTN*, *CRYAB* and *RHOB*. In the tumour microenvironment, the main effector of this pathway, TGF β is a potent cytokine which inhibits immune response targeting cancer cells (483). Conventionally referred to as a tumour suppressor, TGF β also regulates the epithelial mesenchymal transition pathway (484); the latter has been associated with radioresistance (481). Inhibiting TGF β could lead to radiosensitivity through impaired DNA DSB repair via inhibition of the ataxia telangiectasia mutated pathway (485).

4.4.5.8 *The NF κ B pathway*

The TNFA Signalling Via NF κ B gene set of the Hallmark collection was enriched by post-NCRT, non-responder FFPE samples (FDR adjusted q-value= 1%; Table 4-9). Of 195 differentially expressed genes within this set, the top five ranking genes

included *JUNB*, *DUSP1*, *FOS*, *RHOB* and *SERPINE1*. NF κ B which the primary effector of this pathway cross-talks with the PI3K/AKT/mTOR pathway (486-488). Radiation leads to increased expression of the NF κ B (476). NF κ B inhibitor parthenolide was shown to radiosensitise cancer cells (489).

4.5 Discussion

In this study, 3' RNA sequencing was performed on a retrospective cohort of LARC patients using RNA extracted from pre-NCRT FFPE biopsy samples and post-NCRT, FFPE surgical tumour resection specimens. Archived samples were obtained and evaluated by a trained pathologist to verify the presence of tumour tissue using optical microscopy. An additional bioinformatic purity analysis step (ESTIMATE analysis) was introduced to check for stromal contamination and immune system infiltrates. This confirmed that the pre-NCRT specimens were of acceptable standard and did not contain significant differences in levels of stromal or immune system infiltrates between the analysed groups. Genomic markers identified during this study with an association with radiotherapy response can be broadly categorised into those predicting radioresistance or sensitivity. The role of *RPL5P34*, *PIK3CB* and *OSBL*, which were upregulated pre-NCRT, in patients that demonstrated a poor response to NCRT warrants further assessment as biomarkers predicting radioresistance. On the other hand, *FBXW4* was significantly downregulated in non-responder PDOs and may therefore, predict pCR. However, apart from *RPL5P34*, none of the remaining biomarkers recorded FDR adjusted q-values of less than 5% and must therefore, be interpreted with caution due to potential false positives. It is also important to note the results from differential expression analysis of non-

responder pre- (biopsy) versus post-NCRT (tumour) sample RNA may be compromised due to significant differences in stromal contamination between the analysed groups as highlighted by the ESTIMATE analysis (Figure 4-2).

To understand the biological pathways associated with NCRT response, GSEA was performed using RNA expression data comparing pre-NCRT, non-responder with complete responder biopsy samples. Downstream analysis of gene expression data can be challenging given the wide range of available bioinformatics tools and lack of consensus in methodology. GSEA is a widely used gene expression data analysis tool which detects systematic alterations of related genes, grouped into gene sets, within the two categories (449). Davies et al. defines GSEA as a computational technique used to assess statistically significant differential expression of upregulated genes across two phenotypes (451). It is a powerful bioinformatics tool which facilitates real-world translation of large volumes of NGS data. In this study, GSEA revealed several gene sets which were associated with non-responder status at baseline. The PI3K/AKT/mTOR pathway, P53 pathway, oxidative phosphorylation and notch signalling pathways were upregulated in pre-NCRT non-responder biopsy samples. Furthermore, in-depth analysis of individual expression of the various genes and corresponding samples demonstrated upregulation of the above pathways' genes were associated with NCRT resistance (Figure 4-8). This is also in keeping with published literature which has demonstrated upregulation of former pathways and treatment resistance in various cancers (490, 491). The MAPK pathway, epithelial mesenchymal transition, TGF β and NF- κ B signalling pathways were also upregulated in non-responders post-NCRT. However, these results were

again interpreted with caution given the significance biases introduced by the stromal contamination of post-NCRT samples.

There were several limitations within this retrospective study. The sample size was relatively small and could be at risk of selection bias. Use of FFPE samples as opposed to fresh tissue samples could have led to lower quality sequencing data. Three patients in the sample were treated with additional chemotherapy prior to radiotherapy instead of the standard 5FU or Capecitabine alone. However, all three were non-responders and therefore, the impact on outcomes of this research which predominantly focused on the pre-NCRT FFPE biopsy expression profiles is minimal. The time from neoadjuvant treatment to surgery was also different for these samples and this could have an impact on the results. Tumour staging, size and location within the rectum which all have impact on tumour response to NCRT was also not controlled for within this analysis. The ESTIMATE analysis demonstrated potential stromal and immune infiltration contamination of the post-NCRT non-responder samples. Therefore, the results from analyses using these samples were interpreted with caution when interpreting the results. Whilst several individually differentially expressed genes were identified as statistically significantly differentially expressed by nominal p -values, the majority did not record FDR adjusted q -values under 5%. Therefore, the risk of false positives must be considered when interpreting individually differentially expressed genes. However, this was accounted for by using GSEA to obtain meaningful results from the available data.

4.6 Conclusion

Within limitations, this retrospective analysis demonstrated feasibility in extraction of genomic RNA from archived FFPE tumour samples for transcriptomic analysis. The study identified potential biomarkers associated with radioresistance (*RPL5P34*, *PIK3CB* and *OBSL1*) and radiosensitivity (*FBXW4*) in LARC. GSEA revealed several gene sets associated with pathways of biological interest differentially expressed amongst non-responders at baseline. These included several pathways associated with DNA damage repair, cell growth, proliferation and metabolism such as the PI3K/AKT/mTOR pathway, P53 pathway, oxidative phosphorylation and notch signalling pathways which were upregulated in FFPE biopsy samples from patients who subsequently did not respond well to NCRT. Therefore, further validation of these biomarkers and biological pathways using larger sample sizes, fresh donor tissue and *in vitro* experiment models are warranted, given their clinical significance as potential targets for predicting and improving NCRT response in LARC.

Chapter 5: Patient derived organoid models to simulate radiotherapy treatment *in vitro* and transcriptomic analysis

5.1 Introduction

Most preclinical research evaluating the mechanisms behind radioresistance and radiosensitising drugs in rectal cancer have utilised *in vitro* and xenograft experiment models using CRC cell lines. However, there has been limited translation of findings from this research into the clinical environment. This could be attributed to inter-patient variability to treatment response, tumour heterogeneity or acquired resistance to therapies which these traditional experiment models fail to recapitulate (364). Cell line research comprise of an artificial experimental framework where cancer cells are induced into a homogenous clonal expansion within a two-dimensional culture which fails to capture the diverse biological features found in a primary cancer and its microenvironment. There is a need for preclinical research models that resemble this genomic heterogeneity observed in patients, whilst allowing the reliability and flexibility required of an *in vitro* assay. Consequently, the experiment model referred to as patient-derived organoid (PDO), has become increasingly popular (334, 335). PDOs maintain cellular heterogeneity and genetic stability after multiple passages, rendering them a powerful tool in cancer research (364). PDOs have been derived

from primary CRC biopsies and surgical resection specimens replicating the genetic diversity and treatment response to various treatments, within the laboratory (334, 335). Ganesh et al. demonstrated that rectal cancer organoids mirror the clinical response of individual rectal cancer patients undergoing NCRT (334). Yao et al. observed a broad range of intrinsic PDO response variations to conventional chemoradiotherapy (335). These studies suggest that PDOs could serve as tumour avatars which predict rectal cancer response to various treatments. The ability of PDOs to maintain cellular heterogeneity and genetic integrity after multiple passages renders them ideal for *in vitro* experiments spanning several days as well as to understand and confirm the key drivers of treatment resistance and how to overcome these.

5.2 Aims

In this chapter, PDO lines were established and characterised using immunohistochemistry and DNA panel sequencing. *In vitro* irradiation assays were performed to identify radiotherapy resistant (radioresistant) and sensitive (radiosensitive) PDO lines. Pre-treatment, differential gene expression between radioresistant and radiosensitive PDOs, was assessed using 3' and total RNA sequencing. Furthermore, post-irradiation, PDO 3' RNA sequencing was performed to determine differential gene expression between the two groups pre- and post-irradiation. Downstream bioinformatics analyses were performed to identify biological pathways of significance.

5.3 Methods

Fresh tissue samples from patients undergoing surgical resection for CRC were retrieved and PDO lines were derived in the laboratory. Live cultures were regularly tested and ensured clear of mycoplasma (Appendix L). Anonymised demographic and clinicopathological data were obtained using electronic patient records. Genomic and immunohistochemical characterisation was performed. An *in vitro* radiotherapy assay was developed to assess the radiotherapy response of each PDO line. A nominal *p*-value of less than 0.05 was assigned as the level of statistical significance when interpreting the results from a two-way Anova test. Transcriptomic analysis was performed using RNA extracted from PDO lines at baseline through 3' and total RNA sequencing. Pre- and post-irradiation differential gene expression was assessed using 3' RNA sequencing at different radiotherapy doses. PCA was performed. A nominal *p*-value of less than 0.05 and a FDR adjusted *q*-value of less than 0.05 were assigned as the level of statistical significance following 3' RNA and total RNA differential gene expression analyses, respectively. GSEA was performed using MSigDB V4 Hallmark, KEGG and Oncogenic Signatures collections to identify biological pathway of significance. Given the sample size in one of the categories was less than two, differences in classes statistical modelling (a non-parametric test). An FDR adjusted *q*-value less than 0.25 was set as the level of significance to identify gene sets of biological significance following GSEA.

5.4 Results

5.4.1 *Establishing and characterising PDO lines*

5.4.1.1 *Clinicopathological characteristics*

The first six of 16 PDO lines successfully derived using fresh surgical resection specimens from CRC patients in the laboratory were used in experiments. PDO derivation success rate was approximately 50%. The clinicopathological features of the patients from whom the tumours were retrieved are summarised in Table 5-1. The median age of donors was 76 (IQR:74-78). Half (n=3, 50%) were female. Two of the lines (884 and 653) were established from primary rectal tumour surgical resection specimens and one was from a tumour at the rectosigmoid junction (064). The remaining three PDO lines (389, 411, 557) were derived from primary colonic tumours. Four of the PDO lines originated from tumours that were treatment naïve (064, 389, 411 and 557). PDO line 884 was derived from a tumour that had received SCRT and 653 from a tumour that had received NCNRT. The tumour regression grade for the latter tumours were TRS-3 (complete non-responder) and TRS-2 (partial responder) respectively. In addition, PDO line 411 was derived from a tumour harbouring a *BRAF* mutation. Two of the PDO lines (653 and 557) were derived from *KRAS* mutant parent tumours and the parent tumour of 557 demonstrated MSI-H phenotype.

Table 5-1: Patient clinicopathological characteristics

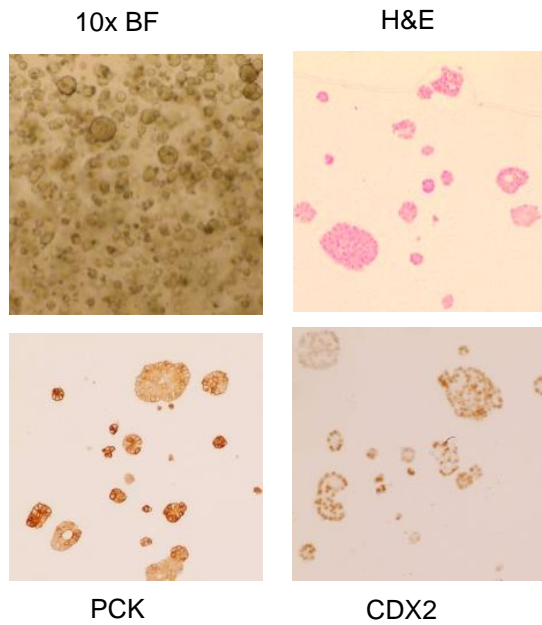
ID	Origin	Age	M/F	Diagnosis	Nx	TRS	TNM	MMR	KRAS	BRAF
884	Rectum	75	M	Locally advanced mid rectal adenocarcinoma	SCRT	TRS-3	pT3, N2a, M0	No loss	wt (N-RAS-mut)	wt
064	Recto-sigmoid	79	M	Rectosigmoid adenocarcinoma	NA	NA	pT2, N1, M0	No loss	wt	wt
389	Colon	82	M	Transverse colon adenocarcinoma	NA	NA	pT4a, N2a, M0	No loss	wt	wt
411	Colon	74	F	Transverse colon adenocarcinoma	NA	NA	pT3, N2b, M0	No loss	wt	mut
653	Rectum	55	F	Locally advanced low rectal adenocarcinoma	NCRT	TRS-2	pT2, N0, M0	No loss	mut	wt
557	Colon	76	F	Ascending colon adenocarcinoma	NA	NA	pT3, N0, M0	Loss of MLH1, PMS2 and MHS6	mut	Not available

TRS – Tumour regression score; Nx – Neoadjuvant treatment, SCRT – short course radiotherapy; wt – wild-type; mut – mutant; NCRT – neoadjuvant chemoradiotherapy; NA – not applicable

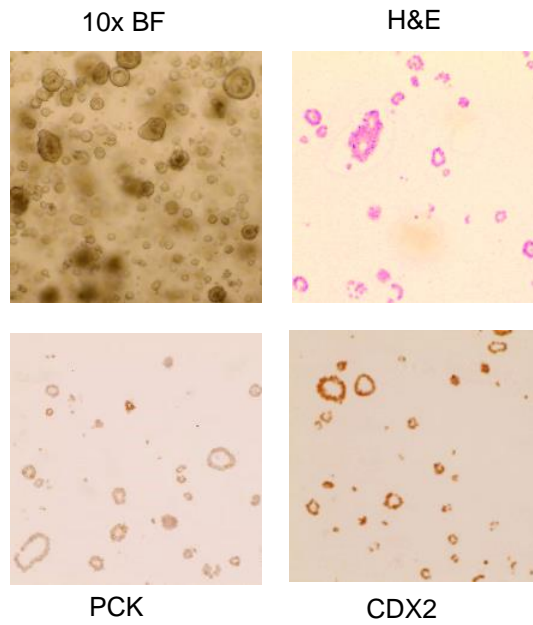
5.4.1.2 *Microscopic characterisations of PDO models*

Mature PDO cultures were visualised under optical microscopy at 10x magnification under bright field light. Distinct clusters of varying densities were identified (Figure 5-1). Immunohistochemical characterisation of the established PDO lines was performed as follows: PDOs were fixed in formalin, immersed in 2% agarose pellets and were embedded in paraffin. The sections were stained using H&E, pancytokeratin and CDX2 to check for tumour status and colorectal origin respectively. Immunohistochemistry demonstrated that PDOs organise into heterogeneous 3D structures with hollow lumens (Figure 5-1). All six PDO lines positively stained with H&E and pancytokeratin. PDO lines 884, 064, 389 and 411 positively stained for CDX2. PDO lines 653 and 557 did not stain with CDX2. CDX2 is an intestinal specific transcription factor. Approximately 20% of colorectal tumours do not express CDX2 and these patients have a poorer prognosis (492, 493).

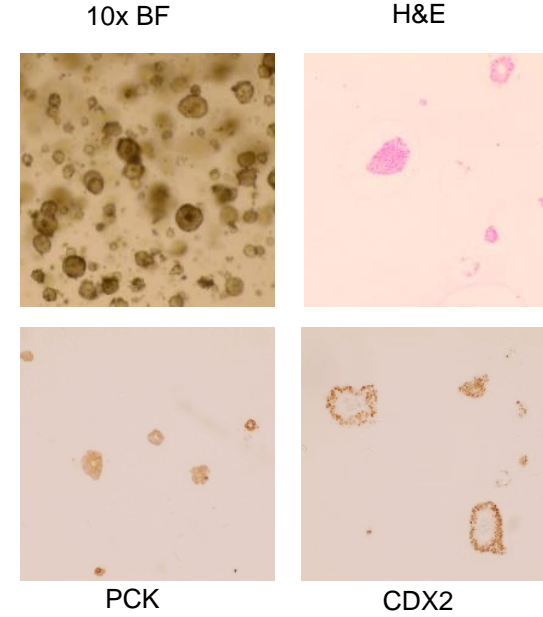
A) PDO 884



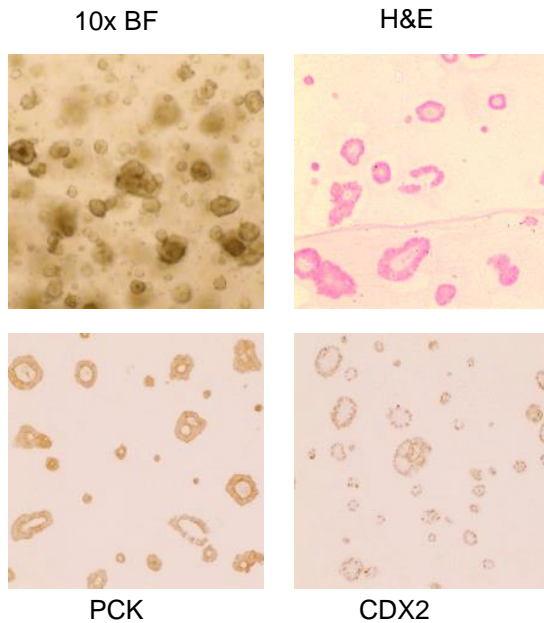
B) PDO 064



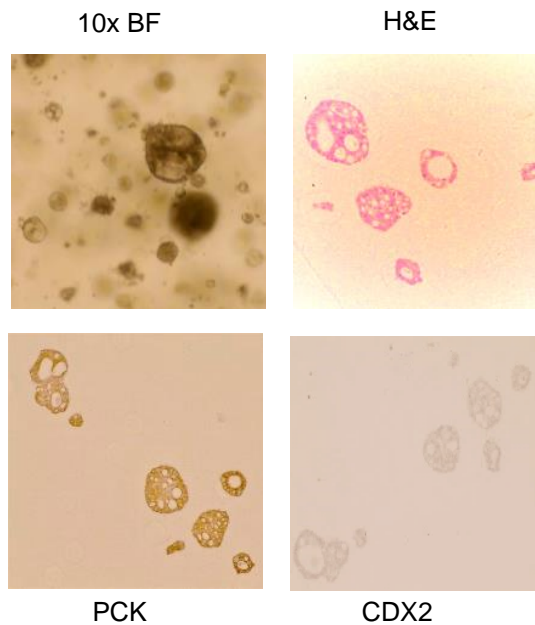
C) PDO 389



D) PDO 411



E) PDO 653



F) PDO 557

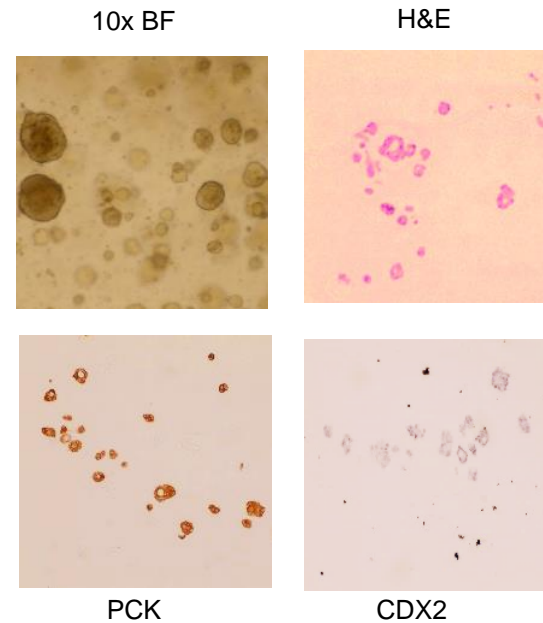


Figure 5-1: Optical microscopy and immunohistochemistry of 6 patient derived organoid lines PDO lines were stained with haematoxylin and eosin (H&E), pancytokeratin (PCK) and CDX2 and visualised under 10x bright field (BF) optimal light microscopy. PDO=patient derived organoid

5.4.1.3 Genomic characterisation

DNA extracted from PDOs were quantified and subjected to quality control. The DIN values ranged from 7.5 to 9.4 (concentration range: 33 to 60ng/ μ l). The DNA quantification and quality control data is displayed in Table 5-2.

Table 5-2: PDO DNA quantification and quality control data

Organoid ID	Alternative ID	DNA concentration (ng/μl)	DIN
884	OA1	60	8.3
411	OA2	54	7.5
653	OA3	33.4	9.4
389	OA4	57	8.9
064	OA5	53	8.1
557	OA6	48.1	8.9

Quantification using Qubit™ 3.0 Fluorometer. DNA integrity number (DIN) values obtained using TapeStation® 2200

Library preparation was performed using a QIAseq™ custom targeted DNA panel and sequencing performed using an Illumina MiSeq™ (see 2.5.3.3). Qiagen Biomedical Genomics Workbench was used for bioinformatics analysis along with the ClinVar database to identify pathological mutations within each PDO line. The mutation profiles of the six PDO lines have been summarised in the heatmap below (Figure 5-2).

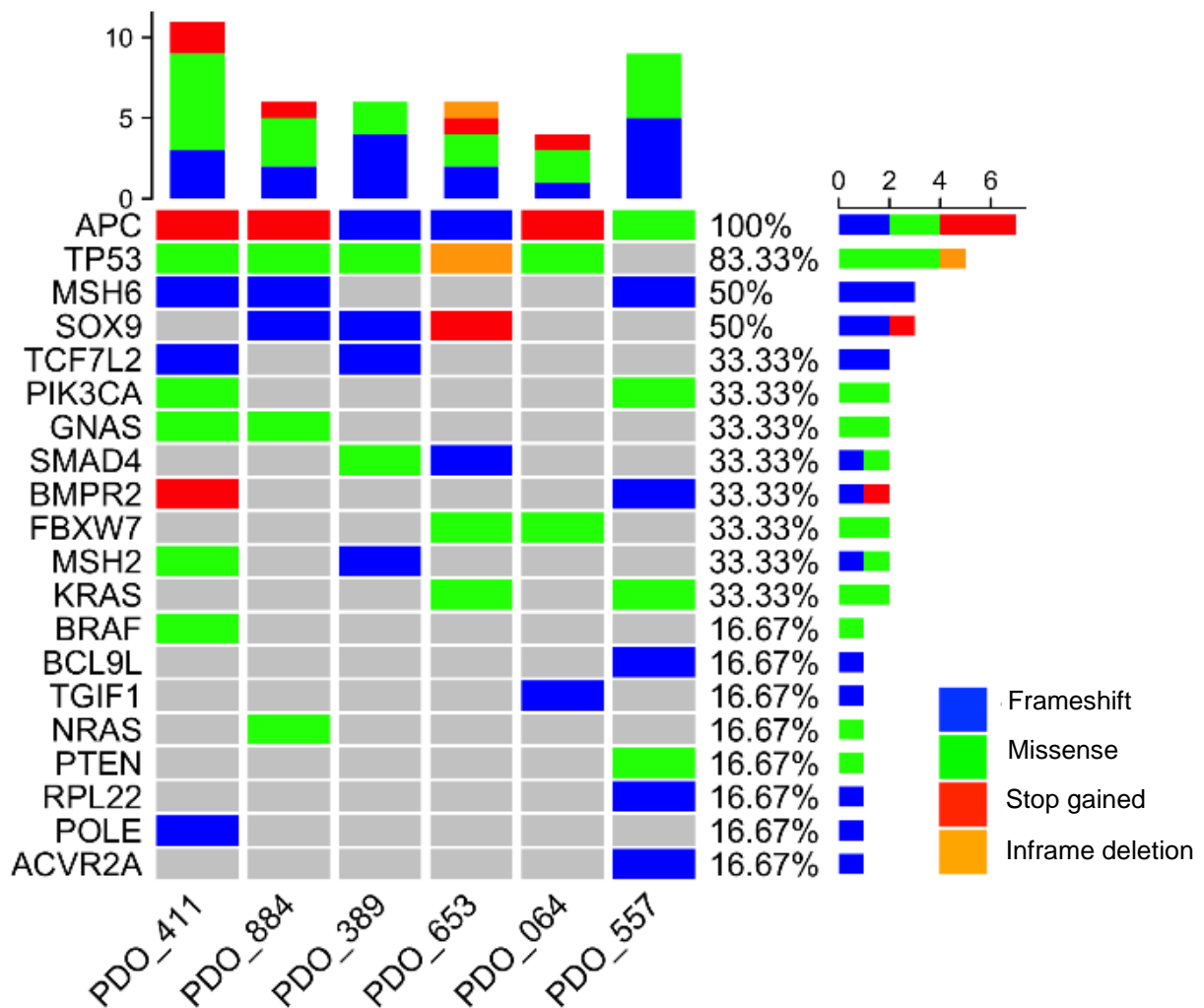


Figure 5-2: Heatmap demonstrating QIAseq™ targeted DNA panel sequencing data. Heatmap generated using ComplexHeatMap OncoPrint R Script (Appendix I). Grey = wild-type. The different colours represent different types of mutations. A detailed list of the pathological mutations identified can be found in Appendix M.

Of the 30 genes on this panel, the six PDO lines harboured 20 genes containing mutations of significance in CRC. All six lines demonstrated APC gene mutations. Pathological p53 mutations R282W, R175H, G245D, R248Q and P191del were present in all PDO lines except 557. MSH6 mutations F1088fs, L1330fs, F1104fs

were detected in 884, 411 and 557, and *SOX9* mutations *Y297fs*, *S323fs*, *Q1378** were observed in 884, 389 and 653, respectively. Mutations on *PIK3CA* (*E545K* and *R88Q*), *GNAS*, *SMAD4* (*R496H* and *W320fs*), *BMP2R*, *FBXW7*, *MSH2*, and *KRAS* (*G12D* and *G13R*) were present in 653 and 557 PDO lines. Lastly, mutations in *BRAF* (*V600E*), *BCL9L*, *TGIF1*, *NRAS*, *PTEN*, *RPL22*, *POLE*, *ACVR2A* were also detected across the different lines.

Genomic characterisation through targeted panel sequencing also demonstrated a comparable mutation profile between the PDO lines and the known mutations within the parent tumour, as identified from the available clinical data. For example, *NRAS* mutations were present in PDO line 884 and its parent tumour. *KRAS* mutations were detected in PDO lines 653 and 557 as well as within their parent tumours. Of note, PDO line 557 was derived from a MSI-H primary tumour and was found to contain a mutation in *MSH6* (*F1104fs*). PDO line 411 was the PDO line with the highest number of pathological mutations. It also demonstrated *MSH2* (*D167V*) and *MSH6* (*L1330fs*) mutations. However, the histopathology report from this patient's tumour stated no loss of dMMR protein expression on immunohistochemistry. The patient from whom PDO line 411 originated, also developed early metastatic recurrence and died within 12 months of surgery. The latter clinical course is in keeping with a MSI-L / MSS phenotype, often associated with a poor prognosis (494).

5.4.2 PDO response to radiotherapy

The response to radiotherapy amongst the six PDO lines was assessed using an *in vitro* experiment model developed within our laboratory (Figure 5-3). The PDOs were plated 5000 cells/well based on previously published experiments using CRC PDO models and preliminary experiments conducted within the laboratory (data not shown). Figure 5-4 summarises the combined results from three independent experiments evaluating radiotherapy response of each of the six PDO lines *in vitro*. The results were normalised to the average experiment endpoint viability from an untreated control plate for each PDO line. The minimum dose administered to a PDO line was 10 Gy (2 Gy/day administered for 5 days). The maximum dose was 200Gy (40 Gy/day administered for 5 days). Four PDO lines (884, 064, 389 and 411) demonstrated lower IC₅₀ values ranging between 10.35 Gy to 20 Gy (Figure 5-4). These were classed as radiosensitive lines. The remaining two PDO lines were classed as radioresistant given the very high IC₅₀ values of 2.41x10⁴ Gy (653) and 2.93x10²⁰ Gy (557) ($p < 0.0001$). The relative organoid viability of radioresistant PDOs were at least 40%, even when treated with extremely high radiotherapy doses (e.g., 200 Gy).

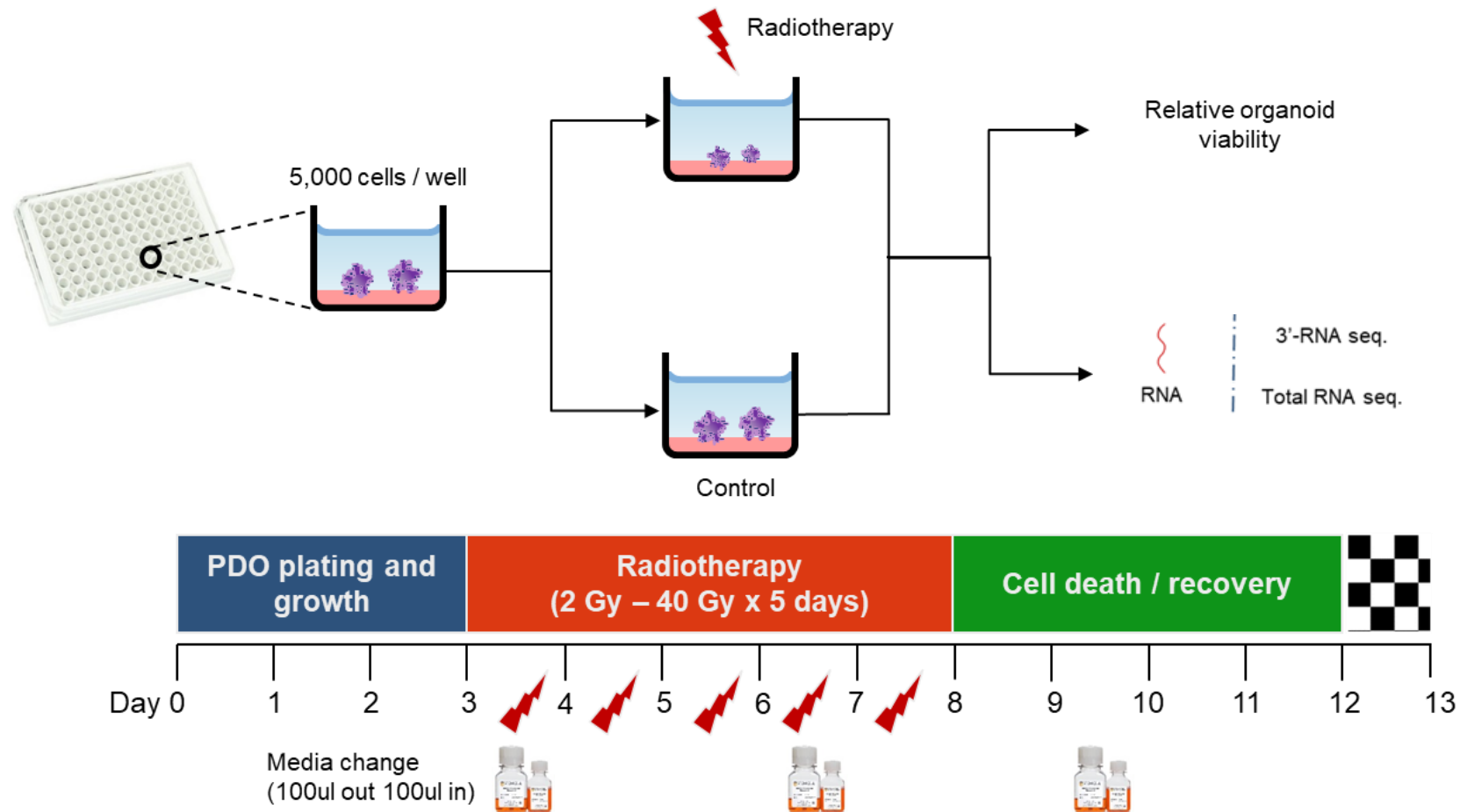


Figure 5-3: An in vitro model to assess PDO radiotherapy response

PDOs were plated (estimated 5000 cell/well) on a Matrigel® bed in 96 well plates. Radiotherapy was commenced on day four at doses ranging from (2 Gy/day to 40 Gy/day for five days). The experiment was completed on day 13 with endpoint PDO viability assessment using CellTiter-Glo® 3D (Promega, USA) and chemiluminescence



Copyright of STEMCELL Technologies (Canada). Image used with permission. Source: [https://www.stemcell.com/cell-](https://www.stemcell.com/cell-separation/immunomagnetic)

separation/immunomagnetic

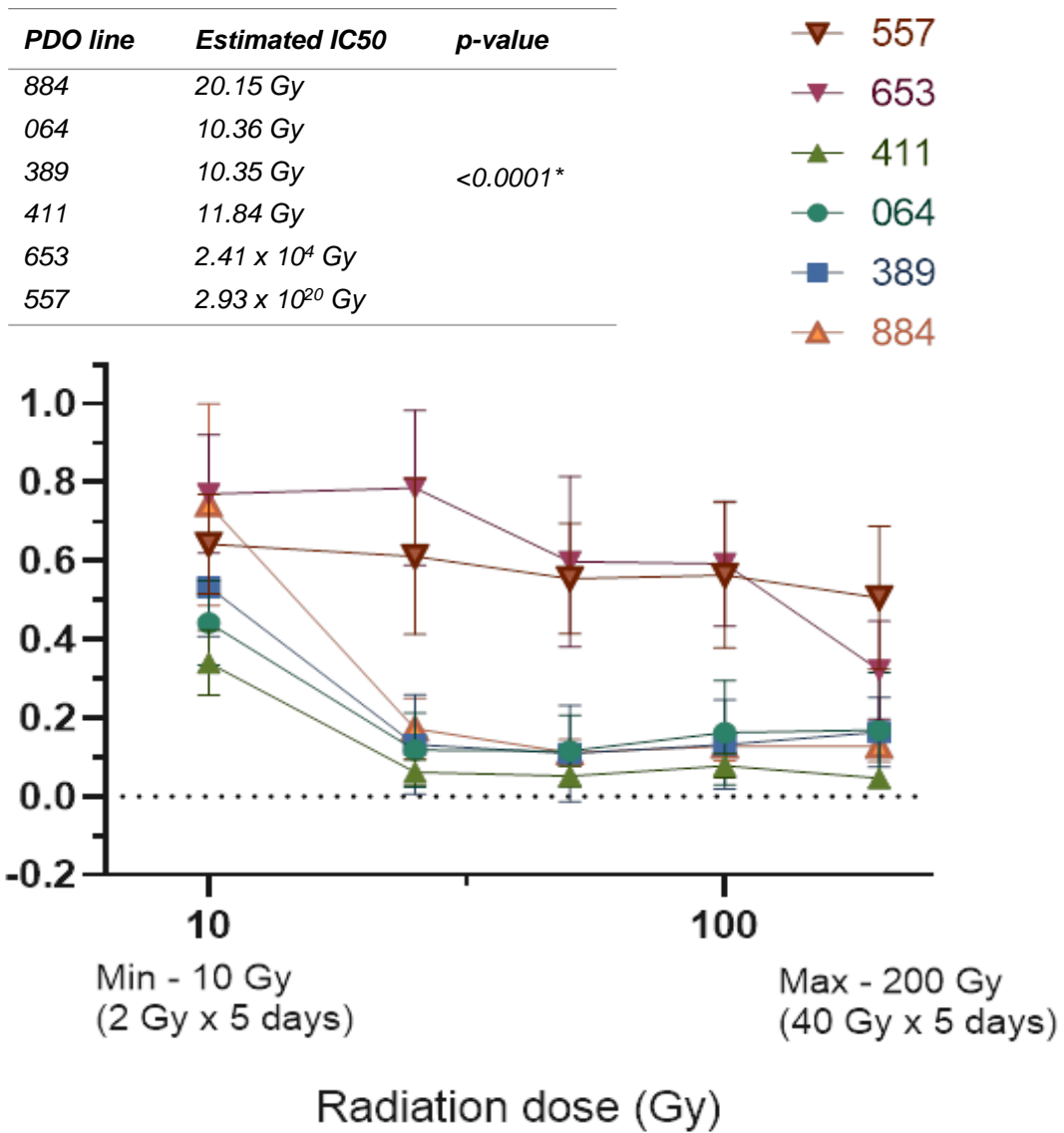


Figure 5-4: Variations in response to radiotherapy in six PDO lines

Six PDO lines, plated estimated 5000 cells/well were irradiated with radiotherapy doses ranging from 5 Gy/day for 5 days (total 25 Gy) to 40 Gy/day for 5 days (200 Gy). Endpoint relative organoid viability was assessed using a chemiluminescence assay. Results from three independent experiments, each containing eight replicates have been presented here. Results were normalised to non-irradiated controls. Maximum inhibitory concentration 50 (IC50) results were calculated and displayed in the table in this figure. Two distinct PDO groups were identified - radioresistant: 653 and 557 versus radiosensitive: 411, 064, 389 and 884. *Statistical significance of mean relative viability difference across the radioresistant versus radiosensitive lines was performed using a two-way Anova test. The x-axis represents radiotherapy doses in the logarithmic scale but re-labelled with non-logarithmically to illustrate the total dose administered.

5.4.3 *Mutations identified in radioresistant versus radiosensitive PDO lines*

Pathological *p53* mutations *R282W*, *R175H*, *G245D* and *R248Q* were identified in all four radiosensitive PDO lines (Table 5-4). One of the two radioresistant lines (653) contained a pathological *p53* mutation (*P191del*). Chen et al. demonstrated that *P53* wild-type status significantly increases the odds of pCR by over 65% and reduces the odds of poor response by 15% ($p < 0.01$) (286). *KRAS* mutations (*G12D* and *G13R*) were identified in the radioresistant PDO lines – 653 and 557. *KRAS* mutation status is a predictor of poor response to anti-EGFR receptor antibody therapy in metastatic CRC, and its correlation with rectal cancer response to NCRT has been widely studied (418, 419, 495). One group found that pathological mutations within codon 13 of the *KRAS* gene were associated with a poor response to NCRT in LARC patients (418). The presence of both *KRAS* and *p53* mutations was also significantly associated with poor response to NCRT (419). Many others have found no significant association between *KRAS* status and response to NCRT in LARC patients (288, 495-497). Furthermore, a systematic review and meta-analysis of 696 patients concluded that *KRAS* status was not predictive of tumour downstaging in these patients (287). *PIK3CA* mutations *E545K* and *R88Q* were detected in one radiosensitive PDO line (411) and one radioresistant PDO line (557), respectively. A previous study failed to demonstrate a statistically significant association between mutated *PIK3CA* and radiotherapy response in LARC patients following NCRT (419).

Several other genetic mutations and their association with NCRT response in rectal cancer have also been explored. Davies et al. demonstrated no association between BRAF status and NCRT response (288), Jiang et al. demonstrated *BRAF* and *SMAD4* were associated with NCRT resistance (420). *SMAD4* mutations *W320fs* and *R496H* were detected in radioresistant PDO line (653) and radiosensitive PDO line (389) respectively. In contrast, only one of the six PDO lines (411) harboured a *BRAF* (*V600E*) mutation. The significance of high microsatellite instability (MSI-H), dMMR phenotype and NCRT response also remains unclear. A systematic review and meta-analysis by O'Connell et al. found no association between MSI-H phenotype and response to NCRT in LARC (289). The radioresistant PDO line 557 had a *MSH6* mutation and its parent tumour which demonstrated dMMR, MSI-H phenotype according to the patient's histopathology report. We also found *MSH6* and *MSH2* mutations in several radiosensitive PDO lines (884, 389 and 411). However, the parent tumours from which these lines originated did not demonstrate dMMR phenotype. Therefore, it is possible that the specific dMMR gene mutations within these lines would not translate to a MSI-H phenotype. Furthermore, the lack of robust immune system modelling significantly limits the capacity to compare MSI-H status and radiotherapy response within this *in vitro* experiment model.

Table 5-3: Frequency of pathological mutations of commonly affected genes in CRC, identified amongst radiosensitive (responder) versus radioresistant (non responder) PDO lines

Pathological mutation	Responders	%	Non Responders	%
<i>P53</i>				
Yes	4	100%	1	50%
No	0	0%	1	50%
<i>KRAS</i>				
Yes	0	0%	2	100%
No	4	100%	0	0%
<i>PIK3CA</i>				
Yes	1	25%	1	50%
No	3	75%	1	50%
<i>BRAF</i>				
Yes	1	25%	0	0%
No	3	75%	2	100%
<i>SMAD4</i>				
Yes	1	25%	1	50%
No	3	75%	1	50%

5.4.4 Pre-irradiation PDO transcriptomic analysis

RNA was extracted from PDOs approximately five days after passage. The extracted genomic RNA was quantified and quality control was performed. Following DNase treatment, the RNA concentrations ranged from 30 to 84 ng/ μ l and RIN values were between 7.8 to 9.5 (Table 5-4).

Table 5-4: PDO RNA quantification and quality control data

Organoid ID	Alternative ID	RNA concentration (ng/ μ l)	RIN
884	OA1	66	9.4
411	OA2	84	7.8
653	OA3	30	7.8
389	OA4	75	9.5
064	OA5	73	9.4
557	OA6	58	8.8

The RNA was normalised and library preparation was performed using Lexogen QuantSeq for 3' RNA sequencing (see 2.5.3.1). NEBNext[®] Ultra[™] II RNA Library Prep Kit for Illumina was used for library preparation for total RNA sequencing (see 2.5.3.2). NGS was performed using a NEXTSeq[™] 500. In both cases, the resulting FASTQ data were uploaded to Partek Flow[®]. Raw gene expression counts were obtained for the six samples using manufacturer developed bioinformatic pipelines.

5.4.5 Pre-irradiation 3' RNA sequencing of PDOs

Downstream bioinformatics analysis was performed with samples grouped by radiation response status (non-responder: 653 and 557 versus responder: 884, 064, 389 and 411) as characterised using the former experiment. PCA revealed sample clustering based on response status (Figure 5-5). The PCA statistic was 76.12%.

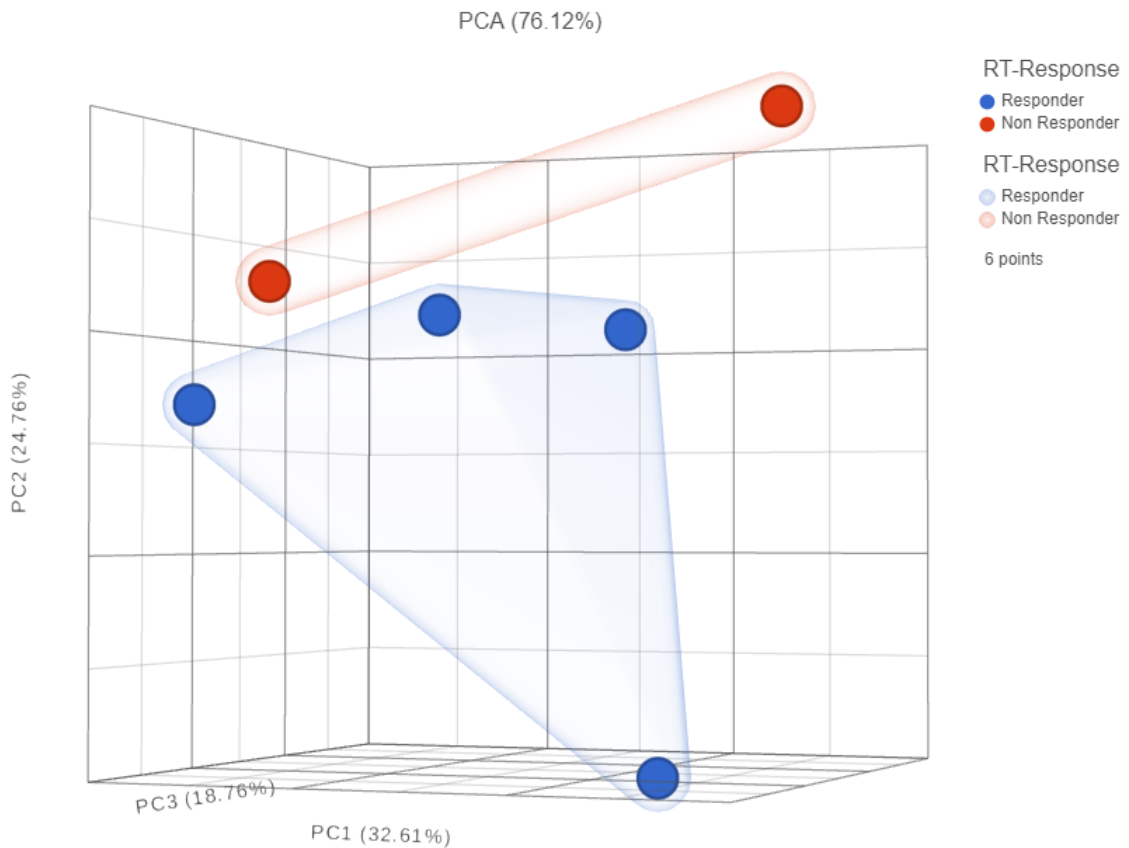


Figure 5-5: Principal component analysis of PDO gene expression between non-responder and responder lines

Principal component analysis (PCA) was performed and plotted. Circles represent individual samples. The shaded area represents sample grouping by response status. The first principal axis along which the largest sample variance was observed was the x-axis (PC1). The y-axis was the second most important direction in which samples showed significant variation (PC2). Non responder samples in red include 653 and 557. Responder samples include 884, 064, 389 and 411 represented by blue dots.

Differential gene expression using GSA revealed 372 upregulated genes and 131 downregulated genes, when filtered using the following parameters: $1.5 < \text{fold change} > -1.5$ and $p < 0.05$. The vast majority of 12,333 genes were not statistically significantly differentially expressed (Figure 5-6).

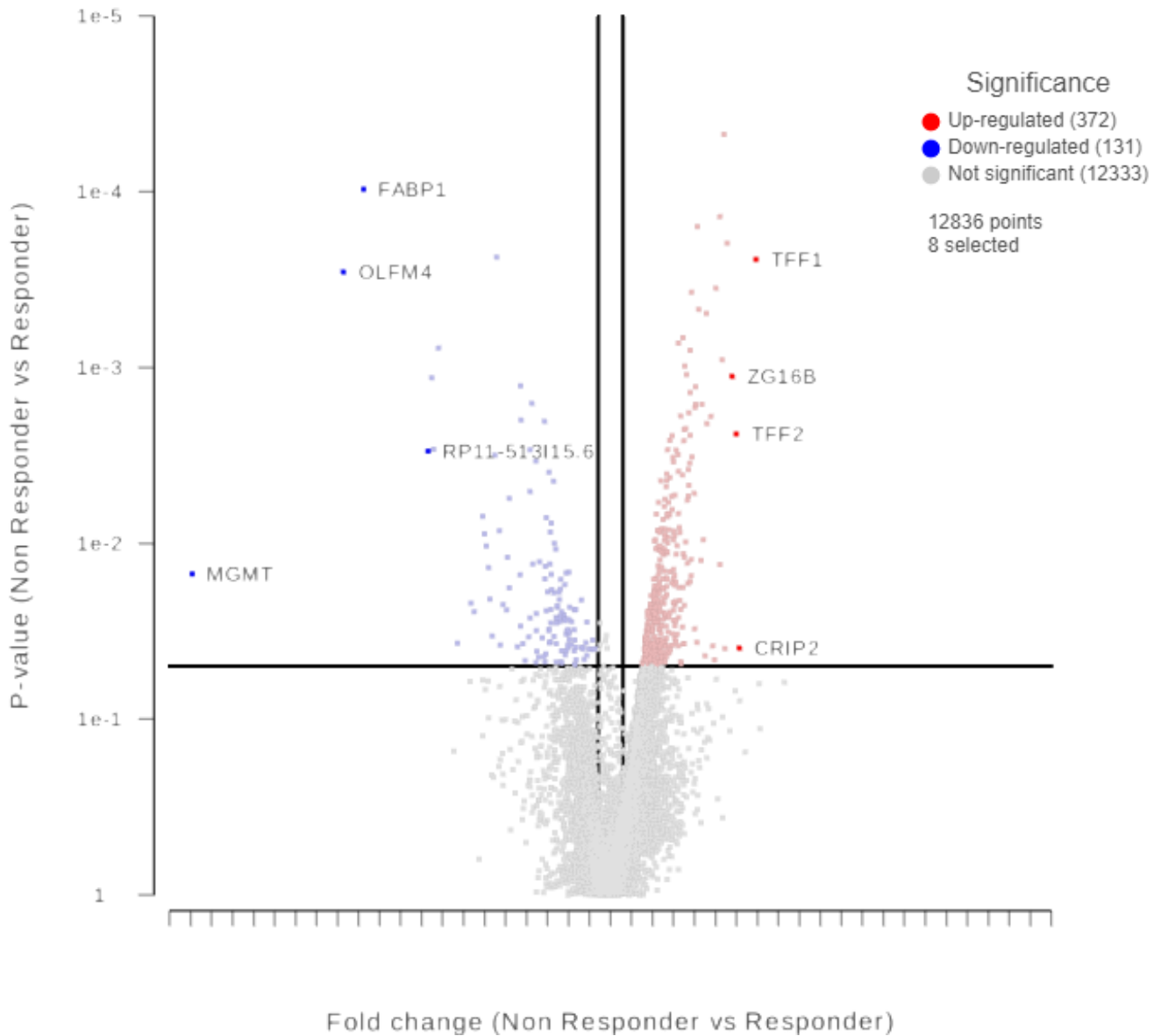


Figure 5-6: Volcano plot representing upregulated and downregulated genes in non-responder PDO lines

The y-axis of the volcano plot represents the p-value which was plotted against the fold change on the x-axis for each of the expressed genes. The red dots represent the significantly upregulated genes, blue dots represent the significantly downregulated genes and the light grey dots represent the non-significant genes. The top four upregulated and downregulated genes have been labelled with their respective gene name. The black horizontal line represents the level of significance at 0.05. The two black vertical lines represent the fold change cut off at -1.5 and 1.5.

5.4.5.1 *Upregulated genes in radioresistant PDOs*

The top 10 of 372 upregulated genes were listed in Table 5-5 based on descending order of fold change, followed by *p*-value. The top ten most upregulated genes included *TFF1*, *CRIP2*, *TFF2*, *ZG16B*, *DCBLD2*, *PLK2*, *MTRNR2L8*, *PON2*, *CLU* and *ARL4D*. *TFF1* and *TFF2* encode the trefoil factor family proteins excreted by mucinous epithelial cells of the gastrointestinal tract (498). These proteins play a crucial role in gastrointestinal tract defence and repair (499). *CRIP2* encodes the LIM domain protein family member cysteine-rich intestinal protein 2 which is found in abundance in endothelial tissues in various organs may serve as a tumour suppressor gene (500, 501). The latter induces radioresistance by inhibiting apoptosis, cell cycle arrest and upregulating pro-survival pathway such as NF- κ B (502, 503). Knockdown of *CRIP2* using siRNA was shown to promote radiosensitivity *in vitro* in NSCLC cell lines (502). *PLK2* encodes the polo-like kinase 2 which is one of five serine/threonine family of protein kinases (PLK 1-5). It regulates the P53 pathway and mTOR pathway and may explain the potential radiosensitising effects of this genes upregulation (504). *PON2* encodes serum paraoxonase / arylesterase 2 which is an anti-apoptotic protein linked to Wnt signalling, and its expression was associated with poor chemoradiotherapy response in oral squamous cell carcinoma patients (505). Clusterin encoded by the *CLU* gene functions as a protein stabiliser and is linked to several cellular processes associated with cell survival, growth and DNA repair (506). Clusterin expression was associated with lack pCR following NCRT in oesophageal squamous cell carcinoma patients (507). Inhibition of Clusterin can radiosensitise various types of cancer cells to chemotherapy and radiotherapy in the laboratory (508). The mechanisms underlying

radiotherapy resistance and the following upregulated genes are unclear. *ZG16b* encodes pancreatic adenocarcinoma upregulated factor which has been found in the secretome of metastatic CRC cells and has a role in CRC progression and metastasis (509). *DCBLD2* expression is dysregulated in various cancers and was associated with increased tumour progression and poor prognosis in CRC cell murine xenografts (510). *MTRNR2L8* is a mitochondrial gene and *ARL4D* is a small GTPase and their exact functions remain uncertain (511)

Table 5-5: Upregulated genes pre-irradiation non-responder PDO lines (653 and 557) on 3' RNA sequencing

Gene symbol	Fold change	p-value	FDR q-value
<i>TFF1</i>	121.57	<0.001	0.446
<i>CRIP2</i>	70.39	0.039	0.949
<i>TFF2</i>	63.74	0.002	0.806
<i>ZG16B</i>	55.35	0.001	0.701
<i>DCBLD2</i>	47.38	<0.001	0.446
<i>PLK2</i>	43.60	0.040	0.949
<i>MTRNR2L8</i>	42.45	<0.001	0.446
<i>PON2</i>	40.00	0.001	0.683
<i>CLU</i>	37.20	<0.001	0.446
<i>ARL4D</i>	37.09	0.013	0.949

5.4.5.2 Downregulated genes in radioresistant PDOs

Of 12,333 expressed genes in the six PDO samples, 131 were downregulated in radioresistant PDO lines. The top 10 were listed in Table 5-6, in ascending order of

fold change and descending order of p -value. The biological mechanisms underpinning radioresistance through downregulation of these genes are unclear. *MGMT* with a fold change of negative 1 million ranked the most downregulated gene in radioresistant PDO lines ($p=0.015$). *MGMT* encodes O6-methylguanine-DNA methyltransferase, a DNA damage repair protein and is usually associated with resistance to DNA damaging therapies such as chemoradiotherapy (512). Promoter methylation of *MGMT* detected in ctDNA and loss of *MGMT* expression detected in tissue from LARC patients, demonstrated a significant association with good response to neoadjuvant therapy (513). Sun et al. demonstrated that higher levels of *MGMT* promoter methylation detected in ctDNA of blood from LARC patients at baseline was associated with a better response to neoadjuvant chemoradiotherapy in 34 LARC patients. *MGMT* hypermethylation and silencing of *MGMT* has been shown to improve radiotherapy response in patients with GBM (514, 515). Our findings contradict the previously published research which begs the question whether the observed downregulation in radioresistant PDO lines is a false positive considering the very high fold change (-1.00×10^6) and FDR adjusted q -value (0.949). *OLFM4* was the second most downregulated gene in radioresistant PDOs (fold change = -6733.15; $p < 0.001$). The latter encodes olfactomedin-4 which is a human intestinal epithelial stem cell marker (516). The *DDC* gene encodes the L-dopa decarboxylase peptide. High *DDC* mRNA expression was associated with earlier stage, well differentiated CRC and longer disease free survival (517). *ABCB1* encodes an ATP binding cassette transported protein and is frequently associated with polymorphisms and therapy response (518). *ABCB1* polymorphism (3435 C>T) was associated with poor response to NCRT in LARC patients (519). *FABP1* encodes fatty acid binding protein 1, *RP11-513/15.6* encodes a ribosomal protein,

AOAH encodes acyloxyacyl hydrolase a protein produced by macrophages and other immune system cells, *DPEP1* encodes dipeptidase 1 which hydrolyses peptides of the beta-lactam ring of various antibiotics; *MYO1A* encodes myosin 1A found in muscle cells and *RUNDC3B* encodes a paralog of the RUN and FYVE domain containing 2 (RUFY2) protein which plays a crucial role in membrane trafficking (520). None of the latter six genes had any association with radiotherapy response in rectal cancer in the published literature reviewed.

Table 5-6: Downregulated genes pre-irradiation non-responder PDO lines (653 and 557) on 3' RNA sequencing

Gene symbol	Fold change	p-value	FDR q-value
<i>MGMT</i>	-1.00x10 ⁶	0.015	0.949
<i>OLFM4</i>	-6733.15	<0.001	0.459
<i>FABP1</i>	-3467.84	<0.001	0.446
<i>RP11-513I15.6</i>	-414.97	0.003	0.833
<i>DDC</i>	-364.93	0.001	0.701
<i>AOAH</i>	-343.93	0.003	0.833
<i>ABCB1</i>	-293.22	0.001	0.640
<i>DPEP1</i>	-156.47	0.037	0.949
<i>MYO1A</i>	-100.48	0.022	0.949
<i>RUNDC3B</i>	-89.98	0.024	0.949

5.4.5.3 Gene clusters identified through hierarchical clustering

Hierarchical clustering revealed two distinct gene clusters upregulated and downregulated in non-responder PDOs. Genes *BLVRA*, *CALB2*, *SLC442*, *RSP26*,

EXTL3, *SSFA2* and *HOMER3* formed a cluster of genes which were overexpressed in non-responders and under expressed in responders. *HEPH*, *PROSER2*, *MTRF1*, *RN7SK*, *RP11-206L.10.2* and *UGT1A6* were downregulated in non-responders (Figure 5-7).

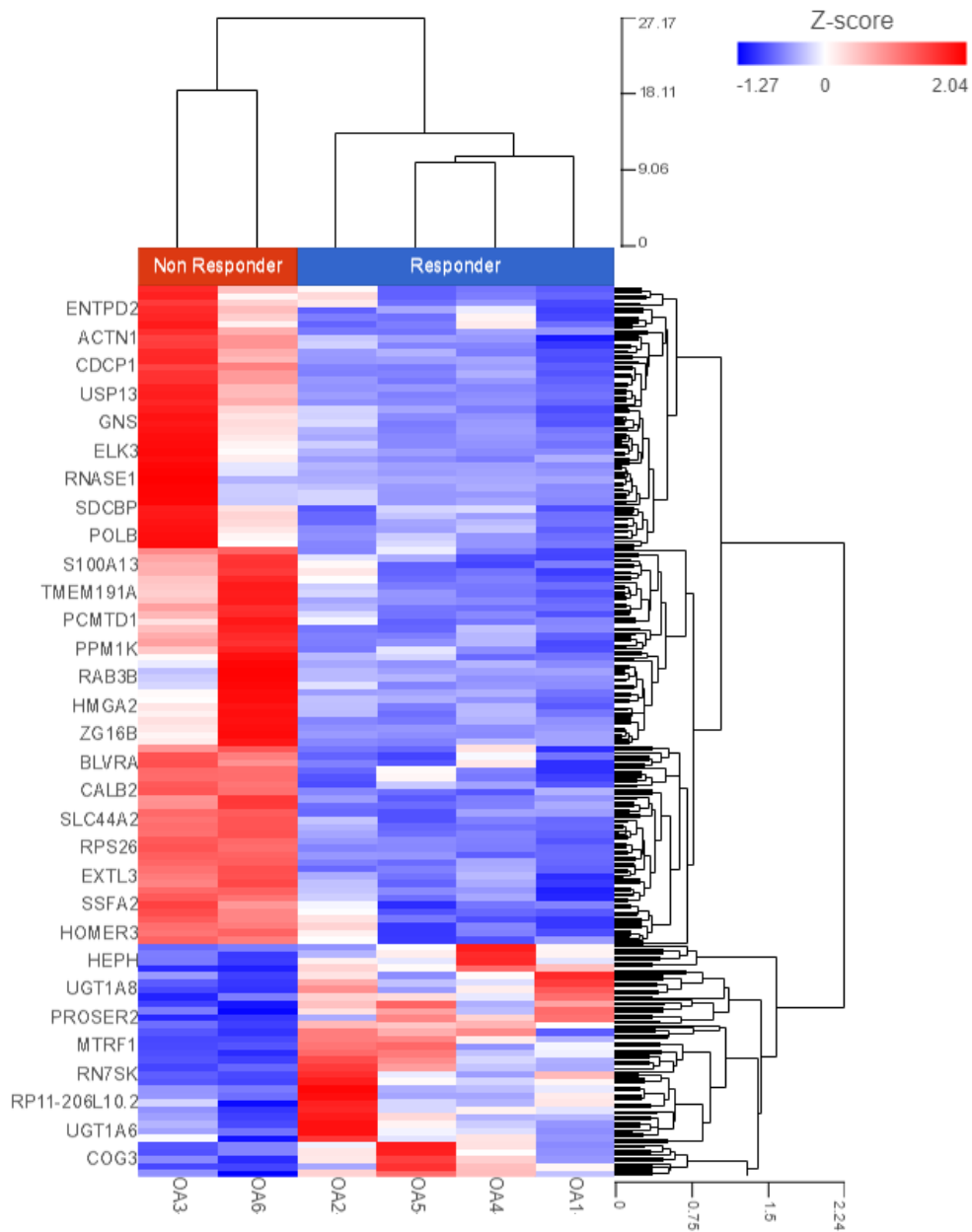


Figure 5-7: Heatmap generated through hierarchical clustering
Hierarchical clustering of samples and genes. A cluster distance metric of average linkage and Euclidean point distance metric were used.

5.4.5.4 GSEA of pre-irradiation PDO lines

5.4.5.4.1 Hallmark collection

Of 50 gene sets of the hallmark collection, 48 were up regulated in the non-responding lines. Twenty six of these were significant at an FDR adjusted q-value of under 0.25 (Table 5-7). Two of the 50 gene sets were upregulated in the four PDO lines demonstrating good response. However, neither gene set were significant at FDR 25% level.

Table 5-7: Hallmark enrichment: Upregulated gene sets in non-responder PDOs (pre-irradiation)

Gene set	Size	ES	FDR q-value	Rank at max
HALLMARK_ANDROGEN_RESPONSE	92	0.85	0.151	900
HALLMARK_COAGULATION	91	0.82	0.077	878
HALLMARK_EPITHELIAL_MESENCHYMAL_TRANSITION	131	0.82	0.108	1538
HALLMARK_MYOGENESIS	134	0.82	0.111	1348
HALLMARK_HYPOXIA	165	0.82	0.189	1010
HALLMARK_TNFA_SIGNALING_VIA_NFKB	173	0.81	0.077	1713
HALLMARK_GLYCOLYSIS	179	0.8	0.237	1050
HALLMARK_APICAL_SURFACE	34	0.79	0.13	965
HALLMARK_CHOLESTEROL_HOMEOSTASIS	69	0.78	0.134	564
HALLMARK_APICAL_JUNCTION	144	0.78	0.226	1891
HALLMARK_APOPTOSIS	140	0.76	0.103	1570
HALLMARK_UV_RESPONSE_DN	123	0.76	0.238	1421
HALLMARK_COMPLEMENT	157	0.75	0.077	2704

<i>HALLMARK_TGF_BETA_SIGNALING</i>	51	0.75	0.117	2234
HALLMARK_NOTCH_SIGNALING	30	0.75	0.135	3386
HALLMARK_INFLAMMATORY_RESPONSE	126	0.73	0.077	1920
HALLMARK_IL2_STAT5_SIGNALING	160	0.73	0.105	1913
HALLMARK_PI3K_AKT_MTOR_SIGNALING	96	0.72	0.077	2274
HALLMARK_REACTIVE_OXYGEN_SPECIES_PATHWAY	45	0.72	0.157	1924
HALLMARK_ADIPOGENESIS	171	0.67	0.23	2521
HALLMARK_KRAS_SIGNALING_DN	98	0.66	0.116	1792
HALLMARK_HEME_METABOLISM	164	0.66	0.121	3193
HALLMARK_INTERFERON_ALPHA_RESPONSE	90	0.65	0.232	2300
HALLMARK_UV_RESPONSE_UP	139	0.64	0.126	1796
HALLMARK_IL6_JAK_STAT3_SIGNALING	63	0.63	0.137	2876
HALLMARK_INTERFERON_GAMMA_RESPONSE	165	0.58	0.236	2056

Upregulated gene sets listed in descending order of enrichment score (ES) followed by ascending order of false discover rate (FDR) adjusted q-value. FDR adjusted q-value cut-off set to less than 0.25.

5.4.5.4.2 KEGG collection

Amongst the 162 gene sets of the KEGG collection, 148 were upregulated in non-responder PDO lines (data not shown). The remaining 14 were upregulated in radiosensitive lines. However, none of the upregulated gene sets in either group were significant at an FDR adjusted q-value of 25%.

5.4.5.4.3 Oncogenic Signatures collection

GSEA using Oncogenic Signatures collection revealed 174 of 187 gene sets were upregulated in non-responder PDO lines (Table 5-8). Of these, 113 were significant at an FDR adjusted q-value of 25%. The remaining gene sets were upregulated in

radiosensitive PDO lines. However, none were significant at FDR adjusted q-value of under 0.25 in the radiosensitive group.

Table 5-8: Oncogenic Signatures enrichment: Upregulated gene sets in non-responder PDOs (pre-irradiation)

Gene set	Size	ES	FDR q-value	Rank at max
CRX_DN.V1_DN	94	0.89	0.171	536
ESC_V6.5_UP_EARLY.V1_DN	122	0.88	0.175	759
SINGH_KRAS_DEPENDENCY_SIGNATURE	20	0.84	0.16	1024
ERBB2_UP.V1_UP	168	0.84	0.165	1274
P53_DN.V2_UP	73	0.83	0.103	1107
CRX_NRL_DN.V1_DN	89	0.81	0.07	1691
RAPA_EARLY_UP.V1_UP	102	0.81	0.225	1034
P53_DN.V1_UP	168	0.81	0.23	1930
CRX_NRL_DN.V1_UP	104	0.8	0.124	552
ESC_V6.5_UP_LATE.V1_DN	137	0.8	0.161	465
MEK_UP.V1_UP	173	0.8	0.181	2084
KRAS.50_UP.V1_DN	18	0.79	0.223	107
RAF_UP.V1_DN	163	0.78	0.099	2304
<i>BMI1_DN.V1_UP</i>	104	0.78	0.224	1440
KRAS.300_UP.V1_UP	74	0.77	0.076	2201
RAF_UP.V1_UP	167	0.76	0.07	1537
KRAS.600_UP.V1_UP	150	0.76	0.07	2057
KRAS.PROSTATE_UP.V1_DN	74	0.76	0.104	555
NRL_DN.V1_DN	93	0.76	0.145	1038
KRAS.LUNG_UP.V1_DN	76	0.76	0.145	2531

ATM_DN.V1_DN	72	0.76	0.246	2174
CAMP_UP.V1_DN	171	0.75	0.12	1698
KRAS.LUNG.BREAST_UP.V1_UP	81	0.74	0.07	1855
CAHOY_ASTROGLIAL	69	0.74	0.07	1417
AKT_UP_MTOR_DN.V1_UP	143	0.74	0.104	2743

The top 25 upregulated gene sets listed in descending order of enrichment score (ES)

followed by ascending order of false discover rate (FDR) adjusted q-value. FDR adjusted q-value cut-off set to less than 0.25.

5.4.6 Pre-irradiation total RNA sequencing of PDOs

Following total RNA sequencing of pre-irradiated PDOs, raw gene counts were obtained using manufacturer designed pipeline on Partek Flow®. The raw gene counts and sample metadata were uploaded to DEBrowser V.1.16.3 operating on RStudio V1.3 running R V4.0.2 and Bioconductor V3.13. Within DEBrowser, the samples were filtered counts per million <0.01 in at least 5 samples. PCA grouped the samples into two clusters according to radiation response (Figure 5-8). The four radiosensitive lines (884, 064, 389 and 411) belonged to one cluster and the two radioresistant lines (653 and 557) did not cluster particularly well.

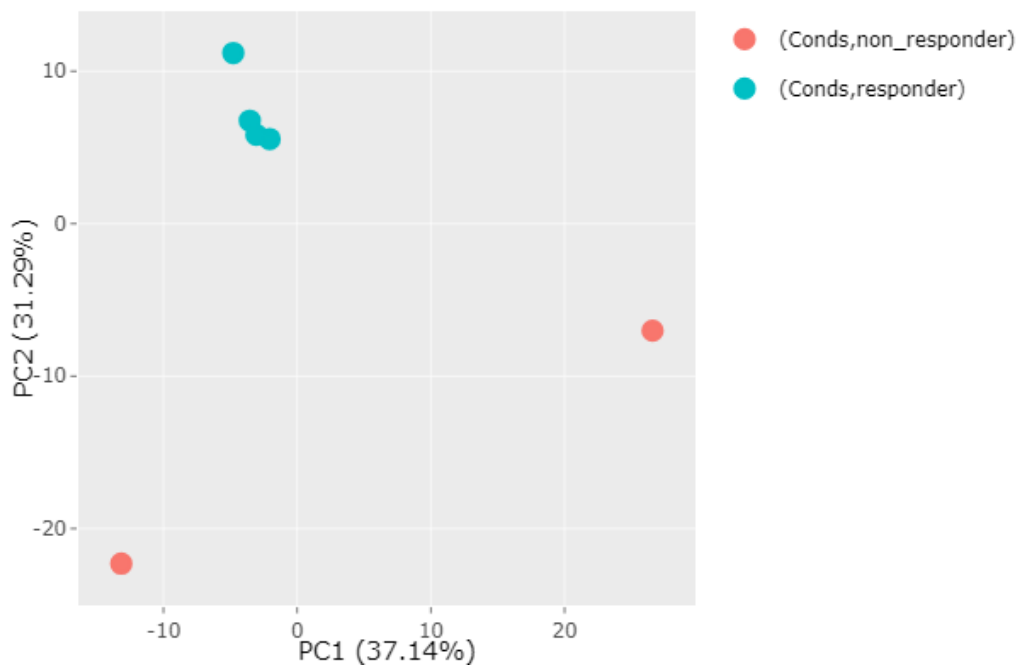


Figure 5-8: Principal component analysis following Total RNA Sequencing of PDO lines (pre-irradiation)

Differential gene expression analysis was performed using DESeq2 (Appendix F) and EnhancedVolcano package (Appendix G) on RStudio to generate a volcano plot demonstrating upregulated and downregulated genes in radioresistant PDO lines (pre-irradiation) (Figure 5-9).

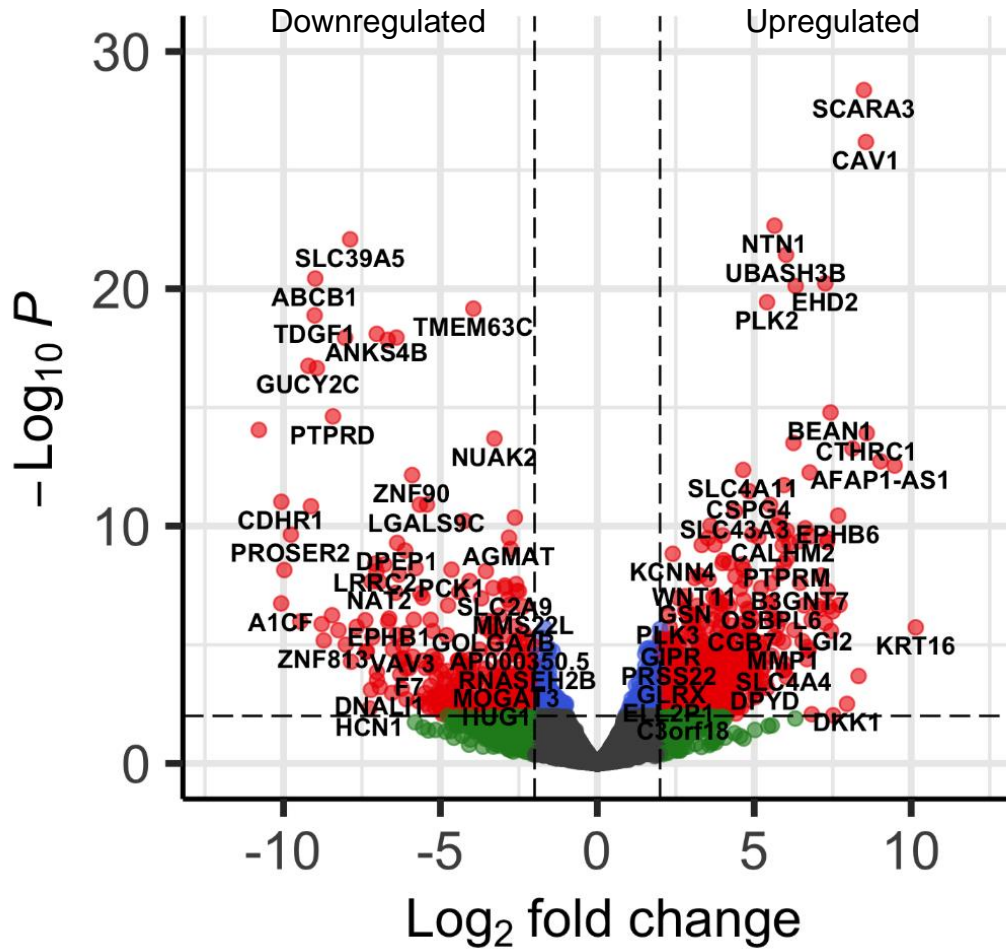


Figure 5-9: Volcano plot representing upregulated and downregulated genes in no-responder PDO lines.

5.4.6.1 Upregulated genes in pre-irradiated radioresistant PDO lines

Differential gene expression analysis was performed on DEBrowser using DESeq2 and the following parameters: DE Method=DESeq2; Fit Type=parametric; betaPrior=FALSE; Test Type=LRT. Subsequently, the results were filtered by fold change (<-1.5 and >1.5) and FDR adjusted q-value (<0.05). There were 323 genes that were upregulated in radioresistant PDO lines and 99 genes upregulated in the radiosensitive PDO lines. The top 10 upregulated genes are listed in Table 5-9.

Table 5-9: Upregulated genes in non-responder PDO lines (653 and 557) - total RNA sequencing of pre-irradiated PDOs

Gene symbol	Fold change	p-value	FDR adjusted q-value
<i>KRT16</i>	1131.90	<0.001	0.00563
<i>MMP7</i>	709.48	<0.001	1.61E-07
<i>AFAP1-AS1</i>	519.39	<0.001	1.61E-07
<i>CTHRC1</i>	383.31	<0.001	7.55E-10
<i>CAV1</i>	376.54	<0.001	1.59E-19
<i>SCARA3</i>	360.12	<0.001	9.20E-22
<i>TNFRSF11B</i>	320.09	<0.001	0.035881
<i>MUC5AC</i>	280.17	<0.001	4.04E-08
<i>CDH11</i>	210.16	<0.001	0.000455
<i>EPHB6</i>	203.85	<0.001	1.04E-06

KRT16 was the most significantly upregulated gene in this sample (fold change = 1131.9; FDR adjusted q-value = 0.006). The former encodes the CK16 cytoskeletal protein and is found in several epithelial tissues (521). *MMP7* was also upregulated in non-responder PDO lines (fold change=709.48; $p<0.001$). This gene encodes the matrix metalloproteinase 7 protein which is closely associated with CRC tumour growth and invasion, and has been found to be upregulated in rectal cancer patients receiving SCRT (308, 522). *AFAP1-AS1* was also upregulated in non-responder PDO lines (fold change = 519.4; $p<0.001$). The latter encodes a long noncoding RNA which is linked to activation of the Wnt / β -catenin signalling pathway and may promote cell growth; thus, promoting radioresistance (523). *CTHRC1* which encodes the collagen triple helix repeat containing 1 protein was also upregulated (fold change=383.31; $p<0.001$). The expression of this protein was first identified in the

intima of injured blood vessels (524), and is also expressed in many solid tumours (525, 526). It is very closely linked to epithelial mesenchymal transition, CRC progression and metastasis (527). *CAV1* was also upregulated in the non-responder PDO lines (fold change = 376.5; $p < 0.001$). Upregulation of *CAV1* has been previously associated with chemoradiotherapy resistance in prostate, lung and pancreatic cancer cells (528-530). The caveolin proteins encoded by the *CAV1* and *CAV2* genes are essential for intra and extracellular exocytosis as well as intracellular signal transduction and regulate several cell functions including cell growth, cell death and migration (531). *SCARA3* was also upregulated in the radioresistant PDO lines (fold change=360.12; $p < 0.001$). The gene encodes a macrophage scavenger receptor-like protein which is expressed in response to oxidative stress (e.g., in response to radiotherapy) (532). These proteins protect cells from death by facilitating the removal of oxidised free radicals (533). Of the remaining four upregulated genes, *MUC5AC* and *EPHB6* also have been linked to prognosis in CRC. *MUC5AC* encodes a mucinous glycoprotein found in colorectal epithelium and lack of its expression has been associated with poor prognosis in CRC (534). *EPHB6* encodes a tyrosine kinase receptor and loss of its expression is linked to poor prognosis in CRC (535). *TNFRSF11B* encodes osteoprotegerin and is associated with Paget's disease (536). *CDH11* encodes cadherin 11, a protein responsible for maintaining cell-cell adhesions. Expression of *CDH11* through its interactions with NF- κ B signalling pathway leads to cell cycle arrest in the G0/G1 phase, apoptosis, suppressed tumour proliferation and metastasis (537). No direct association between the latter four genes and radiotherapy response was found in the reviewed literature.

5.4.6.2 *Downregulated genes in pre-irradiation radioresistant PDO lines*

Differential gene expression analysis identified several genes that were downregulated in radioresistant PDO lines. The top 10 downregulated genes have been displayed in Table 5-10, in descending order of fold change. The results showed some overlap between these genes and those identified as downregulated following 3' RNA sequencing (Table 5-6). For example, the CRC stem cell marker *OLFM4* which was the most downregulated (fold change=-8375.45; $p<0.001$) in this analysis, was also identified as downregulated following 3' RNA sequencing. *FABP1* and *PROSER2*, were also downregulated in both analyses. Other downregulated genes included: *A1CF* which encodes APOBEC1 complementation factor involved in RNA editing and processing events; *CDHR1* which encodes a photoreceptor-specific cadherin cell adhesion molecule; *CYP2B6* which encodes a cytochrome P450 group of catabolising enzymes; *LRRC19* which encodes the leucine-rich-repeat containing protein 19 which is associated NF- κ B signalling pathway activation; *ISX* gene which encodes a transcription factor which regulates gene expression in the intestinal epithelial cells; *TDGF1* which encodes the teratocarcinoma-derived growth factor 1 which is an extracellular membrane-bound signalling protein, which is often abnormal in various tumours. However, the mechanisms which lead to radioresistance following the downregulation of the above genes were unclear and needs further investigation. The only direct association with radiotherapy response was in relation to *GUC2YC*. This gene encodes guanylate cyclase (GC) 2C tyrosine kinase and activates the GC/cGMP pathway and plays an important role in intestinal fluid and electrolyte homeostasis (538). In murine xenografts of CRC cells,

vaccination induced inhibition of GC2C enhanced efficacy of response to radiotherapy (539).

Table 5-10: Downregulated genes in non-responder PDO lines (653 and 557) - total RNA sequencing of pre-irradiated PDOs

Gene symbol	Fold change	p-value	FDR adjusted q-value
<i>OLFM4</i>	-8375.45	<0.001	6.04E-07
<i>FABP1</i>	-1760.23	<0.001	9.66E-05
<i>A1CF</i>	-1076.31	<0.001	0.00099
<i>CDHR1</i>	-1072.11	<0.001	0.001034
<i>CYP2B6</i>	-1004.41	<0.001	2.64E-06
<i>PROSER2</i>	-868.455	<0.001	1.57E-15
<i>LRRC19</i>	-705.509	<0.001	0.002159
<i>GUCY2C</i>	-589.379	<0.001	4.04E-07
<i>ISX</i>	-557.098	<0.001	0.000196
<i>TDGF1</i>	-513.811	<0.001	3.35E-17

5.4.7 Gene enrichment analysis

Gene enrichment was performed on RStudio using DESeq2, MSigDBr and ClusterProfiler R packages. Hallmark, Kegg and Oncogenic Signatures collections of the MSigDB V4 were used. The top 10 of gene sets of each collection has been listed and graphically represented using Pathview and GGPUBR packages (Figure 5-10).

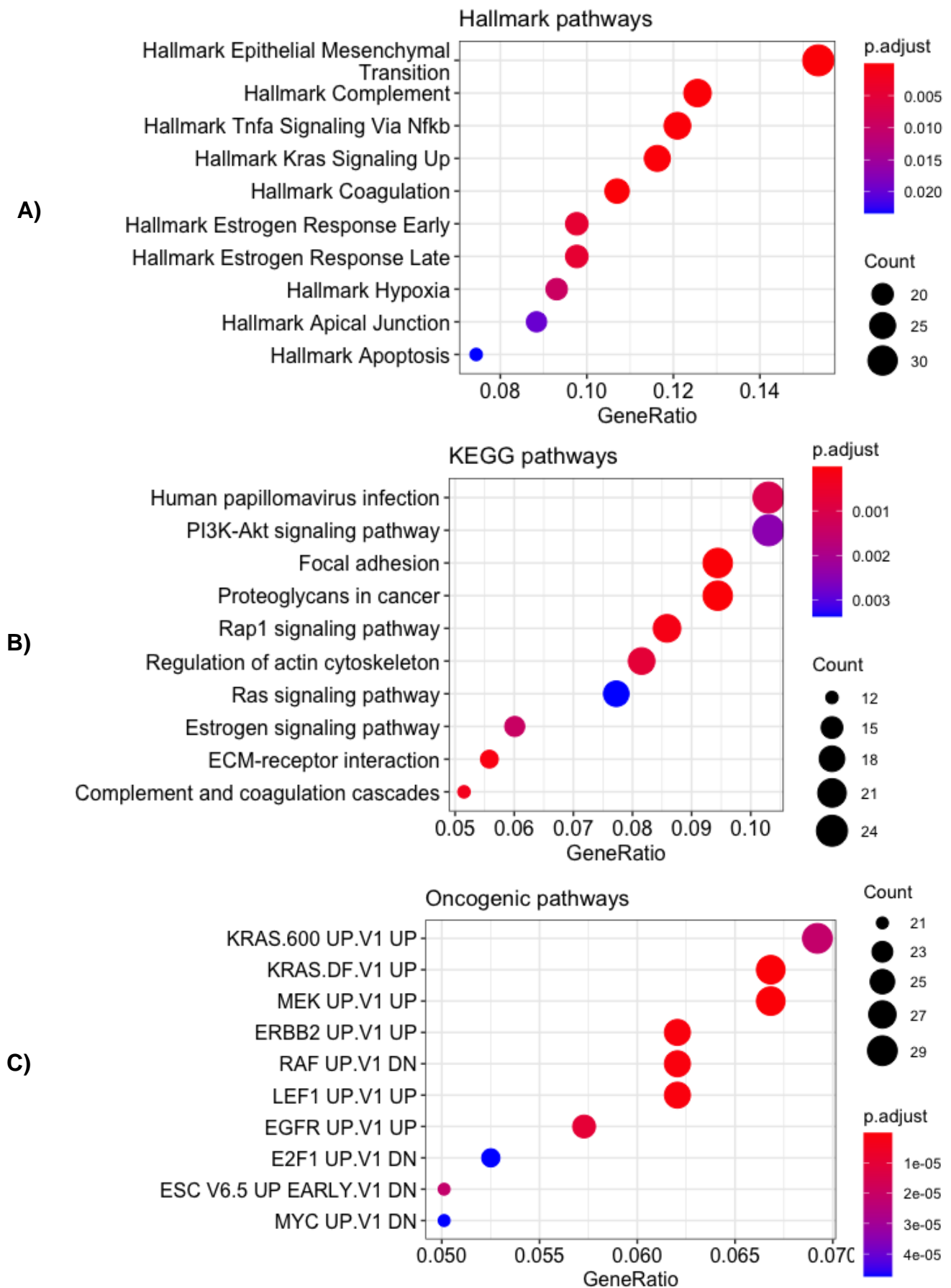
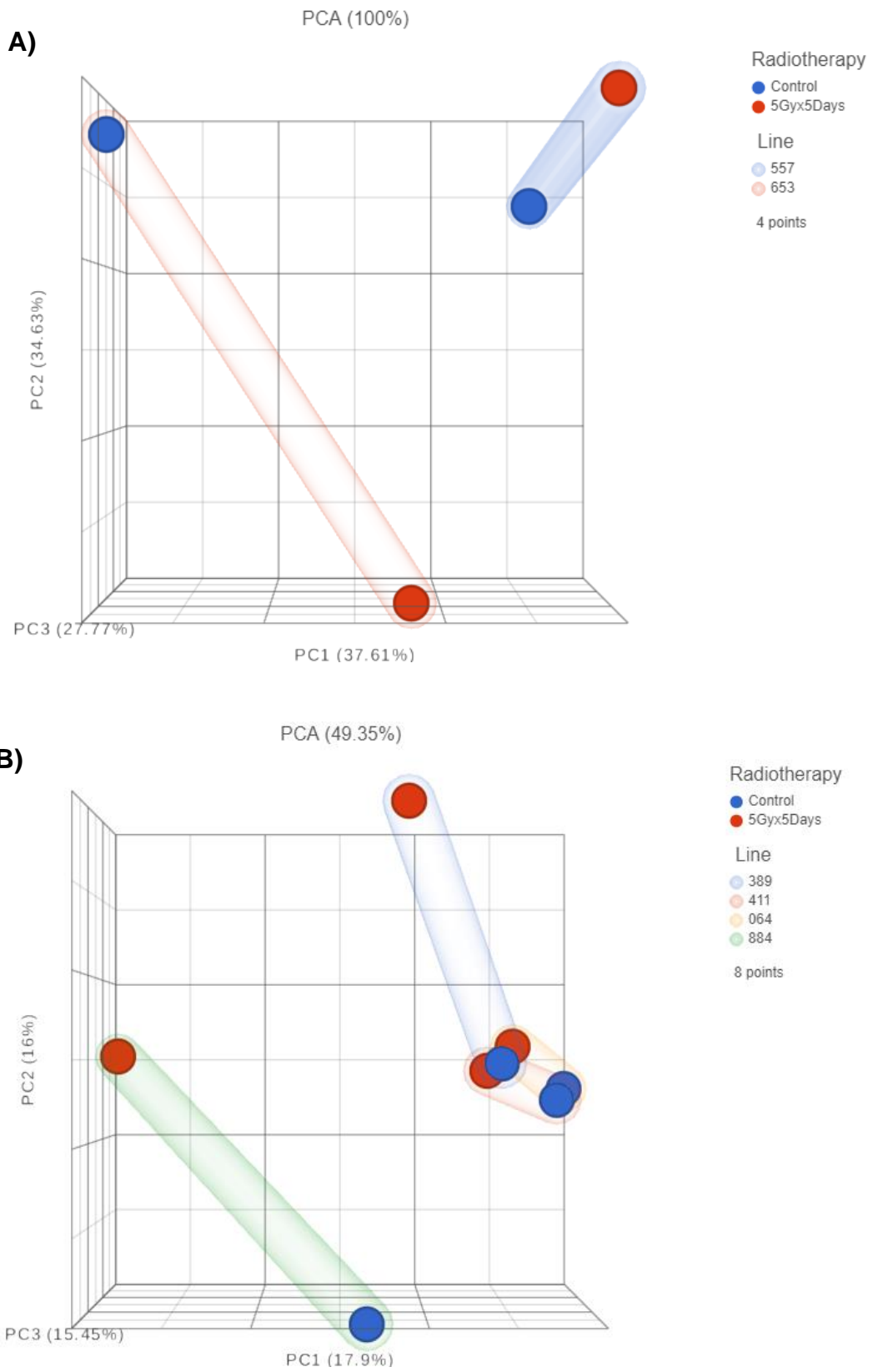


Figure 5-10: Gene sets upregulated in non-responder PDOs
 Enrichment analysis using Hallmark Collection (A), Kegg Collection (B) and Oncogenic Signatures Collection (C) gene sets of MSigDB V4.

Enrichment using the Hallmark collection revealed several significantly upregulated gene sets in pre-irradiated non-responder PDO lines. Whilst there were several upregulated gene sets identified during this analysis, the following were of particular interest given comparable findings from previous experiments. The epithelial mesenchymal transition pathway, TNFA signalling via NF- κ B and KRAS signalling gene sets of the Hallmark collection were upregulated in non-responder PDO lines. Enrichment using the KEGG collection, revealed PI3K/AKT signalling pathway and RAS signalling pathway upregulation in non-responder PDO lines. Furthermore, enrichment using Oncogenic Signatures collection revealed gene sets associated with KRAS, ERBB2 and EGFR pathways were upregulated in non-responder PDO lines.

5.4.8 Pre- and post-irradiation 3' RNA sequencing of PDOs

Three prime RNA sequencing was performed using RNA extracted following irradiation with 25 Gy (5 Gy/day for 5 days) from the six PDO lines. Differential expression analysis was performed between pre versus post-irradiation in non-responder (653 and 557) and responder (389, 411, 064, 884) PDO lines separately. PCA revealed poor clustering of pre- and post-irradiation samples between the radioresistant and radiosensitive PDO groups (Figure 5-11). This suggests a heterogeneous response and distinct transcriptomic changes following radiotherapy amongst individual PDOs.



*Figure 5-11: Principal component analysis of pre- and post- irradiation PDO lines
 A) Radioresistant PDO lines 653 and 557. B) Radiosensitive PDO lines 389, 411, 064 and*

884

5.4.8.1 *Upregulated genes in post-irradiated radioresistant PDO lines*

AC093106.7 (fold change=533.489; $p=0.037$) and *HNRNPCP4* (fold change=170.752; $p=0.047$) were the two most upregulated genes in the post-irradiated radioresistant PDO lines (Table 5-11). However, the significance of these two long noncoding RNA genes on radiotherapy response remains unknown. *IQGAP2* which was upregulated has previously been identified as upregulated in radioresistant cervical cancer tissue (540). In pancreatic cancer patients undergoing chemoradiotherapy, *IQGAP2* upregulation was associated with poor survival (269). *SSB* encodes a protein associated with single strand break repair and its upregulation is closely linked to radiotherapy resistance (541, 542). *NSF*, *TLE4*, and *SFXN1* as well as genes encoding long noncoding RNAs *C15orf48*, *PPP2R5E* and *FAM114A1* had no prior associations with radiotherapy response in the published literature reviewed.

Table 5-11: *Upregulated genes in post-irradiated radioresistant PDO lines*

Gene symbol	Fold change	p-value	FDR q-value
<i>AC093106.7</i>	533.489	0.037	0.924
<i>HNRNPCP4</i>	170.752	0.047	0.924
<i>IQGAP2</i>	62.599	0.043	0.924
<i>TLE4</i>	38.000	0.045	0.924
<i>SSB</i>	25.097	0.029	0.924
<i>NSF</i>	21.128	0.027	0.924

<i>C15orf48</i>	19.829	0.042	0.924
<i>SFXN1</i>	14.750	0.042	0.924
<i>PPP2R5E</i>	11.177	0.015	0.924
<i>FAM114A1</i>	10.726	0.046	0.924

5.4.8.2 *Downregulated genes in post-irradiated radioresistant PDO lines*

The most downregulated gene in post-irradiated radioresistant PDO lines was *POLR2G* (fold change=-166.594; $p=0.047$; Table 5-12). This gene encodes RPB7 DNA-directed RNA polymerase II subunit, which is a substrate of cullin2-RING E3 ligase (CRL2). Increased CRL2 expression is associated with radiosensitivity in GBM patients (543). *FBXL17* encodes the F-box and leucine-rich repeat protein 17 which is a regulator of the hedgehog intracellular signalling pathway (544, 545). Hedgehog pathway inhibition can lead to radiosensitisation of cells and tissues, through the inhibition of DNA repair mechanisms (546, 547). The following genes were also amongst the top-ten most downregulated genes in radioresistant PDO lines following irradiation. However, the relationship between their downregulation and radioresistance is unclear. *MYH14* which encodes NMM IIA cytoskeletal protein was downregulated in post-irradiated radioresistant PDO lines. *TRAPPC1* encodes TrappC1 a subunit of the TRAPP1 protein associated with intracellular signal transduction (548). TrappC4, another subunit of TRAPP1 has been associated with increased phospho-ERK1/2 in CRC (549, 550). *INPPL1* encodes the for src homology 2 domain-containing inositol phosphatase 2 (SHIP2) protein which is associated with the autosomal recessive, inherited condition of opsismodysplasia (551). *FAM120AOS* is a long noncoding RNA. *ATP11B* encodes a p-type ATPase.

ATP11B mRNA expression has been linked poor response to cisplatin in ovarian carcinoma (552, 553). *RPL12P4* encodes a ribosomal protein. *C15orf61* encodes a mitochondrial protein. *MED4* encodes a mediator complex protein essential for gene specific transcription (554).

Table 5-12: Downregulated genes in post-irradiated radioresistant PDO lines

Gene symbol	Fold change	p-value	FDR q-value
<i>POLR2G</i>	-166.594	0.047	0.924
<i>MYH14</i>	-40.948	0.006	0.924
<i>TRAPPC1</i>	-31.272	0.046	0.924
<i>INPPL1</i>	-17.886	0.038	0.924
<i>FBXL17</i>	-17.849	0.016	0.924
<i>FAM120AOS</i>	-17.750	0.040	0.924
<i>ATP11B</i>	-15.042	0.016	0.924
<i>C15orf61</i>	-14.731	0.008	0.924
<i>RPL12P4</i>	-14.661	0.001	0.924
<i>MED4</i>	-13.868	0.049	0.924

5.4.8.3 Upregulated genes in post-irradiated radiosensitive PDO lines

The most upregulated gene amongst the post-irradiated radiosensitive PDO lines was *DGCR8* (fold change=218.96; $p=0.020$; Table 5-13). The gene encodes DiGeorge critical region 8 which is a microRNA biogenesis factor which can promote tumour radioresistance (555). *DGCR8* silencing leads to radiosensitivity in head and neck cancer by downregulating runt-related transcription factor 3, a protein involved

in the control of cellular differentiation and proliferation, by regulating cell cycle transition from G1 beyond the restriction (R) transition point (556, 557). Our findings show upregulation of *DGCR8* following irradiation in radiosensitive PDO lines which could be a false positive (FDR adjusted q-value=0.797). *DNAJB12* encodes an endoplasmic reticulum Hsp70 family protein, the degradation of which in response to cellular stressors leads to cells being primed for apoptosis (558). *FABP5P7* encodes a non-coding RNA. *RP11-762H8.4* encodes a ribosomal protein. *ALDH3B1* encodes Aldehyde dehydrogenase (ALDH) enzyme and catalyses aldehydes derived following lipid peroxidation and is expressed in response to oxidative stress (559). The *OAS3* gene encodes an enzyme from the oligoadenylate synthase family and inhibits cellular protein synthesis. The gene which is an interferon stimulated gene has been previously demonstrated to be upregulated following radiotherapy in breast prostate and glioma cells (560). The *HAUS7* gene encodes a subunit of the augmin protein complex associated with cytoskeletal integrity. *BRCA1* is a human tumour suppressor gene. Commonly associated with breast cancer, it encodes proteins associated with DNA damage repair and facilitates apoptosis of irreparable cells (561). *BRCA1* mutations have failed to demonstrate any significant association with radiotherapy response or resistance in breast cancer patients receiving radiotherapy (562, 563). Its significance in radiosensitising rectal cancer also warrants further investigation. *CDC16* encodes a ubiquitin ligase which is part of the APC complex of proteins. *TCHP* encodes the trichoplein keratin filament binding protein is a tumour suppressor which has the capability and contributes to apoptosis during cellular stress (564).

Table 5-13: Upregulated genes in post-irradiated radiosensitive PDO lines

Gene symbol	Fold change	p-value	FDR q-value
<i>DGCR8</i>	218.96	0.020	0.797
<i>DNAJB12</i>	200.31	0.019	0.797
<i>FABP5P7</i>	195.06	0.024	0.797
<i>RP11-762H8.4</i>	178.64	0.021	0.797
<i>ALDH3B1</i>	154.65	0.021	0.797
<i>OAS3</i>	108.33	0.021	0.797
<i>HAUS7</i>	107.99	0.049	0.797
<i>BRCA1</i>	99.39	0.029	0.797
<i>CDC16</i>	80.00	0.017	0.797
<i>TCHP</i>	69.39	0.032	0.797

5.4.8.4 Downregulated genes in post-irradiated radiosensitive PDO lines

ALDOC, *ANKRD37*, *NDRG1*, *EGLN3* and *GBE1* genes are often upregulated in hypoxic tumours (565). Tumour hypoxia is associated with radiotherapy resistance (474). Downregulation of genes associated with tumour hypoxia may contribute to radiotherapy sensitivity. The most downregulated gene in post-irradiation radiosensitive PDO lines was *FBXW4* (fold change=-92.75; $p=0.025$). Whilst no direct association between *FBXW4* expression and radiotherapy response has been found, Zhang et al. found that reduced *FBXW4* expression is linked to poor disease free survival following NCRT in LARC patients (456). The significance of downregulation of *DCAKD*, ribosomal protein genes *RP11-380G5.3*, *RPL21P28* and

RP11-395B7.7, in enhanced response to radiotherapy in the radiosensitive lines are also unclear.

Table 5-14: Downregulated genes in post-irradiated radiosensitive PDO lines

Gene symbol	Fold change	p-value	FDR q-value
<i>FBXW4</i>	-92.75	0.025	0.797
<i>ALDOC</i>	-33.74	0.029	0.797
<i>ANKRD37</i>	-26.57	0.015	0.797
<i>DCAKD</i>	-18.41	0.034	0.797
<i>EGLN3</i>	-18.30	0.033	0.797
<i>RP11-380G5.3</i>	-17.95	0.026	0.797
<i>NDRG1</i>	-13.17	0.000	0.797
<i>RPL21P28</i>	-12.28	0.009	0.797
<i>RP11-395B7.7</i>	-9.71	0.009	0.797
<i>GBE1</i>	-9.58	0.046	0.797

5.4.8.5 GSEA of PDO lines, pre- versus post-irradiation

GSEA was performed comparing pre- and post-irradiation radioresistant and radiosensitive PDO lines separately. No significantly upregulated pathways were identified at an FDR adjusted q-value less than 0.25 significance level (data not shown).

5.5 Discussion

Traditionally, CRC cell lines and primary tumour tissue have been used in laboratory research evaluating the biological mechanisms surrounding radiotherapy sensitivity and resistance in rectal cancer (566). However, there have been several limitations to such research. Cell lines are clonal expansions of a single cell type and fail to mimic the complex cellular heterogeneity observed within tumour tissue and the intricacies the tumour microenvironment. The retrospective nature of studies involving fresh or archived donor human tissue is also a limitation. Therefore, the use of PDO models has taken centre stage in modern *in vitro* CRC research, given their ability to recapitulate tumour heterogeneity and maintain genetic stability after multiple passages. Research has been conducted successfully using patient derived xenografts (334), as well as PDO coculture with immune system cells (366). In CRC, PDO models have been utilised in experiments evaluating genomic, transcriptomic, proteomic features and treatment response (334, 365, 567). Therefore, PDO models were used in this experiment to simulate radiotherapy response *in vitro* and to perform transcriptomic analysis of radiosensitive and radioresistant PDO lines.

A modified Sato and Cleavers et al. method was used to derive PDO models in the laboratory (362). Of 16 successfully derived PDO models the first six were used in these experiments. Challenges to PDO culture included infection and low success rate. These were overcome by incubating samples in antibiotic containing media during the culture and regular optimisation of the protocol. The fresh tissue samples used for PDO culture included colonic as well as rectal tumour tissue. This was due to the limited availability of rectal cancer donor samples at the time of this research.

Tumours from the colon and rectum both originate from the same glandular crypt epithelium and the biological basis is comparable with common mutational profiles and pathway abnormalities. Whilst rectal cancer is treated with chemoradiotherapy colon cancer is not treated with radiotherapy. This difference in treatment is predominantly owing to the anatomical location of the tumour in an area where radiotherapy can be safely administered as opposed to biological differences. Therefore, the use of PDO lines of colon or rectal lineage is unlikely to be a major confounder within the context of the experiments conducted in this study. Furthermore, most *in vitro* research including those evaluating radiotherapy response have previously been conducted using cell lines derived from colon cancer.

Using the *in vitro* PDO radiotherapy response experiment model (Figure 5-3), four of the six PDO lines were identified as radiosensitive and two as radioresistant (Figure 5-4). There were distinct genomic, immunohistochemical and transcriptomic differences between the two groups. CDX2 expression was absent on immunohistochemistry assessment of the two radioresistant PDO lines. Lack of CDX2 expression is associated with poor prognosis in CRC (492, 493). The two groups also differed in gene mutation profiles (Table 5-3). Pathological *KRAS* mutations were only present in the two radioresistant PDO lines. *KRAS* status and association with NCRT response in LARC is debatable with some research demonstrating an association (7-9), whilst others did not (288, 495-497).

Three-prime and total RNA sequencing was performed to identify differential gene expression between the two groups at baseline and to ensure inter-methodology

validation of results. Corley et al. demonstrated no difference in total RNA sequencing versus 3' RNA sequencing to assess differential gene expression (568). Nevertheless, 3' RNA sequencing is cost effective, fast and provides high quality data including when degraded RNA is used (e.g., from FFPE samples). This research identified several biomarkers related to individual gene expression associated with radiotherapy response status. Pre-irradiation, transcriptomic markers strongly associated with radioresistance included *MMP7* and *CAV1* upregulation. *OLFM4*, *FABP1* and *PROSPER2* upregulation was associated with radiosensitivity. *FBXW4* and *FBXL17* are potential radiosensitivity and radioresistant markers respectively. *FBXW4* downregulation was noted, post-irradiation in radiosensitive PDO lines, implying upregulation pre-irradiation in these lines. An independent retrospective dataset of FFPE LARC biopsy samples also demonstrated *FBXW4* downregulation in non-responders implying upregulation in responders, pre-NCRT.

Several biological pathways associated with radioresistance were identified through GSEA. The PI3K/AKT/mTOR, MAPK, epithelial mesenchymal transition, notch signalling, hypoxia signalling related genes and NF- κ B signalling pathways were upregulated in radioresistant PDOs at baseline. The significance of these pathways in NCRT response was also discussed in Chapter 4. The upregulated pathways were comparable to findings from the independent cohort of retrospective FFPE sample expression profile. GSEA using post-irradiation transcriptomic data did not reveal any significantly upregulated pathways at an FDR q-value significance level of 25%. This may be due to RNA degradation following irradiation particularly amongst radiosensitive PDO lines rendering accurate comparison between the two groups difficult. Other limitations of this research included the small sample size. Most

differentially upregulated and downregulated genes identified during 3'RNA sequencing were not significant at an FDR adjusted q-value less than 0.05. Therefore, GSEA was performed for pathway level analysis and reliable interpretation of the transcriptomic data. Furthermore, the total-RNA sequencing results yielded results with FDR adjusted q-values under 0.05.

5.6 Conclusion

PDO models were successfully derived from surgical resection specimens of CRC patients and an *in vitro* experiment model was established to assess PDO radiotherapy response. The model was replicable and validated for consistency using multiple repeat experiments. The transcriptomic analyses revealed several biomarker genes associated with radiotherapy response status at baseline and potential targets for treatment including several oncogenes and tumour suppressor genes. Several biological pathways were also associated with radiotherapy resistance amongst PDO lines. At baseline, upregulated epithelial mesenchymal transition, PI3K/AKT/mTOR and KRAS signalling pathways may contribute to radioresistance. Following irradiation, upregulation of genes associated with hypoxia and NF- κ B signalling might also be associated with radiotherapy resistance. Further analysis is required to identify the downstream effects of these pathways and a larger sample size to validate these results. The effects of inhibition of pathways identified as upregulated in radioresistant PDO lines), on enhancing radiotherapy response in rectal cancer, requires further research.

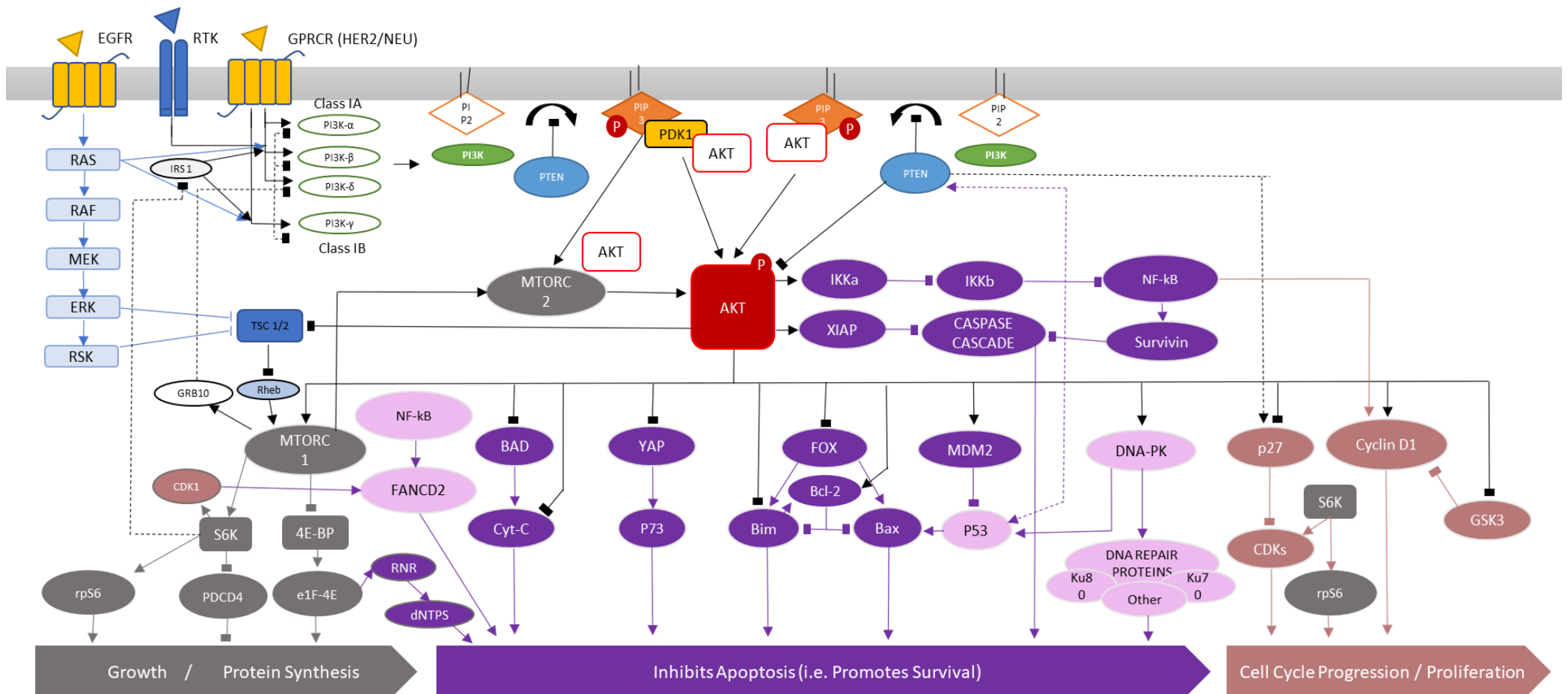
Chapter 6: Does the PI3K AKT mTOR pathway inhibition enhance radiotherapy response?

6.1 Introduction

The PI3K/AKT/mTOR pathway plays a crucial role in cancer pathogenesis, prognosis and treatment resistance (490, 491). Radiotherapy exerts significant stresses to the cellular microenvironment resulting in the activation of pro-survival pathways such as the PI3K/AKT/mTOR pathway (173). The latter pathway has numerous downstream effectors; Its activation leads to cell proliferation, growth, membrane trafficking, cell survival and cell migration (Figure 6-1). It is regulated through several negative feedback loops. The PI3K/AKT/mTOR pathway is activated by substrates binding to G-protein coupled receptor or receptor tyrosine kinase; leading to the activation of membrane bound class-I PI3K proteins (569, 570). Class-I PI3K may also be activated directly by RAS (571). Activated class-I PI3K phosphorylates transmembrane protein phosphatidylinositol-4,5-bisphosphate (PIP₂) to phosphatidylinositol-3,4,5-bisphosphate (PIP₃) (572). Phosphatase and tensin homolog (PTEN) inhibits this process (573). The PI3K/AKT/mTOR pathway has several overlaps with other pathways (Figure 6-1). For example, mTORC1 can be

activated by ERK and RSK of the MAPK pathway, via the inhibition of Tuberous sclerosis proteins (TSC) 1 or 2 (574, 575).

PIP3 activates AKT directly by phosphorylation or indirectly by recruiting phosphoinositide-dependent protein kinase (PDK1) or through mTORC2 (466, 576). Phosphorylated AKT (pAKT) activates mTORC1 which is a principal downstream effector of this pathway regulating cell growth, metabolism and protein synthesis (175). Activated AKT inhibits apoptosis by inhibiting B-cell lymphoma 2 (BCL-2) associated agonist of cell death (BAD), yes-associated protein 1 (YAP), several proteins of the Forkhead (FOX) family, BCL-2-associated X protein (BAX), BCL-2 proteins and by activating Mouse double minute (MDM) 2 homolog - an inhibitor of p53 (466). The caspase cell death cascade is also inhibited through the downstream activation of nuclear factor kappa-light-chain-enhancer of activated B cells (NF- κ B) or X-linked inhibitor of apoptosis protein (XIAP) by pAKT (577). DNA repair pathway proteins such as DNA-dependent protein kinase (DNA-PK) and proteins of the FANCONI anaemia pathway (FANCD2) are also activated by pAKT (578). AKT phosphorylation also leads to cell proliferation, cell cycle progression via the activation of Cyclin D1 and inhibition of p27 an inhibitor of Cyclin Dependent Kinase (CDK) (579). The cumulative effect of AKT activation, thus promoting cell survival, increased metabolism, growth, proliferation, DNA repair and inhibits apoptosis.



Regulatory proteins: phosphatidylinositol-3-Kinase (PI3K) - Class IA (α , β , δ) or Class IB (γ), phosphatidylinositol-4,5-bisphosphate (PIP2), phosphatidylinositol-3,4,5-bisphosphate (PIP3), protein 3-phosphoinositide-dependent protein (PDK1), Tuberous sclerosis proteins 1 and 2 (TSC-1/2), Ras homolog enriched in brain (Rheb), Growth Factor Receptor Bound Protein 10 (GRB10), Insulin receptor substrate 1 (IRS 1), Phosphatase and tensin homolog (PTEN), Protein Kinase B (AKT), Receptor tyrosine kinase (RTK), G-protein coupled receptor (GPCR), Epidermal growth factor receptor (EGFR)

Proteins involved in cell growth and protein synthesis: Mammalian Target of Rapamycin (mTOR), S6 kinase beta-1 (S6K1), Eukaryotic translation initiation factor 4E (eIF4E)-binding protein 1 (4E-BP1), Programmed cell death protein 4 (PDCD4), Ribosomal Protein S6 (rpS6).

Proteins involved in promoting cell survival and inhibiting apoptosis: The I κ B kinase alpha (IKK α), I κ B kinase beta (IKK β), nuclear factor kappa-light-chain-enhancer of activated B cells (NF- κ B), X-linked inhibitor of apoptosis protein (XIAP), BCL2 associated agonist of cell death (BAD), Cytochrome C (Cyt-C), yes-associated protein 1 (YAP), p73, Forkhead box proteins (FOX), B-cell lymphoma 2 protein (Bcl-2), Bcl-2-like protein 11 (Bim), Bcl-2-associated X protein (Bax), Mouse double minute 2 homolog (MDM2), DNA-dependent protein kinase (DNA-PK), Ku-80, Ku-70 Ribonucleotide reductase (RNR), Deoxy nucleoside triphosphate (dNTP), Survivin, Caspase cascade proteins.

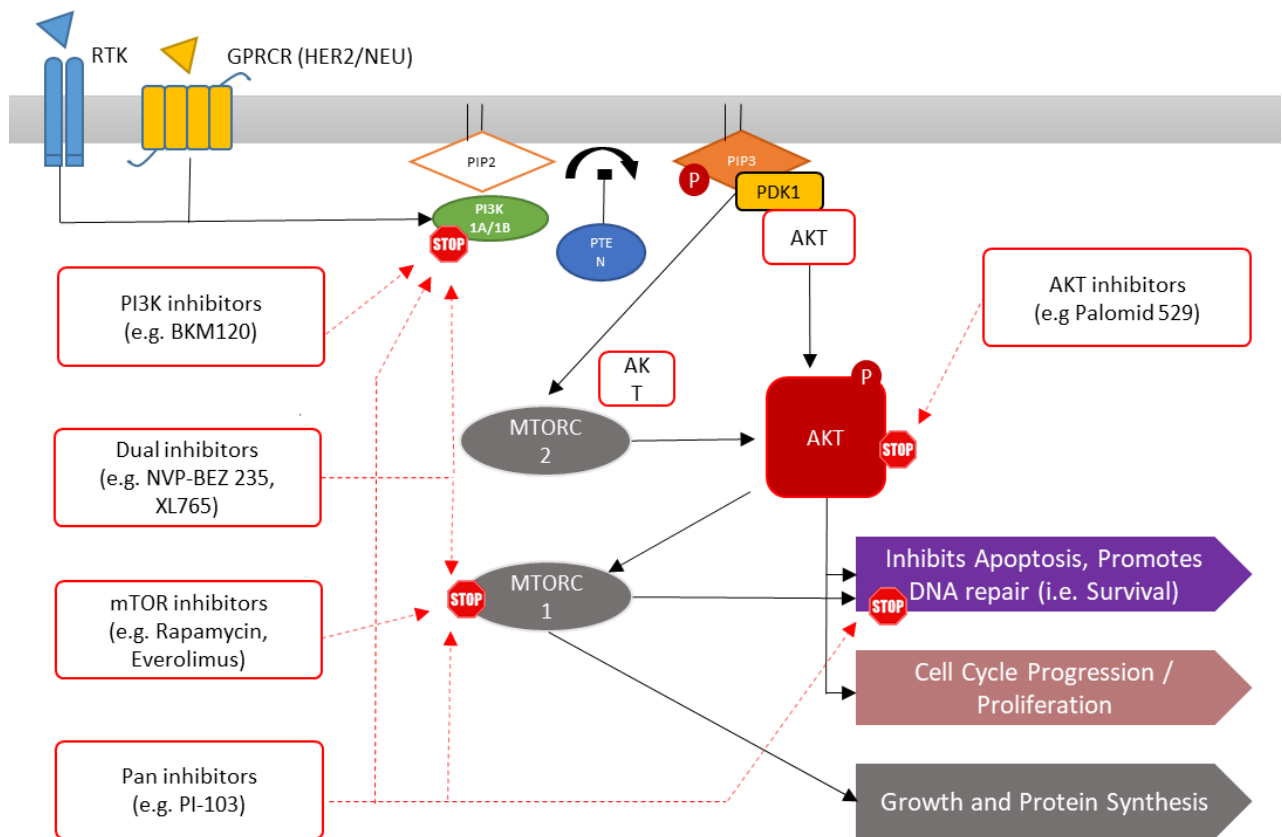
Proteins involved in cell cycle progression and proliferation: Cyclin dependent kinase 1 (Cyclin D1), Glycogen synthase kinase 3 (GSK3), p27, Cyclin dependent kinases (CDKs)

Figure 6-1: The PI3K/AKT/mTOR pathway activation leads to cell growth, increased protein synthesis, inhibited apoptosis, cell cycle progression and proliferation.

This figure was from Wanigasooriya et al, Cancers journal - MDPI publishing group (181), published under CC-BY license. The figure was designed in its entirety by the author of this thesis for former publication. Reproduced with the journals' permission.

6.1.1 Targeted inhibition of the PI3K/AKT/mTOR pathway

The PI3K/AKT/mTOR pathway is often dysregulated in malignancy (176). Mutations within the genes coding for PI3K, PTEN, RAS and EGFR are frequently detected in cancer (466). Tumours harbouring these mutations demonstrate radioresistant properties due to the pathological activation of this pathway (580-583). Multiple groups have also demonstrated that the PI3K/AKT/mTOR pathway activation in response to radiotherapy as a principal mechanism of radioresistance (173, 179-181). This pathway has also been linked to resistance to chemotherapy (182). Consequently, the efficacy of pharmacological inhibition of components of this pathway as cancer treatments has been extensively researched (177). The pathway inhibitors can be classified as single, dual, or multiple pathway component inhibitors based on which components of the pathway they work (Figure 6-2).



Class of inhibitor	Drug	No. of studies utilising drug as a radiosensitiser	
		In-vitro / In-vivo	Clinical trials
PI3K inhibitors	BKM120	4	2
Dual inhibitors	NVP-BE2235	17	0
	NVP-BGT226	1	0
	XL 765	0	1
	PF-05212384	1	0
	PKI-587	1	0
	GSK2126458	1	0
mTOR inhibitors	Rapamycin	9	1
	Everolimus	9	10
	Temsirolimus	2	0
Pan inhibitors	PI-103	5	0
	LY294002	5	0
AKT inhibitors	Palomid 529	1	0
	SH-5	2	0
	MK-2206	2	0

Figure 6-2: Drugs for targeted inhibition of the PI3K/AKT/mTOR pathway

This figure is from Wanigasooriya et al., *Cancers journal* - MDPI publishing group (184),

published under CC-BY license. The figure was designed in its entirety by the author of this thesis for the former publication. Reproduced with journals' permission.

6.1.2 Literature review: The PI3K/AKT/mTOR pathway as a target in colorectal cancer treatment

Whilst most PI3K/AKT/mTOR pathway inhibitors are still being tested in the laboratory or remain in early clinical trials (phase I/II), a few have been approved by the US Food and Drug Administration (FDA) for use in human diseases. Alpellesib a PI3K inhibitor is FDA approved for treatment in *PIK3CA* mutated, HR-positive, HER-2 negative advanced or metastatic breast cancer patients (584). Rapamycin, sirolimus, and everolimus have been widely used as immunosuppressant medications following organ transplantation through their antiproliferative effects (585, 586). Research into the use of PI3K/AKT/mTOR pathway inhibitors in CRC treatment remains in its infancy. A PI3K/AKT/mTOR pathway inhibitor is yet to be FDA approved for CRC treatment. Preclinical research in cell lines has also demonstrated the radiosensitising potential of these drugs in various cancers including breast, colorectal, pancreatic, prostate and lung cancer, certain H&N cancers, and GBM (184). Table 6-1 summarises studies using PI3K/AKT/mTOR pathway inhibitors to radiosensitise CRC cell lines *in vitro* and *in vivo* xenografts derived from CRC cells.

Table 6-1: In vitro and in vivo CRC research utilising PI3K/ AKT / mTOR pathway inhibitors as radiosensitisers

Authors	Year	Drug	Target of inhibition	Outcome
Chen et al. (333)	2019	Dactolisib	PI3K + mTOR	Enhanced apoptosis, disruption of DNA DSB repair
Pal et al. (587)	2016	BI-69A11	AKT inhibitor	Radiosensitisation when combined with COX-2 and radiotherapy
Djuzenova et al. (588)	2016	PI-103	PI3K, mTOR, DNA-PK inhibitor	Enhanced radiosensitisation
Chen et al. (173)	2015	Dactolisib	PI3K + mTOR	Inhibited DNA repair, cell growth and proliferation
Prevo et al. (573)	2008	PI-103	PI3K, mTOR and DNA-PK inhibitor	Radiosensitisation through inhibited AKT phosphorylation
Manegold et al. (589)	2008	Everolimus	mTOR inhibitor	Significant reduction in xenograft tumour size

Several phase I/II clinical trials utilising these drugs as NCRT in rectal cancer patients have also been conducted (Table 6-2). Despite promising results during preclinical research and being well tolerated by LARC patients receiving NCRT, targeted mTOR inhibitors have failed to demonstrate significant increase in pCR rates during early clinical trials (336, 337, 590). Furthermore, a review by Wanigasooriya et al. identified a shift in research in this area towards dual pathway component inhibitors to radiosensitise various cancers (184). GSEA of differentially

expressed genes from earlier experiments demonstrated the significance of PI3K/AKT/mTOR pathway upregulation in radiotherapy resistance (Figure 5-10, Table 4-11). Therefore, dual PI3K and mTOR inhibitors were chosen over single pathway component inhibitors during subsequent experiments to evaluating their radiosensitising potential on HCT116 CRC cell line and PDO lines.

Table 6-2: Clinical trials evaluating the radiosensitising potential of PI3K/AKT/mTOR pathway inhibitors in locally advanced rectal cancer patients

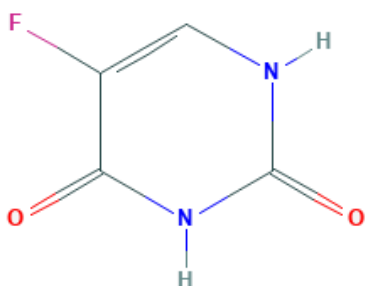
Authors	Year	N	Phase	Regime	Target	Outcome
Gelsomino et al. (336)	2017	12	I/II	Everolimus and radiotherapy	mTOR inhibitor	Safe in combination
Buijsen et al (337)	2015	44	I/II	Rapamycin and radiotherapy	mTOR inhibitor	No significant increase in pCR
Bertolini et al. (590)	2014	12	1b	Everolimus, 5FU and radiotherapy	mTOR inhibitor	

6.1.3 The chosen radiosensitising drugs

The three drugs chosen for subsequent assays included 5FU and dual PI3K and mTOR inhibitors, apitolisib and dactolisib. Given that 5FU is the standard chemotherapy used as neoadjuvant treatment in LARC patients this was chosen as the standard control in these experiments.

6.1.3.1 5FU

This chemotherapy agent is widely used in the treatment of various cancers. It is a uracil analogue which disrupts RNA synthesis and inhibits the enzyme thymidylate synthase (Figure 6-3), and is metabolised in the liver by the dihydropyrimidine dehydrogenase enzyme (242). The seminal German rectal cancer study group trial demonstrated significantly lower local recurrence rates following neoadjuvant treatment with 5FU and radiotherapy in LARC patients (220). Since then, intravenous 5FU or its pro-drug capecitabine which is available orally, continue to be used as the main radiosensitising agent in NCRT regimens administered to LARC patients.



Source: PubChem

URL: <https://pubchem.ncbi.nlm.nih.gov>

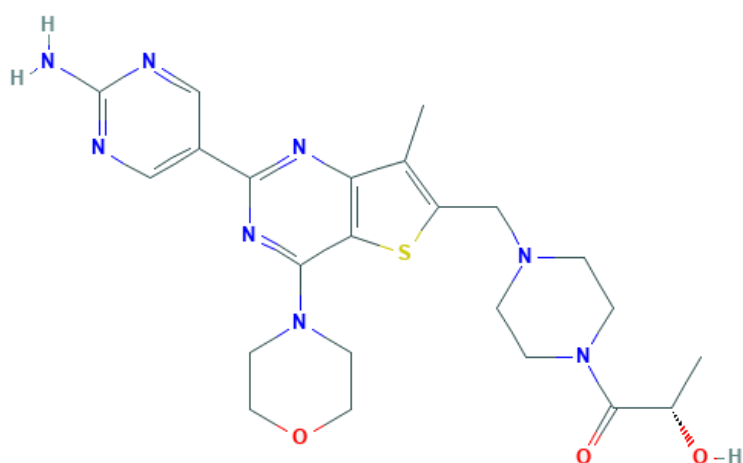
Description: Data deposited in or computed by PubChem.

Figure 6-3: Chemical structure of 5FU (591)

6.1.3.2 Apitolisib

Apitolisib (GDC-0980) is an orally administered antineoplastic drug which competitively binds and inhibits PI3K p110 $\alpha/\gamma/\delta/\beta$ and mTOR (Figure 6-4) (592, 593). Several Phase I and II clinical trials have been conducted using this drug in renal cell carcinoma, endometrial cancer, breast, CRC and other solid tumours (594-596). The largest multi-centre phase II trial recruited over 120 patients with solid malignant tumours, which included 8 CRC patients, found target modulation at doses greater

than 16mg and reported a maximum safe tolerate dose of 40mg once a day in patients (596). Research has also demonstrated maximum safe plasma concentrations (C_{max}) ranging from 0.320μM to 0.380μM, where an oral daily dose of 30mg or 40mg of apitolisib was administered to patients, respectively (596). Furthermore, the drug has been used in *in vitro* CRC liver metastasis derived PDO drug assays (365). No preclinical or clinical research combining apitolisib with radiotherapy was found.



Source: PubChem

URL: <https://pubchem.ncbi.nlm.nih.gov>

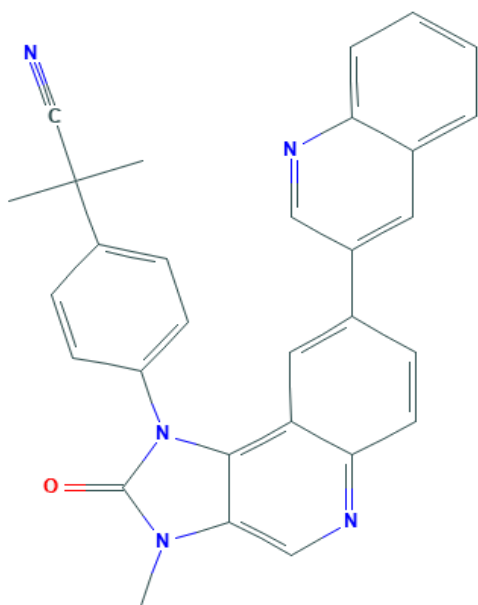
Description: Data deposited in or
computed by PubChem

Figure 6-4: The chemical structure of apitolisib (592)

6.1.3.3 Dactolisib

Dactolisib (NVP-BEZ235) is a competitive dual inhibitor of PI3K at p110α/γ/δ/β subunits and mTOR (p70S6K) (Figure 6-5) (597). Dactolisib has demonstrated radiosensitisation of CRC (173, 333), breast cancer (598, 599), endometrial cancer (600), prostate cancer (601-603), non-small cell lung cancer (583, 604), H&N cancer (179, 605-607), GBM (605, 608-611), sarcoma (606) and bladder transitional cell carcinoma (607) cell lines *in vitro* or *in vivo*. Phase I and II clinical trials have also been safely conducted in humans using dactolisib as a single agent or combined

with other anti-cancer therapies (612, 613). However, there were no clinical trials combining radiotherapy with dactolisib. Cmax values of 0.100 μ M, 0.220 μ M and 0.520 μ M have been reported following the administration of 200mg, 400mg or 800mg of oral dactolisib administration respectively to patients (612).



Source: PubChem

URL: <https://pubchem.ncbi.nlm.nih.gov>

Description: Data deposited in or
computed by PubChem

Figure 6-5: The chemical structure of dactolisib (614)

6.2 Methods

In vitro chemoradiotherapy experiment models were developed using HCT116 *KRAS* +/- CRC cell line and locally derived PDO lines described in the previous chapter.

HCT116 was chosen given its reputation as a stable CRC cell line used in numerous previous *in vitro* studies, including those evaluating radiotherapy response (173, 333). Standard treatment, using 5FU (+/- radiotherapy) were compared against dual PI3K and mTOR inhibitors, apitolisib and dactolisib (+radiotherapy). Several pilot seeding density experiments and feasibility experiments were conducted using HCT116 and six PDO lines. Data were represented as normalised bar charts or

dose-response curves. The effect of dual inhibitors on pAKT inhibition was assessed using HCT116 cell line and western blots targeting pAKT (phospho-Ser473). Image densitometry was performed followed by student t-test to determine statistical significance of inhibition. Subsequently, experiments were conducted to demonstrate the inhibitory potential of these drugs with or without radiotherapy. Where feasible, IC50 values were calculated and Welch's t-tests (chosen due to unequal variance in results) were performed to test for statistical significance. Live cell and PDO cultures were regularly tested for and ensured clear of mycoplasma (Appendix L).

6.3 Results

6.3.1 CRC cell line chemoradiotherapy assays

6.3.1.1 Optimum seeding density

The HCT116 cell line was initially plated at different cell counts to establish an optimum cell count for subsequent experiments.

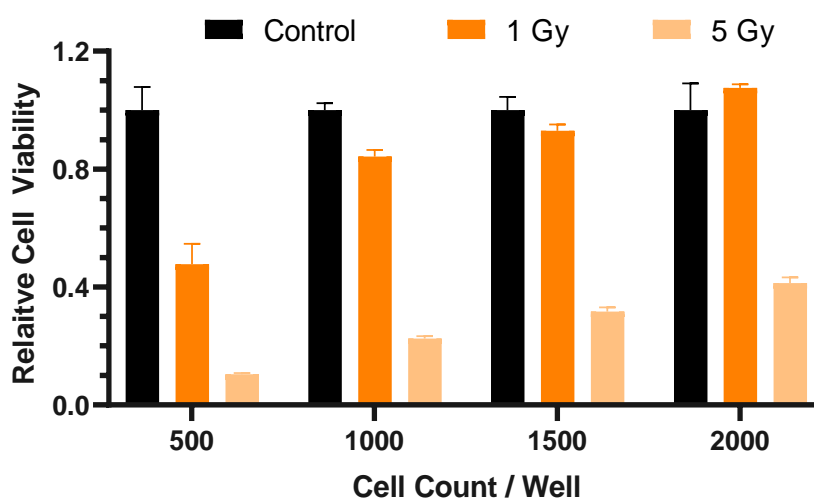


Figure 6-6: HCT116 optimum seeding density experiment

At 1000 cells / well and 1 Gy/day radiotherapy administered for five days, a 16% reduction in cell viability was observed compared to the untreated control (Figure 6-6). Therefore, approximately 84% of viable cells were available to assess any potential radiosensitising effects of the drugs used in subsequent experiments. In contrast at 500 cells/well radiotherapy resulted in the loss of over 50% viable cells. At 1500 or 2000 cells per well and 1 Gy/day for 5 days radiotherapy had minimal or no effect on cells. Furthermore, the use of higher radiotherapy dose (5 Gy or 5 days) at any of the different cell counts resulted in a greater than 50% loss of viable cells. Given that 1000 cells/well and 1 Gy/day radiotherapy administered for five days demonstrated a visible effect of radiotherapy response but at the same time left enough residual cells to demonstrate the possible effect of radiosensitising agents the latter parameters were used for subsequent experiments.

6.3.1.2 Improving CRC cell line response to radiation

HCT116 was treated in vitro using 5FU, apitolisib or dactolisib with or without radiotherapy administered in 1 Gy fraction per day for five days. The dose-response curves in Figure 6-7 summarise the combined results from three independent experiments using this cell line and the former treatments. Radiotherapy administered as a standalone treatment had minimal effect on endpoint cell viability (<10% reduction in relative cell viability). All three drugs demonstrated a dose dependent reduction in cell viability. At face value, when combined with radiotherapy, dactolisib demonstrated a synergistic effect but 5FU and apitolisib could demonstrate additive effects.

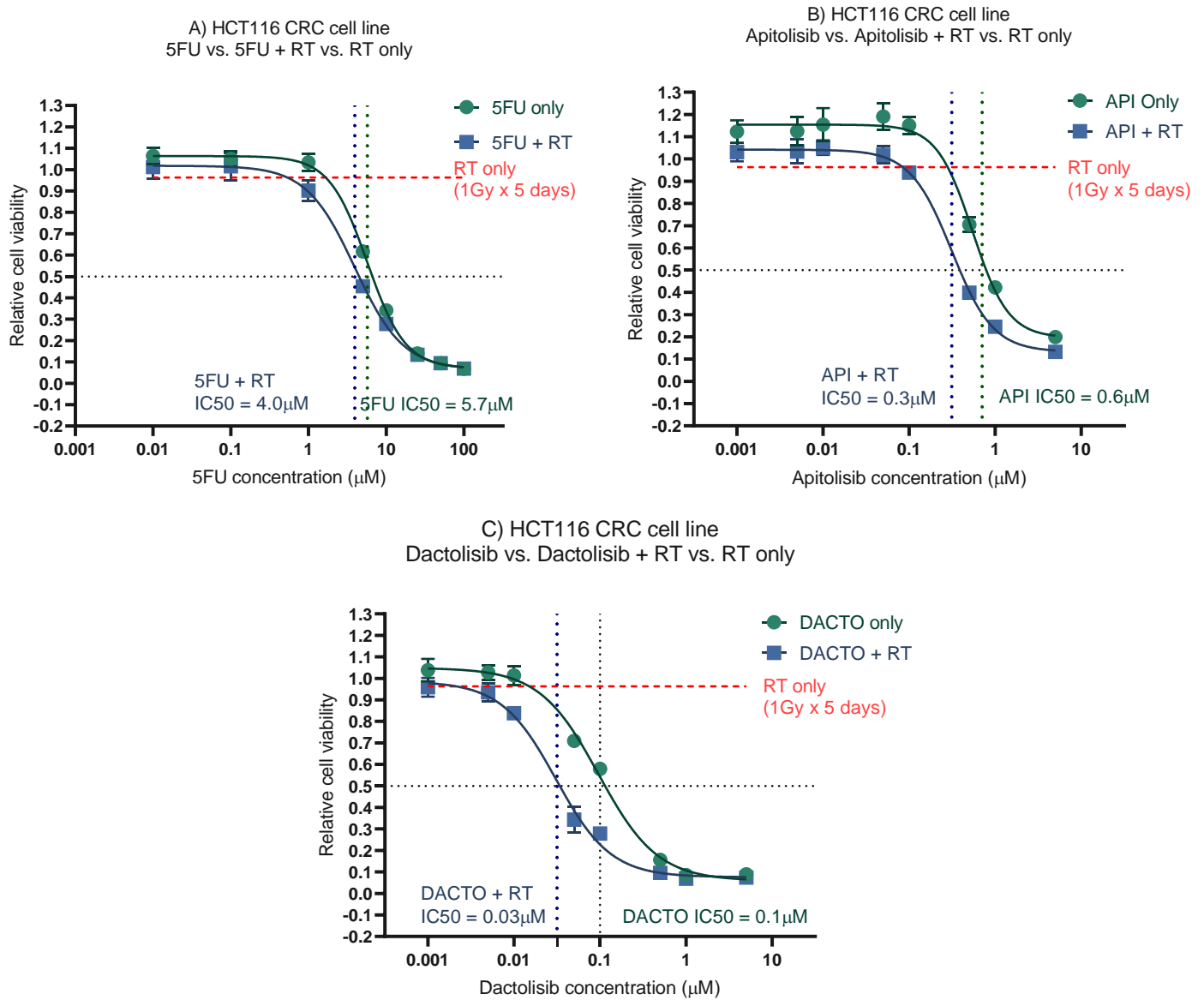


Figure 6-7: HCT116 cell viability and half maximum inhibitory concentrations (IC50) after treatment with 5FU, apitolisib or dactolisib with or without radiotherapy
HCT116 cells were treated with a range of different doses of 5FU, apitolisib and dactolisib with or without radiotherapy (1 Gy/day for 5 days). Experiment endpoint cell viability was assessed using chemiluminescence. Results were normalised to untreated controls and dose-response curves were generated. RT= radiotherapy, 5FU= 5-fluorouracil, API= apitolisib, DACTO=dactolisib

A Welch's t-test revealed that all three drugs significantly radiosensitised the HCT116 CRC cell line ($p < 0.05$). The IC₅₀ for HCT116 treated with dual PI3K/mTOR inhibitors apitolisib and dactolisib were 0.6 μM, 0.1 μM without radiotherapy, and 0.3 μM, 0.03 μM in the presence of radiotherapy, respectively (Table 6-3). These values were below the previously published C_{max} values for these drugs (596, 612). Furthermore, previous studies have demonstrated similar IC₅₀ values using in HCT116 CRC treated with 5FU and Dactolisib (615).

Table 6-3: HCT116 half maximum inhibitory concentrations (IC₅₀) after treatment with 5FU, apitolisib or dactolisib with or without radiotherapy

	IC₅₀ (μM) (95% CI)	p-value*
5FU	5.702 (5.506 – 5.905)	0.018
5FU + RT	3.950 (3.692 – 4.227)	
Apitolisib	0.547 (0.511 – 0.585)	<0.001
Apitolisib + RT	0.314 (0.294 – 0.335)	
Dactolisib	0.096 (0.090 – 0.104)	0.010
Dactolisib + RT	0.031 (0.028 – 0.034)	

RT= radiotherapy, 5FU= 5-fluorouracil, API= apitolisib, DACTO=dactolisib. Results from a Welch's t-test (Appendix N).

6.3.1.3 Optimum radiotherapy dose and time point for protein extraction to detect pAKT in a CRC cell line following irradiation

Western blots were performed using protein extracted at different time points following irradiation of HCT116 cell with a single fraction of 5 Gy or 10 Gy radiotherapy (Figure 6-8).

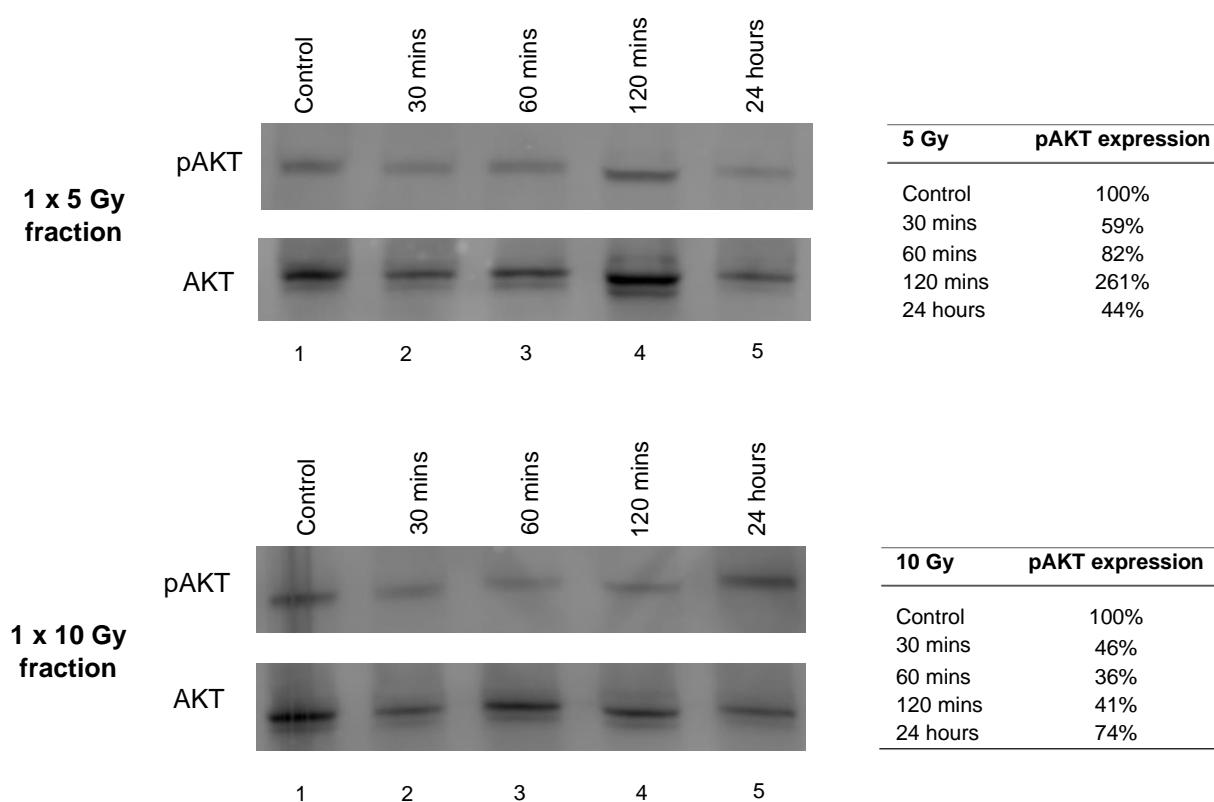


Figure 6-8: AKT phosphorylation in HCT116 cells over time following a single 5 Gy or 10 Gy radiotherapy fraction.

HCT116 was irradiated with a single 5 Gy or 10 Gy fraction and protein was extracted at different time points after irradiation to evaluate extent of AKT phosphorylation over time.

The numbers (1 to 5) below each lane represent the lane number. Image densitometry was performed and results normalised to untreated control in lane 1 and the results displayed in the two tables next to each blot. Raw western blot images can be found in Appendix O.

A single radiotherapy fraction as opposed to a daily dose for five days (e.g., 1 Gy/day for 5 days) was chosen due to logistical reasons. The total dose administered of 5 Gy was within the range of the experiment in section 6.3.1.2. Following treatment with a single 5 Gy fraction, AKT phosphorylation was initially suppressed relative to the control, detected at around 30 minutes after irradiation. This was followed by a gradual increase in pAKT levels. AKT phosphorylation in irradiated cells was first detectable at a level higher than the control, 2 hours after irradiation following treatment with a 5 Gy fraction. Whilst there was also an increase in baseline AKT detected at 2 hours, the rise in pAKT (261%) was considerably higher compared to AKT (132%) on image densitometry analysis. At 24 hours, the pAKT level had decreased to below 50% relative to the control. After a 10 Gy fraction of radiotherapy, maximum pAKT levels were detected relative to the control at 24 hours. There was AKT inhibition following irradiation between 30 minutes and 2 hours. At 24 hours pAKT levels appear to return to baseline control levels. Whether there was delayed pathway activation between 30 minutes and 24 hours is difficult to establish given that AKT phosphorylation at these time points were not assessed.

The lack of detectable significant increase in pAKT after irradiation would render the use of the other time points or the 10 Gy dose a logistical challenge for subsequent experiments. Therefore, a decision was made not to use 10 Gy for subsequent pathway analysis experiments. However, a 5 Gy radiotherapy fraction appears to lead to high pAKT phosphorylation (relative to the control) detectable 2 hours after irradiation. Furthermore, it is the daily radiotherapy dose which is administered to

LARC patients receiving SCRT. Furthermore, Chen et al. had previously demonstrated AKT phosphorylation in HCT116, maximally detected after 1 hour following irradiation with a single 5 Gy fraction(173). Therefore, a decision was made to proceed with the single 5 Gy fraction for the next experiment and protein was extracted 2 hours after treatment.

6.3.1.4 Radiation induced AKT phosphorylation is inhibited by dual PI3K and mTOR blockers in irradiated HCT116 cells

Western blots were performed using protein extracted from HCT116 cells treated with radiotherapy with or without drug treatment. The concentrations of drugs chosen for this experiment was based on the IC50 results from the experiment in section .

The results from these experiments also confirmed that treatment with a single 5 Gy radiotherapy fraction led to a significant increase in AKT phosphorylation, relative to the control in HCT116 cells, at 2 hours post-irradiation ($p=0.027$; Figure 6-9).

Standard treatment with 5 μ M of 5FU alone or 5 μ M 5FU with a single 5 Gy radiotherapy fraction did not significantly suppress AKT phosphorylation ($p>0.05$).

However, following treatment with 0.1 μ M of dual PI3K and mTOR inhibitors (dactolisib or apitolisib) there was complete suppression of AKT phosphorylation.

Furthermore, AKT phosphorylation continued to remain suppressed following administration of radiotherapy to HCT116 cells in the presence of apitolisib or dactolisib. The total level of AKT and GAPDH were lower in lanes 5, 6 and AKT levels were lower in lane 7. These lanes corresponded to cells treated with apitolisib and dactolisib with or without radiotherapy. This effect was observed across all independent experiment repeats (see Appendix O). There was a concern as to

whether the loss of pAKT signal in lanes 5 and 6 was due to a net reduction in AKT. However, in lane 7 and 8 the levels of AKT and GAPDH return to levels detected in the untreated control indicating the possibility of an experiment error.

This experiment demonstrated that radiotherapy leads to significant AKT phosphorylation following irradiation detected at 2 hours after irradiation in keeping with the preliminary experiment in section 6.3.1.3. It also demonstrated that dactolisib and apitolisib effectively inhibit phosphorylation of AKT. Both apitolisib and dactolisib are potent inhibitors of PI3K and mTOR. The latter is a key activator of downstream components of this pathway responsible for DNA DSB repair, cell growth, proliferation and migration. These results were replicated and validated through three independent repeat experiments.

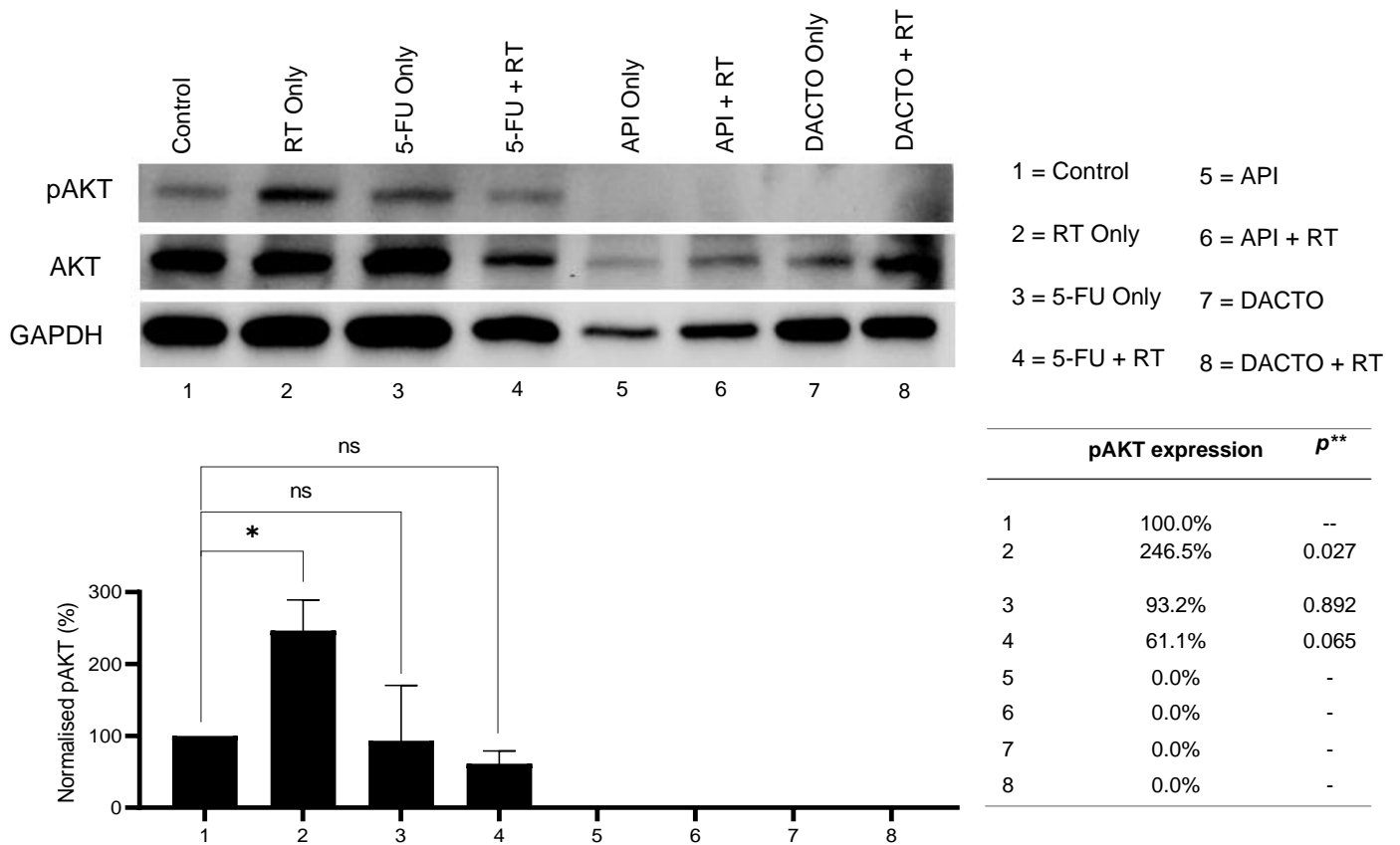


Figure 6-9: AKT phosphorylation following treatment with 5FU, apitolisib, dactolisib and irradiation.

HCT116 cells were treated with a single 5 Gy fraction of radiotherapy (in isolation) or single dose of 5FU (5mM), apitolisib, dactolisib (in isolation) or the drugs in former doses combined with radiotherapy (a single 5 Gy fraction). Protein was extracted and western blots performed. The best blot of three repeat experiments demonstrated here. Image densitometry was performed and results normalised to untreated controls in lane 1 in each experiment. The numbers (1 to 10) represent the lane number and treatment each treatment condition. RT- radiotherapy– API - apitolisib, Dacto – dactolisib, ns – not statistically significantly different, * statistically significantly different. Raw western blot images can be found in Appendix O. ** Results from a student t-test (Appendix P)

6.3.2 PDO in vitro chemoradiotherapy assays

The four radiosensitive PDO lines (884, 064, 389, 411) and two radioresistant PDO lines (653 and 557) identified in earlier experiments were chosen for combined PDO drug and radiotherapy assays.

6.3.2.1 Determining the optimal PDO seeding density

In these pilot experiments, PDO lines 884 and 064 were plated at 10,000, 5,000 and 2,500 cells/wells of PDOs in 96-well culture plates and treated with 50 μ M of 5FU on the third day after incubation (Figure 6-10).

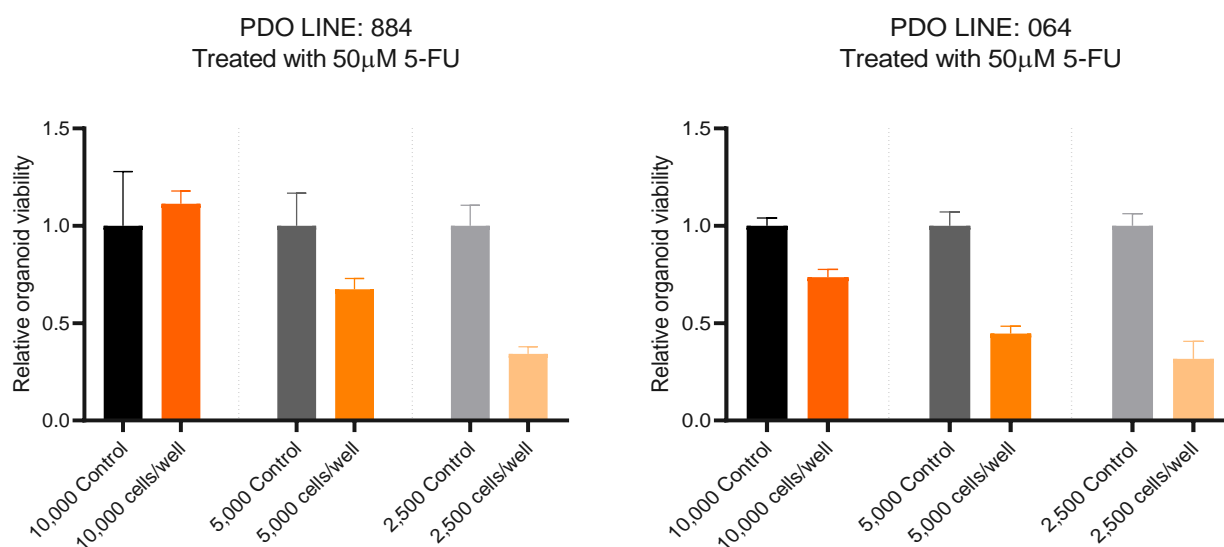


Figure 6-10: The effect of high dose 5FU on different seeding densities of two PDO lines

The PDOs were incubated for five days under treatment conditions and endpoint cell viability was assessed on the sixth day after plating. The drug dose of 50 μ M was chosen given that it was a high enough dose to observe an inhibitory effect even at very high cell counts. The two PDO lines were chosen at random and were readily

available for this preliminary experiment. The results for both lines showed maximum confluence was reached by day five, independent of initial seeding density. A greater inhibitory effect of the drug was maximally observed at an initial seeding density of 2,500 cells/well for both lines. At a 10,000 cells/well, despite a relatively high dose of 5FU, failed to demonstrate any growth inhibition in PDO line 884 and a small effect observed in 064. Given these findings and previously published literature pertaining to PDO drug assays utilising 3000 to 5000 cells/well a decision was made to proceed with a seeding density of 5000 cells/well of PDOs for subsequent experiments. Previous experiments had also confirmed that 5000 cells/well of PDOs provided a suitable seeding density for irradiation experiments.

6.3.2.2 Pilot experiments reveal feasibility of in vitro PDO drug and radiotherapy assays using dual PI3K and mTOR inhibitors

The inhibitory potential of the experimental drugs chosen and effects of radiotherapy were assessed using several pilot experiments. PDOs were plated 5000 cells/well and treated with fixed doses of 5FU (25 μ M), apitolisib (1 μ M), dactolisib (1 μ M), 5FU and apitolisib or 5FU and dactolisib, with or without radiotherapy (5 Gy/day fractions for five days). The drug doses were chosen at random and the radiotherapy regime emulated SCRT regimen administered to patients. Four replicates for each experiment conditions were performed in a single experiment. The bar charts below represent results from these experiments normalised to untreated control wells containing PDOs in DMSO (0.1%) in Human Intesticult™ Component A and B.

6.3.2.2.1 5FU +/- radiotherapy

Treatment of the six PDO lines with 5FU demonstrated varying responses to 5FU (Figure 6-11). PDO line 884 appears to be most resistant to treatment with 5FU. This was a PDO line derived from a rectal tumour of a patient following SCRT. PDO lines 653 and 557 were most responsive. These two PDO lines were deemed radioresistant in earlier experiments. The reason for this observed effect is unclear. The response to 5FU was similar across 064, 389 and 411. Radiotherapy in the presence of 5FU did not significantly inhibit the six PDO lines.

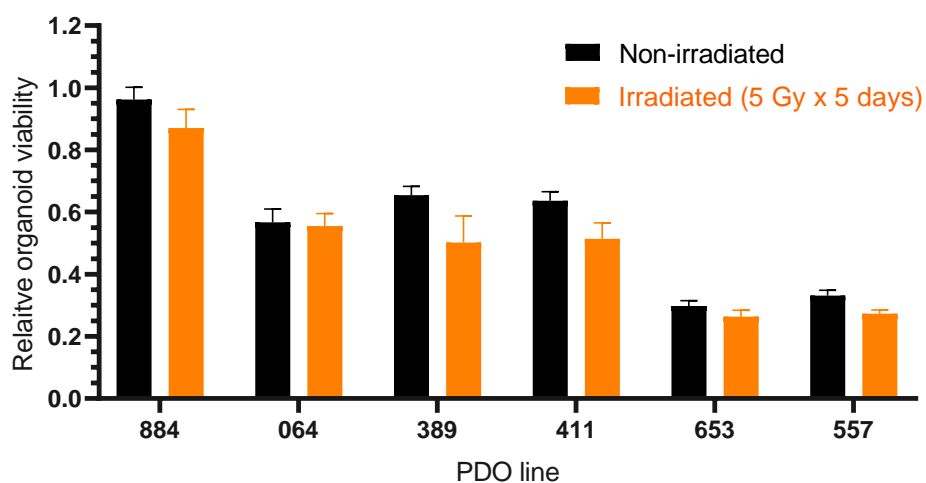


Figure 6-11: Six PDO lines treated with 5FU with or without radiotherapy.

6.3.2.2.2 Apitolisib +/- radiotherapy

Apitolisib on its own did not inhibit PDO growth in any of the six PDO lines (Figure 6-12). However, in the presence of apitolisib irradiated PDOs demonstrated substantial inhibition (40-50%) of PDO survival across all six PDO lines, almost uniformly.

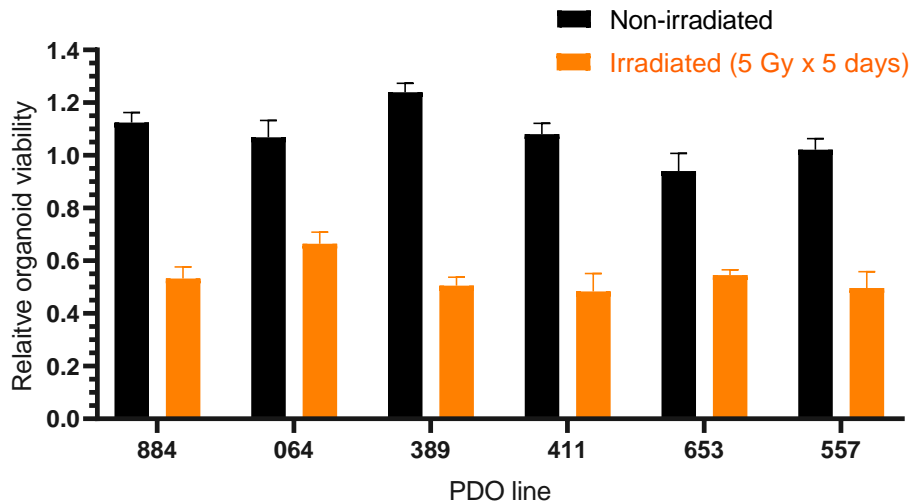


Figure 6-12: Six PDO lines treated with apitolisib with or without radiotherapy

6.3.2.2.3 5FU and apitolisib +/- radiotherapy

Combining 5FU with apitolisib led to a reduction in PDO viability (>40%) across all six PDO lines (Figure 6-13). Combining the two drugs with radiotherapy led to further inhibition of PDO survival. The radioresistant PDO lines 653 and 557 were the most responsive to treatment.

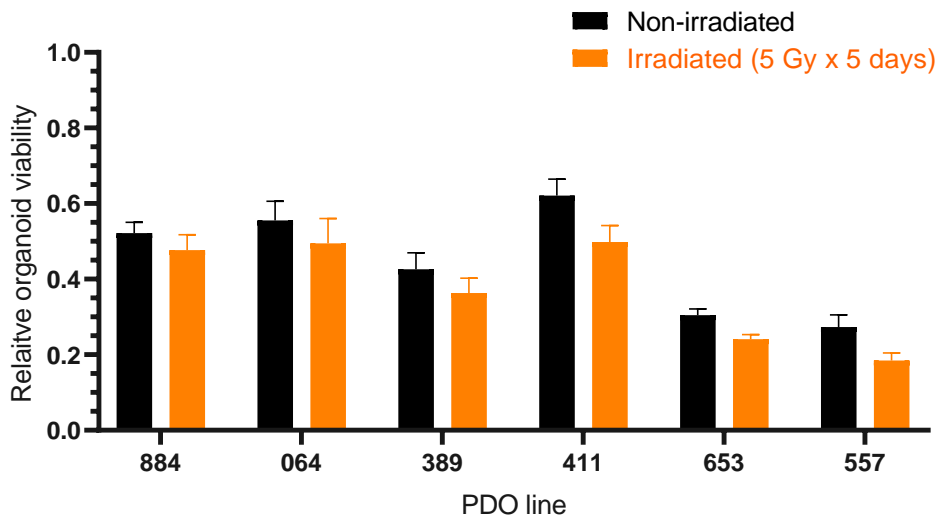


Figure 6-13: Six PDO lines treated with 5FU and apitolisib with or without radiotherapy.

6.3.2.2.4 Dactolisib +/- radiotherapy

Dactolisib demonstrated varying degrees of inhibition of PDO survival across the six lines (Figure 6-14). However, PDO line 411 did not respond well to dactolisib treatment. This PDO line contained the most mutations amongst the six PDO lines (Figure 5-2). However, when combined with radiotherapy there was inhibition of PDO survival. PDO lines 064, 389, 653 and 557 were most responsive to dactolisib treatment with or without radiotherapy.

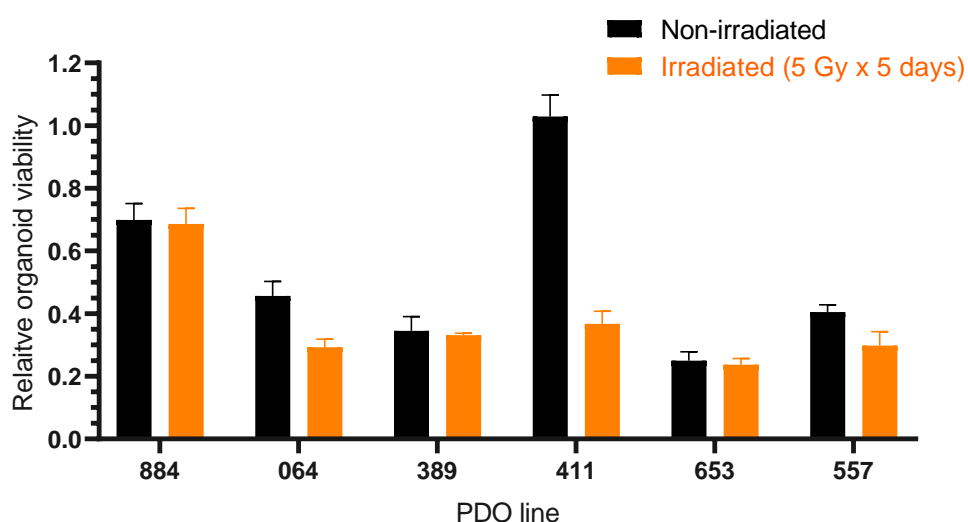


Figure 6-14: Six PDO lines treated with dactolisib with or without radiotherapy.

6.3.2.2.5 5FU and dactolisib +/- radiotherapy

Marked PDO survival inhibition was observed across all six PDO lines when treated with 5FU and dactolisib (Figure 6-15). PDO lines demonstrating the biggest response were 064, 389 and 653. Combining with radiotherapy may have led to further inhibition of PDO survival.

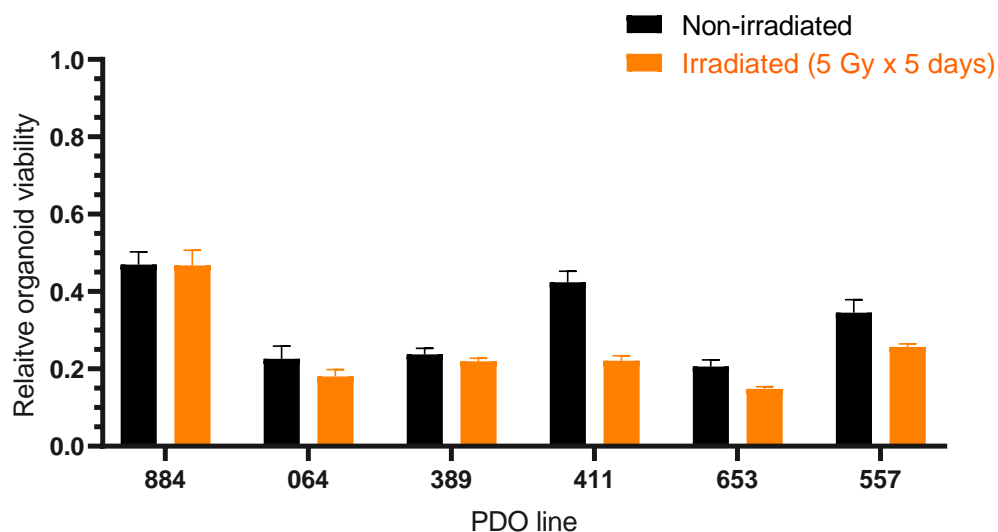


Figure 6-15: Six PDO lines treated with 5FU and dactolisib with or without radiotherapy.

6.3.2.3 Dual PI3K and mTOR inhibitors radiosensitise radioresistant PDO lines

Radioresistant PDO lines (653 and 557) were treated with the dual PI3K/mTOR inhibitors apitolisib and dactolisib, alone or in combination with radiotherapy to evaluate their radiosensitising potential (Figure 6-16). Dose-response graphs represent combined results from three independent experiments normalised to untreated control wells containing PDOs in DMSO (0.1%) in Human Intesticult™ Component A and B (Figure 6-17). When administered as a single agent, both apitolisib and dactolisib were less effective at inhibiting tumour viability requiring higher doses to reduce cell viability by 50%.

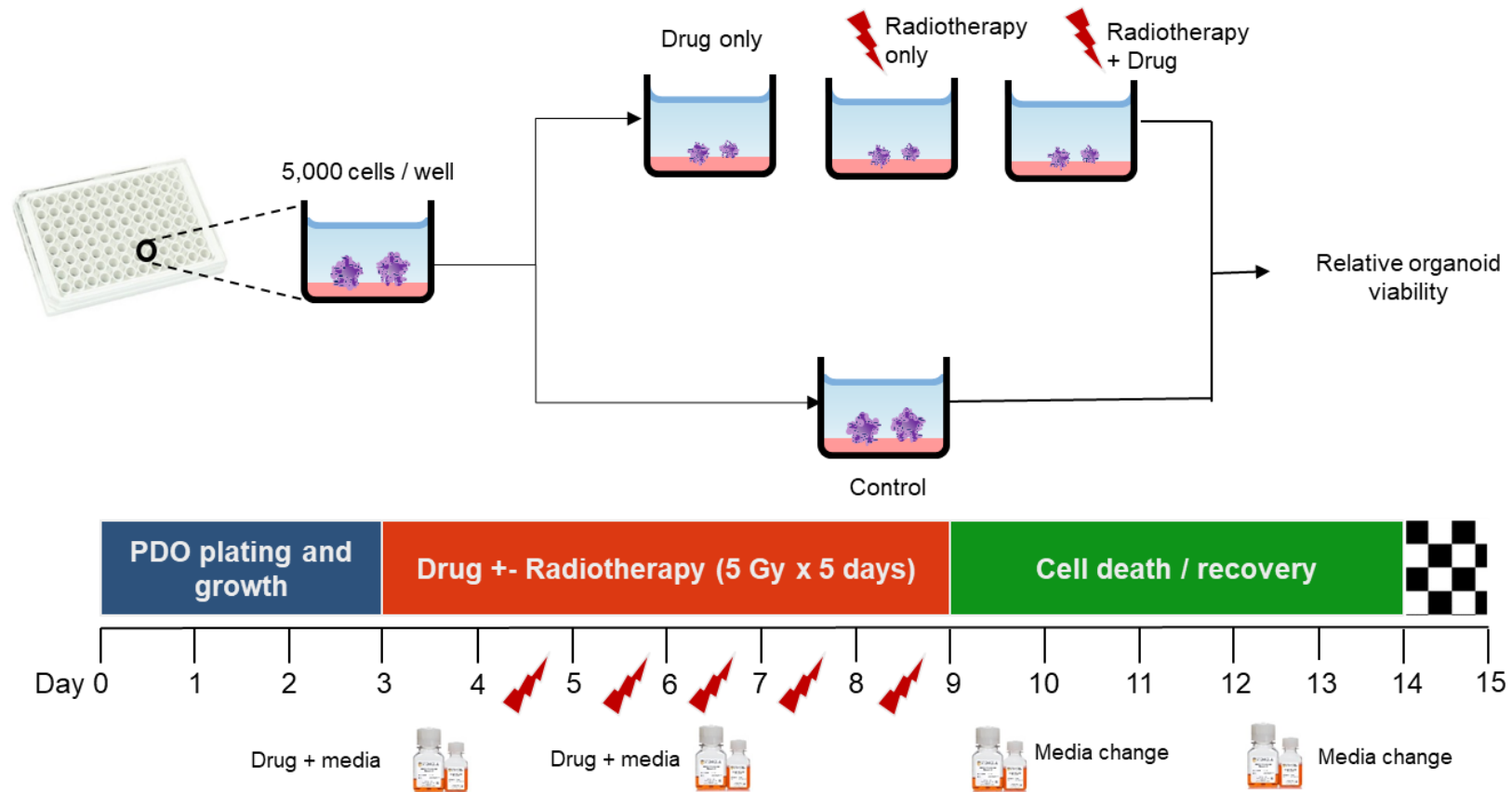


Figure 6-16: Schematic representation of PDO chemoradiotherapy assays

PDOs were plated (estimated 5000 cell/well) on a Matrigel® bed in 96 well plates. Drug (5FU, apitolisib, dactolisib) and DMSO (0.1%) in varying concentrations were added on the fourth day and radiotherapy was commenced (5 Gy/day for five days) starting on the fifth day. The experiment was completed on day 15 with endpoint PDO viability assessment using CellTiter-Glo® 3D (Promega, USA) and chemiluminescence.



Copyright of STEMCELL Technologies (Canada). Image used with permission. Source: [https://www.stemcell.com/cell-](https://www.stemcell.com/cell-separation/immunomagnetic)

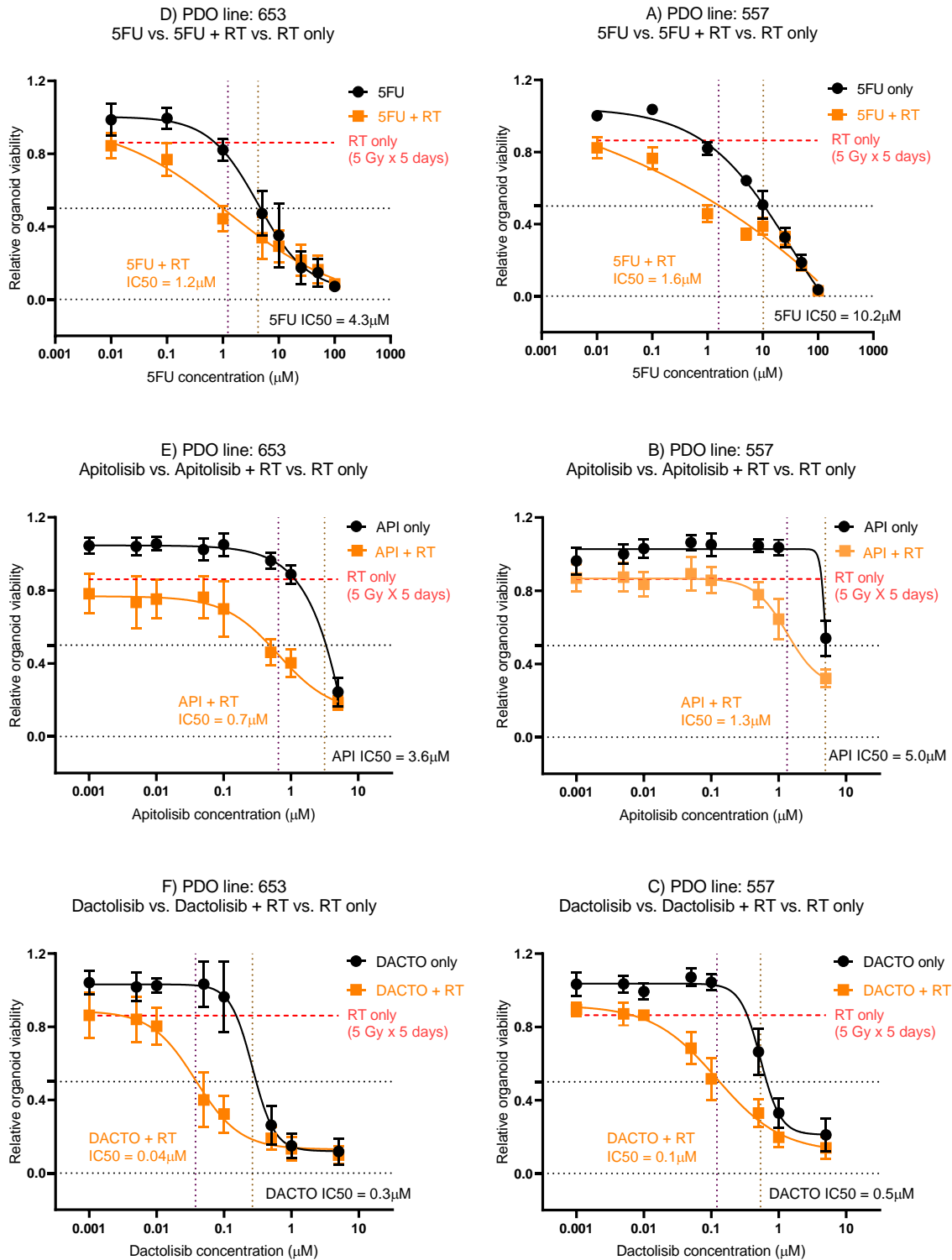


Figure 6-17: Radiotherapy resistant PDO lines 557 and 653 treated with 5FU, apitolisib and dactolisib with or without radiotherapy.
 PDO lines were plated at an estimated 5000 cells / well and treated with was treated with eight different concentrations of 5FU, Apatolisib (API) or Dactolisib (DACTO), with or without

radiotherapy (5 Gy/day for 5 days). Endpoint cell viability was assessed using CellTiter-Glo® 3D (Promega, USA) and chemiluminescence. The data is presented normalised to control (containing 0.1% DMSO in organoid culture media). The x-axis represents log transformed drug dose concentrations (μM). 5FU – 5-fluorouracil, API – apitolisib, Dacto – dactolisib, RT – radiotherapy.

The IC50 values obtained following treatment of radioresistant PDOs (557 and 653) with 5FU alone and 5FU with radiotherapy were 4.3 μM , 1.2 μM and 10.2 μM , 1.6 μM respectively (Table 6-4). The IC50 following Apitolisib-only treatment for lines 557 and 653 were 5.0 μM and 3.6 μM respectively; combined with radiotherapy the IC50 was 1.3 μM and 0.7 μM . The IC50 following Dactolisib-only treatment for lines 557 and 653 were 0.5 μM and 0.3 μM respectively; combined with radiotherapy the IC50 was 0.1 μM and 0.04 μM . A Welch's t-test revealed that all three drugs significantly radiosensitised the PDO lines ($p < 0.05$). On assessment of the dose-response curves dactolisib combined with radiotherapy likely demonstrates a synergistic effect but the observed radiosensitisation for apitolisib and 5FU treated PDO lines could be an additive effect.

Table 6-4: IC50 values following treatment of radioresistant PDO lines with 5FU, apitolisib or dactolisib with or without radiotherapy.

	653 IC50 (μM) (95% CI)	p-value	557 IC50 (μM) (95% CI)	p-value*
5FU	4.266 (3.287-5.538)	0.035	4.300 (NA)	0.035
5FU + RT	1.232 (0.527-2.879)		1.200 (NA)	
API	3.600 (NA)	<0.001	4.951 (NA)	<0.001
API + RT	0.651 (0.386-1.099)		1.335 (0.835-2.134)	
DACTO	0.265 (0.213-0.330)	0.015	0.538 (0.497-0.583)	0.002
DACTO + RT	0.038 (0.028-0.050)		0.122 (0.093-0.159)	

API – apitolisib, Dacto – dactolisib, RT – radiotherapy. Half maximal inhibitory concentrations (IC50) for each of the drugs with or without radiotherapy were obtained using Prism (GraphPad, USA). A statistically significant difference in radiosensitisation across all three drugs (radiotherapy effect; Results from paired-sample t-test*, $p < 0.05$, Appendix Q). NA – Unable to compute 95% CI yielding (0.000-infinity).

6.3.2.4 *In vitro* PDO drug assays using dual PI3K and mTOR inhibitors

The four radiosensitive PDO lines (884,064,389 and 411) were plated 5000 cells/well and treated with 5FU, apitolisib and dactolisib for five days. The dose response curves in Figure 6-18 represent combined results from two independent experiments normalised to untreated control wells containing DMSO (0.1%) in Human Intesticult™ Component A and B.

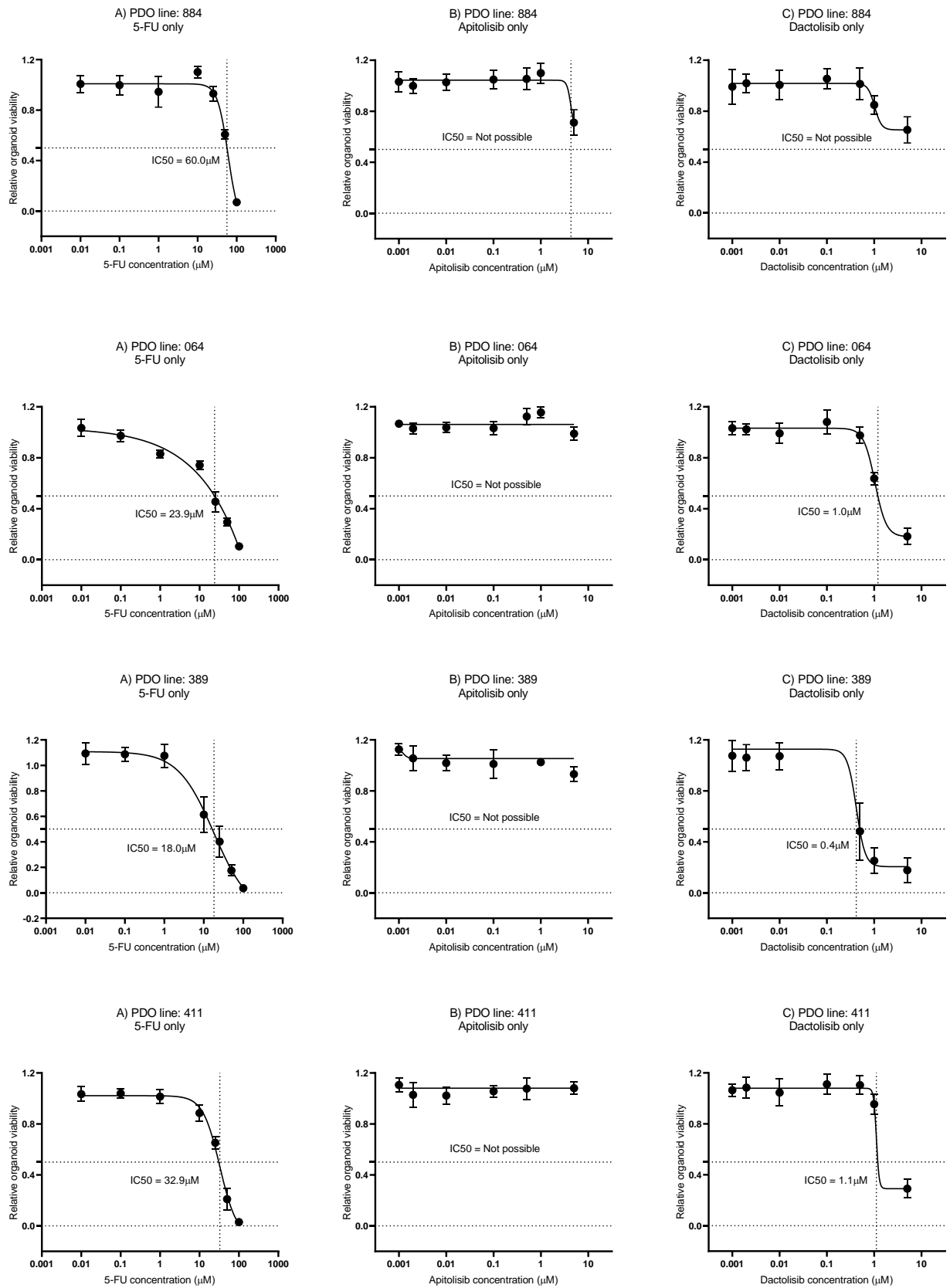


Figure 6-18: Dose response curves and IC50 values following treatment of radiosensitive PDO lines with 5FU, apitolisib or dactolisib

Four PDO lines were plated at an estimated 5000 cells/well and were cultured for three days in 96-well plates on a bed of Matrigel® before commencing treatment with 5FU, apitolisib and dactolisib in varying concentration for six days. Chemotherapy containing media was removed at the end of the sixth day and replaced with fresh organoid culture media and PDOs were left for further six days to allow for cell recovery or death. The endpoint cell viability was assessed on day 15 using CellTiter-Glo® 3D (Promega, USA) and chemiluminescence. The data is presented normalised to control (containing 0.1% DMSO in organoid culture media). The x-axis represents log transformed drug dose concentrations (μM).

Apitolisib failed to demonstrate a reduction in PDO viability across all four lines, whilst 5FU inhibited all four lines and dactolisib inhibited three lines except 884. PDO line 884 was the most drug resistant PDO line with the highest IC50 value recorded after 5FU treatment (60.0 μM) and failing to inhibit PDO viability with apitolisib treatment and dactolisib treatment. Interestingly, PDO line 411 demonstrated did not respond well to dactolisib treatment and this was in keeping with findings in pilot experiments in Figure 6-14. Furthermore, when compared with IC50 results from PDO lines 653 and 557 treated with 5FU, apitolisib or dactolisib, the former four radiosensitive lines appear more resistant to the drugs tested (Table 6-5). Higher IC50 values or a lack of inhibition of PDO viability was observed following treatment of these radiosensitive PDO lines with 5FU, apitolisib or dactolisib.

Table 6-5: A summary of half maximum inhibitory concentration (IC50) results for the six PDO lines following treatment with 5FU, apitolisib or dactolisib.

	Radiotherapy response	Half maximum inhibitory concentration (IC50)		
		5FU	Apitolisib	Dactolisib
884	Radiosensitive	60.0µM	NA	NA
064	Radiosensitive	23.9µM	NA	1.0µM
389	Radiosensitive	18.0µM	NA	0.4µM
411	Radiosensitive	32.9µM	NA	1.1µM
653	Radioresistant	4.3µM	5.0µM	0.5µM
557	Radioresistant	4.3µM	3.6µM	0.3µM

NA – not available as there was no inhibition following treatment

6.4 Discussion

Drug and radiotherapy assays were successfully performed *in vitro* using HCT116 CRC cell line and six PDO lines. The variation in response across the different PDO lines reflected the inter-patient tumour variability and heterogeneity of cells within a tumour population. Dual PI3K and mTOR inhibitors dactolisib and apitolisib were used in these *in vitro* assays and replicated, consistently generating reliable and reproducible results. The PI3K/AKT/mTOR pathway significance in radiotherapy resistance and response has long been researched and established.

Chemoradiotherapy resistant tumours demonstrate the ability to evade apoptosis, enhanced DNA double-strand breaks repair, changes to cellular metabolism, resistance to hypoxia, poor inflammation and abundance of tumour stem cell populations (331). The PI3K/AKT/mTOR pathway regulates several of these functions (570). Pathway activation leads to several downstream effectors

responsible for cell proliferation, migration, growth and DNA repair (616). The pathway is implicated in the pathogenesis as well as chemoradiotherapy resistance in various cancers (490, 491). Mutations within genes coding for components within this pathway are frequently detected in malignancy.(466)

Several pharmacological inhibitors targeting the PI3K/AKT/mTOR pathway are commercially widely available and several are being trialled as cancer treatment (617, 618). Furthermore, the radiosensitising potential of these inhibitors is currently being assessed in several tumour types (184). In CRC, studies using cell lines and cell line- derived xenografts have shown that PI3K/mTOR inhibitors dactolisib and PI-103 improve the efficacy of ionizing radiation (173, 333, 573, 588). As the long-term treatment with PI-103 before irradiation could cause reactivation of PI3K and MAPK pro-survival pathways (333), this was not included in our assays.

Furthermore, PI-103 may have short half-life in humans due to rapid metabolism, rendering it less effective (619). Furthermore, early clinical trials evaluating the radiosensitising effects of selective mTOR inhibitors such as everolimus, rapamycin or sirolimus failed to increase pCR rates (336, 337, 620). Emerging evidence points towards the effectiveness of using dual pathway component inhibitors to ensure effective radiosensitisation (184). Therefore, dual PI3K and mTOR inhibitors (apitolisib and dactolisib) were chosen. Both drugs have safely undergone Phase I/II clinical trials in humans in various cancers (596, 612).

In these experiments, dactolisib showed radiosensitising effects in HCT116 and radioresistant PDOs, with an IC50 lower than the previously published Cmax in

humans. Apitolisib radiosensitised HCT116. However, it did not demonstrate a potentially clinically useful radiosensitising effect in the radioresistant PDO lines; the IC50 for apitolisib-treated radioresistant PDOs exceeded the previously published Cmax in humans. Furthermore, the chemoradiotherapy assays utilising 5FU and apitolisib did not conclusively show whether the observed effects were synergistic or additive. However, for PDOs and HCT116 treated with dactolisib and radiotherapy, the dose-response curves were more in keeping with synergism. Future experiments with several rectal cancer cell lines and PDOs treated with a fixed dose of drug and radiotherapy and radiotherapy alone with results normalised to an untreated control will aid to objectively ascertain whether the observations made are due to synergistic or additive effects. Interestingly, the radioresistant PDOs appear to be five to -fold more sensitive to 5 to 15 fold more sensitive to 5FU compared to the radioresistant PDO lines. This phenotype could be used to define and explore targets related to DNA/RNA synthesis associated with radiotherapy resistance in future experiments.

The results also demonstrated phosphorylation of AKT, when HCT116 was treated with clinically comparable doses of radiotherapy, maximally detected at 2-hours after irradiation (Figure 6-8 and Figure 6-9). This was in keeping with findings published by Chen et al (173). Nevertheless, the results from this preliminary experiment (Figure 6-8) were interpreted with caution given they were from a single experiment run as opposed to multiple independent experiments. The lack of a loading control in the western blots in Figure 6-8 was a limitation. It is also important to note that there was a higher level of AKT in lane 4 and this could have had an impact on the very high levels of pAKT detected in lane 4. However, image densitometry revealed that whilst the difference in AKT was approximately 1.4 times compared to the control,

there was over 2.6 times rise in pAKT compared to untreated controls. Furthermore, results from three subsequent independent repeat experiments (summarised in Figure 6-9) demonstrated an average pAKT rise of over 2.5 times the control at 2 hours after irradiation in keeping with the results from the preliminary experiment in Figure 6-8. The radiotherapy regime used for pathway analysis was different from the cell viability experiments for logistical reasons (1Gy/day for 5 days as opposed to a one off 5 Gy dose) even though the total dose administered was the same.

Western blots showed complete pAKT suppression in apitolisib and dactolisib-treated cells. In contrast, treatment with 5FU did not significantly reduce pAKT expression. Results from this experiment was also interpreted with caution particularly in relation to apitolisib given the low AKT and GAPDH levels detected in lanes 5 and 6. A use of a proteasome inhibitor in the future could be beneficial to identify if the drugs have a direct effect on total AKT levels. Nevertheless, the overall findings were in keeping with numerous other research attributing the effects of dual PI3K and mTOR inhibitors in suppressing AKT phosphorylation (184). Suppressed AKT phosphorylation likely leads to the inhibition of several downstream pathway functions such as DNA damage repair, cell survival, proliferation and migration (184); which in turn would lead to radiosensitisation. Future research should focus on the effects on downstream targets of the PI3K/AKT/mTOR pathway (e.g., DNA-PK involved in NHEJ, ribosomal protein s6 and eukaryotic translation initiation factor 4E involved in protein synthesis) following dual PI3K and mTOR inhibitor treatment to validate these hypotheses. Research has previously demonstrated that dactolisib in particular is a potent inhibitor of ataxia telangiectasia mutated checkpoint protein and DNA-dependent protein kinase catalytic subunit protein (611, 621). Dactolisib has

also been shown to directly inhibit ataxia telangiectasia and rad3 related protein (ATR) which is responsible for DNA damage repair (622). The ATR and mTOR pathway are intertwined with ATR leading to direct phosphorylation of mTOR and phosphorylated mTOR also upregulates the main effector of ATR, checkpoint kinase 1 (responsible for coordinating cell cycle response following DNA damage) (623). Direct ATR inhibition could potentially explain the greater potency of dactolisib observed in these experiments compared to apitolisib which is not known to be an ATR inhibitor.

There were several limitations in this research. Only one cell line was used and it was a colon cancer cell line as opposed to a rectal cancer cell line. The PDO sample size was small due to limited availability of viable, experiment-ready organoid models and also resource limitations. This experiment model did not incorporate the microenvironment factors which may play a crucial role in NCRT response. A potential solution to this could be patient derived xenografts where tumour organoids may be grafted on to animal hosts (e.g., mice). There were also strengths. This experiment model provides a reliable and reproducible model for chemoradiotherapy assays using PDO lines. This research was one of the first to test PI3K/AKT/mTOR pathway inhibitors and their impact on radiotherapy response using CRC PDO lines.

6.5 Conclusion

In vitro chemoradiotherapy assays using PDO lines are feasible in CRC and serves as a valuable adjunct to traditional models of such assays utilising CRC cell lines. This experiment model may be replicated to test other potential treatment for CRC *in vitro*. Irradiation of CRC cells leads to phosphorylation of AKT. PI3K/AKT/mTOR pathway inhibition using dual PI3K and mTOR inhibitors plays a significant role in enhancing radiotherapy response and warrants further research using additional rectal cancer cell lines, PDO and PDX models to further validate these findings, identify downstream effects of dual PI3K and mTOR inhibition on proteins and pathways associated with DNA damage repair.

Chapter 7: General Discussion

Ionizing radiation (e.g., x-ray) is widely used to treat cancer with or without chemotherapy. However, significant challenges arise due to radioresistance. Chemotherapy agents such as 5FU and oxaliplatin have been traditionally used to radiosensitize cancers to radiotherapy. However, the efficacy of these drugs is limited. Radiotherapy is routinely used as neoadjuvant treatment in patients with LARC. Approximately 10-30% of patients who receive NCRT demonstrate pCR and these patients have a survival advantage over their non-responding counterparts (250, 251, 258). The non-responders undergo NCRT, enduring the side-effects of treatment with no benefit (262, 263). Furthermore, their surgery might be delayed and subsequent surgery following radiotherapy often more challenging and associated with increased risk of post-operative complications such as anastomotic leak (624). Various strategies to improve pCR have been explored. The use of total neoadjuvant chemoradiotherapy strategies where LARC patients are treated with either SCRT followed by chemotherapy then surgery or long course NCRT followed by additional chemotherapy and surgery have shown marginally higher pCR rates over traditional NCRT (625-627). However, much needs to be done to combat radioresistance, improve pCR rates and consequently improve survival in LARC patients, and to better predict therapy response in patients.

Numerous clinicopathological factors contribute to radioresistance. The intrinsic tumour biology and extrinsic tumour microenvironment are affected by radiotherapy. Radiotherapy leads to complex intracellular and extracellular transformations which contribute to treatment resistance. Several genetic mutations, gene expression profiles, gene signatures, methylation arrays as well biological pathways have been linked to good or poor response following NCRT in LARC. In keeping with preceding research, this project expanded upon previously published methodology to identify novel markers of radioresistance. The laboratory research comprised of several distinct components. The retrospective component involved transcriptomic analysis of RNA extracted from archived FFPE patient samples of non-responder versus responder patients. The prospective components included derivation of PDO models, establishment of a novel *in vitro* model to identify radiotherapy response status. Subsequent pre-and post-irradiation genomic and transcriptomic analyses were performed from locally derived PDO models. Having identified a potential biological target for improving radioresistance dual PI3K and mTOR inhibitors were used to assess their radiosensitising potential *in vitro* using CRC cell line and PDO models.

Within the retrospective cohort, differential gene expression analysis identified upregulated *PIK3CB* in non-responders. Wei-Dong et al. demonstrated a significant association between more abundant PIK3CB expression by immunohistochemistry and poor response to NCRT in LARC patients (453). Prior research, including from our own laboratory had demonstrated that genetic alternations within the AKT pathway genes could be associated with NCRT response in LARC (628). Amongst the PDO lines there were *PIK3CA* mutations detected in two of the PDO lines (411

and 557), one of which (557) was a radioresistant PDO line. Nevertheless, Russo et al. found no clear association between *PIK3CA* mutation and radiotherapy response (290). Upregulation of the PI3K/AKT/mTOR pathway was also detected on GSEA in non-responder pre-irradiation FFPE samples and non-responder PDO lines. Several associations with F-Box protein component gene up or downregulation and radiotherapy response was also identified amongst the FFPE cohort and PDO samples before and after irradiation. This pathway is downstream of the PI3K/AKT/mTOR pathway.

Buckley et al. identified ten potential hallmarks of gastrointestinal cancer which are targets for improving radiosensitivity (331). Amongst these was PI3K/AKT/mTOR pathway inhibition which the authors concluded was responsible for radioresistance through sustained growth and survival signalling following radiotherapy induced cellular injury. The pathway has been a popular target of interest for treatment in various cancers with several drugs having undergone successful early clinical trials. Furthermore, research aimed at PI3K/AKT/mTOR pathway inhibition to promote radiosensitivity is also being considered across different cancers (184).

Nevertheless, the existing evidence-base exploring this pathway's significance in LARC was limited. Therefore, targeted PI3K/AKT/mTOR pathway inhibition to promote radiosensitivity in LARC was further explored in this research. In addition, the genomic and transcriptomic analyses performed in this research pointed towards this pathway and its various components as potential biologically significant targets in the quest to improve radiotherapy response in LARC.

Genetic mutations and association with radiotherapy response status was assessed through panel sequencing of PDO models. Pathological *KRAS* mutations (G12D and G13R) were detected in both radioresistant PDO lines whilst the radiosensitive lines were wild-type *KRAS*. Duldulao et al. had previously demonstrated a significant association with *KRAS* codon 13 mutations and incomplete or poor response following NCRT in LARC patients (119). Similarly, the presence of both *KRAS* and *p53* mutations have previously been linked to poor response (419). For example, pathological *p53* mutations were detected across five of the PDO lines including all four radioresistant lines. However, one of the radioresistant PDO lines (557) did not have any *p53* mutations. This is contradictory to previous research involving patient tumour samples where wild-type *p53* was associated with higher odds of pCR and lower relative risk of poor response, following NCRT in LARC (286). Several other pathological mutations identified were not unique to the radiosensitive or radioresistant lines and therefore, showed no clear associations with radiation response. GSEA identified upregulated *KRAS* signalling amongst non-responder patient cohort and radioresistant PDO lines, pre-irradiation. *KRAS* mutation status and radiation response has been extensively researched with no clear consensus on its association with radiosensitivity or resistance. Furthermore, there was no clear association with *p53*, *PIK3CA*, *SMAD4*, *dMMR* gene mutations and radiotherapy response in this analysis.

Several potential target genes of interest were identified as predictors of NCRT response during this research. However, some of these had previously published links to radiotherapy response in cancer. These included *MMP7*, *CAV1*, *OLFM4*, *FABP1*, *FBXW4*, *FBXL17*, *RPL5P34*, and *OBSL1*. The role of these genes in

radiotherapy response has been discussed in earlier chapters. Other upregulated pathways potentially associated with radiotherapy resistance identified during this research included the epithelial mesenchymal transition, oxidative phosphorylation, TGF β , NF- κ B signalling, MAPK, notch signalling and hypoxia signalling pathways. Research has shown that all these pathways have a role to play in chemoradiotherapy response in various cancers (see Chapter 4). The role of these biological pathways in rectal cancer radiotherapy response warrants further investigation. Of particular interest is hypoxia signalling. Tumour hypoxia and chemoradiotherapy response has been extensively researched. Tumour hypoxia leads to chemoradiotherapy resistance and poor prognosis in various cancers (473, 474). Hypoxic tumour cells frequently express HIF1 α and VEGF promoting oxidative phosphorylation and angiogenesis promoting tumour cell survival (475, 476).

Dual pathway inhibitors were chosen given the findings from a comprehensive literature review highlighting their superiority over single component inhibitors (184). The use of isolated mTOR inhibitors will likely lead to reactivation of the pathway through the numerous feedback loops and pro-survival mechanisms (Figure 6-1). Furthermore, several of these drugs had failed to demonstrate enhanced radiosensitivity amongst patients during early clinical trials in various cancers including in rectal cancer. Preliminary research conducted in our laboratory (data not shown) had also demonstrated limited efficacy of single pathway inhibitors such as everolimus and rapamycin in enhancing radiosensitivity amongst PDO lines. Therefore, dual pathway inhibitors apitolisib and dactolisib were chosen. Exposure to stressful stimuli can activate the PI3K/AKT/mTOR pathway. Western blots revealed that radiotherapy leads to a statistically significant increase in AKT phosphorylation

suggesting the activation of the pathway following radiotherapy. *In vitro* treatment with dual inhibitors successfully suppressed AKT phosphorylation. AKT is the main effector of the PI3K/AKT/mTOR pathway. Its activation leads to downstream activation of several pathways leading to DNA repair and protein synthesis. Overall, the pathway regulates several key intracellular functions including cell growth, proliferation and autophagy (Figure 6-1). Additionally, glucose metabolism and angiogenesis may also indirectly be regulated by this pathway (629).

In vitro drug assays involving the HCT116 CRC cell line and two radioresistant PDO lines (653 and 557) showed statistically significant radiosensitising effects following treatment with radiotherapy and either dactolisib or apitolisib (Figure 6-7 and Figure 6-17). The two drugs also demonstrated chemo-sensitising effects when administered with 5FU without any radiotherapy, to all six PDO lines. The radiosensitising effects were more pronounced with dactolisib compared to apitolisib, particularly amongst the PDO lines. In isolation, dactolisib demonstrated significant cyto-toxic potential effect across all PDO lines. However, apitolisib did not demonstrate any significant efficacy when administered by itself (Table 6-5). The direct inhibition of ATR by dactolisib could explain the differences observed. There is also crosstalk between ATR and mTOR. The inhibition of the PI3K/AKT/mTOR pathway may also inhibit ATR and consequently checkpoint kinase1 inhibiting cell cycle progression. Therefore, the role of dual pathway inhibitors in radiosensitisation through mTOR / ATR / checkpoint kinase 1 mediated inhibition of DNA damage repair, cell cycle arrest or cell death, warrants further investigation. Another possible yet less plausible explanation for the observed difference in effect between apitolisib and dactolisib could be the higher molecular weight of apitolisib reducing its ability to

traverse to the depths of the 3D PDO cultures. This again highlights the differences between 2D and 3D culture experiments and variable results and how 3D cultures may provide real-world comparable results. Nevertheless, pathway analysis through western blots of protein extracted from drug and radiotherapy treated HCT116 revealed suppressed AKT phosphorylation following dactolisib as well as apitolisib treatment confirming that the drugs are effective inhibitors of the main effector of the PI3K/AKT/mTOR pathway.

The mechanisms by which PI3K/AKT/mTOR pathway inhibition leads to radiosensitisation is linked to the inhibition of AKT phosphorylation. AKT activated through phosphorylation leads to the activation of mTORC1 through phosphorylation which in turn leads to downstream activation of proteins associated with protein synthesis (e.g., ribosomal protein S6, eukaryotic translation initiation factor 4E) associated with cell growth and proliferation. Furthermore, proteins such as BAD, FOX, YAP and the activation of p53 via MDM2 as well as DNA-PK lead to DNA repair and inhibition of autophagy. Activation of cyclinD1 and activation of CKDs by inhibition of p27 lead to downstream cell cycle progression. Therefore, pathway activation (e.g., secondary to radiotherapy) leads to a pro-survival state. The inhibition of the pathway likely leads to the suppression of downstream pro-survival effectors leading to radiosensitivity. Further research is warranted on these downstream effectors and whether these could serve as novel therapeutic targets considering the concerns associated with side effects secondary to upstream PI3K and mTOR inhibition.

Chapter 8: Future Work

The proposed future work can be subcategorised into laboratory research and clinical research. Future research should focus on developing a validated predictive score to determine patient response to NCRT pre-treatment. To achieve the complete translational potential of this research a phase II clinical trial should be considered using dual PI3K and mTOR inhibitors.

8.1 Laboratory research

8.1.1 *Additional genomic, transcriptomic and immunohistochemistry work*

Gene signatures capable of predicting NCRT response at baseline could be derived from the available transcriptomic data from FFPE samples used in this research and validated using a previously published test dataset or transcriptomic analysis of fresh LARC biopsy or tumour tissues extracted from a prospective cohort of patients. The sensitivity, specificity, positive and negative predictive values of these signatures at detecting NCRT response should be further analysed. QPCR validation of target genes such as *MMP7*, *CAV1*, *OLFM4*, *FABP1*, *PROSPER2*, *FBXW4*, *FBXL17*, *PIK3CB*, *RPL5P34*, and *OBSL1* from this research should be performed using RNA extracted from fresh tumour tissue, irradiated CRC cell lines and PDO lines. This research also identified that CDX2 expression was absent in both radioresistant PDO lines. The significance of absent CDX2 expression as a predictive marker in

NCRT resistance must be further evaluated. Immunohistochemistry and QPCR analysis of pre-NCRT rectal cancer biopsies from a large cohort of LARC patients and correlation between CDX2 expression and corresponding post-operative TRG should be considered. RNA extracted from the radioresistant PDO lines following very high doses of irradiation (20 Gy/day or 40 Gy/day for 5 days) should be analysed for differential gene expression and GSEA to identify the biological basis of cellular resistance at the extreme end of radiation exposure.

DNA extracted from FFPE patient samples and PDO models should be used to perform methylation arrays to identify differentially methylated regions and their associations with response. Differentially methylated regions can provide insight into potential targets associated with radiotherapy response. The use of ctDNA as a predictor for NCRT response should be explored. The presence of mutations in *KRAS*, *p53*, *BRAF*, *SMAD4*, *PIK3CA* and *PIK3CB* genes in ctDNA and associations with NCRT response in LARC patients should be assessed in more detail. Access to the 100,000 Genomes Project (Genomics England, UK) data from LARC patients undergoing NCRT may prove useful as a grouped analysis. CtDNA from plasma extracted before, during and after NCRT and genomic analysis of biopsies, post-NCRT surgical resection specimens from LARC patients could be analysed to identify ctDNA based predictors of response. Such a study must be a prospective study spanning several years to also include a 3 to 5 year follow up period to assess predictors of improved overall and disease free survival following NCRT in LARC patients.

8.1.2 Downstream PI3K/AKT/mTOR pathway component analysis

This research highlighted the potential of dual PI3K and mTOR inhibitors at radiosensitising and chemo sensitising CRC cells, but the exact mechanisms remain unknown. The proteomic analyses in this research aimed at pathway analysis was limited to pAKT. However, additional western blots from extracted protein could be performed to identify effects of these drugs and irradiation on pathway downstream targets of the pathway such as DNA-PK, eukaryotic translation initiation factor 4E and ATR. It is essential to evaluate the effect of dactolisib and apitolisib on ATR. Whilst dactolisib has been shown to be a direct inhibitor of ATR, the effects of apitolisib on ATR is unknown. This will also help identify whether the main mechanism by which dual PI3K and mTOR inhibitors promote cytotoxicity and radioresistance is through inhibition of mTOR, ATR and checkpoint kinase 1 mediated DNA damage repair.

These pathway analysis proteomics experiments should also be conducted using a broader panel of rectal cancer cell lines comprising of multiple replicates to further validate the results. Furthermore, proteomic studies should be extended to PDO models and not limited to CRC cell lines. The pathway analysis experiments conducted using the HCT116 CRC cell line in this research as well as additional pathway component analysis experiments should be performed using PDO models to demonstrate that the results can be effectively replicated using PDO models. There were significant limitations to extracting phosphorylated proteins in this research owing to the prolonged Matrigel® dissolution stage, involved in extracting

protein from PDO models. This prolonged incubation often renders phosphatase inhibitors inert or ineffective. Several measures have been proposed to overcome this problem, including the use of flash-freezing techniques. The transcriptomic analyses conducted in this study also identified several biological pathways which are associated with radiotherapy resistance (e.g., epithelial mesenchymal transition, oxidative phosphorylation, MAPK signalling and TGF β pathway, NF- κ B, notch and hypoxia signalling). Using siRNAs or clustered regularly interspaced short palindromic repeats (CRISPR) and CRISPR-associated protein 9 mediated knockdown of targets within these different biological pathways should be performed to better comprehend their associations with radiotherapy response.

8.1.3 Additional in vitro chemoradiotherapy assays

To further validate the findings from this research the chemoradiotherapy assays will be replicated using additional rectal cancer cell lines and dual PI3K and mTOR inhibitors as well as 5FU (current standard treatment). Endpoint assessment will utilise chemiluminescence and colony forming assays. The latter will ensure comparable methodology in line with previously published *in vitro* research cancer radiotherapy research. Additional PDO lines, preferably derived from oncological therapy naïve rectal tumour surgical resection specimens or pre-treatment biopsies will also be used to replicate PDO chemoradiotherapy assay experiments described in this research. Following genomic and immunohistochemical characterisation, the individual PDO line response to radiotherapy will be determined using the experiment model described in Chapter 4, Figure 5-3. The PDO counts at the start of each experiment will be standardised using the method described in this research

and validated using novel digital image based cell counting methodology. To ensure that the observed effects are due synergy and additive, fixed drug and radiotherapy dose experiments will be conducted using the cell lines as well as PDO lines.

8.1.4 Patient derived xenografts models

Provided that the additional *in vitro* cell line and PDO experiments described above further validates the radiosensitising potential of dual PI3K and mTOR inhibitors, PDX models should be used to evaluate their use as systemic therapy or local treatment (enema form) in improving radiotherapy response. A concern with potent PI3K/AKT/mTOR pathway inhibitors is systemic toxicity and side effects (630). An alternative method of drug delivery could be considered where the drug is administered per rectum as an enema as opposed to oral therapy. The proposed methodology for an *in vivo* animal study evaluating a systemic and local dual PI3K and mTOR inhibitor therapy is as follows. Pre-NCRT biopsies from rectal cancer patients should be sampled to derive PDO models in the laboratory. Immune nude mice will be grafted with successfully derived PDO models. The methodology published by Ganesh et al. will be used to generate PDX models (334). The test group mice may then be treated with oral or per rectum apitolisib or dactolisib with oral capecitabine. A clinically relevant dose regime of radiotherapy will be administered. The comparator group will be administered capecitabine and radiotherapy and the control group will receive radiotherapy only. PDOs from one patient will be grafted to several murine models to develop corresponding PDX models for each patient. A power calculation will be performed to identify the number of PDX models required for each patient. Each mouse will be allocated to test,

comparator or control group. Endpoint residual tumour volume can be assessed through murine endoscopy, cross sectional imaging and post-mortem tumour weight assessment. Tumour regression, cCR and pCR rates should be assessed.

Comparisons can be made between the pCR, cCR rates from patients undergoing NCRT to the *in vitro* models developed the laboratory. Genomic, transcriptomic and proteomic analyses of pre-treatment biopsies and post-treatment tumour specimens from patients and murine models could provide internal validation of the model utilised, confirm maintenance of genetic stability and tumour heterogeneity, and identify targets for treatment as well as mechanisms behind radioresistance or radiosensitivity, amongst the PDO models and PDX models.

8.2 Clinical research

Phase I/II clinical trials have previously been conducted with dactolisib in humans.

However, none of these involved LARC patients or radiotherapy. Dactolisib was chosen given its greater potency and consistent radiosensitising and chemo

sensitising effects compared to apitolisib. A phase II double blinded clinical trial of

LARC patients randomised systemic oral dactolisib (200mg or 400mg once a day for 28 days) with or without capecitabine or placebo and radiotherapy (50.4 Gy)

administered as daily fractions over 28 days, should be conducted (Figure 8-1).

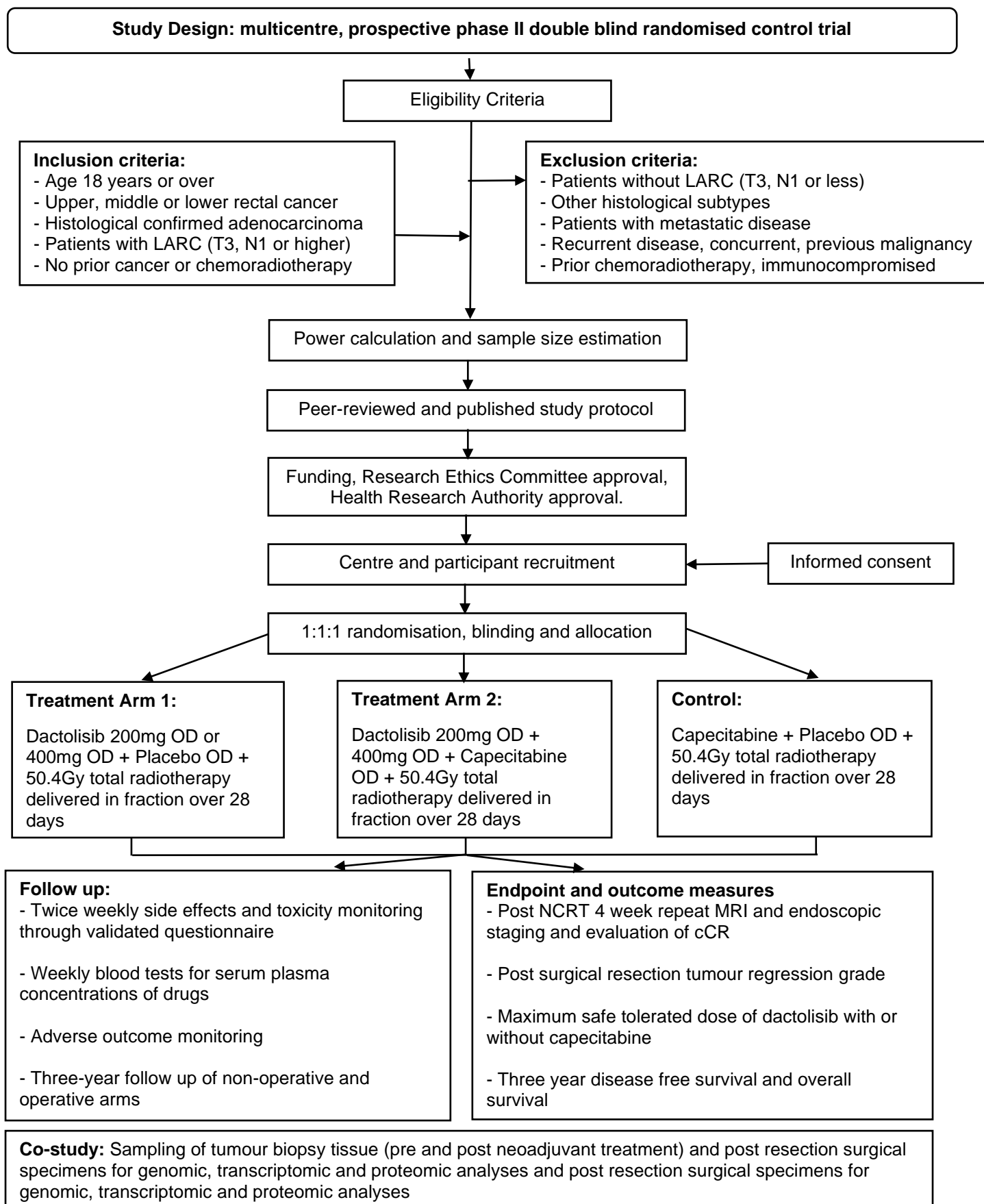


Figure 8-1: Proposed phase II double blinded clinical trial to evaluate the safety and efficacy of dual PI3K and mTOR inhibitor dactolisib (with or without capecitabine) and radiotherapy versus current standard treatment in LARC patients

The dactolisib doses 200mg and 400mg oral once a day were shown to be safe in humans in a previous phase II randomised control trial (612). The control arm may comprise of patients receiving standard treatment (capecitabine) with placebo and radiotherapy. The main aim of this phase II study is to evaluate the safety and efficacy of dactolisib in combination with NCRT in LARC patients. The study could also identify safe, effective maximally tolerated plasma concentrations and dose-finding study in patients with LARC undergoing neoadjuvant radiotherapy with dactolisib with or without capecitabine. The primary outcome measure would be proportions of patients achieving cCR versus downstaging versus no response or disease progression at four weeks after each treatment regimen, assessed on cross-sectional imaging (MRI, CT scan) and flexible sigmoidoscopy. Secondary outcome measures should include the following: pCR versus TRG detected on post-surgical resection specimen histopathological assessment; maximal safe tolerated dose of dactolisib in LARC patients receiving a combination of radiotherapy with or without capecitabine. Additional outcome measures include intra-operative time, surgical complications assessed using the Clavien-Dindo classification (631), length of hospital stay and 30-day readmission rate following surgery. A small group of patients with cCR may proceed to “watch and wait.” These patients alongside patients undergoing surgical resection should be followed up for three years to determine local recurrence rates, disease free survival and overall survival in each treatment arm. The trial will pave the way to a subsequent phase III clinical trial further evaluating the efficacy of dual PI3K and mTOR inhibitor dactolisib as neoadjuvant treatment in LARC. A co-study may also be conducted alongside the primary trial to evaluate the biological mechanisms surrounding this pathway blockade. Pre-treatment biopsy, post-treatment biopsy samples and post-surgical

tumour resection specimens should be sampled for genomic, transcriptomic and proteomic analyses. The effect of dactolisib on downstream PI3K/AKT/mTOR pathway proteins, specifically associated with DNA DSB repair, protein synthesis and cell growth can be assessed through western blots and immunohistochemistry. Genomic and transcriptomic analysis of tissues sampled during this trial could reveal other pathways closely associated with radiotherapy response.

Thesis Conclusion

- PDO models were derived from fresh donor tissue. Genomic, transcriptomic and immunohistochemistry analyses were performed using these PDO lines.
- *In vitro* experiment models were developed to simulate neoadjuvant therapy using PDO models. They were highly effective, reliable and recapitulated clinically utilised treatment regimens.
- Through retrospective (FFPE samples) and prospective (PDOs) transcriptomic analyses several potential target genes of interest (*MMP7*, *CAV1*, *OLFM4*, *FABP1*, *FBXW4*, *FBXL17*, *PIK3CB*, *RPL5P34*, and *OBSL1*) were identified as predictors of NCRT response in LARC patients, pre-NCRT.
- PDO model genomic analyses revealed an association between *KRAS G12D* and *G13R* mutations and radiotherapy resistance. There was no clear association with *p53*, *PIK3CA*, *SMAD4*, dMMR gene mutations and radiotherapy response.

- An association with loss of CDX2 expression and radiotherapy resistance also warrants further investigation.
- GSEA revealed an upregulation of the following pathway and radioresistance: PI3K/AKT/mTOR, epithelial mesenchymal transition, oxidative phosphorylation, TGF β , NF- κ B signalling, MAPK, notch and hypoxia signalling pathways.
- There was overlap between the upregulated pathways associated with radioresistance in the retrospective FFPE patient sample cohort and prospective PDO samples.
- Previous research has shown that the PI3K/AKT/mTOR pathway is a key oncogenic pathway associated with radiotherapy resistance in various cancers. Pathway inhibition leads to radiosensitivity in various cancers.
- Transcriptomic analyses revealed upregulation of this pathway at baseline and radiotherapy resistance across two independent datasets (FFPE samples and PDO samples).
- Using *in vitro* experiment models, within limitation PI3K/AKT/mTOR pathway activation through AKT phosphorylation was demonstrated up to 2 hours after

exposure to ionizing x-ray radiation. Dual PI3K and mTOR inhibitors effectively inhibited AKT phosphorylation, the main effector of this pathway.

- Dactolisib showed the greatest potential by radiosensitising HCT116 and two radioresistant PDO lines. More research is needed to evaluate whether this was a synergistic or additive effect.
- The differences between the responses to Apitolisib and Dactolisib and radiotherapy warrants further research particularly focusing on the role of ATR inhibition by dactolisib.
- The use of dual PI3K and mTOR inhibitors in LARC patients as an adjunct or alternative to standard chemotherapy alongside radiotherapy warrants further preclinical and clinical investigation.

References

1. Cancer Research UK. Bowel cancer incidence statistics. [internet]. [22nd Jan 2018]. Available from: <http://www.cancerresearchuk.org/health-professional/cancer-statistics/statistics-by-cancer-type/bowel-cancer/incidence>.
2. Kolligs FT. Diagnostics and epidemiology of colorectal cancer. *Visceral medicine*. 2016;32(3):158-64.
3. Cancer Research UK. Bowel cancer risk. [internet].2015 [cited 2019 January 16]. Available from: <https://www.cancerresearchuk.org/health-professional/cancer-statistics/statistics-by-cancer-type/bowel-cancer/risk-factors#heading-Zero>.
4. Cancer Research UK. Cancer mortality for common cancers. [internet].2016 [cited 2019 January 16]. Available from: <https://www.cancerresearchuk.org/health-professional/cancer-statistics/mortality/common-cancers-compared#heading-One>.
5. Leal J. Cancer costs the UK economy £15.8bn a year [internet].2012 [cited 2018 December 12]. Available from: <http://www.ox.ac.uk/news/2012-11-07-cancer-costs-uk-economy-%C2%A3158bn-year>.
6. Favoriti P, Carbone G, Greco M, Pirozzi F, Pirozzi REM, Corcione F. Worldwide burden of colorectal cancer: a review. *Updates in Surgery*. 2016;68(1):7-11.
7. Bishehsari F, Mahdavinia M, Vacca M, Malekzadeh R, Mariani-Costantini R. Epidemiological transition of colorectal cancer in developing countries: environmental factors, molecular pathways, and opportunities for prevention. *World Journal of Gastroenterology: WJG*. 2014;20(20):6055.
8. Center MM, Jemal A, Smith RA, Ward E. Worldwide variations in colorectal cancer. *CA: a cancer journal for clinicians*. 2009;59(6):366-78.
9. Arnold M, Sierra MS, Laversanne M, Soerjomataram I, Jemal A, Bray F. Global patterns and trends in colorectal cancer incidence and mortality. *Gut*. 2017;66(4):683-91.
10. Ouakrim DA, Pizot C, Boniol M, Malvezzi M, Boniol M, Negri E, et al. Trends in colorectal cancer mortality in Europe: retrospective analysis of the WHO mortality database. *BMJ*. 2015;351:h4970.
11. Center MM, Jemal A, Ward E. International trends in colorectal cancer incidence rates. *Cancer Epidemiology and Prevention Biomarkers*. 2009;18(6):1688-94.
12. Miller KD, Siegel RL, Lin CC, Mariotto AB, Kramer JL, Rowland JH, et al. Cancer treatment and survivorship statistics, 2016. *CA: a cancer journal for clinicians*. 2016;66(4):271-89.
13. Millan M, Merino S, Caro A, Feliu F, Escuder J, Francesch T. Treatment of colorectal cancer in the elderly. *World Journal of Gastrointestinal Oncology*. 2015;7(10):204.
14. Meyer JE, Narang T, Schnoll-Sussman FH, Pochapin MB, Christos PJ, Sherr DL. Increasing incidence of rectal cancer in patients aged younger than 40 years. *Cancer*. 2010;116(18):4354-9.
15. Vuik FE, Nieuwenburg SA, Bardou M, Lansdorp-Vogelaar I, Dinis-Ribeiro M, Bento MJ, et al. Increasing incidence of colorectal cancer in young adults in Europe over the last 25 years. *Gut*. 2019;gutjnl-2018-317592.
16. Jeon J, Du M, Schoen RE, Hoffmeister M, Newcomb PA, Berndt SI, et al. Determining risk of colorectal cancer and starting age of screening based on lifestyle, environmental, and genetic factors. *Gastroenterology*. 2018;154(8):2152-64. e19.
17. Jasperson KW, Tuohy TM, Neklason DW, Burt RW. Hereditary and familial colon cancer. *Gastroenterology*. 2010;138(6):2044-58.
18. Lin OS. Acquired risk factors for colorectal cancer. *Cancer Epidemiology*: Springer; 2009. p. 361-72.

19. Siegel RL, Miller KD, Fedewa SA, Ahnen DJ, Meester RG, Barzi A, et al. Colorectal cancer statistics, 2017. *CA: a cancer journal for clinicians*. 2017;67(3):177-93.
20. Broomé U, Bergquist A, editors. Primary sclerosing cholangitis, inflammatory bowel disease, and colon cancer. *Seminars in Liver Disease*; 2006: Copyright© 2006 by Thieme Medical Publishers, Inc., 333 Seventh Avenue, New
21. Wang R, Leong RW. Primary sclerosing cholangitis as an independent risk factor for colorectal cancer in the context of inflammatory bowel disease: a review of the literature. *World Journal of Gastroenterology*. 2014;20(27):8783.
22. Buell JF, Gross TG, Woodle ES. Malignancy after transplantation. *Transplantation*. 2005;80(2S):S254-S64.
23. Astin M, Griffin T, Neal RD, Rose P, Hamilton W. The diagnostic value of symptoms for colorectal cancer in primary care: a systematic review. *Br J Gen Pract*. 2011;61(586):e231-e43.
24. Stein DE, Clark S, Wexner S, Mahmoud N, Paulson EC, Atkin G, et al. *BMJ Best Practice*. [internet]. Jan 2018. [cited 2019 February 11]. Available from: <https://bestpractice.bmj.com/topics/en-gb/258/pdf/258.pdf>.
25. Acher P, Al-Mishlab T, Rahman M, Bates T. Iron-deficiency anaemia and delay in the diagnosis of colorectal cancer. *Colorectal Disease*. 2003;5(2):145-8.
26. National Collaborating Centre for Cancer. Colorectal cancer: the diagnosis and management of colorectal cancer 2011 [cited 2019 February 25]. Available from: <https://www.ncbi.nlm.nih.gov/books/NBK116639/>.
27. Hugen N, Van de Velde C, De Wilt J, Nagtegaal I. Metastatic pattern in colorectal cancer is strongly influenced by histological subtype. *Annals of Oncology*. 2014;25(3):651-7.
28. Baer C, Menon R, Bastawrous S, Bastawrous A. Emergency presentations of colorectal cancer. *Surgical Clinics of North America*. 2017;97(3):529-45.
29. Cuffy M, Abir F, Audisio RA, Longo WE. Colorectal cancer presenting as surgical emergencies. *Surgical Oncology*. 2004;13(2-3):149-57.
30. Larsen MB, Njor S, Ingeholm P, Andersen B. Effectiveness of colorectal cancer screening in detecting earlier-stage disease—a nationwide cohort study in Denmark. *Gastroenterology*. 2018;155(1):99-106.
31. U.S. National Institute of Health. National Cancer Institute. SEER Training Modules. Colorectal Cancer. [internet]. [cited 2019 January 22]. Available from: <https://training.seer.cancer.gov/colorectal/anatomy/>.
32. Stintzing S, Tejpar S, Gibbs P, Thiebach L, Lenz H-J. Understanding the role of primary tumour localisation in colorectal cancer treatment and outcomes. *European Journal of Cancer*. 2017;84:69-80.
33. Cancer Research UK. Distribution of Cases Diagnosed By Anatomical Site, UK [internet]. 2018 [cited 2019 January 23]. Available from: https://www.cancerresearchuk.org/sites/default/files/cstream-node/inc_anatomicalsites_bowel.pdf.
34. Hemminki K, Santi I, Weires M, Thomsen H, Sundquist J, Bermejo JLJ. Tumor location and patient characteristics of colon and rectal adenocarcinomas in relation to survival and TNM classes. *BMC Cancer*. 2010;10(1):688.
35. Matalon SA, Mamon HJ, Fuchs CS, Doyle LA, Tirumani SH, Ramaiya NH, et al. Anorectal cancer: critical anatomic and staging distinctions that affect use of radiation therapy. *Radiographics*. 2015;35(7):2090-107.
36. Compton CC, Byrd DR, Garcia-Aguilar J, Kurtzman SH, Olawaiye A, Washington MK. Colon and rectum. *AJCC cancer staging atlas*: Springer; 2012. p. 185-201.
37. Kenig J, Richter P. Definition of the rectum and level of the peritoneal reflection—still a matter of debate? *Videosurgery and Other Miniinvasive Techniques*. 2013;8(3):183.
38. U.S. National Institute of Health. National Cancer Institute. SEER Training Modules. Digestive System. [internet]. [cited 2019 February 25]. Available from: <https://training.seer.cancer.gov/anatomy/digestive/regions/intestine.html>.
39. American Joint Committee on Cancer. Colon and rectum. *AJCC cancer staging manual*: Springer; 2002. p. 113-23.

40. Salerno G, Sinnatamby C, Branagan G, Daniels I, Heald R, Moran B. Defining the rectum: surgically, radiologically and anatomically. *Colorectal Disease*. 2006;8:5-9.
41. McMullen TP, Easson AM, Cohen Z, Swallow CJ. The investigation of primary rectal cancer by surgeons: current pattern of practice. *Canadian journal of surgery*. 2005;48(1):19.
42. Heald R, Moran B, editors. *Embryology and anatomy of the rectum*. Seminars in Surgical Oncology; 1998: Wiley Online Library.
43. Nivatvongs S, Stern HS, Fryd DS. The length of the anal canal. *Diseases of the Colon & Rectum*. 1981;24(8):600-1.
44. Jorge JMN, Habr-Gama A, surgery r. *Anatomy and embryology of the colon, rectum, and anus*. The ASCRS textbook of colon. 2007:1-22.
45. Mik M, Berut M, Dziki L, Trzcinski R, Dziki A. Right-and left-sided colon cancer—clinical and pathological differences of the disease entity in one organ. *Archives of medical science: AMS*. 2017;13(1):157.
46. Ellis H, Mahadevan VJS. *Anatomy of the caecum, appendix and colon*. Surgery. 2014;32(4):155-8.
47. Benninger B. Splenomesenteric vein: formally recognising a clinically relevant section of the portal venous drainage system. *Folia morphologica*. 2013;72(1):63-6.
48. Looney W. Lymphatic distribution of the colon and rectum. *The American Journal of Surgery*. 1939;46(1):143-8.
49. Hasan RM, Mahdi BM. *New Concepts in the Management of Septic Perianal Conditions*. Academic Press; 2018. p. 1-7.
50. Ramirez PT, Frumovitz M, Abu-Rustum NR. *Principles of Gynecologic Oncology Surgery*. Principles of Gynecologic Oncology Surgery: Elsevier; 2018. p. 3-49.
51. Li F-y. Colorectal cancer, one entity or three. *Journal of Zhejiang University Science B*. 2009;10(3):219-29.
52. Riihimäki M, Hemminki A, Sundquist J, Hemminki K. Patterns of metastasis in colon and rectal cancer. *Scientific Reports*. 2016;6:29765.
53. McGraw S, Thakkar J, Mehta D. Inguinal lymph node metastasis of colon cancer. *Indian journal of medical paediatric oncology*. 2011;32(3):168.
54. Sakorafas GH, Zouros E, Peros G. Applied vascular anatomy of the colon and rectum: clinical implications for the surgical oncologist. *Surgical Oncology*. 2006;15(4):243-55.
55. Markowitz SD, Dawson DM, Willis J, Willson JK. Focus on colon cancer. *Cancer Cell*. 2002;1(3):233-6.
56. Jaladanki RN, Wang J-Y, editors. *Regulation of gastrointestinal mucosal growth*. Colloquium series on integrated systems physiology: from molecule to function; 2011: Morgan & Claypool Life Sciences.
57. Tanaka E, Noguchi T, Nagai K, Akashi Y, Kawahara K, Shimada T. Morphology of the epithelium of the lower rectum and the anal canal in the adult human. *Medical molecular morphology*. 2012;45(2):72-9.
58. Spit M, Koo B-K, Maurice MM. Tales from the crypt: intestinal niche signals in tissue renewal, plasticity and cancer. *Open biology*. 2018;8(9):180120.
59. Wedel T, Roblick U, Gleiß J, Schiedeck T, Bruch H-P, Kühnel W, et al. Organization of the enteric nervous system in the human colon demonstrated by wholemount immunohistochemistry with special reference to the submucous plexus. *Annals of Anatomy-Anatomischer Anzeiger*. 1999;181(4):327-37.
60. Klimstra D, Arnold R, Capella C, Bosman FT, Carneiro F, Hruban RH, Theise ND (eds): *WHO Classification of Tumours of the Digestive System*. Lyon, IARC. 2010.
61. Fleming M, Ravula S, Tatishchev SF, Wang HL. Colorectal carcinoma: Pathologic aspects. *Journal of Gastrointestinal Oncology*. 2012;3(3):153.
62. Salati SA, Al Kadi A. Anal cancer—a review. *International journal of health sciences*. 2012;6(2):206.
63. Hill M, Morson B, Bussey H. Aetiology of adenoma—carcinoma sequence in large bowel. *The Lancet*. 1978;311(8058):245-7.

64. Leslie A, Carey F, Pratt N, Steele R. The colorectal adenoma–carcinoma sequence. *British Journal of Surgery*. 2002;89(7):845-60.
65. De Leon MP, Di Gregorio C. Pathology of colorectal cancer. *Digestive Liver Disease*. 2001;33(4):372-88.
66. Rex DK, Ahnen DJ, Baron JA, Batts KP, Burke CA, Burt RW, et al. Serrated lesions of the colorectum: review and recommendations from an expert panel. *The American journal of gastroenterology*. 2012;107(9):1315.
67. Hermsen M, Postma C, Baak J, Weiss M, Rapallo A, Sciutto A, et al. Colorectal adenoma to carcinoma progression follows multiple pathways of chromosomal instability. *Gastroenterology*. 2002;123(4):1109-19.
68. Winawer SJ, Zauber AG, Ho MN, O'Brien MJ, Gottlieb LS, Sternberg SS, et al. Prevention of colorectal cancer by colonoscopic polypectomy. *New England Journal of Medicine*. 1993;329(27):1977-81.
69. Jørgensen O, Kronborg O, Fenger C. The Funen adenoma follow-up study: Incidence and death from colorectal carcinoma in an adenoma surveillance program. *Scandinavian journal of gastroenterology*. 1993;28(10):869-74.
70. Hoff G, Sauar J, Vatn M, Larsen S, Langmark F, Moen I, et al. Polypectomy of adenomas in the prevention of colorectal cancer: 10 years' follow-up of the Telemark Polyp Study IA prospective, controlled population study. *Scandinavian journal of gastroenterology*. 1996;31(10):1006-10.
71. Krishnamurthy N, Kurzrock R. Targeting the Wnt/beta-catenin pathway in cancer: Update on effectors and inhibitors. *Cancer treatment reviews*. 2018;62:50-60.
72. Fodde R. The APC gene in colorectal cancer. *European journal of cancer*. 2002;38(7):867-71.
73. Nguyen HT, Duong HQ. The molecular characteristics of colorectal cancer: Implications for diagnosis and therapy. *Oncology letters*. 2018;16(1):9-18.
74. Armelao F, de Pretis G. Familial colorectal cancer: a review. *World journal of gastroenterology: WJG*. 2014;20(28):9292.
75. Lichtenstein P, Holm NV, Verkasalo PK, Iliadou A, Kaprio J, Koskenvuo M, et al. Environmental and heritable factors in the causation of cancer—analyses of cohorts of twins from Sweden, Denmark, and Finland. *New England journal of medicine*. 2000;343(2):78-85.
76. Calvert PM, Frucht H. The genetics of colorectal cancer. *Annals of internal medicine*. 2002;137(7):603-12.
77. Pino MS, Chung DC. The chromosomal instability pathway in colon cancer. *Gastroenterology*. 2010;138(6):2059-72.
78. Grady WM, Carethers JM. Genomic and epigenetic instability in colorectal cancer pathogenesis. *Gastroenterology*. 2008;135(4):1079-99.
79. Vilar E, Gruber SB. Microsatellite instability in colorectal cancer—the stable evidence. *Nature reviews Clinical oncology*. 2010;7(3):153.
80. Pardal R, Clarke MF, Morrison SJ. Applying the principles of stem-cell biology to cancer. *Nature Reviews Cancer*. 2003;3(12):895-902.
81. Chen W, Swanson BJ, Frankel WL. Molecular genetics of microsatellite-unstable colorectal cancer for pathologists. *Diagnostic pathology*. 2017;12(1):1-12.
82. Ellegren H. Microsatellites: simple sequences with complex evolution. *Nature reviews genetics*. 2004;5(6):435-45.
83. Harfe BD, Jinks-Robertson S. DNA mismatch repair and genetic instability. *Annual review of genetics*. 2000;34(1):359-99.
84. Iacopetta B, Li W, Grieu F, Ruzskiewicz A, Kawakami K. BRAF mutation and gene methylation frequencies of colorectal tumours with microsatellite instability increase markedly with patient age. *Gut*. 2006;55(8):1213-.
85. Wright C, Dent O, Newland R, Barker M, Chapuis P, Bokey E, et al. Low level microsatellite instability may be associated with reduced cancer specific survival in sporadic stage C colorectal carcinoma. *Gut*. 2005;54(1):103-8.

86. Boland CR, Goel A. Microsatellite instability in colorectal cancer. *Gastroenterology*. 2010;138(6):2073-87. e3.
87. Karimi M, Von Salomé J, Aravidis C, Silander G, Askmalm MS, Henriksson I, et al. A retrospective study of extracolonic, non-endometrial cancer in Swedish Lynch syndrome families. *Hereditary cancer in clinical practice*. 2018;16(1):16.
88. Kawakami H, Zaanan A, Sinicrope FA. Microsatellite instability testing and its role in the management of colorectal cancer. *Current treatment options in oncology*. 2015;16(7):30.
89. Tutlewska K, Lubinski J, Kurzawski G. Germline deletions in the EPCAM gene as a cause of Lynch syndrome—literature review. *Hereditary cancer in clinical practice*. 2013;11(1):9.
90. Wang L, Cunningham JM, Winters JL, Guenther JC, French AJ, Boardman LA, et al. BRAF mutations in colon cancer are not likely attributable to defective DNA mismatch repair. *Cancer research*. 2003;63(17):5209-12.
91. The National Institute for Health and Care Excellence (NICE). Molecular testing strategies for Lynch syndrome in people with colorectal cancer - Diagnostics guidance [DG27] [internet]. 2017 [cited 2020 April 23]. Available from: <https://www.nice.org.uk/guidance/dg27/chapter/1-Recommendations>.
92. Munemitsu S, Albert I, Souza B, Rubinfeld B, Polakis P. Regulation of intracellular beta-catenin levels by the adenomatous polyposis coli (APC) tumor-suppressor protein. *Proceedings of the National Academy of Sciences*. 1995;92(7):3046-50.
93. Miyaki M, Iijima T, Kimura J, Yasuno M, Mori T, Hayashi Y, et al. Frequent mutation of β -catenin and APC genes in primary colorectal tumors from patients with hereditary nonpolyposis colorectal cancer. *Cancer research*. 1999;59(18):4506-9.
94. Miyaki M, Konishi M, Kikuchi-Yanoshita R, Enomoto M, Igari T, Tanaka K, et al. Characteristics of somatic mutation of the adenomatous polyposis coli gene in colorectal tumors. *Cancer research*. 1994;54(11):3011-20.
95. Leoz ML, Carballal S, Moreira L, Ocaña T, Balaguer F. The genetic basis of familial adenomatous polyposis and its implications for clinical practice and risk management. *The application of clinical genetics*. 2015;8:95.
96. Scott RJ. Familial adenomatous polyposis (FAP) and other polyposis syndromes. *Hereditary Cancer in Clinical Practice*. 2003;1(1):19.
97. Anaya DA, Chang GJ, Rodriguez-Bigas MA. Extracolonic manifestations of hereditary colorectal cancer syndromes. *Clinics in colon and rectal surgery*. 2008;21(04):263-72.
98. Groen EJ, Roos A, Muntinghe FL, Enting RH, de Vries J, Kleibeuker JH, et al. Extra-intestinal manifestations of familial adenomatous polyposis. *Annals of surgical oncology*. 2008;15(9):2439-50.
99. Lamlum H, Ilyas M, Rowan A, Clark S, Johnson V, Bell J, et al. The type of somatic mutation at APC in familial adenomatous polyposis is determined by the site of the germline mutation: a new facet to Knudson's' two-hit' hypothesis. *Nature medicine*. 1999;5(9):1071-5.
100. Fearnhead NS, Britton MP, Bodmer WF. The abc of apc. *Human molecular genetics*. 2001;10(7):721-33.
101. Armaghany T, Wilson JD, Chu Q, Mills G. Genetic alterations in colorectal cancer. *Gastrointestinal cancer research: GCR*. 2012;5(1):19.
102. Mori Y, Nagse H, Ando H, Horii A, Ichii S, Nakatsuru S, et al. Somatic mutations of the APC gene in colorectal tumors: mutation cluster region in the APC gene. *Human molecular genetics*. 1992;1(4):229-33.
103. Hiltunen MO, Alhonen L, Koistinaho J, Myöhänen S, Pääkkönen M, Marin S, et al. Hypermethylation of the APC (adenomatous polyposis coli) gene promoter region in human colorectal carcinoma. *International journal of cancer*. 1997;70(6):644-8.
104. Sampson JR, Jones S, Dolwani S, Cheadle JP. MutYH (MYH) and colorectal cancer. Portland Press Ltd.; 2005.
105. Krokan HE, Bjørås M. Base excision repair. *Cold Spring Harbor perspectives in biology*. 2013;5(4):a012583.

106. Kuno T, Matsubara N, Tsuda S, Kobayashi M, Hamanaka M, Yamagishi D, et al. Alterations of the base excision repair gene MUTYH in sporadic colorectal cancer. *Oncology reports*. 2012;28(2):473-80.
107. Isobe M, Emanuel B, Givol D, Oren M, Croce CM. Localization of gene for human p53 tumour antigen to band 17p13. *Nature*. 1986;320(6057):84-5.
108. Agarwal ML, Agarwal A, Taylor WR, Stark GR. p53 controls both the G2/M and the G1 cell cycle checkpoints and mediates reversible growth arrest in human fibroblasts. *Proceedings of the National Academy of Sciences*. 1995;92(18):8493-7.
109. Weinberg RL, Veprintsev DB, Bycroft M, Fersht AR. Comparative binding of p53 to its promoter and DNA recognition elements. *Journal of molecular biology*. 2005;348(3):589-96.
110. Harper JW, Adami GR, Wei N, Keyomarsi K, Elledge SJ. The p21 Cdk-interacting protein Cip1 is a potent inhibitor of G1 cyclin-dependent kinases. *Cell*. 1993;75(4):805-16.
111. Jänicke R, Sohn D, Schulze-Osthoff K. The dark side of a tumor suppressor: anti-apoptotic p53. *Cell Death & Differentiation*. 2008;15(6):959-76.
112. Van Den Berg F, Tigges A, Schipper M, Den Hartog-Jager F, Kroes W, Walboomers J. Expression of the nuclear oncogene p53 in colon tumours. *The Journal of pathology*. 1989;157(3):193-9.
113. Crawford L, Pim D, Lamb P. The cellular protein p53 in human tumours. *Molecular biology & medicine*. 1984;2(4):261.
114. Munro A, Lain S, Lane D. P53 abnormalities and outcomes in colorectal cancer: a systematic review. *British journal of cancer*. 2005;92(3):434-44.
115. Knijn N, Mekenkamp L, Klomp M, Vink-Börger M, Tol J, Teerenstra S, et al. KRAS mutation analysis: a comparison between primary tumours and matched liver metastases in 305 colorectal cancer patients. *British journal of cancer*. 2011;104(6):1020-6.
116. Timar J, Kashofer K. Molecular epidemiology and diagnostics of KRAS mutations in human cancer. *Cancer and Metastasis Reviews*. 2020:1-10.
117. Bamford S, Dawson E, Forbes S, Clements J, Pettett R, Dogan A, et al. The COSMIC (Catalogue of Somatic Mutations in Cancer) database and website. *British journal of cancer*. 2004;91(2):355-8.
118. Mendoza MC, Er EE, Blenis J. The Ras-ERK and PI3K-mTOR pathways: cross-talk and compensation. *Trends in biochemical sciences*. 2011;36(6):320-8.
119. Arrington AK, Heinrich EL, Lee W, Duldulao M, Patel S, Sanchez J, et al. Prognostic and predictive roles of KRAS mutation in colorectal cancer. *International journal of molecular sciences*. 2012;13(10):12153-68.
120. Han C-B, Li F, Ma J-T, Zou H-W. Concordant KRAS mutations in primary and metastatic colorectal cancer tissue specimens: a meta-analysis and systematic review. *Cancer investigation*. 2012;30(10):741-7.
121. Therkildsen C, Bergmann TK, Henrichsen-Schnack T, Ladelund S, Nilbert M. The predictive value of KRAS, NRAS, BRAF, PIK3CA and PTEN for anti-EGFR treatment in metastatic colorectal cancer: A systematic review and meta-analysis. *Acta oncologica*. 2014;53(7):852-64.
122. Lievre A, Bachet J-B, Le Corre D, Boige V, Landi B, Emile J-F, et al. KRAS mutation status is predictive of response to cetuximab therapy in colorectal cancer. *Cancer research*. 2006;66(8):3992-5.
123. Karakas B, Bachman K, Park B. Mutation of the PIK3CA oncogene in human cancers. *British journal of cancer*. 2006;94(4):455-9.
124. Samuels Y, Wang Z, Bardelli A, Silliman N, Ptak J, Szabo S, et al. High frequency of mutations of the PIK3CA gene in human cancers. *Science*. 2004.
125. Nosho K, Kawasaki T, Longtine JA, Fuchs CS, Ohnishi M, Suemoto Y, et al. PIK3CA mutation in colorectal cancer: relationship with genetic and epigenetic alterations. *Neoplasia*. 2008;10(6):534-41.
126. Liao X, Morikawa T, Lochhead P, Imamura Y, Kuchiba A, Yamauchi M, et al. Prognostic role of PIK3CA mutation in colorectal cancer: cohort study and literature review. *Clinical cancer research*. 2012;18(8):2257-68.

127. Wang Q, Shi Y-I, Zhou K, Wang L-I, Yan Z-x, Liu Y-I, et al. PIK3CA mutations confer resistance to first-line chemotherapy in colorectal cancer. *Cell death & disease*. 2018;9(7):1-11.
128. Sartore-Bianchi A, Martini M, Molinari F, Veronese S, Nichelatti M, Artale S, et al. PIK3CA mutations in colorectal cancer are associated with clinical resistance to EGFR-targeted monoclonal antibodies. *Cancer research*. 2009;69(5):1851-7.
129. He Y, Van't Veer LJ, Mikolajewska-Hanclich I, van Velthuysen M-LF, Zeestraten EC, Nagtegaal ID, et al. PIK3CA mutations predict local recurrences in rectal cancer patients. *Clinical cancer research*. 2009;15(22):6956-62.
130. Zhang J, Roberts TM, Shivdasani RA. Targeting PI3K signaling as a therapeutic approach for colorectal cancer. *Gastroenterology*. 2011;141(1):50-61.
131. Shiau C, Tsao M-S. *Molecular Testing in Lung Cancer*. *Diagnostic Molecular Pathology*: Elsevier; 2017. p. 287-303.
132. Davies H, Bignell GR, Cox C, Stephens P, Edkins S, Clegg S, et al. Mutations of the BRAF gene in human cancer. *Nature*. 2002;417(6892):949-54.
133. Richtig G, Hoeller C, Kashofer K, Aigelsreiter A, Heinemann A, Kwong L, et al. Beyond the BRAFV 600E hotspot: biology and clinical implications of rare BRAF gene mutations in melanoma patients. *British Journal of Dermatology*. 2017;177(4):936-44.
134. Seligmann JF, Fisher D, Smith CG, Richman SD, Elliott F, Brown S, et al. Investigating the poor outcomes of BRAF-mutant advanced colorectal cancer: analysis from 2530 patients in randomised clinical trials. *Annals of Oncology*. 2017;28(3):562-8.
135. Deng G, Bell I, Crawley S, Gum J, Terdiman JP, Allen BA, et al. BRAF mutation is frequently present in sporadic colorectal cancer with methylated hMLH1, but not in hereditary nonpolyposis colorectal cancer. *Clinical Cancer Research*. 2004;10(1):191-5.
136. Monahan KJ, Bradshaw N, Dolwani S, Desouza B, Dunlop MG, East JE, et al. Guidelines for the management of hereditary colorectal cancer from the British society of gastroenterology (BSG)/Association of coloproctology of great Britain and Ireland (ACPGBI)/United Kingdom cancer genetics group (UKCGG). *Gut*. 2020;69(3):411-44.
137. Wieduwilt M, Moasser M. The epidermal growth factor receptor family: biology driving targeted therapeutics. *Cellular and Molecular Life Sciences*. 2008;65(10):1566-84.
138. Seo AN, Kwak Y, Kim D-W, Kang S-B, Choe G, Kim WH, et al. HER2 status in colorectal cancer: its clinical significance and the relationship between HER2 gene amplification and expression. *PloS one*. 2014;9(5):e98528.
139. Ross JS, Fakih M, Ali SM, Elvin JA, Schrock AB, Suh J, et al. Targeting HER2 in colorectal cancer: The landscape of amplification and short variant mutations in ERBB2 and ERBB3. *Cancer*. 2018;124(7):1358-73.
140. Bertucci F, Borie N, Ginestier C, Groulet A, Charafe-Jauffret E, Adélaïde J, et al. Identification and validation of an ERBB2 gene expression signature in breast cancers. *Oncogene*. 2004;23(14):2564-75.
141. Cooke T, Reeves J, Lanigan A, Stanton P. HER2 as a prognostic and predictive marker for breast cancer. *Annals of oncology*. 2001;12:S23-S8.
142. Essapen S, Thomas H, Green M, De Vries C, Cook MG, Marks C, et al. The expression and prognostic significance of HER-2 in colorectal cancer and its relationship with clinicopathological parameters. *International journal of oncology*. 2004;24(2):241-8.
143. Park DI, Kang MS, Oh SJ, Kim HJ, Cho YK, Sohn CI, et al. HER-2/neu overexpression is an independent prognostic factor in colorectal cancer. *International journal of colorectal disease*. 2007;22(5):491.
144. Takahashi N, Iwasa S, Taniguchi H, Sasaki Y, Shoji H, Honma Y, et al. Prognostic role of ERBB2, MET and VEGFA expression in metastatic colorectal cancer patients treated with anti-EGFR antibodies. *British journal of cancer*. 2016;114(9):1003-11.
145. Loree JM, Bailey AM, Johnson AM, Yu Y, Wu W, Bristow CA, et al. Molecular landscape of ERBB2/ERBB3 mutated colorectal cancer. *JNCI: Journal of the National Cancer Institute*. 2018;110(12):1409-17.
146. Sartore-Bianchi A, Trusolino L, Martino C, Bencardino K, Lonardi S, Bergamo F, et al. Dual-targeted therapy with trastuzumab and lapatinib in treatment-refractory, KRAS

codon 12/13 wild-type, HER2-positive metastatic colorectal cancer (HERACLES): a proof-of-concept, multicentre, open-label, phase 2 trial. *The Lancet Oncology*. 2016;17(6):738-46.

147. Vaiopoulos AG, Athanasoula KC, Papavassiliou AG. Epigenetic modifications in colorectal cancer: molecular insights and therapeutic challenges. *Biochimica et Biophysica Acta (BBA)-Molecular Basis of Disease*. 2014;1842(7):971-80.

148. Juo Y, Johnston F, Zhang D, Juo H, Wang H, Pappou E, et al. Prognostic value of CpG island methylator phenotype among colorectal cancer patients: a systematic review and meta-analysis. *Annals of Oncology*. 2014;25(12):2314-27.

149. Kokelaar R, Jones H, Beynon J, Evans M, Harris D. Meta-analysis of the prognostic value of CpG island methylator phenotype in rectal cancer. *International journal of colorectal disease*. 2018;33(8):995-1000.

150. Brookes AJ. The essence of SNPs. *Gene*. 1999;234(2):177-86.

151. Wen J, Xu Q, Yuan Y. Single nucleotide polymorphisms and sporadic colorectal cancer susceptibility: a field synopsis and meta-analysis. *Cancer cell international*. 2018;18(1):155.

152. Horvat M, Potočnik U, Repnik K, Kavalar R, Štabuc B. Single nucleotide polymorphisms as prognostic and predictive factors of adjuvant chemotherapy in colorectal cancer of stages I and II. *Gastroenterology research and practice*. 2016;2016.

153. Paez D, Gerger A, Zhang W, Yang D, Labonte M, Benhanim L, et al. Association of common gene variants in the WNT/ β -catenin pathway with colon cancer recurrence. *The pharmacogenomics journal*. 2014;14(2):142-50.

154. Absenger G, Benhaim L, Szkandera J, Zhang W, Yang D, Labonte M, et al. The cyclin D1 (CCND1) rs9344 G> A polymorphism predicts clinical outcome in colon cancer patients treated with adjuvant 5-FU-based chemotherapy. *The pharmacogenomics journal*. 2014;14(2):130-4.

155. Deenen MJ, Tol J, Burylo AM, Doodeman VD, De Boer A, Vincent A, et al. Relationship between single nucleotide polymorphisms and haplotypes in DPYD and toxicity and efficacy of capecitabine in advanced colorectal cancer. *Clinical Cancer Research*. 2011;17(10):3455-68.

156. Seck K, Riemer S, Kates R, Ullrich T, Lutz V, Harbeck N, et al. Analysis of the DPYD gene implicated in 5-fluorouracil catabolism in a cohort of Caucasian individuals. *Clinical cancer research*. 2005;11(16):5886-92.

157. Henricks LM, Lunenburg CA, Meulendijks D, Gelderblom H, Cats A, Swen JJ, et al. Translating DPYD genotype into DPD phenotype: using the DPYD gene activity score. *Pharmacogenomics*. 2015;16(11):1275-84.

158. Ma Y, Zhang P, Yang J, Liu Z, Yang Z, Qin H. Candidate microRNA biomarkers in human colorectal cancer: systematic review profiling studies and experimental validation. *International journal of cancer*. 2012;130(9):2077-87.

159. Mármol I, Sánchez-de-Diego C, Pradilla Dieste A, Cerrada E, Rodríguez Yoldi MJ. Colorectal carcinoma: a general overview and future perspectives in colorectal cancer. *International journal of molecular sciences*. 2017;18(1):197.

160. Carter JV, Galbraith NJ, Yang D, Burton JF, Walker SP, Galandiuk S. Blood-based microRNAs as biomarkers for the diagnosis of colorectal cancer: a systematic review and meta-analysis. *British journal of cancer*. 2017;116(6):762-74.

161. Guinney J, Dienstmann R, Wang X, De Reyniès A, Schlicker A, Sonesson C, et al. The consensus molecular subtypes of colorectal cancer. *Nature medicine*. 2015;21(11):1350-6.

162. Isella C, Brundu F, Bellomo SE, Galimi F, Zanella E, Porporato R, et al. Selective analysis of cancer-cell intrinsic transcriptional traits defines novel clinically relevant subtypes of colorectal cancer. *Nature communications*. 2017;8(1):1-16.

163. Flahaut M, Meier R, Coulon A, Nardou K, Niggli F, Martinet D, et al. The Wnt receptor FZD1 mediates chemoresistance in neuroblastoma through activation of the Wnt/ β -catenin pathway. *Oncogene*. 2009;28(23):2245-56.

164. Eisenmann D. Wnt signaling. *WormBook: the online review of C elegans biology*[PubMed]2005. p. pp. 1–17.

165. Holcombe R, Marsh J, Waterman M, Lin F, Milovanovic T, Truong T. Expression of Wnt ligands and Frizzled receptors in colonic mucosa and in colon carcinoma. *Molecular Pathology*. 2002;55(4):220.
166. Woodward WA, Chen MS, Behbod F, Alfaro MP, Buchholz TA, Rosen JM. WNT/ β -catenin mediates radiation resistance of mouse mammary progenitor cells. *Proceedings of the National Academy of Sciences*. 2007;104(2):618-23.
167. Fang JY, Richardson BC. The MAPK signalling pathways and colorectal cancer. *The lancet oncology*. 2005;6(5):322-7.
168. Shen L, Toyota M, Kondo Y, Lin E, Zhang L, Guo Y, et al. Integrated genetic and epigenetic analysis identifies three different subclasses of colon cancer. *Proceedings of the National Academy of Sciences*. 2007;104(47):18654-9.
169. Berg M, Soreide K. EGFR and downstream genetic alterations in KRAS/BRAF and PI3K/AKT pathways in colorectal cancer—implications for targeted therapy. *Discovery medicine*. 2012;14(76):207-14.
170. Lewis TS, Shapiro PS, Ahn NG. Signal transduction through MAP kinase cascades. *Advances in cancer research*. 74: Elsevier; 1998. p. 49-139.
171. Yen A, Roberson MS, Varvayanis S, Lee AT. Retinoic acid induced mitogen-activated protein (MAP)/extracellular signal-regulated kinase (ERK) kinase-dependent MAP kinase activation needed to elicit HL-60 cell differentiation and growth arrest. *Cancer research*. 1998;58(14):3163-72.
172. Kirstein MM, Lange A, Prenzler A, Manns MP, Kubicka S, Vogel A. Targeted therapies in metastatic colorectal cancer: a systematic review and assessment of currently available data. *The oncologist*. 2014;19(11):1156.
173. Chen Y-H, Wei M-F, Wang C-W, Lee H-W, Pan S-L, Gao M, et al. Dual phosphoinositide 3-kinase/mammalian target of rapamycin inhibitor is an effective radiosensitizer for colorectal cancer. *Cancer Letters*. 2015;357(2):582-90.
174. Li D, Lu Z, Xu Z, Ji J, Zheng Z, Lin S, et al. Spironolactone promotes autophagy via inhibiting PI3K/AKT/mTOR signalling pathway and reduce adhesive capacity damage in podocytes under mechanical stress. *Bioscience Reports*. 2016;36(4):e00355.
175. Laplante M, Sabatini DM. mTOR signaling at a glance. *Journal of Cell Science*. 2009;122(20):3589-94.
176. Osaki M, Oshimura Ma, Ito H. PI3K-Akt pathway: its functions and alterations in human cancer. *Apoptosis*. 2004;9(6):667-76.
177. LoRusso PM. Inhibition of the PI3K/AKT/mTOR pathway in solid tumors. *Journal of clinical oncology*. 2016;34(31):3803.
178. Goel A, Arnold CN, Niedzwiecki D, Carethers JM, Dowell JM, Wasserman L, et al. Frequent inactivation of PTEN by promoter hypermethylation in microsatellite instability-high sporadic colorectal cancers. *Cancer research*. 2004;64(9):3014-21.
179. Yu C-C, Hung S-K, Lin H-Y, Chiou W-Y, Lee M-S, Liao H-F, et al. Targeting the PI3K/AKT/mTOR signaling pathway as an effectively radiosensitizing strategy for treating human oral squamous cell carcinoma in vitro and in vivo. *Oncotarget*. 2017;8(40):68641.
180. Toulany M, Rodemann HP. Potential of Akt mediated DNA repair in radioresistance of solid tumors overexpressing erbB-PI3K-Akt pathway. *Translational Cancer Research*. 2013;2(3):190-202.
181. Holler M, Grottke A, Mueck K, Manes J, Jücker M, Rodemann HP, et al. Dual targeting of Akt and mTORC1 impairs repair of DNA double-strand breaks and increases radiation sensitivity of human tumor cells. *PLoS One*. 2016;11(5):e0154745.
182. Burris HA. Overcoming acquired resistance to anticancer therapy: focus on the PI3K/AKT/mTOR pathway. *Cancer chemotherapy and pharmacology*. 2013;71(4):829-42.
183. Porta C, Paglino C, Mosca A. Targeting PI3K/Akt/mTOR signaling in cancer. *Frontiers in oncology*. 2014;4:64.
184. Wanigasooriya K, Tyler R, Barros-Silva JD, Sinha Y, Ismail T, Beggs AD. Radiosensitising Cancer Using Phosphatidylinositol-3-Kinase (PI3K), Protein Kinase B (AKT) or Mammalian Target of Rapamycin (mTOR) Inhibitors. *Cancers*. 2020;12(5):1278.

185. Xu Y, Pasche B. TGF- β signaling alterations and susceptibility to colorectal cancer. *Human molecular genetics*. 2007;16(R1):R14-R20.
186. Itatani Y, Kawada K, Sakai Y. Transforming growth factor- β signaling pathway in colorectal cancer and its tumor microenvironment. *International journal of molecular sciences*. 2019;20(23):5822.
187. Huang C-Y, Chung C-L, Hu T-H, Chen J-J, Liu P-F, Chen C-L. Recent progress in TGF- β inhibitors for cancer therapy. *Biomedicine & Pharmacotherapy*. 2021;134:111046.
188. Huynh LK, Hipolito CJ, Ten Dijke P. A Perspective on the Development of TGF- β Inhibitors for Cancer Treatment. *Biomolecules*. 2019;9(11):743.
189. Pagès F, Mlecnik B, Marliot F, Bindea G, Ou F-S, Bifulco C, et al. International validation of the consensus Immunoscore for the classification of colon cancer: a prognostic and accuracy study. *The Lancet*. 2018;391(10135):2128-39.
190. Ogino S, Giannakis M. Immunoscore for (colorectal) cancer precision medicine. *The Lancet*. 2018;391(10135):2084-6.
191. Zhang R, Qi F, Zhao F, Li G, Shao S, Zhang X, et al. Cancer-associated fibroblasts enhance tumor-associated macrophages enrichment and suppress NK cells function in colorectal cancer. *Cell death & disease*. 2019;10(4):1-14.
192. Herrera M, Herrera A, Domínguez G, Silva J, García V, García JM, et al. Cancer-associated fibroblast and M2 macrophage markers together predict outcome in colorectal cancer patients. *Cancer science*. 2013;104(4):437-44.
193. Peña C, Céspedes MV, Lindh MB, Kiflemariam S, Mezheyeuski A, Edqvist P-H, et al. STC1 expression by cancer-associated fibroblasts drives metastasis of colorectal cancer. *Cancer research*. 2013;73(4):1287-97.
194. Goswami KK, Ghosh T, Ghosh S, Sarkar M, Bose A, Baral R. Tumor promoting role of anti-tumor macrophages in tumor microenvironment. *Cellular immunology*. 2017;316:1-10.
195. Yin Y, Yao S, Hu Y, Feng Y, Li M, Bian Z, et al. The immune-microenvironment confers chemoresistance of colorectal cancer through macrophage-derived IL6. *Clinical Cancer Research*. 2017;23(23):7375-87.
196. Ternes D, Karta J, Tsenkova M, Wilmes P, Haan S, Letellier E. Microbiome in Colorectal Cancer: How to Get from Meta-omics to Mechanism? *Trends in Microbiology*. 2020;28(5):401-23.
197. Ahn J, Sinha R, Pei Z, Dominianni C, Wu J, Shi J, et al. Human gut microbiome and risk for colorectal cancer. *Journal of the National Cancer Institute*. 2013;105(24):1907-11.
198. Sánchez-Alcoholado L, Ramos-Molina B, Otero A, Laborda-Illanes A, Ordóñez R, Medina JA, et al. The Role of the Gut Microbiome in Colorectal Cancer Development and Therapy Response. *Cancers*. 2020;12(6):1406.
199. Cunningham C, Leong K, Clark S, Plumb A, Taylor S, Geh I, et al. Association of Coloproctology of Great Britain & Ireland (ACPGBI): Guidelines for the Management of Cancer of the Colon, Rectum and Anus (2017)—Diagnosis, Investigations and Screening. *Colorectal Disease*. 2017;19(Suppl S1):9-17.
200. Richter JM, Campbell EJ, Chung DC. Interval colorectal cancer after colonoscopy. *Clinical colorectal cancer*. 2015;14(1):46-51.
201. Than M, Witherspoon J, Shami J, Patil P, Saklani A. Diagnostic miss rate for colorectal cancer: an audit. *Annals of gastroenterology: quarterly publication of the Hellenic Society of Gastroenterology*. 2015;28(1):94.
202. Kuipers EJ, Rösch T, Bretthauer M. Colorectal cancer screening—optimizing current strategies and new directions. *Nature reviews Clinical oncology*. 2013;10(3):130.
203. McKigney N, Coyne PE. *Bowel cancer screening*. Surgery (Oxford). 2019.
204. Vasilyev S, Smirnova E, Popov D, Semenov A, Eklund C, Hendolin P, et al. A new-generation fecal immunochemical test (FIT) is superior to quaiac-based test in detecting colorectal neoplasia among colonoscopy referral patients. *Anticancer Research*. 2015;35(5):2873-80.
205. UK Government. *Bowel Cancer Screening Programme Overview*. [internet].2018 [cited 2020 April 14]. Available from: <https://www.gov.uk/guidance/bowel-cancer-screening-programme-overview>.

206. Haq AI, Schneeweiss J, Kalsi V, Arya M. The Dukes staging system: a cornerstone in the clinical management of colorectal cancer. *The Lancet Oncology*. 2009;10(11):1128.
207. Brown G, Rimmer M, Williams S. Colon, rectum and anal cancer. In: Nicholson T (ed). *Recommendations for cross-sectional imaging in cancer management*. London: The Royal College of Radiologists; 2014 [cited 2019 February 26]. Available from: https://www.rcr.ac.uk/system/files/publication/field_publication_files/BFCR%2814%292_12_Colon.pdf.
208. Gollins S, Moran B, Adams R, Cunningham C, Bach S, Myint AS, et al. Association of Coloproctology of Great Britain & Ireland (ACPGBI): Guidelines for the Management of Cancer of the Colon, Rectum and Anus (2017)–Multidisciplinary Management. *Colorectal Disease*. 2017;19(S1):37-66.
209. Ahuja NK, Sauer BG, Wang AY, White GE, Zabolotsky A, Koons A, et al. Performance of endoscopic ultrasound in staging rectal adenocarcinoma appropriate for primary surgical resection. *Clinical Gastroenterology and Hepatology*. 2015;13(2):339-44.
210. MacDermid E, Hooton G, MacDonald M, McKay G, Grose D, Mohammed N, et al. Improving patient survival with the colorectal cancer multi-disciplinary team. *Colorectal Disease*. 2009;11(3):291-5.
211. Li M, Li J, Zhao A, Gu J. Colorectal cancer or colon and rectal cancer? *Oncology*. 2007;73(1-2):52-7.
212. Paschke S, Jafarov S, Staib L, Kreuzer E-D, Maulbecker-Armstrong C, Roitman M, et al. Are colon and rectal cancer two different tumor entities? A proposal to abandon the term colorectal cancer. *International journal of molecular sciences*. 2018;19(9):2577.
213. Cancer Genome Atlas Network. Comprehensive molecular characterization of human colon and rectal cancer. *Nature*. 2012;487(7407):330.
214. Moran B, Karandikar S, Geh I. Association of Coloproctology of Great Britain & Ireland (ACPGBI): Guidelines for the Management of Cancer of the Colon, Rectum and Anus (2017)-Introduction. *Colorectal Disease*. 2017;19(S1):6-8.
215. Seymour MT, Morton D, Investigators IFT. FOxTROT: an international randomised controlled trial in 1052 patients (pts) evaluating neoadjuvant chemotherapy (NAC) for colon cancer. *American Society of Clinical Oncology*; 2019.
216. Kokelaar R, Evans M, Davies M, Harris D, Beynon J. Locally advanced rectal cancer: management challenges. *OncoTargets and therapy*. 2016;9:6265.
217. Glynne-Jones R, Wyrwicz L, Tiret E, Brown G, Rödel C, Cervantes A, et al. Rectal cancer: ESMO Clinical Practice Guidelines for diagnosis, treatment and follow-up. *Annals of Oncology*. 2017;28:iv22-iv40.
218. Dewdney A, Cunningham D, Chau I. Selecting patients with locally advanced rectal cancer for neoadjuvant treatment strategies. *The Oncologist*. 2013;18(7):833-42.
219. Glynne-Jones R, Kronfli M. Locally advanced rectal cancer: a comparison of management strategies. *Drugs*. 2011;71(9):1153-77.
220. Sauer R, Becker H, Hohenberger W, Rödel C, Wittekind C, Fietkau R, et al. Preoperative versus postoperative chemoradiotherapy for rectal cancer. *New England Journal of Medicine*. 2004;351(17):1731-40.
221. Wasserberg N. Interval to surgery after neoadjuvant treatment for colorectal cancer. *World Journal of Gastroenterology: WJG*. 2014;20(15):4256.
222. Nacion AJD, Park YY, Kim NK. Contemporary management of locally advanced rectal cancer: Resolving issues, controversies and shifting paradigms. *Chinese Journal of Cancer Research*. 2018;30(1):131.
223. Craven I, Crellin A, Cooper R, Melcher A, Byrne P, Sebag-Montefiore D. Preoperative radiotherapy combined with 5 days per week capecitabine chemotherapy in locally advanced rectal cancer. *British journal of cancer*. 2007;97(10):1333.
224. Bosset J-F, Collette L, Calais G, Mineur L, Maingon P, Radosevich-Jelic L, et al. Chemotherapy with preoperative radiotherapy in rectal cancer. *New England Journal of Medicine*. 2006;355(11):1114-23.
225. Aghili M, Sotoudeh S, Ghalehtaki R, Babaei M, Farazmand B, Fazeli M-S, et al. Preoperative short course radiotherapy with concurrent and consolidation chemotherapies

followed by delayed surgery in locally advanced rectal cancer: preliminary results. *Radiation Oncology Journal*. 2018;36(1):17.

226. Pettersson D, Löhrinc E, Holm T, Iversen H, Cedermark B, Glimelius B, et al. Tumour regression in the randomized Stockholm III Trial of radiotherapy regimens for rectal cancer. *British Journal of Surgery*. 2015;102(8):972-8.

227. Bujko K, Pietrzak L, Partycki M, Szczepkowski M, Wyrwicz L, Rupiński M, et al. The feasibility of short-course radiotherapy in a watch-and-wait policy for rectal cancer. *Acta Oncologica*. 2017;56(9):1152-4.

228. Latkauskas T, Pauzas H, Kairevice L, Petrauskas A, Saladzinskas Z, Janciauskiene R, et al. Preoperative conventional chemoradiotherapy versus short-course radiotherapy with delayed surgery for rectal cancer: results of a randomized controlled trial. *BMC Cancer*. 2016;16(1):927.

229. Millard T, Kunk PR, Ramsdale E, Rahma OE. Current debate in the oncologic management of rectal cancer. *World Journal of Gastrointestinal Oncology*. 2016;8(10):715.

230. van den Broek CB, Vermeer TA, Bastiaannet E, Rutten HJ, van de Velde CJ, Marijnen CA. Impact of the interval between short-course radiotherapy and surgery on outcomes of rectal cancer patients. *European Journal of Cancer*. 2013;49(15):3131-9.

231. Figueiredo N, Panteleimonitis S, Popeskou S, Cunha JF, Qureshi T, Beets GL, et al. Delaying surgery after neoadjuvant chemoradiotherapy in rectal cancer has no influence in surgical approach or short-term clinical outcomes. *European Journal of Surgical Oncology*. 2018;44(4):484-9.

232. Macchia G, Gambacorta MA, Masciocchi C, Chiloiro G, Mantello G, di Benedetto M, et al. Time to surgery and pathologic complete response after neoadjuvant chemoradiation in rectal cancer: a population study on 2094 patients. *Clinical and translational radiation oncology*. 2017;4:8-14.

233. Garrer WY, El HH, Gad ZS, Namour AE, Abo SA. Appropriate Timing of Surgery after Neoadjuvant ChemoRadiation Therapy for Locally Advanced Rectal Cancer. *Asian Pacific journal of cancer prevention: APJCP*. 2016;17(9):4381-9.

234. Tulchinsky H, Shmueli E, Figer A, Klausner JM, Rabau M. An interval > 7 weeks between neoadjuvant therapy and surgery improves pathologic complete response and disease-free survival in patients with locally advanced rectal cancer. *Annals of Surgical Oncology*. 2008;15(10):2661-7.

235. Spiotto M, Fu Y-X, Weichselbaum RR. The intersection of radiotherapy and immunotherapy: mechanisms and clinical implications. *Science Immunology*. 2016;1(3).

236. Pitroda SP, Pashtan IM, Logan HL, Budke B, Darga TE, Weichselbaum RR, et al. DNA repair pathway gene expression score correlates with repair proficiency and tumor sensitivity to chemotherapy. *Science translational medicine*. 2014;6(229):229ra42-ra42.

237. Lukas J, Lukas C. Shielding broken DNA for a quick fix. *Science*. 2013;339(6120):652-3.

238. Panier S, Durocher D. Push back to respond better: regulatory inhibition of the DNA double-strand break response. *Nature Reviews Molecular Cell Biology*. 2013;14(10):661.

239. Vignard J, Mirey G, Salles B, Oncology. Ionizing-radiation induced DNA double-strand breaks: a direct and indirect lighting up. *Radiotherapy*. 2013;108(3):362-9.

240. Barker HE, Paget JT, Khan AA, Harrington KJ. The tumour microenvironment after radiotherapy: mechanisms of resistance and recurrence. *Nature reviews Cancer*. 2015;15(7):409-25.

241. Golden EB, Apetoh L, editors. Radiotherapy and immunogenic cell death. *Seminars in radiation oncology*; 2015: Elsevier.

242. Longley DB, Harkin DP, Johnston PG. 5-fluorouracil: mechanisms of action and clinical strategies. *Nature reviews cancer*. 2003;3(5):330-8.

243. Kim SH, Chang HJ, Kim DY, Park JW, Baek JY, Kim SY, et al. What is the ideal tumor regression grading system in rectal cancer patients after preoperative chemoradiotherapy? *Cancer research and treatment: official journal of Korean Cancer Association*. 2016;48(3):998.

244. Mandard AM, Dalibard F, Mandard JC, Marnay J, Henry-Amar M, Petiot JF, et al. Pathologic assessment of tumor regression after preoperative chemoradiotherapy of esophageal carcinoma. Clinicopathologic correlations. *Cancer*. 1994;73(11):2680-6.
245. Ryan R, Gibbons D, Hyland J, Treanor D, White A, Mulcahy H, et al. Pathological response following long-course neoadjuvant chemoradiotherapy for locally advanced rectal cancer. *Histopathology*. 2005;47(2):141-6.
246. Dworak O, Keilholz L, Hoffmann A. Pathological features of rectal cancer after preoperative radiochemotherapy. *International journal of colorectal disease*. 1997;12(1):19-23.
247. Xu L, Cai S, Xiao T, Chen Y, Qiu H, Wu B, et al. Prognostic significance of tumour regression grade after neoadjuvant chemoradiotherapy for a cohort of patients with locally advanced rectal cancer: an 8-year retrospective single-institutional study. *Colorectal Disease*. 2017;19(7):O263-O71.
248. Valentini V, Van Stiphout RG, Lammering G, Gambacorta MA, Barba MC, Bebenek M, et al. Nomograms for predicting local recurrence, distant metastases, and overall survival for patients with locally advanced rectal cancer on the basis of European randomized clinical trials. *Journal of clinical oncology*. 2011;29(23):3163-72.
249. George TJ, Allegra CJ, Yothers G. Neoadjuvant rectal (NAR) score: a new surrogate endpoint in rectal cancer clinical trials. *Current colorectal cancer reports*. 2015;11(5):275-80.
250. Maas M, Nelemans PJ, Valentini V, Das P, Rödel C, Kuo L-J, et al. Long-term outcome in patients with a pathological complete response after chemoradiation for rectal cancer: a pooled analysis of individual patient data. *The Lancet Oncology*. 2010;11(9):835-44.
251. Pucciarelli S, Toppan P, Friso ML, Russo V, Pasetto L, Urso E, et al. Complete pathologic response following preoperative chemoradiation therapy for middle to lower rectal cancer is not a prognostic factor for a better outcome. *Diseases of the colon & rectum*. 2004;47(11):1798-807.
252. Hoendervangers S, Couwenberg AM, Intven MP, van Grevenstein WM, Verkooijen HM. Comparison of pathological complete response rates after neoadjuvant short-course radiotherapy or chemoradiation followed by delayed surgery in locally advanced rectal cancer. *European Journal of Surgical Oncology*. 2018;44(7):1013-7.
253. Rödel C, Martus P, Papadopoulos T, Füzesi L, Klimpfing M, Fietkau R, et al. Prognostic significance of tumor regression after preoperative chemoradiotherapy for rectal cancer. *Journal of Clinical Oncology*. 2005;23(34):8688-96.
254. Martin S, Heneghan H, Winter D. Systematic review and meta-analysis of outcomes following pathological complete response to neoadjuvant chemoradiotherapy for rectal cancer. *British Journal of Surgery*. 2012;99(7):918-28.
255. Capirci C, Valentini V, Cionini L, De Paoli A, Rodel C, Glynne-Jones R, et al. Prognostic value of pathologic complete response after neoadjuvant therapy in locally advanced rectal cancer: long-term analysis of 566 ypCR patients. *International Journal of Radiation Oncology* Biology* Physics*. 2008;72(1):99-107.
256. Dinaux A, Amri R, Bordeianou L, Hong T, Wo J, Blaszkowsky L, et al. The impact of pathologic complete response in patients with neoadjuvantly treated locally advanced rectal cancer—a large single-center experience. *Journal of Gastrointestinal Surgery*. 2017;21(7):1153-8.
257. Sigurdson ER, Benson III AB, Minsky B. 78 *Cancer of the Rectum*.
258. García-Aguilar J, de Anda EH, Sirivongs P, Lee S-H, Madoff RD, Rothenberger DA. A pathologic complete response to preoperative chemoradiation is associated with lower local recurrence and improved survival in rectal cancer patients treated by mesorectal excision. *Diseases of the colon & rectum*. 2003;46(3):298-304.
259. Dossa F, Chesney TR, Acuna SA, Baxter NN. A watch-and-wait approach for locally advanced rectal cancer after a clinical complete response following neoadjuvant chemoradiation: a systematic review and meta-analysis. *The Lancet Gastroenterology and Hepatology*. 2017;2(7):501-13.

260. Fokas E, Liersch T, Fietkau R, Hohenberger W, Beissbarth T, Hess C, et al. Tumor regression grading after preoperative chemoradiotherapy for locally advanced rectal carcinoma revisited: updated results of the CAO. *J Clin Oncol*. 2014;32(15):1554-62.
261. Fokas E, Ströbel P, Fietkau R, Ghadimi M, Liersch T, Grabenbauer GG, et al. Tumor regression grading after preoperative chemoradiotherapy as a prognostic factor and individual-level surrogate for disease-free survival in rectal cancer. *JNCI: Journal of the National Cancer Institute*. 2017;109(12):dix095.
262. Battersby NJ, Juul T, Christensen P, Janjua AZ, Branagan G, Emmertsen KJ, et al. Predicting the risk of bowel-related quality-of-life impairment after restorative resection for rectal cancer: a multicenter cross-sectional study. *Diseases of the Colon & Rectum*. 2016;59(4):270-80.
263. Lange MM, Van De Velde CJ. Urinary and sexual dysfunction after rectal cancer treatment. *Nature reviews Urology*. 2011;8(1):51.
264. Ryan JE, Warriar SK, Lynch AC, Ramsay RG, Phillips WA, Heriot AG. Predicting pathological complete response to neoadjuvant chemoradiotherapy in locally advanced rectal cancer: a systematic review. *Colorectal Disease*. 2016;18(3):234-46.
265. Clarke T, White D, Osborne M, Shaw A, Smart NJ, Daniels IR. Predicting response to neoadjuvant chemoradiotherapy in locally advanced rectal cancer with serum biomarkers. *The Annals of The Royal College of Surgeons of England*. 2017;99(5):373-7.
266. Park YA, Sohn SK, Seong J, Baik SH, Lee KY, Kim NK, et al. Serum CEA as a predictor for the response to preoperative chemoradiation in rectal cancer. *Journal of Surgical Oncology*. 2006;93(2):145-50.
267. Huh JW, Kim HR, Kim YJ. Clinical prediction of pathological complete response after preoperative chemoradiotherapy for rectal cancer. *Diseases of the Colon & Rectum*. 2013;56(6):698-703.
268. Yoon SM, Kim DY, Kim TH, Jung KH, Chang HJ, Koom WS, et al. Clinical parameters predicting pathologic tumor response after preoperative chemoradiotherapy for rectal cancer. *International Journal of Radiation Oncology* Biology* Physics*. 2007;69(4):1167-72.
269. Zeng W-G, Liang J-W, Wang Z, Zhang X-M, Hu J-J, Hou H-R, et al. Clinical parameters predicting pathologic complete response following neoadjuvant chemoradiotherapy for rectal cancer. *Chinese Journal of Cancer*. 2015;34(3):41.
270. Kim HJ, Choi G-S, Park JS, Park S, Kawai K, Watanabe T. Clinical significance of thrombocytosis before preoperative chemoradiotherapy in rectal cancer: predicting pathologic tumor response and oncologic outcome. *Annals of Surgical Oncology*. 2015;22(2):513-9.
271. Lee SD, Park JW, Park KS, Lim S-B, Chang HJ, Kim DY, et al. Influence of anemia on tumor response to preoperative chemoradiotherapy for locally advanced rectal cancer. *International journal of colorectal disease*. 2009;24(12):1451.
272. Bozkaya Y, Özdemir NY, Erdem GU, Güner EK, Ürün Y, Demirci NS, et al. Clinical predictive factors associated with pathologic complete response in locally advanced rectal cancer. *Journal of Oncological Sciences*. 2018;4(1):5-10.
273. Restivo A, Zorcolo L, Cocco IMF, Manunza R, Margiani C, Marongiu L, et al. Elevated CEA levels and low distance of the tumor from the anal verge are predictors of incomplete response to chemoradiation in patients with rectal cancer. *Annals of Surgical Oncology*. 2013;20(3):864-71.
274. Yan H, Wang R, Zhu K, Zhao W, Jiang S, Feng R, et al. Predictors of sensitivity to preoperative chemoradiotherapy of rectal adenocarcinoma. *Tumori Journal*. 2011;97(6):717-23.
275. Kang JH, Kim YC, Kim H, Kim YW, Hur H, Kim JS, et al. Tumor volume changes assessed by three-dimensional magnetic resonance volumetry in rectal cancer patients after preoperative chemoradiation: the impact of the volume reduction ratio on the prediction of pathologic complete response. *International Journal of Radiation Oncology* Biology* Physics*. 2010;76(4):1018-25.

276. Kleiman A, Al-Khamis A, Farsi A, Kezouh A, Vuong T, Gordon PH, et al. Normalization of CEA levels post-neoadjuvant therapy is a strong predictor of pathologic complete response in rectal cancer. *Journal of Gastrointestinal Surgery*. 2015;19(6):1106-12.
277. Peng J, Lin J, Qiu M, Wu X, Lu Z, Chen G, et al. Clinical factors of post-chemoradiotherapy as valuable indicators for pathological complete response in locally advanced rectal cancer. *Clinics*. 2016;71(8):449-54.
278. Lee JH, Kim SH, Jang HS, Chung HJ, Oh ST, Lee DS, et al. Preoperative elevation of carcinoembryonic antigen predicts poor tumor response and frequent distant recurrence for patients with rectal cancer who receive preoperative chemoradiotherapy and total mesorectal excision: a multi-institutional analysis in an Asian population. *International journal of colorectal disease*. 2013;28(4):511-7.
279. Song JH, Kim SH, Lee JH, Cho HM, Kim DY, Kim TH, et al. Significance of histologic tumor grade in rectal cancer treated with preoperative chemoradiotherapy followed by curative surgery: a multi-institutional retrospective study. *Radiotherapy and Oncology*. 2016;118(2):387-92.
280. Yeo S-G, Kim DY, Chang HJ, Park JW, Oh JH, Kim BC, et al. Reappraisal of pretreatment carcinoembryonic antigen in patients with rectal cancer receiving preoperative chemoradiotherapy. *Tumori Journal*. 2013;99(1):93-9.
281. Yang K-L, Yang S-H, Liang W-Y, Kuo Y-J, Lin J-K, Lin T-C, et al. Carcinoembryonic antigen (CEA) level, CEA ratio, and treatment outcome of rectal cancer patients receiving pre-operative chemoradiation and surgery. *Radiation Oncology*. 2013;8(1):43.
282. Perez RO, São Julião GP, Habr-Gama A, Kiss D, Proscurshim I, Campos FG, et al. The role of carcinoembryonic antigen in predicting response and survival to neoadjuvant chemoradiotherapy for distal rectal cancer. *Diseases of the Colon & Rectum*. 2009;52(6):1137-43.
283. Zhou J, Wang C, Lin G, Xiao Y, Jia W, Xiao G, et al. Serial circulating tumor DNA in predicting and monitoring the effect of neoadjuvant chemoradiotherapy in patients with rectal cancer: a prospective multicenter study. *Clinical Cancer Research*. 2020.
284. Pazdirek F, Minarik M, Benesova L, Halkova T, Belsanova B, Macek M, et al. Monitoring of Early Changes of Circulating Tumor DNA in the Plasma of Rectal Cancer Patients Receiving Neoadjuvant Concomitant Chemoradiotherapy: Evaluation for Prognosis and Prediction of Therapeutic Response. *Frontiers in Oncology*. 2020;10.
285. Sun Y-w, Chi P, Lin H-m, Lu X-r, Huang Y, Xu Z-b, et al. Effect of Neoadjuvant Chemoradiotherapy on Locally Advanced Rectal Mucinous Adenocarcinoma: A Propensity Score-Matched Study. *Gastroenterology research and practice*. 2017;2017.
286. Chen M-B, Wu X-Y, Yu R, Li C, Wang L-Q, Shen W, et al. P53 status as a predictive biomarker for patients receiving neoadjuvant radiation-based treatment: a meta-analysis in rectal cancer. *PloS one*. 2012;7(9):e45388.
287. Clancy C, Burke JP, Coffey JC. KRAS mutation does not predict the efficacy of neoadjuvant chemoradiotherapy in rectal cancer: a systematic review and meta-analysis. *Surgical oncology*. 2013;22(2):105-11.
288. Davies JM, Trembath D, Deal AM, Funkhouser WK, Calvo BF, Finnegan T, et al. Phospho-ERK and AKT status, but not KRAS mutation status, are associated with outcomes in rectal cancer treated with chemoradiotherapy. *Radiation Oncology*. 2011;6(1):114.
289. O'Connell E, Reynolds I, McNamara D, Prehn J, Burke J. Microsatellite instability and response to neoadjuvant chemoradiotherapy in rectal cancer: A systematic review and meta-analysis. *Surgical Oncology*. 2020.
290. Russo AL, Ryan DP, Borger DR, Wo JY, Szymonifka J, Liang W-Y, et al. Mutational and clinical predictors of pathologic complete response in the treatment of locally advanced rectal cancer. *Journal of gastrointestinal cancer*. 2014;45(1):34-9.
291. Maring ED, Tawadros PS, Steer CJ, Lee JT. Systematic review of candidate single-nucleotide polymorphisms as biomarkers for responsiveness to neoadjuvant chemoradiation for rectal cancer. *Anticancer research*. 2015;35(7):3761-6.

292. Yang Y, Wu G, Jin L, Wang K, Bai Z, Wang J, et al. Association of thymidylate synthase polymorphisms with the tumor response to preoperative chemoradiotherapy in rectal cancer: a systematic review and meta-analysis. *The pharmacogenomics journal*. 2017;17(3):265-73.
293. Páez D, Salazar J, Paré L, Pertriz L, Targarona E, Del Rio E, et al. Pharmacogenetic study in rectal cancer patients treated with preoperative chemoradiotherapy: polymorphisms in thymidylate synthase, epidermal growth factor receptor, GSTP1, and DNA repair genes. *International Journal of Radiation Oncology* Biology* Physics*. 2011;81(5):1319-27.
294. Grimminger PP, Brabender J, Warnecke-Eberz U, Narumiya K, Wandhöfer C, Drebber U, et al. XRCC1 gene polymorphism for prediction of response and prognosis in the multimodality therapy of patients with locally advanced rectal cancer. *Journal of Surgical Research*. 2010;164(1):e61-e6.
295. Sebio A, Salazar J, Paez D, Berenguer-Llargo A, Del Rio E, Tobena M, et al. EGFR ligands and DNA repair genes: genomic predictors of complete response after capecitabine-based chemoradiotherapy in locally advanced rectal cancer. *The pharmacogenomics journal*. 2015;15(1):77-83.
296. Spindler K-LG, Nielsen JN, Lindebjerg J, Brandslund I, Jakobsen A. Prediction of response to chemoradiation in rectal cancer by a gene polymorphism in the epidermal growth factor receptor promoter region. *International Journal of Radiation Oncology* Biology* Physics*. 2006;66(2):500-4.
297. Hu-Lieskovan S, Vallbohmer D, Zhang W, Yang D, Pohl A, Labonte MJ, et al. EGF61 polymorphism predicts complete pathologic response to cetuximab-based chemoradiation independent of KRAS status in locally advanced rectal cancer patients. *Clinical Cancer Research*. 2011;17(15):5161-9.
298. Williamson JS, Harris DA, Beynon J, Jenkins GJ. Review of the development of DNA methylation as a marker of response to neoadjuvant therapy and outcomes in rectal cancer. *Clinical epigenetics*. 2015;7(1):1-9.
299. Sun W, Sun Y, Zhu M, Wang Z, Zhang H, Xin Y, et al. The role of plasma cell-free DNA detection in predicting preoperative chemoradiotherapy response in rectal cancer patients. *Oncology reports*. 2014;31(3):1466-72.
300. Ebert MP, Tänzer M, Balluff B, Burgermeister E, Kretzschmar AK, Hughes DJ, et al. TFAP2E–DKK4 and chemoresistance in colorectal cancer. *New England Journal of Medicine*. 2012;366(1):44-53.
301. Ha YJ, Kim CW, Roh SA, Cho DH, Park JL, Kim SY, et al. Epigenetic regulation of KLHL34 predictive of pathologic response to preoperative chemoradiation therapy in rectal cancer patients. *International Journal of Radiation Oncology* Biology* Physics*. 2015;91(3):650-8.
302. Yokoi K, Yamashita K, Ishii S, Tanaka T, Nishizawa N, Tsutsui A, et al. Comprehensive molecular exploration identified promoter DNA methylation of the CRBP1 gene as a determinant of radiation sensitivity in rectal cancer. *British journal of cancer*. 2017;116(8):1046-56.
303. Molinari C, Casadio V, Foca F, Zingaretti C, Giannini M, Avanzolini A, et al. Gene methylation in rectal cancer: predictive marker of response to chemoradiotherapy? *Journal of cellular physiology*. 2013;228(12):2343-9.
304. Jo P, Jung K, Grade M, Conradi L-C, Wolff HA, Kitz J, et al. CpG island methylator phenotype infers a poor disease-free survival in locally advanced rectal cancer. *Surgery*. 2012;151(4):564-70.
305. Williamson JS, Jones HG, Williams N, Griffiths AP, Jenkins G, Beynon J, et al. Extramural vascular invasion and response to neoadjuvant chemoradiotherapy in rectal cancer: influence of the CpG island methylator phenotype. *World journal of gastrointestinal oncology*. 2017;9(5):209.
306. Watanabe T, Komuro Y, Kiyomatsu T, Kanazawa T, Kazama Y, Tanaka J, et al. Prediction of sensitivity of rectal cancer cells in response to preoperative radiotherapy by DNA microarray analysis of gene expression profiles. *Cancer research*. 2006;66(7):3370-4.

307. Rimkus C, Friederichs J, Boulesteix AI, Theisen J, Mages J, Becker K, et al. Microarray-based prediction of tumor response to neoadjuvant radiochemotherapy of patients with locally advanced rectal cancer. *Clinical gastroenterology and hepatology*. 2008;6(1):53-61.
308. Nishioka M, Shimada M, Kurita N, Iwata T, Morimoto S, Yoshikawa K, et al. Gene expression profile can predict pathological response to preoperative chemoradiotherapy in rectal cancer. *Cancer Genomics-Proteomics*. 2011;8(2):87-92.
309. Toiyama Y, Inoue Y, Saigusa S, Okugawa Y, Yokoe T, Tanaka K, et al. Gene expression profiles of epidermal growth factor receptor, vascular endothelial growth factor and hypoxia-inducible factor-1 with special reference to local responsiveness to neoadjuvant chemoradiotherapy and disease recurrence after rectal cancer surgery. *Clinical Oncology*. 2010;22(4):272-80.
310. Saigusa S, Tanaka K, Toiyama Y, Matsushita K, Kawamura M, Okugawa Y, et al. Gene expression profiles of tumor regression grade in locally advanced rectal cancer after neoadjuvant chemoradiotherapy. *Oncology reports*. 2012;28(3):855-61.
311. Saigusa S, Inoue Y, Tanaka K, Toiyama Y, Matsushita K, Kawamura M, et al. Clinical significance of LGR5 and CD44 expression in locally advanced rectal cancer after preoperative chemoradiotherapy. *International journal of oncology*. 2012;41(5):1643-52.
312. Huh JW, Lee JH, Kim HR. Pretreatment expression of 13 molecular markers as a predictor of tumor responses after neoadjuvant chemoradiation in rectal cancer. *Annals of surgery*. 2014;259(3):508-15.
313. Watanabe T, Kobunai T, Akiyoshi T, Matsuda K, Ishihara S, Nozawa K. Prediction of response to preoperative chemoradiotherapy in rectal cancer by using reverse transcriptase polymerase chain reaction analysis of four genes. *Diseases of the colon & rectum*. 2014;57(1):23-31.
314. Ghadimi BM, Grade M, Difilippantonio MJ, Varma S, Simon R, Montagna C, et al. Effectiveness of gene expression profiling for response prediction of rectal adenocarcinomas to preoperative chemoradiotherapy. *Journal of clinical oncology: official journal of the American Society of Clinical Oncology*. 2005;23(9):1826.
315. Lopes-Ramos CM, Habr-Gama A, de Souza Quevedo B, Felício NM, Bettoni F, Koyama FC, et al. Overexpression of miR-21-5p as a predictive marker for complete tumor regression to neoadjuvant chemoradiotherapy in rectal cancer patients. *BMC medical genomics*. 2014;7(1):68.
316. Millino C, Maretto I, Pacchioni B, Digito M, De Paoli A, Canzonieri V, et al. Gene and MicroRNA expression are predictive of tumor response in rectal adenocarcinoma patients treated with preoperative chemoradiotherapy. *Journal of cellular physiology*. 2017;232(2):426-35.
317. Kim I-J, Lim S-B, Kang HC, Chang HJ, Ahn S-A, Park H-W, et al. Microarray gene expression profiling for predicting complete response to preoperative chemoradiotherapy in patients with advanced rectal cancer. *Diseases of the colon & rectum*. 2007;50(9):1342-53.
318. Kheirlesei EA, Miller N, Chang KH, Curran C, Hennessey E, Sheehan M, et al. miRNA expressions in rectal cancer as predictors of response to neoadjuvant chemoradiation therapy. *International journal of colorectal disease*. 2013;28(2):247-60.
319. Baba Y, Noshō K, Shima K, Hayashi M, Meyerhardt JA, Chan AT, et al. Phosphorylated AKT expression is associated with PIK3CA mutation, low stage, and favorable outcome in 717 colorectal cancers. *Cancer*. 2011;117(7):1399-408.
320. Zlobec I, Vuong T, Compton C, Lugli A, Michel R, Hayashi S, et al. Combined analysis of VEGF and EGFR predicts complete tumour response in rectal cancer treated with preoperative radiotherapy. *British journal of cancer*. 2008;98(2):450-6.
321. Farkas R, Pozsgai E, Schally AV, Szigeti A, Szigeti E, Laszlo Z, et al. Possible predictors of histopathological response to neoadjuvant chemoradiotherapy for rectal cancer. *Journal of cancer research and clinical oncology*. 2012;138(3):387-95.
322. Iwata T, Shimada M, Kurita N, Nishioka M, Morimoto S, Yoshikawa K, et al. Evaluation of relation of RAD51 and the effect of chemo-radiation therapy for advanced rectal cancer. *Hepato-gastroenterology*. 2012;59(116):990-3.

323. Kamran SC, Lennerz JK, Margolis CA, Liu D, Reardon B, Wankowicz SA, et al. Integrative molecular characterization of resistance to neoadjuvant chemoradiation in rectal cancer. *Clinical Cancer Research*. 2019;25(18):5561-71.
324. Alderdice M, Dunne PD, Cole AJ, O'Reilly PG, McArt DG, Bingham V, et al. Natural killer-like signature observed post therapy in locally advanced rectal cancer is a determinant of pathological response and improved survival. *Modern Pathology*. 2017;30(9):1287-98.
325. El Sissy C, Kirilovsky A, Van den Eynde M, Muşină A-M, Anitei M-G, Romero A, et al. A diagnostic biopsy-adapted immunoscore predicts response to neoadjuvant treatment and selects patients with rectal cancer eligible for a watch-and-wait strategy. *Clinical Cancer Research*. 2020;26(19):5198-207.
326. Shen L, Yi Y, Wang Y, Zhang J, Xia F, Zhang Z. Gut Microbiome Predicts Neoadjuvant Chemoradiotherapy Response in Locally Advanced Rectal Cancer Patients. *International Journal of Radiation Oncology, Biology, Physics*. 2020;108(3):S46-S7.
327. Sun Y, Dou X, Li W, Liu C, Yu J, Yue J. Longitudinal Analysis of Fecal Microbiome Diversity during the Neoadjuvant Concurrent Chemoradiotherapy of Patients with Locally Advanced Rectal Cancer. *International Journal of Radiation Oncology, Biology, Physics*. 2020;108(3):e579-e80.
328. Toomey S, Gunther J, Carr A, Weksberg DC, Thomas V, Salvucci M, et al. Genomic and Transcriptomic Characterisation of Response to Neoadjuvant Chemoradiotherapy in Locally Advanced Rectal Cancer. *Cancers*. 2020;12(7):1808.
329. Jang B-S, Chang JH, Chie EK, Kim K, Park JW, Kim MJ, et al. Gut microbiome composition is associated with a pathologic response after preoperative chemoradiation in rectal cancer patients. *International Journal of Radiation Oncology* Biology* Physics*. 2020.
330. Van't Veer LJ, Bernards R. Enabling personalized cancer medicine through analysis of gene-expression patterns. *Nature*. 2008;452(7187):564-70.
331. Buckley AM, Lynam-Lennon N, O'Neill H, O'Sullivan J. Targeting hallmarks of cancer to enhance radiosensitivity in gastrointestinal cancers. *Nature Reviews Gastroenterology & Hepatology*. 2020:1-16.
332. Spitzner M, Emons G, Kramer F, Gaedcke J, Rave-Fränk M, Scharf J-G, et al. A gene expression signature for chemoradiosensitivity of colorectal cancer cells. *International Journal of Radiation Oncology* Biology* Physics*. 2010;78(4):1184-92.
333. Chen Y-H, Wang C-W, Wei M-F, Tzeng Y-S, Lan K-H, Cheng A-L, et al. Maintenance BEZ235 Treatment Prolongs the Therapeutic Effect of the Combination of BEZ235 and Radiotherapy for Colorectal Cancer. *Cancers*. 2019;11(8):1204.
334. Ganesh K, Wu C, O'Rourke KP, Szeglin BC, Zheng Y, Sauvé C-EG, et al. A rectal cancer organoid platform to study individual responses to chemoradiation. *Nature medicine*. 2019;25(10):1607-14.
335. Yao Y, Xu X, Yang L, Zhu J, Wan J, Shen L, et al. Patient-Derived Organoids Predict Chemoradiation Responses of Locally Advanced Rectal Cancer. *Cell stem cell*. 2019.
336. Gelsomino F, Bertolini F, Luppi G, Spallanzani A, Pettorelli E, Bonetti LR, et al. A Dose-finding and Biomarker Evaluation Phase Ib Study of Everolimus in Association With 5-Fluorouracil and Pelvic Radiotherapy as Neoadjuvant Treatment of Locally Advanced Rectal Cancer (E-LARC Study). *Clinical Colorectal Cancer*. 2017;16(4):410-5. e1.
337. Buijsen J, van den Bogaard J, Jutten B, Belgers E, Sosef M, Leijtens JW, et al. A phase I-II study on the combination of rapamycin and short course radiotherapy in rectal cancer. *Radiotherapy and Oncology*. 2015;116(2):214-20.
338. Rödel C, Arnold D, Hipp M, Liersch T, Dellas K, Ilesalnieks I, et al. Phase I-II trial of cetuximab, capecitabine, oxaliplatin, and radiotherapy as preoperative treatment in rectal cancer. *International Journal of Radiation Oncology* Biology* Physics*. 2008;70(4):1081-6.
339. Helbling D, Bodoky G, Gautschi O, Sun H, Bosman F, Gloor B, et al. Neoadjuvant chemoradiotherapy with or without panitumumab in patients with wild-type KRAS, locally advanced rectal cancer (LARC): a randomized, multicenter, phase II trial SAKK 41/07. *Annals of oncology*. 2013;24(3):718-25.

340. Mardjuadi FI, Carrasco J, Coche J-C, Sempoux C, Jouret-Mourin A, Scalliet P, et al. Panitumumab as a radiosensitizing agent in KRAS wild-type locally advanced rectal cancer. *Targeted oncology*. 2015;10(3):375-83.
341. O'Neil BH, Raftery L, Calvo BF, Chakravarthy AB, Ivanova A, Myers MO, et al. A phase I study of bortezomib in combination with standard 5-fluorouracil and external-beam radiation therapy for the treatment of locally advanced or metastatic rectal cancer. *Clinical colorectal cancer*. 2010;9(2):119-25.
342. Sanoff HK, Moon DH, Moore DT, Boles J, Bui C, Blackstock W, et al. Phase I/II trial of nano-camptothecin CRLX101 with capecitabine and radiotherapy as neoadjuvant treatment for locally advanced rectal cancer. *Nanomedicine: Nanotechnology, Biology and Medicine*. 2019;18:189-95.
343. Yamazaki T, Gunderson AJ, Gilchrist M, Whiteford M, Kiely MX, Hayman A, et al. Galunisertib plus neoadjuvant chemoradiotherapy in patients with locally advanced rectal cancer: a single-arm, phase 2 trial. *The Lancet Oncology*. 2022.
344. Hanna CR, O'Cathail SM, Graham JS, Saunders M, Samuel L, Harrison M, et al. Durvalumab (MEDI 4736) in combination with extended neoadjuvant regimens in rectal cancer: a study protocol of a randomised phase II trial (PRIME-RT). *Radiation Oncology*. 2021;16(1):1-9.
345. van der Geest LG, Koopman M, Verhoef C, Elferink MA, de Wilt JH. Nationwide trends in incidence, treatment and survival of colorectal cancer patients with synchronous metastases. *Clinical & experimental metastasis*. 2015;32(5):457-65.
346. Mentha G, Majno P, Andres A, Rubbia-Brandt L, Morel P, Roth A. Neoadjuvant chemotherapy and resection of advanced synchronous liver metastases before treatment of the colorectal primary. *British journal of surgery*. 2006;93(7):872-8.
347. Viganò L. Treatment strategy for colorectal cancer with resectable synchronous liver metastases: Is any evidence-based strategy possible? *World Journal of Hepatology*. 2012;4(8):237.
348. Adam R, de Gramont A, Figueras J, Kokudo N, Kunstlinger F, Loyer E, et al. Managing synchronous liver metastases from colorectal cancer: a multidisciplinary international consensus. *Cancer treatment reviews*. 2015;41(9):729-41.
349. van der Kruijssen DE, Elias SG, Vink GR, van Rooijen KL, Mol L, Punt CJ, et al. Sixty-Day Mortality of Patients With Metastatic Colorectal Cancer Randomized to Systemic Treatment vs Primary Tumor Resection Followed by Systemic Treatment: The CAIRO4 Phase 3 Randomized Clinical Trial. *JAMA surgery*. 2021.
350. Edwards M, Chadda S, Zhao Z, Barber B, Sykes D. A systematic review of treatment guidelines for metastatic colorectal cancer. *Colorectal Disease*. 2012;14(2):e31-e47.
351. De Cuba E, Kwakman R, Knol D, Bonjer H, Meijer G, Te Velde E. Cytoreductive surgery and HIPEC for peritoneal metastases combined with curative treatment of colorectal liver metastases: systematic review of all literature and meta-analysis of observational studies. *Cancer treatment reviews*. 2013;39(4):321-7.
352. Law W, Choi H, Chu K. Comparison of stenting with emergency surgery as palliative treatment for obstructing primary left-sided colorectal cancer. *British journal of Surgery*. 2003;90(11):1429-33.
353. Lyons N, Pathak S, Daniels IR, Spiers A, Smart NJ. Percutaneous management of pulmonary metastases arising from colorectal cancer; a systematic review. *European Journal of Surgical Oncology (EJSO)*. 2015;41(11):1447-55.
354. Solbiati L, Livraghi T, Goldberg SN, Ierace T, Meloni F, Dellanoce M, et al. Percutaneous radio-frequency ablation of hepatic metastases from colorectal cancer: long-term results in 117 patients. *Radiology*. 2001;221(1):159-66.
355. Engelhardt EG, Révész D, Tamminga HJ, Punt CJ, Koopman M, Onwuteaka-Philipsen BD, et al. Clinical usefulness of tools to support decision-making for palliative treatment of metastatic colorectal Cancer: a systematic review. *Clinical colorectal cancer*. 2018;17(1):e1-e12.

356. Galandiuk S, Wieand H, Moertel C, Cha S, Fitzgibbons Jr R, Pemberton J, et al. Patterns of recurrence after curative resection of carcinoma of the colon and rectum. *Surgery, gynecology & obstetrics*. 1992;174(1):27-32.
357. Yang TX, Morris DL, Chua TC. Pelvic exenteration for rectal cancer: a systematic review. *Diseases of the colon & rectum*. 2013;56(4):519-31.
358. Quaresma M, Coleman MP, Rachet B. 40-year trends in an index of survival for all cancers combined and survival adjusted for age and sex for each cancer in England and Wales, 1971–2011: a population-based study. *The Lancet*. 2015;385(9974):1206-18.
359. Zlobec I, Lugli A. Prognostic and predictive factors in colorectal cancer. *Postgraduate medical journal*. 2008;84(994):403-11.
360. Chen T-M, Huang Y-T, Wang G-C. Outcome of colon cancer initially presenting as colon perforation and obstruction. *World journal of surgical oncology*. 2017;15(1):164.
361. Lee Y-C, Lee Y-L, Chuang J-P, Lee J-C. Differences in survival between colon and rectal cancer from SEER data. *PloS one*. 2013;8(11):e78709.
362. Sato T, Stange DE, Ferrante M, Vries RG, Van Es JH, Van Den Brink S, et al. Long-term expansion of epithelial organoids from human colon, adenoma, adenocarcinoma, and Barrett's epithelium. *Gastroenterology*. 2011;141(5):1762-72.
363. Dutta D, Heo I, Clevers H. Disease modeling in stem cell-derived 3D organoid systems. *Trends in Molecular Medicine*. 2017;23(5):393-410.
364. Drost J, Clevers H. Organoids in cancer research. *Nature Reviews Cancer*. 2018;18(7):407-18.
365. Vlachogiannis G, Hedayat S, Vatsiou A, Jamin Y, Fernández-Mateos J, Khan K, et al. Patient-derived organoids model treatment response of metastatic gastrointestinal cancers. *Science*. 2018;359(6378):920-6.
366. Schnalzger TE, de Groot MH, Zhang C, Mosa MH, Michels BE, Röder J, et al. 3D model for CAR-mediated cytotoxicity using patient-derived colorectal cancer organoids. *The EMBO journal*. 2019;38(12):e100928.
367. Dijkstra KK, Cattaneo CM, Weeber F, Chalabi M, van de Haar J, Fanchi LF, et al. Generation of tumor-reactive T cells by co-culture of peripheral blood lymphocytes and tumor organoids. *Cell*. 2018;174(6):1586-98. e12.
368. Matano M, Date S, Shimokawa M, Takano A, Fujii M, Ohta Y, et al. Modeling colorectal cancer using CRISPR-Cas9-mediated engineering of human intestinal organoids. *Nature medicine*. 2015;21(3):256-62.
369. Takeda H, Kataoka S, Nakayama M, Ali MA, Oshima H, Yamamoto D, et al. CRISPR-Cas9-mediated gene knockout in intestinal tumor organoids provides functional validation for colorectal cancer driver genes. *Proceedings of the National Academy of Sciences*. 2019;116(31):15635-44.
370. Covaris. Protocol: truXTRAC® FFPE total NA Kit -Column (25) [internet].no date [cited 2020 March 02]. Available from: https://covaris.com/wp-content/uploads/pn_010434.pdf.
371. Thermo Fisher Scientific. User Guide: TURBO DNA-free Kit (English) [internet]. [cited 2020 March 02]. Available from: https://assets.thermofisher.com/TFS-Assets/LSG/manuals/1907M_turbodnafree_UG.pdf.
372. Qiagen. AllPrep DNA/RNA Mini Kit, Part 1 (EN) [internet].no date [cited 2020 March 02]. Available from: <https://www.qiagen.com/us/resources/resourcedetail?id=c1d0a03f-554c-402f-93eb-9940ed76921d&lang=en>.
373. Qiagen. AllPrep DNA/RNA Mini Kit, Part 2 (EN) [internet].no date [cited 2020 March 02]. Available from: <https://www.qiagen.com/us/resources/resourcedetail?id=cb6b6bff-6193-4206-bdfd-18047a6b5fee&lang=en>.
374. Agilent. Agilent Genomic DNA ScreenTape System Quick Guide [internet].no date [cited 2020 March 02]. Available from: https://www.agilent.com/cs/library/usermanuals/Public/ScreenTape_gDNA_QG.pdf.
375. Agilent. Agilent High Sensitivity RNA ScreenTape System Quick Guide [internet].no date [cited 2020 March 02]. Available from: https://www.agilent.com/cs/library/usermanuals/public/ScreenTape_HSRNA_QG.pdf.

376. Agilent. Agilent High Sensitivity D1000 ScreenTape System Quick Guide [internet].no date [cited 2020 March 02]. Available from: https://www.agilent.com/cs/library/usermanuals/Public/ScreenTape_HSD1000_QG.pdf.
377. Lexogen. 3' mRNA-Seq Library Prep Kit: User Guide [internet].(no date) [cited 2021 October 30]. Available from: https://www.lexogen.com/wp-content/uploads/2021/08/015UG009V0260_QuantSeq_Illumina_2021-08-16.pdf.
378. Lexogen. PCR Add-on Kit for Illumina: Instruction Manual [internet].no date [cited 2021 October 10]. Available from: https://www.lexogen.com/wp-content/uploads/2020/11/020IM064V0131_PCR-Add-on-for-Illumina_2020-11-04.pdf.
379. New England BioLabs. Protocol for use with NEBNext® rRNA Depletion Kit (Human/Mouse/Rat) (E6310, E6350) [internet].no date [cited 2021 October 10]. Available from: <https://international.neb.com/protocols/2017/04/06/nebnext-rna-depletion-kit-human-mouse-rat-with-rna-sample-purification-beads>.
380. New England BioLabs. Instruction Manual: NEBNext® Ultra™ II DNA Library Prep Kit for Illumina® [internet].no date [cited 2021 October 10]. Available from: <https://international.neb.com/-/media/nebus/files/manuals/manuale7103-e7645.pdf?rev=339d6c65a9314c9e988851a9d671fd9a&hash=2AF765847CD54F1B7464205F7920A50F>.
381. Qiagen. QIAseq Targeted DNA Panel Handbook [internet].no date [cited 2020 March 02]. Available from: <https://www.qiagen.com/qb/resources/resourcedetail?id=8907edbe-a462-4883-ae1b-2759657e7fd0&lang=en>.
382. Law CW, Chen Y, Shi W, Smyth GK. voom: Precision weights unlock linear model analysis tools for RNA-seq read counts. *Genome biology*. 2014;15(2):1-17.
383. Vera-Ramirez L, Vodnala SK, Nini R, Hunter KW, Green JE. Autophagy promotes the survival of dormant breast cancer cells and metastatic tumour recurrence. *Nature communications*. 2018;9(1):1-12.
384. Lexogen. Lexogen QuantSeq Data USING PARTEK® FLOW® SOFTWARE [internet].(no date) [cited 2019 October 23]. Available from: https://www.lexogen.com/wp-content/uploads/2017/12/015PF156V0100_PartekFlow_Lexogen.pdf.
385. Benjamini Y, Hochberg Y. Controlling the false discovery rate: a practical and powerful approach to multiple testing. *Journal of the Royal statistical society: series B (Methodological)*. 1995;57(1):289-300.
386. Love MI, Huber W, Anders S. Moderated estimation of fold change and dispersion for RNA-seq data with DESeq2. *Genome biology*. 2014;15(12):1-21.
387. Broad Institute. Gene Set Enrichment Analysis (GSEA) User Guide [internet].(no date) [cited 2021 July 03]. Available from: https://www.gsea-msigdb.org/gsea/doc/GSEAUUserGuideTEXT.htm#_Interpreting_GSEA_Results.
388. Kuehn H, Liberzon A, Reich M, Mesirov JP. Using GenePattern for gene expression analysis. *Current protocols in bioinformatics*. 2008;22(1):7.12. 1-7.. 39.
389. Biological Industries. EZ-PCR™ Mycoplasma Detection Kit [internet].no date [cited 2020 March 02]. Available from: <https://www.bioind.com/media/wysiwyg/product/mycoplasma/BI-USA-EZ-PCR-Mycoplasma-Detection-protocol-2019.pdf>.
390. Garland ML, Vather R, Bunkley N, Pearse M, Bissett IP. Clinical tumour size and nodal status predict pathologic complete response following neoadjuvant chemoradiotherapy for rectal cancer. *International journal of colorectal disease*. 2014;29(3):301-7.
391. De Felice F, Izzo L, Musio D, Magnante AL, Bulzonetti N, Pugliese F, et al. Clinical predictive factors of pathologic complete response in locally advanced rectal cancer. *Oncotarget*. 2016;7(22):33374.
392. Patel SV, Roxburgh CS, Vakiani E, Shia J, Smith JJ, Temple LK, et al. Distance to the anal verge is associated with pathologic complete response to neoadjuvant therapy in locally advanced rectal cancer. *Journal of Surgical Oncology*. 2016;114(5):637-41.
393. Han YD, Kim WR, Park SW, Cho MS, Hur H, Min BS, et al. Predictors of pathologic complete response in rectal cancer patients undergoing total mesorectal excision after preoperative chemoradiation. *Medicine*. 2015;94(45).

394. Das P, Skibber JM, Rodriguez-Bigas MA, Feig BW, Chang GJ, Wolff RA, et al. Predictors of tumor response and downstaging in patients who receive preoperative chemoradiation for rectal cancer. *Cancer*. 2007;109(9):1750-5.
395. Al-Sukhni E, Attwood K, Mattson DM, Gabriel E, Nurkin SJ. Predictors of pathologic complete response following neoadjuvant chemoradiotherapy for rectal cancer. *Annals of Surgical Oncology*. 2016;23(4):1177-86.
396. Reggiani Bonetti L, Lioni S, Domati F, Pagliani G, Mattioli E, Barresi V. Histological grading based on poorly differentiated clusters is predictive of tumour response and clinical outcome in rectal carcinoma treated with neoadjuvant chemoradiotherapy. *Histopathology*. 2017;71(3):393-405.
397. Qiu HZ, Wu B, Xiao Y, Lin GL. Combination of differentiation and T stage can predict unresponsiveness to neoadjuvant therapy for rectal cancer. *Colorectal Disease*. 2011;13(12):1353-60.
398. McCawley N, Clancy C, O'Neill BD, Deasy J, McNamara DA, Burke JP. Mucinous rectal adenocarcinoma is associated with a poor response to neoadjuvant chemoradiotherapy: a systematic review and meta-analysis. *Diseases of the Colon & Rectum*. 2016;59(12):1200-8.
399. Du D, Su Z, Wang D, Liu W, Wei Z. Optimal interval to surgery after neoadjuvant chemoradiotherapy in rectal cancer: a systematic review and meta-analysis. *Clinical colorectal cancer*. 2018;17(1):13-24.
400. Maffione A, Chondrogiannis S, Capirci C, Galeotti F, Fornasiero A, Crepaldi G, et al. Early prediction of response by 18F-FDG PET/CT during preoperative therapy in locally advanced rectal cancer: a systematic review. *European Journal of Surgical Oncology (EJSO)*. 2014;40(10):1186-94.
401. Martoni A, Di Fabio F, Pinto C, Castellucci P, Pini S, Ceccarelli C, et al. Prospective study on the FDG-PET/CT predictive and prognostic values in patients treated with neoadjuvant chemoradiation therapy and radical surgery for locally advanced rectal cancer. *Annals of Oncology*. 2011;22(3):650-6.
402. Krug B, Crott R, de Canniere L, D'Hondt L, Vander Borght T. A systematic review of the predictive value of 18 F-fluoro-2-deoxyglucose positron emission tomography on survival in locally advanced rectal cancer after neoadjuvant chemoradiation. *Colorectal Disease*. 2013;15(11):e627-e33.
403. Barbaro B, Vitale R, Valentini V, Illuminati S, Vecchio FM, Rizzo G, et al. Diffusion-weighted magnetic resonance imaging in monitoring rectal cancer response to neoadjuvant chemoradiotherapy. *International Journal of Radiation Oncology* Biology* Physics*. 2012;83(2):594-9.
404. Sun Y, Li J, Shen L, Wang X, Tong T, Gu Y. Predictive value of MRI-detected extramural vascular invasion in stage T3 rectal cancer patients before neoadjuvant chemoradiation. *Diagnostic and Interventional Radiology*. 2018;24(3):128.
405. Kim IY, You SH, Kim YW. Neutrophil-lymphocyte ratio predicts pathologic tumor response and survival after preoperative chemoradiation for rectal cancer. *BMC Surgery*. 2014;14(1):94.
406. Caputo D, Caricato M, Coppola A, La Vaccara V, Fiore M, Coppola R. Neutrophil to lymphocyte ratio (NLR) and derived neutrophil to lymphocyte ratio (d-NLR) predict non-responders and postoperative complications in patients undergoing radical surgery after neo-adjuvant radio-chemotherapy for rectal adenocarcinoma. *Cancer investigation*. 2016;34(9):440-51.
407. Sung S, Son SH, Park EY, Kay CS. Prognosis of locally advanced rectal cancer can be predicted more accurately using pre-and post-chemoradiotherapy neutrophil-lymphocyte ratios in patients who received preoperative chemoradiotherapy. *PloS one*. 2017;12(3):e0173955.
408. Ishikawa D, Nishi M, Takasu C, Kashihara H, Tokunaga T, Higashijima J, et al. The role of neutrophil-to-lymphocyte ratio on the effect of CRT for patients with rectal cancer. *in vivo*. 2020;34(2):863-8.

409. Nagasaki T, Akiyoshi T, Fujimoto Y, Konishi T, Nagayama S, Fukunaga Y, et al. Prognostic impact of neutrophil-to-lymphocyte ratio in patients with advanced low rectal cancer treated with preoperative chemoradiotherapy. *Digestive surgery*. 2015;32(6):496-503.
410. Shen J, Zhu Y, Wu W, Zhang L, Ju H, Fan Y, et al. Prognostic role of neutrophil-to-lymphocyte ratio in locally advanced rectal cancer treated with neoadjuvant chemoradiotherapy. *Medical science monitor: international medical journal of experimental and clinical research*. 2017;23:315.
411. Yeo S-G, Kim DY, Kim TH, Kim SY, Baek JY, Chang HJ, et al. Carbohydrate antigen 19-9 levels associated with pathological responses to preoperative chemoradiotherapy in rectal cancer. *Asian Pac J Cancer Prev*. 2014;15(13):5383-7.
412. Song J, Huang X, Chen Z, Chen M, Lin Q, Li A, et al. Predictive value of carcinoembryonic antigen and carbohydrate antigen 19-9 related to downstaging to stage 0–I after neoadjuvant chemoradiotherapy in locally advanced rectal cancer. *Cancer Management and Research*. 2018;10:3101.
413. Carpinetti P, Donnard E, Bettoni F, Asprino P, Koyama F, Rozanski A, et al. The use of personalized biomarkers and liquid biopsies to monitor treatment response and disease recurrence in locally advanced rectal cancer after neoadjuvant chemoradiation. *Oncotarget*. 2015;6(35):38360.
414. Sclafani F, Chau I, Cunningham D, Hahne JC, Vlachogiannis G, Eltahir Z, et al. KRAS and BRAF mutations in circulating tumour DNA from locally advanced rectal cancer. *Scientific Reports*. 2018;8(1):1445.
415. Spitz FR, Giacco GG, Hess K, Larry L, Rich TA, Janjan N, et al. p53 immunohistochemical staining predicts residual disease after chemoradiation in patients with high-risk rectal cancer. *Clinical Cancer Research*. 1997;3(10):1685-90.
416. Hur H, Kim NK, Min BS, Baik SH, Lee KY, Koom WS, et al. Can a biomarker-based scoring system predict pathologic complete response after preoperative chemoradiotherapy for rectal cancer? *Diseases of the colon & rectum*. 2014;57(5):592-601.
417. Rebischung C, Gérard JP, Gayet J, Thomas G, Hamelin R, Laurent-Puig P. Prognostic value of P53 mutations in rectal carcinoma. *International journal of cancer*. 2002;100(2):131-5.
418. Duldulao MP, Lee W, Nelson RA, Li W, Chen Z, Kim J, et al. Mutations in specific codons of the KRAS oncogene are associated with variable resistance to neoadjuvant chemoradiation therapy in patients with rectal adenocarcinoma. *Annals of surgical oncology*. 2013;20(7):2166-71.
419. Garcia-Aguilar J, Chen Z, Smith DD, Li W, Madoff RD, Cataldo P, et al. Identification of a biomarker profile associated with resistance to neoadjuvant chemoradiation therapy in rectal cancer. *Annals of surgery*. 2011;254(3):486.
420. Jiang D, Wang X, Wang Y, Philips D, Meng W, Xiong M, et al. Mutation in BRAF and SMAD4 associated with resistance to neoadjuvant chemoradiation therapy in locally advanced rectal cancer. *Virchows Archiv*. 2019;475(1):39-47.
421. Hanssen-Bauer A, Solvang-Garten K, Akbari M, Otterlei M. X-ray repair cross complementing protein 1 in base excision repair. *International journal of molecular sciences*. 2012;13(12):17210-29.
422. Guzman MJ, Shao J, Sheng H. Pro-neoplastic effects of amphiregulin in colorectal carcinogenesis. *Journal of gastrointestinal cancer*. 2013;44(2):211-21.
423. Xu Q, Long Q, Zhu D, Fu D, Zhang B, Han L, et al. Targeting amphiregulin (AREG) derived from senescent stromal cells diminishes cancer resistance and averts programmed cell death 1 ligand (PD-L1)-mediated immunosuppression. *Aging cell*. 2019;18(6):e13027.
424. Yin M, Yan J, Martinez-Balibrea E, Graziano F, Lenz H-J, Kim H-J, et al. ERCC1 and ERCC2 Polymorphisms Predict Clinical Outcomes of Oxaliplatin-Based Chemotherapies in Gastric and Colorectal Cancer: A Systemic Review and Meta-analysisNER Gene Polymorphisms and Platinum Therapy. *Clinical cancer research*. 2011;17(6):1632-40.
425. Jeong JH, Hong YS, Park Y, Kim J, Kim JE, Kim K-p, et al. Phase 1 study of preoperative chemoradiation therapy with temozolomide and capecitabine in patients with

- locally advanced rectal cancer. *International Journal of Radiation Oncology* Biology* Physics*. 2016;96(2):289-95.
426. Cai X, Yao Z, Li L, Huang J. Role of DKK4 in tumorigenesis and tumor progression. *International journal of biological sciences*. 2018;14(6):616.
427. Su C-W, Lin C-W, Yang W-E, Yang S-F. TIMP-3 as a therapeutic target for cancer. *Therapeutic advances in medical oncology*. 2019;11:1758835919864247.
428. Tsang J, Vencken S, Sharaf O, Leen E, Kay E, McNamara D, et al. Global DNA methylation is altered by neoadjuvant chemoradiotherapy in rectal cancer and may predict response to treatment—a pilot study. *European Journal of Surgical Oncology (EJSO)*. 2014;40(11):1459-66.
429. Gaedcke J, Leha A, Claus R, Weichenhan D, Jung K, Kitz J, et al. Identification of a DNA methylation signature to predict disease-free survival in locally advanced rectal cancer. *Oncotarget*. 2014;5(18):8123.
430. Exner R, Pulverer W, Diem M, Spaller L, Woltering L, Schreiber M, et al. Potential of DNA methylation in rectal cancer as diagnostic and prognostic biomarkers. *British journal of cancer*. 2015;113(7):1035-45.
431. Garajová I, Slabý O, Svoboda M, Fabian P, Silák J, Smerdová T, et al. Gene expression profiling in prediction of tumor response to neoadjuvant concomitant chemoradiotherapy in patients with locally advanced rectal carcinoma: pilot study. *Casopis lekaru ceskych*. 2008;147(7):381-6.
432. Palma P, Cano C, Conde-Muiño R, Comino A, Bueno P, Ferrón JA, et al. Expression profiling of rectal tumors defines response to neoadjuvant treatment related genes. *PloS one*. 2014;9(11):e112189.
433. Conde-Muiño R, Cano C, Sánchez-Martín V, Herrera A, Comino A, Medina PP, et al. Preoperative chemoradiotherapy for rectal cancer: the sensitizer role of the association between miR-375 and c-Myc. *Oncotarget*. 2017;8(47):82294.
434. D'Angelo E, Fassan M, Maretto I, Pucciarelli S, Zanon C, Digito M, et al. Serum miR-125b is a non-invasive predictive biomarker of the pre-operative chemoradiotherapy responsiveness in patients with rectal adenocarcinoma. *Oncotarget*. 2016;7(19):28647.
435. D'Angelo E, Zanon C, Sensi F, Digito M, Rugge M, Fassan M, et al. miR-194 as predictive biomarker of responsiveness to neoadjuvant chemoradiotherapy in patients with locally advanced rectal adenocarcinoma. *Journal of clinical pathology*. 2018;71(4):344-50.
436. Drebber U, Lay M, Wedemeyer I, VALLböHMER D, Bollschweiler E, Brabender J, et al. Altered levels of the onco-microRNA 21 and the tumor-suppressor microRNAs 143 and 145 in advanced rectal cancer indicate successful neoadjuvant chemoradiotherapy. *International journal of oncology*. 2011;39(2):409-15.
437. Du B, Wang X, Wu D, Wang T, Yang X, Wang J, et al. MicroRNA expression profiles identify biomarkers for predicting the response to chemoradiotherapy in rectal cancer. *Molecular medicine reports*. 2018;18(2):1909-16.
438. Machackova T, Trachtova K, Prochazka V, Grolich T, Farkasova M, Fiala L, et al. Tumor microRNAs Identified by Small RNA Sequencing as Potential Response Predictors in Locally Advanced Rectal Cancer Patients Treated With Neoadjuvant Chemoradiotherapy. *Cancer Genomics-Proteomics*. 2020;17(3):249-57.
439. Svoboda M, Sana J, Fabian P, Kocakova I, Gombosova J, Nekvindova J, et al. MicroRNA expression profile associated with response to neoadjuvant chemoradiotherapy in locally advanced rectal cancer patients. *Radiation oncology*. 2012;7(1):195.
440. Casado E, García VM, Sánchez JJ, Blanco M, Maurel J, Feliu J, et al. A combined strategy of SAGE and quantitative PCR provides a 13-gene signature that predicts preoperative chemoradiotherapy response and outcome in rectal cancer. *Clinical Cancer Research*. 2011;17(12):4145-54.
441. Li Y, Castellano JJ, Moreno I, Martínez-Rodenas F, Hernandez R, Canals J, et al. LincRNA-p21 Levels Relates to Survival and Post-Operative Radiotherapy Benefit in Rectal Cancer Patients. *Life*. 2020;10(9):172.

442. Benitez JC, Campayo M, Díaz T, Ferrer C, Acosta-Plasencia M, Monzo M, et al. Lincp21-RNA as Predictive Response Marker for Preoperative Chemoradiotherapy in Rectal Cancer. *Journal of Personalized Medicine*. 2021;11(5):420.
443. Wong MH, Xue A, Baxter RC, Pavlakis N, Smith RC. Upstream and downstream co-inhibition of mitogen-activated protein kinase and PI3K/Akt/mTOR pathways in pancreatic ductal adenocarcinoma. *Neoplasia*. 2016;18(7):425-35.
444. So A, Dardillac E, Muhammad A, Chailleux C, Sesma-Sanz L, Ragu S, et al. RAD51 protects against nonconservative DNA double-strand break repair through a nonenzymatic function. *Nucleic acids research*. 2022;50(5):2651-66.
445. Du L, Wang H, He L, Zhang J, Ni B, Wang X, et al. CD44 is of functional importance for colorectal cancer stem cells. *Clinical cancer research*. 2008;14(21):6751-60.
446. Feeney G, Sehgal R, Sheehan M, Hogan A, Regan M, Joyce M, et al. Neoadjuvant radiotherapy for rectal cancer management. *World journal of gastroenterology*. 2019;25(33):4850.
447. Carlson JJ, Roth JA. The impact of the Oncotype Dx breast cancer assay in clinical practice: a systematic review and meta-analysis. *Breast cancer research and treatment*. 2013;141(1):13-22.
448. Welsh JB, Sapinoso LM, Su AI, Kern SG, Wang-Rodriguez J, Moskaluk CA, et al. Analysis of gene expression identifies candidate markers and pharmacological targets in prostate cancer. *Cancer research*. 2001;61(16):5974-8.
449. Subramanian A, Tamayo P, Mootha VK, Mukherjee S, Ebert BL, Gillette MA, et al. Gene set enrichment analysis: a knowledge-based approach for interpreting genome-wide expression profiles. *Proceedings of the National Academy of Sciences*. 2005;102(43):15545-50.
450. Mootha VK, Lindgren CM, Eriksson K-F, Subramanian A, Sihag S, Lehar J, et al. PGC-1 α -responsive genes involved in oxidative phosphorylation are coordinately downregulated in human diabetes. *Nature genetics*. 2003;34(3):267-73.
451. Davies MN, Meaburn EL, Schalkwyk LC. Gene set enrichment; a problem of pathways. *Briefings in functional genomics*. 2010;9(5-6):385-90.
452. Yoshihara K, Shahmoradgoli M, Martínez E, Vegesna R, Kim H, Torres-Garcia W, et al. Inferring tumour purity and stromal and immune cell admixture from expression data. *Nature communications*. 2013;4(1):1-11.
453. Yu W-D, Peng Y-F, Pan H-D, Wang L, Li K, Gu J. Phosphatidylinositol 3-kinase CB association with preoperative radiotherapy response in rectal adenocarcinoma. *World journal of gastroenterology: WJG*. 2014;20(43):16258.
454. Do Canto LM, Barros-Filho MC, Rainho CA, Marinho D, Kupper BEC, Begnami MDFdS, et al. Comprehensive Analysis of DNA Methylation and Prediction of Response to Neoadjuvant Therapy in Locally Advanced Rectal Cancer. *Cancers*. 2020;12(11):3079.
455. Lee TH, Perrem K, Harper JW, Lu KP, Zhou XZ. The F-box protein FBX4 targets PIN2/TRF1 for ubiquitin-mediated degradation and regulates telomere maintenance. *Journal of Biological Chemistry*. 2006;281(2):759-68.
456. Zhang Y, Xu M, Chen J, Chen K, Zhuang J, Yang Y, et al. Prognostic value of the FOXK family expression in patients with locally advanced rectal cancer following neoadjuvant chemoradiotherapy. *OncoTargets and therapy*. 2020;13:9185.
457. National Library of Medicine. ATF6B activating transcription factor 6 beta [Homo sapiens (human)] [internet].no date [cited 2022 March 02]. Available from: <https://www.ncbi.nlm.nih.gov/gene/1388>.
458. National Library of Medicine. SERPINH1 serpin family H member 1 [Homo sapiens (human)] [internet].no date [cited 2022 March 02]. Available from: <https://www.ncbi.nlm.nih.gov/gene/871>.
459. National Library of Medicine. PHACTR4 phosphatase and actin regulator 4 [Homo sapiens (human)] [internet].no date [cited 2022 March 02]. Available from: <https://www.ncbi.nlm.nih.gov/gene/65979>.

460. National Library of Medicine. YRDC yrdC N6-threonylcarbamoyltransferase domain containing [Homo sapiens (human)] [internet].no date [cited 2022 March 02]. Available from: <https://www.ncbi.nlm.nih.gov/gene/79693>.
461. National Library of Medicine. B2M beta-2-microglobulin [Homo sapiens (human)] [internet].no date [cited 2022 March 02]. Available from: <https://www.ncbi.nlm.nih.gov/gene/567>.
462. National Library of Medicine. PDIA3 protein disulfide isomerase family A member 3 [Homo sapiens (human)] [internet].no date [cited 2022 March 02]. Available from: [ncbi.nlm.nih.gov/gene/2923](https://www.ncbi.nlm.nih.gov/gene/2923).
463. Frederick M, Skinner HD, Kazi SA, Sikora AG, Sandulache VC. High expression of oxidative phosphorylation genes predicts improved survival in squamous cell carcinomas of the head and neck and lung. *Scientific reports*. 2020;10(1):1-14.
464. Ju F, Li N, Wang W, Yuan H. Effects of varying radiation dosages on MMP1 expression, and MMP1 knockdown on the viability and migration of SW620 cells. *Molecular medicine reports*. 2019;19(4):2503-8.
465. Egerman MA, Glass DJ. Signaling pathways controlling skeletal muscle mass. *Critical reviews in biochemistry and molecular biology*. 2014;49(1):59-68.
466. Manning BD, Toker A. AKT/PKB signaling: navigating the network. *Cell*. 2017;169(3):381-405.
467. Gudkov AV, Komarova EA. The role of p53 in determining sensitivity to radiotherapy. *Nature Reviews Cancer*. 2003;3(2):117-29.
468. Gallo O, Chiarelli I, Boddi V, Bocciolini C, Bruschini L, Porfirio B. Cumulative prognostic value of p53 mutations and bcl-2 protein expression in head-and-neck cancer treated by radiotherapy. *International journal of cancer*. 1999;84(6):573-9.
469. Viktorsson K, De Petris L, Lewensohn R. The role of p53 in treatment responses of lung cancer. *Biochemical and biophysical research communications*. 2005;331(3):868-80.
470. Pawlik TM, Keyomarsi K. Role of cell cycle in mediating sensitivity to radiotherapy. *International Journal of Radiation Oncology* Biology* Physics*. 2004;59(4):928-42.
471. Tavassoli M, Suh Y-e. Hypoxia in Head and Neck Cancer. *Squamous cell Carcinoma*: Springer; 2017. p. 59-95.
472. Nayak AP, Kapur A, Barroilhet L, Patankar MS. Oxidative phosphorylation: a target for novel therapeutic strategies against ovarian cancer. *Cancers*. 2018;10(9):337.
473. Ashton TM, McKenna WG, Kunz-Schughart LA, Higgins GS. Oxidative phosphorylation as an emerging target in cancer therapy. *Clinical Cancer Research*. 2018;24(11):2482-90.
474. Ganci F, Sacconi A, Mancio V, Spriano G, Fontemaggi G, Carlini P, et al. Radioresistance in head and neck squamous cell carcinoma—possible molecular markers for local recurrence and new putative therapeutic strategies. *Contemp Issues Head Neck Cancer Manag*. 2015;37:763-70.
475. Moeller B, Dewhirst M. HIF-1 and tumour radiosensitivity. *British journal of cancer*. 2006;95(1):1-5.
476. Mortezaee K, Parwaie W, Motevaseli E, Mirtavoos-Mahyari H, Musa AE, Shabeeb D, et al. Targets for improving tumor response to radiotherapy. *International immunopharmacology*. 2019;76:105847.
477. Saito N, Aoki K, Hirai N, Fujita S, Iwama J, Hiramoto Y, et al. Effect of Notch expression in glioma stem cells on therapeutic response to chemo-radiotherapy in recurrent glioblastoma. *Brain tumor pathology*. 2015;32(3):176-83.
478. Giuranno L, Wansleeben C, Iannone R, Arathoon L, Hounjet J, Groot AJ, et al. NOTCH signaling promotes the survival of irradiated basal airway stem cells. *American Journal of Physiology-Lung Cellular and Molecular Physiology*. 2019;317(3):L414-L23.
479. Shen ED, Zeng Q. Inhibition of the Numb/Notch signaling pathway increases radiation sensitivity in human nasopharyngeal carcinoma cells. *The Kaohsiung journal of medical sciences*. 2019;35(8):474-85.

480. Peng JH, Wang XL, Ran L, Song JL, Zhang ZT, Liu X, et al. Inhibition of Notch signaling pathway enhanced the radiosensitivity of breast cancer cells. *Journal of cellular biochemistry*. 2018;119(10):8398-409.
481. Lee SY, Jeong EK, Ju MK, Jeon HM, Kim MY, Kim CH, et al. Induction of metastasis, cancer stem cell phenotype, and oncogenic metabolism in cancer cells by ionizing radiation. *Molecular cancer*. 2017;16(1):1-25.
482. Zhou S, Zhang M, Zhou C, Wang W, Yang H, Ye W. The role of epithelial-mesenchymal transition in regulating radioresistance. *Critical reviews in oncology/hematology*. 2020;150:102961.
483. Farhood B, Hoseini-Ghahfarokhi M, Motevaseli E, Mirtavoos-Mahyari H, Musa AE, Najafi M. TGF- β in radiotherapy: Mechanisms of tumor resistance and normal tissues injury. *Pharmacological research*. 2020;155:104745.
484. Heldin C-H, Landström M, Moustakas A. Mechanism of TGF- β signaling to growth arrest, apoptosis, and epithelial-mesenchymal transition. *Current opinion in cell biology*. 2009;21(2):166-76.
485. Andarawewa KL, Paupert J, Pal A, Barcellos-Hoff MH. New rationales for using TGF beta inhibitors in radiotherapy. *International journal of radiation biology*. 2007;83(11-12):803-11.
486. Ozes ON, Mayo LD, Gustin JA, Pfeffer SR, Pfeffer LM, Donner DB. NF- κ B activation by tumour necrosis factor requires the Akt serine-threonine kinase. *Nature*. 1999;401(6748):82-5.
487. Meng F, D'Mello SR. NF- κ B stimulates Akt phosphorylation and gene expression by distinct signaling mechanisms. *Biochimica et Biophysica Acta (BBA)-Gene Structure and Expression*. 2003;1630(1):35-40.
488. Wang H, Wang H, Zhang W, Huang HJ, Liao WS, Fuller GN. Analysis of the activation status of Akt, NF κ B, and Stat3 in human diffuse gliomas. *Laboratory investigation*. 2004;84(8):941-51.
489. Watson C, Miller DA, Chin-Sinex H, Losch A, Hughes W, Sweeney C, et al. Suppression of NF- κ B activity by parthenolide induces X-ray sensitivity through inhibition of split-dose repair in TP53 null prostate cancer cells. *Radiation research*. 2009;171(4):389-96.
490. Jiang N, Dai Q, Su X, Fu J, Feng X, Peng J. Role of PI3K/AKT pathway in cancer: the framework of malignant behavior. *Molecular biology reports*. 2020;47(6):4587-629.
491. Xu F, Na L, Li Y, Chen L. Roles of the PI3K/AKT/mTOR signalling pathways in neurodegenerative diseases and tumours. *Cell & bioscience*. 2020;10:1-12.
492. Aasebø K, Dragomir A, Sundström M, Mezheyeuski A, Edqvist P-H, Eide GE, et al. CDX2: a prognostic marker in metastatic colorectal cancer defining a better BRAF mutated and a worse KRAS mutated subgroup. *Frontiers in oncology*. 2020;10:8.
493. Dalerba P, Sahoo D, Paik S, Guo X, Yothers G, Song N, et al. CDX2 as a prognostic biomarker in stage II and stage III colon cancer. *New England Journal of Medicine*. 2016;374(3):211-22.
494. Kohonen-Corish MR, Daniel JJ, Chan C, Lin BP, Kwun SY, Dent OF, et al. Low microsatellite instability is associated with poor prognosis in stage C colon cancer. *Journal of Clinical Oncology*. 2005;23(10):2318-24.
495. Martellucci J, Alemanno G, Castiglione F, Bergamini C, Valeri A. Role of KRAS mutation as predictor of pathologic response after neoadjuvant chemoradiation therapy for rectal cancer. *Updates in surgery*. 2015;67(1):47-53.
496. Derbel O, Wang Q, Desseigne F, Rivoire M, Meeus P, Peyrat P, et al. Impact of KRAS, BRAF and PI3KCA mutations in rectal carcinomas treated with neoadjuvant radiochemotherapy and surgery. *BMC cancer*. 2013;13(1):1-6.
497. Gaedcke J, Grade M, Jung K, Schirmer M, Jo P, Obermeyer C, et al. KRAS and BRAF mutations in patients with rectal cancer treated with preoperative chemoradiotherapy. *Radiotherapy and Oncology*. 2010;94(1):76-81.
498. Busch M, Dünker N. Trefoil factor family peptides—friends or foes? *Biomolecular concepts*. 2015;6(5-6):343-59.

499. Im S, Yoo C, Jung J-H, Choi HJ, Yoo J, Kang CS. Reduced expression of TFF1 and increased expression of TFF3 in gastric cancer: correlation with clinicopathological parameters and prognosis. *International journal of medical sciences*. 2013;10(2):133.
500. Cheung AKL, Ko JM, Lung HL, Chan KW, Stanbridge EJ, Zabarovsky E, et al. Cysteine-rich intestinal protein 2 (CRIP2) acts as a repressor of NF- κ B-mediated proangiogenic cytokine transcription to suppress tumorigenesis and angiogenesis. *Proceedings of the National Academy of Sciences*. 2011;108(20):8390-5.
501. Lo PHY, Ko JMY, Yu ZY, Law S, Wang LD, Li J-L, et al. The LIM domain protein, CRIP2, promotes apoptosis in esophageal squamous cell carcinoma. *Cancer letters*. 2012;316(1):39-45.
502. Li F, Bing Z, Chen W, Ye F, Liu Y, Ding L, et al. Prognosis biomarker and potential therapeutic target CRIP2 associated with radiosensitivity in NSCLC cells. *Biochemical and biophysical research communications*. 2021.
503. Ahmed KM, Li JJ. NF- κ B-mediated adaptive resistance to ionizing radiation. *Free Radical Biology and Medicine*. 2008;44(1):1-13.
504. Xia X, Cao F, Yuan X, Zhang Q, Chen W, Yu Y, et al. Low expression or hypermethylation of PLK2 might predict favorable prognosis for patients with glioblastoma multiforme. *PeerJ*. 2019;7:e7974.
505. Krüger M, Amort J, Wilgenbus P, Helmstaedter JP, Grechowa I, Ebert J, et al. The anti-apoptotic PON2 protein is Wnt/ β -catenin-regulated and correlates with radiotherapy resistance in OSCC patients. *Oncotarget*. 2016;7(32):51082.
506. Shannan B, Seifert M, Boothman D, Tilgen W, Reichrath J. Clusterin and DNA repair: a new function in cancer for a key player in apoptosis and cell cycle control. *Journal of molecular histology*. 2006;37(5-7):183-8.
507. He LR, Liu MZ, Li BK, Rao HL, Liao YJ, Zhang LJ, et al. Clusterin as a predictor for chemoradiotherapy sensitivity and patient survival in esophageal squamous cell carcinoma. *Cancer science*. 2009;100(12):2354-60.
508. García-Aranda M, Téllez T, Muñoz M, Redondo M. Clusterin inhibition mediates sensitivity to chemotherapy and radiotherapy in human cancer. *Anti-cancer drugs*. 2017;28(7):702-16.
509. Barderas R, Mendes M, Torres S, Bartolomé RA, López-Lucendo M, Villar-Vázquez R, et al. In-depth characterization of the secretome of colorectal cancer metastatic cells identifies key proteins in cell adhesion, migration, and invasion. *Molecular & Cellular Proteomics*. 2013;12(6):1602-20.
510. He J, Huang H, Du Y, Peng D, Zhou Y, Li Y, et al. Association of DCBLD2 upregulation with tumor progression and poor survival in colorectal cancer. *Cellular Oncology (2211-3428)*. 2020;43(3).
511. Yu J, Ka S-O, Kwon K-B, Lee S-M, Park J-W, Park B-H. Overexpression of the small GTPase Arl4D suppresses adipogenesis. *International journal of molecular medicine*. 2011;28(5):793-8.
512. Yu W, Zhang L, Wei Q, Shao A. O6-methylguanine-DNA methyltransferase (MGMT): challenges and new opportunities in glioma chemotherapy. *Frontiers in oncology*. 2020;9:1547.
513. Shalaby SM, Amal S, Abdelaziz LA, Abd-Elbary E, Khairy MM. Promoter methylation and expression of DNA repair genes MGMT and ERCC1 in tissue and blood of rectal cancer patients. *Gene*. 2018;644:66-73.
514. Rivera AL, Pelloski CE, Gilbert MR, Colman H, De La Cruz C, Sulman EP, et al. MGMT promoter methylation is predictive of response to radiotherapy and prognostic in the absence of adjuvant alkylating chemotherapy for glioblastoma. *Neuro-oncology*. 2010;12(2):116-21.
515. Thon N, Eigenbrod S, Grasbon-Frodl EM, Lutz J, Kreth S, Popperl G, et al. Predominant influence of MGMT methylation in non-resectable glioblastoma after radiotherapy plus temozolomide. *Journal of Neurology, Neurosurgery & Psychiatry*. 2011;82(4):441-6.

516. Wang X-Y, Chen S-H, Zhang Y-N, Xu C-F. Olfactomedin-4 in digestive diseases: a mini-review. *World journal of gastroenterology*. 2018;24(17):1881.
517. Kontos C, Papadopoulos I, Fragoulis E, Scorilas A. Quantitative expression analysis and prognostic significance of L-DOPA decarboxylase in colorectal adenocarcinoma. *British journal of cancer*. 2010;102(9):1384-90.
518. Zawadzka I, Jeleń A, Pietrzak J, Żebrowska-Nawrocka M, Michalska K, Szmajda-Krygier D, et al. The impact of ABCB1 gene polymorphism and its expression on non-small-cell lung cancer development, progression and therapy—preliminary report. *Scientific reports*. 2020;10(1):1-10.
519. Cecchin E, Agostini M, Pucciarelli S, De Paoli A, Canzonieri V, Sigon R, et al. Tumor response is predicted by patient genetic profile in rectal cancer patients treated with neo-adjuvant chemo-radiotherapy. *The pharmacogenomics journal*. 2011;11(3):214-26.
520. Kitagishi Y, Matsuda S. RUFY, Rab and Rap family proteins involved in a regulation of cell polarity and membrane trafficking. *International journal of molecular sciences*. 2013;14(3):6487-98.
521. Yuanhua L, Pudong Q, Wei Z, Yuan W, Delin L, Yan Z, et al. TFAP2A induced KRT16 as an oncogene in lung adenocarcinoma via EMT. *International journal of biological sciences*. 2019;15(7):1419.
522. Stene C, Polistena A, Gaber A, Nodin B, Ottochian B, Adawi D, et al. MMP7 modulation by short-and long-term radiotherapy in patients with rectal cancer. *in vivo*. 2018;32(1):133-8.
523. Bi Z, Li Q, Dinglin X, Xu Y, You K, Hong H, et al. Nanoparticles (NPs)-Mediated LncRNA AFAP1-AS1 Silencing to Block Wnt/ β -Catenin Signaling Pathway for Synergistic Reversal of Radioresistance and Effective Cancer Radiotherapy. *Advanced Science*. 2020;7(18):2000915.
524. Pyagay P, Heroult M, Wang Q, Lehnert W, Belden J, Liaw L, et al. Collagen triple helix repeat containing 1, a novel secreted protein in injured and diseased arteries, inhibits collagen expression and promotes cell migration. *Circulation research*. 2005;96(2):261-8.
525. Tang L, Dai DL, Su M, Martinka M, Li G, Zhou Y. Aberrant expression of collagen triple helix repeat containing 1 in human solid cancers. *Clinical cancer research*. 2006;12(12):3716-22.
526. Wang P, Wang YC, Chen XY, Shen ZY, Cao H, Zhang YJ, et al. CTHRC1 is upregulated by promoter demethylation and transforming growth factor- β 1 and may be associated with metastasis in human gastric cancer. *Cancer science*. 2012;103(7):1327-33.
527. Ni S, Ren F, Xu M, Tan C, Weng W, Huang Z, et al. CTHRC1 overexpression predicts poor survival and enhances epithelial-mesenchymal transition in colorectal cancer. *Cancer medicine*. 2018;7(11):5643-54.
528. Ketteler J, Klein D. Caveolin-1, cancer and therapy resistance. *International journal of cancer*. 2018;143(9):2092-104.
529. Hehlhans S, Eke I, Storch K, Haase M, Baretton GB, Cordes N. Caveolin-1 mediated radioresistance of 3D grown pancreatic cancer cells. *Radiotherapy and Oncology*. 2009;92(3):362-70.
530. Klein D, Schmitz T, Verhelst V, Panic A, Schenck M, Reis H, et al. Endothelial Caveolin-1 regulates the radiation response of epithelial prostate tumors. *Oncogenesis*. 2015;4(5):e148-e.
531. Williams TM, Lisanti MP. The Caveolin genes: from cell biology to medicine. *Annals of medicine*. 2004;36(8):584-95.
532. Cao M, Cai J, Yuan Y, Shi Y, Wu H, Liu Q, et al. A four-gene signature-derived risk score for glioblastoma: prospects for prognostic and response predictive analyses. *Cancer biology & medicine*. 2019;16(3):595.
533. Brown CO, Schibler J, Fitzgerald MP, Singh N, Salem K, Zhan F, et al. Scavenger receptor class A member 3 (SCARA3) in disease progression and therapy resistance in multiple myeloma. *Leukemia research*. 2013;37(8):963-9.

534. Kocer B, Soran A, Erdogan S, Karabeyoglu M, Yildirim O, Eroglu A, et al. Expression of MUC5AC in colorectal carcinoma and relationship with prognosis. *Pathology international*. 2002;52(7):470-7.
535. Peng L, Tu P, Wang X, Shi S, Zhou X, Wang J. Loss of EphB6 protein expression in human colorectal cancer correlates with poor prognosis. *Journal of molecular histology*. 2014;45(5):555-63.
536. Cundy T, Hegde M, Naot D, Chong B, King A, Wallace R, et al. A mutation in the gene TNFRSF11B encoding osteoprotegerin causes an idiopathic hyperphosphatasia phenotype. *Human Molecular Genetics*. 2002;11(18):2119-27.
537. Yuan S, Li L, Xiang S, Jia H, Luo T. Cadherin-11 is inactivated due to promoter methylation and functions in colorectal cancer as a tumour suppressor. *Cancer management and research*. 2019;11:2517.
538. Steinbrecher KA, Harmel-Laws E, Garin-Laflam MP, Mann EA, Bezerra LD, Hogan SP, et al. Murine guanylate cyclase C regulates colonic injury and inflammation. *The Journal of Immunology*. 2011;186(12):7205-14.
539. Witek M, Snook A, Magee M, Waldman S. Single Dose Tumor Irradiation Primes the Immune System for Therapeutic Cancer Vaccination. *International Journal of Radiation Oncology, Biology, Physics*. 2013;87(2):S109.
540. Fu Z-c, Wang F-m, Cai J-m. Gene expression changes in residual advanced cervical cancer after radiotherapy: indicators of poor prognosis and radioresistance? *Medical science monitor: international medical journal of experimental and clinical research*. 2015;21:1276.
541. Witte G, Urbanke C, Curth U. DNA polymerase III χ subunit ties single-stranded DNA binding protein to the bacterial replication machinery. *Nucleic acids research*. 2003;31(15):4434-40.
542. Park S, Lee H, Lee B, Lee S-H, Sun J-M, Park W-Y, et al. Dna damage response and repair pathway alteration and its association with tumor mutation burden and platinum-based chemotherapy in SCLC. *Journal of Thoracic Oncology*. 2019;14(9):1640-50.
543. Zheng S, Wu Y, Li Z. Integrating cullin2-RING E3 ligase as a potential biomarker for glioblastoma multiforme prognosis and radiosensitivity profiling. *Radiotherapy and Oncology*. 2021;154:36-44.
544. Yan Z, Cheng M, Hu G, Wang Y, Zeng S, Huang A, et al. Positive feedback of SuFu negating protein 1 on Hedgehog signaling promotes colorectal tumor growth. *Cell death & disease*. 2021;12(2):1-20.
545. Raducu M, Fung E, Serres S, Infante P, Barberis A, Fischer R, et al. SCF (Fbx17) ubiquitylation of Sufu regulates Hedgehog signaling and medulloblastoma development. *The EMBO journal*. 2016;35(13):1400-16.
546. Hehlgans S, Booms P, Güllülü Ö, Sader R, Rödel C, Balermipas P, et al. Radiation sensitization of basal cell and head and neck squamous cell carcinoma by the hedgehog pathway inhibitor vismodegib. *International journal of molecular sciences*. 2018;19(9):2485.
547. Meng E, Hanna A, Samant RS, Shevde LA. The impact of hedgehog signaling pathway on DNA repair mechanisms in human cancer. *Cancers*. 2015;7(3):1333-48.
548. Brunet S, Sacher M. In sickness and in health: the role of TRAPP and associated proteins in disease. *Traffic*. 2014;15(8):803-18.
549. Zhao S-L, Hong J, Xie Z-Q, Tang J-T, Su W-Y, Du W, et al. TRAPPC4-ERK2 interaction activates ERK1/2, modulates its nuclear localization and regulates proliferation and apoptosis of colorectal cancer cells. *PLoS One*. 2011;6(8):e23262.
550. Kong X, Qian J, Chen L-S, Wang Y-C, Wang J-L, Chen H, et al. Synbindin in extracellular signal-regulated protein kinase spatial regulation and gastric cancer aggressiveness. *Journal of the National Cancer Institute*. 2013;105(22):1738-49.
551. Abumansour IS, Iskandarani RM, Edrees A, Javed F, Taher F, Hakeem GF. Prenatal-onset INPPL1-related skeletal dysplasia in two unrelated families: Diagnosis and prediction of lethality. *Clinical Case Reports*. 2021;9(5):e04079.
552. Moreno-Smith M, Halder J, Meltzer PS, Gonda TA, Mangala LS, Rupaimoole R, et al. ATP11B mediates platinum resistance in ovarian cancer. *The Journal of clinical investigation*. 2013;123(5):2119-30.

553. Elsnerova K, Mohelnikova-Duchonova B, Cerovska E, Ehrlichova M, Gut I, Rob L, et al. Gene expression of membrane transporters: Importance for prognosis and progression of ovarian carcinoma. *Oncology reports*. 2016;35(4):2159-70.
554. Napoli C, Sessa M, Infante T, Casamassimi A. Unraveling framework of the ancestral Mediator complex in human diseases. *Biochimie*. 2012;94(3):579-87.
555. Hang Q, Zeng L, Wang L, Nie L, Yao F, Teng H, et al. Non-canonical function of DGCR8 in DNA double-strand break repair signaling and tumor radioresistance. *Nature communications*. 2021;12(1):1-18.
556. Zhang C, Chen H, Deng Z, Long D, Xu L, Liu Z. DGCR8/miR-106 Axis Enhances Radiosensitivity of Head and Neck Squamous Cell Carcinomas by Downregulating RUNX3. *Frontiers in Medicine*. 2020;7:880.
557. Lee J-W, Kim D-M, Jang J-W, Park T-G, Song S-H, Lee Y-S, et al. RUNX3 regulates cell cycle-dependent chromatin dynamics by functioning as a pioneer factor of the restriction-point. *Nature communications*. 2019;10(1):1-17.
558. Sopha P, Ren HY, Grove DE, Cyr DM. Endoplasmic reticulum stress-induced degradation of DNAJB12 stimulates BOK accumulation and primes cancer cells for apoptosis. *Journal of Biological Chemistry*. 2017;292(28):11792-803.
559. Marchitti SA, Orlicky DJ, Brocker C, Vasiliou V. Aldehyde dehydrogenase 3B1 (ALDH3B1): immunohistochemical tissue distribution and cellular-specific localization in normal and cancerous human tissues. *Journal of Histochemistry & Cytochemistry*. 2010;58(9):765-83.
560. Tsai M-H, Cook JA, Chandramouli GV, DeGraff W, Yan H, Zhao S, et al. Gene expression profiling of breast, prostate, and glioma cells following single versus fractionated doses of radiation. *Cancer research*. 2007;67(8):3845-52.
561. Khanna KK, Jackson SP. DNA double-strand breaks: signaling, repair and the cancer connection. *Nature genetics*. 2001;27(3):247-54.
562. Gaffney DK, Brohet RM, Lewis CM, Holden JA, Buys SS, Neuhausen SL, et al. Response to radiation therapy and prognosis in breast cancer patients with BRCA1 and BRCA2 mutations. *Radiotherapy and oncology*. 1998;47(2):129-36.
563. Pierce LJ, Strawderman M, Narod SA, Oliviotto I, Eisen A, Dawson L, et al. Effect of radiotherapy after breast-conserving treatment in women with breast cancer and germline BRCA1/2 mutations. *Journal of Clinical Oncology*. 2000;18(19):3360-9.
564. Nishimura Y, Kasahara K, Inagaki M. Intermediate filaments and IF-associated proteins: from cell architecture to cell proliferation. *Proceedings of the Japan Academy, Series B*. 2019;95(8):479-93.
565. Toustrup K, Sørensen BS, Nordmark M, Busk M, Wiuf C, Alsner J, et al. Development of a hypoxia gene expression classifier with predictive impact for hypoxic modification of radiotherapy in head and neck cancer. *Cancer research*. 2011;71(17):5923-31.
566. Lin S, Shen Z, Yang Y, Qiu Y, Wang Y, Wang X. Expression profiles of radio-resistant genes in colorectal cancer cells. *Radiation Medicine and Protection*. 2021;2(2):48-54.
567. Ooft SN, Weeber F, Dijkstra KK, McLean CM, Kaing S, van Werkhoven E, et al. Patient-derived organoids can predict response to chemotherapy in metastatic colorectal cancer patients. *Science translational medicine*. 2019;11(513).
568. Corley SM, Troy NM, Bosco A, Wilkins MR. QuantSeq. 3' Sequencing combined with Salmon provides a fast, reliable approach for high throughput RNA expression analysis. *Scientific reports*. 2019;9(1):1-15.
569. Vivanco I, Sawyers CL. The phosphatidylinositol 3-kinase-AKT pathway in human cancer. *Nature Reviews Cancer*. 2002;2(7):489.
570. Engelman JA, Luo J, Cantley LC. The evolution of phosphatidylinositol 3-kinases as regulators of growth and metabolism. *Nature Reviews Genetics*. 2006;7(8):606.
571. Rodriguez-Viciano P, Warne PH, Dhand R, Vanhaesebroeck B, Gout I, Fry MJ, et al. Phosphatidylinositol-3-OH kinase direct target of Ras. *Nature*. 1994;370(6490):527.

572. Chalhoub N, Baker SJ. PTEN and the PI3-kinase pathway in cancer. *Annual Review of Pathological Mechanical Disease*. 2009;4:127-50.
573. Prevo R, Deutsch E, Sampson O, Diplexcito J, Cengel K, Harper J, et al. Class I PI3 kinase inhibition by the pyridinylfuranopyrimidine inhibitor PI-103 enhances tumor radiosensitivity. *Cancer Research*. 2008;68(14):5915-23.
574. Ma L, Chen Z, Erdjument-Bromage H, Tempst P, Pandolfi PP. Phosphorylation and functional inactivation of TSC2 by Erk: implications for tuberous sclerosis and cancer pathogenesis. *Cell*. 2005;121(2):179-93.
575. Shaw RJ, Cantley LC. Ras, PI (3) K and mTOR signalling controls tumour cell growth. *Nature*. 2006;441(7092):424.
576. Sarbassov DD, Guertin DA, Ali SM, Sabatini DM. Phosphorylation and regulation of Akt/PKB by the rictor-mTOR complex. *Science*. 2005;307(5712):1098-101.
577. Romashkova JA, Makarov SS. NF- κ B is a target of AKT in anti-apoptotic PDGF signalling. *Nature*. 1999;401(6748):86.
578. Liu Q, Turner KM, Alfred Yung W, Chen K, Zhang W. Role of AKT signaling in DNA repair and clinical response to cancer therapy. *Neuro-oncology*. 2014;16(10):1313-23.
579. Choi YJ, Anders L. Signaling through cyclin D-dependent kinases. *Oncogene*. 2014;33(15):1890.
580. Zhang H, Wang S, Cacalano N, Zhu H, Liu Q, Xie M, et al. Oncogenic Y68 frame shift mutation of PTEN represents a mechanism of docetaxel resistance in endometrial cancer cell lines. *Scientific Reports*. 2019;9(1):2111.
581. Lockney NA, Yang TJ, Barron D, Gelb E, Gelblum DY, Yorke E, et al. PIK3CA mutation is associated with increased local failure in lung stereotactic body radiation therapy (SBRT). *Clinical Translational Radiation Oncology*. 2017;7:91.
582. Wang M, Han J, Marcar L, Black J, Liu Q, Li X, et al. Radiation Resistance in KRAS-Mutated Lung Cancer Is Enabled by Stem-like Properties Mediated by an Osteopontin-EGFR Pathway. *Cancer Research*. 2017;77(8):2018-28.
583. Konstantinidou G, Bey EA, Rabellino A, Schuster K, Maira MS, Gazdar AF, et al. Dual phosphoinositide 3-kinase/mammalian target of rapamycin blockade is an effective radiosensitizing strategy for the treatment of non-small cell lung cancer harboring K-RAS mutations. *Cancer Research*. 2009;69(19):7644-52.
584. Narayan P, Prowell TM, Gao JJ, Fernandes LL, Li E, Jiang X, et al. FDA Approval Summary: Alpelisib plus fulvestrant for patients with HR-positive, HER2-negative, PIK3CA-mutated, advanced or metastatic breast cancer. *Clinical Cancer Research*. 2020.
585. Baroja-Mazo A, Revilla-Nuin B, Ramírez P, Pons JA. Immunosuppressive potency of mechanistic target of rapamycin inhibitors in solid-organ transplantation. *World journal of transplantation*. 2016;6(1):183.
586. Klawitter J, Nashan B, Christians U. Everolimus and sirolimus in transplantation-related but different. *Expert opinion on drug safety*. 2015;14(7):1055-70.
587. Pal I, Dey KK, Chaurasia M, Parida S, Das S, Rajesh Y, et al. Cooperative effect of BI-69A11 and celecoxib enhances radiosensitization by modulating DNA damage repair in colon carcinoma. *Tumor Biology*. 2016;37(5):6389-402.
588. Djuzenova CS, Fiedler V, Katzer A, Michel K, Deckert S, Zimmermann H, et al. Dual PI3K-and mTOR-inhibitor PI-103 can either enhance or reduce the radiosensitizing effect of the Hsp90 inhibitor NVP-AUY922 in tumor cells: the role of drug-irradiation schedule. *Oncotarget*. 2016;7(25):38191.
589. Manegold PC, Paringer C, Kulka U, Krimmel K, Eichhorn ME, Wilkowski R, et al. Antiangiogenic therapy with mammalian target of rapamycin inhibitor RAD001 (Everolimus) increases radiosensitivity in solid cancer. *Clinical Cancer Research*. 2008;14(3):892-900.
590. Bertolini F, Pettorelli E, Meduri B, Zironi S, Fontana A, Gelsomino F, et al. A Phase Ib Study of Everolimus, 5-Fluorouracil (5-Fu) and Pelvic Radiotherapy (Rt) As Neo-Adjuvant Treatment for Locally Advanced Rectal Cancer (Larc). *Annals of Oncology*. 2014;25:iv202.
591. National Center for Biotechnology Information. PubChem Compound Summary for CID 3385, 5-Fluorouracil [internet].2021 [cited 2021 April 2]. Available from: <https://pubchem.ncbi.nlm.nih.gov/compound/5-Fluorouracil>.

592. National Center for Biotechnology Information. PubChem Compound Summary for CID 25254071, Apitolisib [internet].2021 [cited 2021 April 2]. Available from: <https://pubchem.ncbi.nlm.nih.gov/compound/Apitolisib>.
593. Sutherland DP, Bao L, Berry M, Castanedo G, Chuckowree I, Dotson J, et al. Discovery of a potent, selective, and orally available class I phosphatidylinositol 3-kinase (PI3K)/mammalian target of rapamycin (mTOR) kinase inhibitor (GDC-0980) for the treatment of cancer. *Journal of medicinal chemistry*. 2011;54(21):7579-87.
594. Powles T, Lackner MR, Oudard S, Escudier B, Ralph C, Brown JE, et al. Randomized open-label phase II trial of apitolisib (GDC-0980), a novel inhibitor of the PI3K/mammalian target of rapamycin pathway, versus everolimus in patients with metastatic renal cell carcinoma. *Journal of Clinical Oncology*. 2016;34(14):1660.
595. Makker V, Recio FO, Ma L, Matulonis UA, Lauchle JO, Parmar H, et al. A multicenter, single-arm, open-label, phase 2 study of apitolisib (GDC-0980) for the treatment of recurrent or persistent endometrial carcinoma (MAGGIE study). *Cancer*. 2016;122(22):3519-28.
596. Dolly SO, Wagner AJ, Bendell JC, Kindler HL, Krug LM, Seiwert TY, et al. Phase I study of apitolisib (GDC-0980), dual phosphatidylinositol-3-kinase and mammalian target of rapamycin kinase inhibitor, in patients with advanced solid tumors. *Clinical Cancer Research*. 2016;22(12):2874-84.
597. Maira S-M, Stauffer F, Brueggen J, Furet P, Schnell C, Fritsch C, et al. Identification and characterization of NVP-BEZ235, a new orally available dual phosphatidylinositol 3-kinase/mammalian target of rapamycin inhibitor with potent in vivo antitumor activity. *Molecular cancer therapeutics*. 2008;7(7):1851-63.
598. Fatehi D, Soltani A, Ghatrehsamani M. SRT1720, a potential sensitizer for radiotherapy and cytotoxicity effects of NVP-BEZ235 in metastatic breast cancer cells. *Pathology Research Practice*. 2018;214(6):889-95.
599. Kuger S, Cörek E, Polat B, Kämmerer U, Flentje M, Djuzenova CS. Novel PI3K and mTOR inhibitor NVP-BEZ235 radiosensitizes breast cancer cell lines under normoxic and hypoxic conditions. *Breast cancer: basic clinical research*. 2014;8:BCBCR. S13693.
600. Miyasaka A, Oda K, Ikeda Y, Sone K, Fukuda T, Inaba K, et al. PI3K/mTOR pathway inhibition overcomes radioresistance via suppression of the HIF1- α /VEGF pathway in endometrial cancer. *Gynecologic Oncology*. 2015;138(1):174-80.
601. Chang L, Graham P, Hao J, Ni J, Bucci J, Cozzi P, et al. PI3K/Akt/mTOR pathway inhibitors enhance radiosensitivity in radioresistant prostate cancer cells through inducing apoptosis, reducing autophagy, suppressing NHEJ and HR repair pathways. *Cell Death and Disease*. 2014;5(10):e1437.
602. Potiron VA, Abderrhamani R, Giang E, Chiavassa S, Di Tomaso E, Maira S-M, et al. Radiosensitization of prostate cancer cells by the dual PI3K/mTOR inhibitor BEZ235 under normoxic and hypoxic conditions. *Radiotherapy and Oncology*. 2013;106(1):138-46.
603. Zhu W, Fu W, Hu L. NVP-BEZ235, dual phosphatidylinositol 3-kinase/mammalian target of rapamycin inhibitor, prominently enhances radiosensitivity of prostate cancer cell line PC-3. *Cancer Biotherapy and Radiopharmaceuticals*. 2013;28(9):665-73.
604. Kim KW, Myers CJ, Jung DK, Lu B. NVP-BEZ-235 enhances radiosensitization via blockade of the PI3K/mTOR pathway in cisplatin-resistant non-small cell lung carcinoma. *Genes and Cancer*. 2014;5(7-8):293.
605. Cerniglia GJ, Karar J, Tyagi S, Christofidou-Solomidou M, Rengan R, Koumenis C, et al. Inhibition of autophagy as a strategy to augment radiosensitization by the dual phosphatidylinositol 3-kinase/mammalian target of rapamycin inhibitor NVP-BEZ235. *Molecular Pharmacology*. 2012;82(6):1230-40.
606. Fokas E, Yoshimura M, Prevo R, Higgins G, Hackl W, Maira S-M, et al. NVP-BEZ235 and NVP-BGT226, dual phosphatidylinositol 3-kinase/mammalian target of rapamycin inhibitors, enhance tumor and endothelial cell radiosensitivity. *Radiation Oncology*. 2012;7(1):48.

607. Fokas E, Im JH, Hill S, Yameen S, Stratford M, Beech J, et al. Dual inhibition of the PI3K/mTOR pathway increases tumor radiosensitivity by normalizing tumor vasculature. *Cancer Research*. 2011;72(1):239-48.
608. Del Alcazar CRG, Hardebeck MC, Mukherjee B, Tomimatsu N, Gao X, Yan J, et al. Inhibition of DNA double-strand break repair by the dual PI3K/mTOR inhibitor NVP-BEZ235 as a strategy for radiosensitization of glioblastoma. *Clinical Cancer Research*. 2014;20(5):1235-48.
609. Kuger S, Graus D, Brendtke R, Günther N, Katzer A, Lutyj P, et al. Radiosensitization of glioblastoma cell lines by the dual PI3K and mTOR inhibitor NVP-BEZ235 depends on drug-irradiation schedule. *Translational Oncology*. 2013;6(2):169.
610. Wang W-j, Long L-m, Yang N, Zhang Q-q, Ji W-j, Zhao J-h, et al. NVP-BEZ235, a novel dual PI3K/mTOR inhibitor, enhances the radiosensitivity of human glioma stem cells in vitro. *Acta Pharmacologica Sinica*. 2013;34(5):681.
611. Mukherjee B, Tomimatsu N, Amancherla K, Camacho CV, Pichamoorthy N, Burma S. The dual PI3K/mTOR inhibitor NVP-BEZ235 is a potent inhibitor of ATM-and DNA-PKCs-mediated DNA damage responses. *Neoplasia*. 2012;14(1):34-IN8.
612. Wise-Draper TM, Moorthy G, Salkeni MA, Karim NA, Thomas HE, Mercer CA, et al. A phase Ib study of the dual PI3K/mTOR inhibitor dactolisib (BEZ235) combined with everolimus in patients with advanced solid malignancies. *Targeted oncology*. 2017;12(3):323-32.
613. Massard C, Chi KN, Castellano D, de Bono J, Gravis G, Dirix L, et al. Phase Ib dose-finding study of abiraterone acetate plus buparlisib (BKM120) or dactolisib (BEZ235) in patients with castration-resistant prostate cancer. *European journal of cancer*. 2017;76:36-44.
614. National Center for Biotechnology Information. PubChem Compound Summary for CID 11977753, Dactolisib. [internet].2021 [cited 2021 April 2]. Available from: <https://pubchem.ncbi.nlm.nih.gov/compound/Dactolisib>.
615. Briffa R, Um I, Faratian D, Zhou Y, Turnbull AK, Langdon SP, et al. Multi-scale genomic, transcriptomic and proteomic analysis of colorectal cancer cell lines to identify novel biomarkers. *PloS one*. 2015;10(12):e0144708.
616. Jason S, Cui W. Proliferation, survival and metabolism: the role of PI3K/AKT/mTOR signalling in pluripotency and cell fate determination. *Development*. 2016;143(17):3050-60.
617. Mayer IA, Arteaga CL. The PI3K/AKT pathway as a target for cancer treatment. *Annual review of medicine*. 2016;67:11-28.
618. Alzahrani AS, editor PI3K/Akt/mTOR inhibitors in cancer: at the bench and bedside. *Seminars in cancer biology*; 2019: Elsevier.
619. Chiarini F, Falà F, Tazzari PL, Ricci F, Astolfi A, Pession A, et al. DUAL INHIBITION OF CLASS IA PHOSPHATIDYLINOSITOL 3-KINASE AND mTOR AS A NEW THERAPEUTIC OPTION FOR T-CELL ACUTE LYMPHOBLASTIC LEUKEMIA. *Cancer research*. 2009;69(8).
620. Ma DJ, Galanis E, Anderson SK, Schiff D, Kaufmann TJ, Peller PJ, et al. A phase II trial of everolimus, temozolomide, and radiotherapy in patients with newly diagnosed glioblastoma: NCCTG N057K. *Neuro-oncology*. 2014;17(9):1261-9.
621. Shen C, Houghton PJ. The mTOR pathway negatively controls ATM by up-regulating miRNAs. *Proceedings of the National Academy of Sciences*. 2013;110(29):11869-74.
622. Frøsina G, Profumo A, Marubbi D, Marcello D, Ravetti JL, Daga A. ATR kinase inhibitors NVP-BEZ235 and AZD6738 effectively penetrate the brain after systemic administration. *Radiation Oncology*. 2018;13(1):1-7.
623. Lamm N, Rogers S, Cesare AJ. The mTOR pathway: Implications for DNA replication. *Progress in Biophysics and Molecular Biology*. 2019;147:17-25.
624. Matthiessen P, Hallböök O, Andersson M, Rutegård J, Sjödahl R. Risk factors for anastomotic leakage after anterior resection of the rectum. *Colorectal Disease*. 2004;6(6):462-9.
625. Bahadoer RR, Dijkstra EA, van Etten B, Marijnen CA, Putter H, Kranenbarg EM-K, et al. Short-course radiotherapy followed by chemotherapy before total mesorectal excision

(TME) versus preoperative chemoradiotherapy, TME, and optional adjuvant chemotherapy in locally advanced rectal cancer (RAPIDO): a randomised, open-label, phase 3 trial. *The Lancet Oncology*. 2021;22(1):29-42.

626. Cercek A, Roxburgh CS, Strombom P, Smith JJ, Temple LK, Nash GM, et al. Adoption of total neoadjuvant therapy for locally advanced rectal cancer. *JAMA oncology*. 2018;4(6):e180071-e.

627. Fokas E, Allgäuer M, Polat B, Klautke G, Grabenbauer GG, Fietkau R, et al. Randomized phase II trial of chemoradiotherapy plus induction or consolidation chemotherapy as total neoadjuvant therapy for locally advanced rectal cancer: CAO/ARO/AIO-12. *Journal of Clinical Oncology*. 2019;37(34):3212-22.

628. Stockton JD, Tee L, Whalley C, James J, Dilworth M, Wheat R, et al. Complete response to neoadjuvant chemoradiotherapy in rectal cancer is associated with RAS/AKT mutations and high tumour mutational burden. *Radiation Oncology*. 2021;16(1):1-12.

629. Karar J, Maity A. PI3K/AKT/mTOR pathway in angiogenesis. *Frontiers in molecular neuroscience*. 2011;4:51.

630. Dienstmann R, Rodon J, Serra V, Tabernero J. Picking the point of inhibition: a comparative review of PI3K/AKT/mTOR pathway inhibitors. *Molecular cancer therapeutics*. 2014;13(5):1021-31.

Appendices

A) Consent form

UNIVERSITY OF
BIRMINGHAM

HBRC-201119-0251

University Hospital **NHS**
Birmingham
NHS Foundation Trust

DONATION OF SAMPLES TO THE HUMAN BIOMATERIALS RESOURCE CENTRE

Adult Patient Consent Form

Please initial each box if you agree with the statement and sign the bottom of the form

1. I have read the Information Sheet entitled 'DONATION OF SAMPLES TO THE HUMAN BIOMATERIALS RESOURCE CENTRE' dated 11-Oct-2016 (Version 2.0) and had the opportunity to ask questions.
2. I consent to the storage of my samples (may be tissue, blood or other body fluids) in the Human Biomaterials Resource Centre and for their use in ethically approved medical research projects, including genetic studies. I understand that occasionally samples may not be stored but may be released directly to approved projects.
3. I understand that donated samples may sometimes be used in ethically approved medical research which uses animals, but only when this is absolutely necessary and no alternative approach is available.
4. I understand that giving my samples for research is completely voluntary and that I am free to withdraw my consent at any time without giving a reason, and without my medical care or treatment being affected.
5. I understand that my health records may be accessed for research, both now and in the future, but that all extracted information will be anonymised.
6. I understand that my samples may be used by local researchers or by research institutions elsewhere in the UK and overseas, including private/commercial companies that do medical research. I understand that I will not receive any personal financial reward for donating my samples.

Please enter initials

Please enter initials

Please enter initials

Please enter initials

Please enter initials

Please enter initials

Attach patient sticker here

PATIENT		PERSON TAKING CONSENT	
Name		Name	
Date		Role	
Signature		Date	
		Signature	

B) PDO count estimation example

PDO lines	064	884	389	411	557	653
Passage	77	77	73	57	34	56
No. of wells 24 well plate	9	9	9	9	9	9

	064	884	389	411	557	653
Read 1	5.35×10^5	4.44×10^5	4.35×10^5	5.29×10^5	3.24×10^5	2.20×10^5
Read 2	4.80×10^5	5.18×10^5	4.20×10^5	6.60×10^5	3.18×10^5	2.69×10^5
Read 3	5.00×10^5	4.09×10^5	4.15×10^5	6.79×10^5	3.29×10^5	2.15×10^5
Read 4	4.86×10^5	5.18×10^5	4.09×10^5	6.77×10^5	3.69×10^5	2.47×10^5
Average in 1ml	5.02×10^5	4.72×10^5	4.24×10^5	6.61×10^5	3.35×10^5	2.38×10^5
In 3ml						
To get 190,000 cells (38 wells – including 10 spare x 5000 cells per well of PDOs)						
Volume of PDO in required form 3ml solution	378 μ l	403 μ l	448 μ l	287 μ l	567 μ l	798 μ l
Remaining media volume	3422 μ l	3397 μ l	3352 μ l	351 μ l3	3233 μ l	3002 μ l

C) List of genes and mutations covered by the
 QIASeq® Custom Targeted DNA sequencing panel

Gene	bp ROI	bp not covered by fragments <= 150 bp	bp not covered by fragments <= 250 bp
<i>MSH6</i>	4183	0	0
<i>BRAF</i>	2660	0	0
<i>TCF7L2</i>	2425	0	0
<i>BCL9L</i>	4580	0	0
<i>TP53</i>	1383	0	0
<i>B2M</i>	413	0	0
<i>TGIF1</i>	1365	0	0
<i>NRAS</i>	610	0	0
<i>PIK3CA</i>	3407	0	0
<i>GNAS</i>	4186	0	0
<i>SMAD4</i>	1769	0	0
<i>BMPR2</i>	3247	0	0
<i>PTEN</i>	1302	0	0
<i>RPL22</i>	619	0	0
<i>SMAD2</i>	1504	0	0
<i>ATM</i>	9791	0	0
<i>POLE</i>	7351	0	0
<i>ARID1A</i>	7058	0	0
<i>FBXW7</i>	2758	0	0
<i>RNF43</i>	2442	0	0
<i>MLH1</i>	2461	0	0

<i>MSH2</i>	3107	0	0
<i>KRAS</i>	737	0	0
<i>ELF3</i>	1256	0	0
<i>POLD1</i>	3662	0	0
<i>CTNNB1</i>	2486	0	0
<i>ZFP36L2</i>	1505	0	0
<i>APC</i>	8857	0	0
<i>SOX9</i>	1560	0	0
<i>ACVR2A</i>	1652	0	0

Supplementary Table 1: Genes tested using the QIASeq™ (Qiagen, Germany) custom targeted DNA sequencing panel

track name='QIaseq_DNA_panel.CDHS-14542Z-1197.roi'

description='QIaseq_DNA_panel.CDHS-14542Z-1197.roi'

chr1	6246726	6246881	RPL22
chr1	6252984	6253119	RPL22
chr1	6257706	6257821	RPL22
chr1	6259424	6259638	RPL22
chr1	27022889	27024036	ARID1A
chr1	27056136	27056359	ARID1A
chr1	27057637	27058100	ARID1A
chr1	27059161	27059288	ARID1A
chr1	27087341	27087592	ARID1A
chr1	27087869	27087969	ARID1A
chr1	27088637	27088815	ARID1A
chr1	27089458	27089781	ARID1A
chr1	27092706	27092862	ARID1A
chr1	27092942	27093062	ARID1A
chr1	27094275	27094495	ARID1A
chr1	27097604	27097822	ARID1A
chr1	27098985	27099128	ARID1A
chr1	27099297	27099483	ARID1A
chr1	27099831	27099992	ARID1A
chr1	27100065	27100213	ARID1A
chr1	27100287	27100394	ARID1A
chr1	27100814	27101716	ARID1A
chr1	27102062	27102203	ARID1A
chr1	27105508	27107252	ARID1A
chr1	115251150	115251280	NRAS
chr1	115252184	115252354	NRAS
chr1	115256415	115256604	NRAS
chr1	115258665	115258786	NRAS
chr1	201980259	201980432	ELF3
chr1	201981079	201981311	ELF3
chr1	201981466	201981569	ELF3
chr1	201981762	201981892	ELF3
chr1	201981973	201982033	ELF3
chr1	201982069	201982169	ELF3
chr1	201982304	201982431	ELF3
chr1	201982951	201983157	ELF3
chr1	201984331	201984456	ELF3
chr10	89624221	89624310	PTEN
chr10	89653776	89653871	PTEN
chr10	89685264	89685319	PTEN
chr10	89690797	89690851	PTEN
chr10	89692764	89693013	PTEN
chr10	89711869	89712021	PTEN
chr10	89717604	89717781	PTEN
chr10	89720645	89720880	PTEN
chr10	89725038	89725234	PTEN
chr10	114710510	114710709	TCF7L2
chr10	114710960	114711037	TCF7L2

chr10	114711236	114711371	TCF7L2
chr10	114724309	114724388	TCF7L2
chr10	114799778	114799890	TCF7L2
chr10	114849150	114849304	TCF7L2
chr10	114886632	114886645	TCF7L2
chr10	114889618	114889751	TCF7L2
chr10	114900937	114901080	TCF7L2
chr10	114903676	114903789	TCF7L2
chr10	114905764	114905861	TCF7L2
chr10	114910736	114910887	TCF7L2
chr10	114911478	114911648	TCF7L2
chr10	114912086	114912204	TCF7L2
chr10	114917774	114917833	TCF7L2
chr10	114918420	114918481	TCF7L2
chr10	114919673	114919756	TCF7L2
chr10	114920372	114920455	TCF7L2
chr10	114921332	114921349	TCF7L2
chr10	114925308	114925736	TCF7L2
chr11	108098346	108098428	ATM
chr11	108098497	108098620	ATM
chr11	108099899	108100055	ATM
chr11	108106391	108106566	ATM
chr11	108114674	108114850	ATM
chr11	108115509	108115758	ATM
chr11	108117685	108117859	ATM
chr11	108119654	108119834	ATM
chr11	108121422	108121804	ATM
chr11	108122558	108122763	ATM
chr11	108123538	108123644	ATM
chr11	108124535	108124771	ATM
chr11	108126936	108127072	ATM
chr11	108128202	108128338	ATM
chr11	108129707	108129807	ATM
chr11	108137892	108138074	ATM
chr11	108139131	108139341	ATM
chr11	108141785	108141878	ATM
chr11	108141972	108142138	ATM
chr11	108143253	108143339	ATM
chr11	108143443	108143584	ATM
chr11	108150212	108150340	ATM
chr11	108151716	108151900	ATM
chr11	108153431	108153611	ATM
chr11	108154948	108155205	ATM
chr11	108158321	108158447	ATM
chr11	108159698	108159835	ATM
chr11	108160323	108160533	ATM
chr11	108163340	108163525	ATM
chr11	108164034	108164209	ATM
chr11	108165648	108165791	ATM
chr11	108168008	108168114	ATM

<i>chr11</i>	108170435	108170617	ATM
<i>chr11</i>	108172369	108172521	ATM
<i>chr11</i>	108173574	108173761	ATM
<i>chr11</i>	108175396	108175584	ATM
<i>chr11</i>	108178618	108178716	ATM
<i>chr11</i>	108180881	108181047	ATM
<i>chr11</i>	108183132	108183230	ATM
<i>chr11</i>	108186544	108186643	ATM
<i>chr11</i>	108186732	108186845	ATM
<i>chr11</i>	108188094	108188253	ATM
<i>chr11</i>	108190675	108190790	ATM
<i>chr11</i>	108192022	108192152	ATM
<i>chr11</i>	108196031	108196276	ATM
<i>chr11</i>	108196779	108196957	ATM
<i>chr11</i>	108198366	108198490	ATM
<i>chr11</i>	108199742	108199970	ATM
<i>chr11</i>	108200935	108201153	ATM
<i>chr11</i>	108202165	108202289	ATM
<i>chr11</i>	108202600	108202769	ATM
<i>chr11</i>	108203483	108203632	ATM
<i>chr11</i>	108204607	108204700	ATM
<i>chr11</i>	108205690	108205841	ATM
<i>chr11</i>	108206566	108206693	ATM
<i>chr11</i>	108213943	108214103	ATM
<i>chr11</i>	108216464	108216640	ATM
<i>chr11</i>	108218000	108218097	ATM
<i>chr11</i>	108224487	108224612	ATM
<i>chr11</i>	108225532	108225606	ATM
<i>chr11</i>	108235803	108235950	ATM
<i>chr11</i>	108236046	108236240	ATM
<i>chr11</i>	118769118	118770222	BCL9L
<i>chr11</i>	118770620	118770912	BCL9L
<i>chr11</i>	118771322	118773622	BCL9L
<i>chr11</i>	118773693	118773788	BCL9L
<i>chr11</i>	118773939	118774166	BCL9L
<i>chr11</i>	118778186	118778316	BCL9L
<i>chr11</i>	118778973	118779369	BCL9L
<i>chr11</i>	118780617	118780653	BCL9L
<i>chr12</i>	25362723	25362850	KRAS
<i>chr12</i>	25368369	25368499	KRAS
<i>chr12</i>	25378542	25378712	KRAS
<i>chr12</i>	25380162	25380351	KRAS
<i>chr12</i>	25398202	25398323	KRAS
<i>chr12</i>	133201277	133201401	POLE
<i>chr12</i>	133201485	133201585	POLE
<i>chr12</i>	133202225	133202361	POLE
<i>chr12</i>	133202697	133202908	POLE
<i>chr12</i>	133208895	133209099	POLE
<i>chr12</i>	133209244	133209386	POLE
<i>chr12</i>	133210766	133210969	POLE

<i>chr12</i>	133212472	133212615	POLE
<i>chr12</i>	133214594	133214730	POLE
<i>chr12</i>	133215705	133215889	POLE
<i>chr12</i>	133218227	133218442	POLE
<i>chr12</i>	133218757	133218988	POLE
<i>chr12</i>	133219086	133219320	POLE
<i>chr12</i>	133219400	133219587	POLE
<i>chr12</i>	133219804	133219921	POLE
<i>chr12</i>	133219987	133220151	POLE
<i>chr12</i>	133220417	133220568	POLE
<i>chr12</i>	133225509	133225663	POLE
<i>chr12</i>	133225886	133226106	POLE
<i>chr12</i>	133226257	133226480	POLE
<i>chr12</i>	133233716	133233849	POLE
<i>chr12</i>	133233929	133234020	POLE
<i>chr12</i>	133234448	133234561	POLE
<i>chr12</i>	133235875	133236100	POLE
<i>chr12</i>	133237549	133237755	POLE
<i>chr12</i>	133238107	133238275	POLE
<i>chr12</i>	133240584	133240739	POLE
<i>chr12</i>	133240950	133241053	POLE
<i>chr12</i>	133241882	133242041	POLE
<i>chr12</i>	133244083	133244239	POLE
<i>chr12</i>	133244936	133245093	POLE
<i>chr12</i>	133245215	133245328	POLE
<i>chr12</i>	133245391	133245530	POLE
<i>chr12</i>	133248795	133248913	POLE
<i>chr12</i>	133249207	133249430	POLE
<i>chr12</i>	133249744	133249868	POLE
<i>chr12</i>	133250155	133250298	POLE
<i>chr12</i>	133251978	133252108	POLE
<i>chr12</i>	133252315	133252411	POLE
<i>chr12</i>	133252674	133252795	POLE
<i>chr12</i>	133253126	133253244	POLE
<i>chr12</i>	133253943	133254034	POLE
<i>chr12</i>	133254158	133254310	POLE
<i>chr12</i>	133256077	133256242	POLE
<i>chr12</i>	133256534	133256637	POLE
<i>chr12</i>	133256758	133256813	POLE
<i>chr12</i>	133257187	133257278	POLE
<i>chr12</i>	133257718	133257870	POLE
<i>chr12</i>	133263834	133263906	POLE
<i>chr15</i>	45003739	45003816	B2M
<i>chr15</i>	45007615	45007927	B2M
<i>chr15</i>	45008521	45008545	B2M
<i>chr17</i>	7572921	7573013	TP53
<i>chr17</i>	7573921	7574038	TP53
<i>chr17</i>	7576531	7576589	TP53
<i>chr17</i>	7576619	7576662	TP53
<i>chr17</i>	7576847	7576931	TP53

<i>chr17</i>	7577013	7577160	TP53
<i>chr17</i>	7577493	7577613	TP53
<i>chr17</i>	7578171	7578294	TP53
<i>chr17</i>	7578365	7578559	TP53
<i>chr17</i>	7579306	7579595	TP53
<i>chr17</i>	7579694	7579726	TP53
<i>chr17</i>	7579833	7579917	TP53
<i>chr17</i>	56432298	56432352	RNF43
<i>chr17</i>	56434823	56436189	RNF43
<i>chr17</i>	56437504	56437617	RNF43
<i>chr17</i>	56438138	56438310	RNF43
<i>chr17</i>	56439899	56440014	RNF43
<i>chr17</i>	56440630	56440772	RNF43
<i>chr17</i>	56440881	56440966	RNF43
<i>chr17</i>	56448266	56448399	RNF43
<i>chr17</i>	56492681	56492943	RNF43
<i>chr17</i>	70117527	70117968	SOX9
<i>chr17</i>	70118854	70119118	SOX9
<i>chr17</i>	70119678	70120533	SOX9
<i>chr18</i>	3447732	3447800	TGIF1
<i>chr18</i>	3449624	3449659	TGIF1
<i>chr18</i>	3450482	3450508	TGIF1
<i>chr18</i>	3451972	3452385	TGIF1
<i>chr18</i>	3456346	3456583	TGIF1
<i>chr18</i>	3457357	3457943	TGIF1
<i>chr18</i>	45368192	45368326	SMAD2
<i>chr18</i>	45371705	45371860	SMAD2
<i>chr18</i>	45372028	45372176	SMAD2
<i>chr18</i>	45374840	45375063	SMAD2
<i>chr18</i>	45377639	45377703	SMAD2
<i>chr18</i>	45391424	45391509	SMAD2
<i>chr18</i>	45394688	45394833	SMAD2
<i>chr18</i>	45395608	45395812	SMAD2
<i>chr18</i>	45396840	45396940	SMAD2
<i>chr18</i>	45422886	45423132	SMAD2
<i>chr18</i>	48573411	48573670	SMAD4
<i>chr18</i>	48575050	48575235	SMAD4
<i>chr18</i>	48575659	48575699	SMAD4
<i>chr18</i>	48581145	48581368	SMAD4
<i>chr18</i>	48584489	48584619	SMAD4
<i>chr18</i>	48584704	48584831	SMAD4
<i>chr18</i>	48586230	48586291	SMAD4
<i>chr18</i>	48591787	48591981	SMAD4
<i>chr18</i>	48593383	48593562	SMAD4
<i>chr18</i>	48603002	48603151	SMAD4
<i>chr18</i>	48604620	48604842	SMAD4
<i>chr19</i>	50902103	50902315	POLD1
<i>chr19</i>	50902622	50902746	POLD1
<i>chr19</i>	50905029	50905186	POLD1
<i>chr19</i>	50905250	50905386	POLD1

<i>chr19</i>	50905456	50905635	POLD1
<i>chr19</i>	50905705	50905797	POLD1
<i>chr19</i>	50905863	50906003	POLD1
<i>chr19</i>	50906304	50906481	POLD1
<i>chr19</i>	50906744	50906859	POLD1
<i>chr19</i>	50909433	50909584	POLD1
<i>chr19</i>	50909658	50909779	POLD1
<i>chr19</i>	50910234	50910436	POLD1
<i>chr19</i>	50910578	50910677	POLD1
<i>chr19</i>	50911958	50912163	POLD1
<i>chr19</i>	50912373	50912497	POLD1
<i>chr19</i>	50912770	50912928	POLD1
<i>chr19</i>	50916677	50916783	POLD1
<i>chr19</i>	50916993	50917141	POLD1
<i>chr19</i>	50918066	50918252	POLD1
<i>chr19</i>	50918689	50918852	POLD1
<i>chr19</i>	50918975	50919088	POLD1
<i>chr19</i>	50919647	50919790	POLD1
<i>chr19</i>	50919861	50919985	POLD1
<i>chr19</i>	50920296	50920359	POLD1
<i>chr19</i>	50920423	50920531	POLD1
<i>chr19</i>	50921093	50921209	POLD1
<i>chr2</i>	43451452	43452896	ZFP36L2
<i>chr2</i>	43453398	43453459	ZFP36L2
<i>chr2</i>	47630325	47630546	MSH2
<i>chr2</i>	47635534	47635699	MSH2
<i>chr2</i>	47637227	47637516	MSH2
<i>chr2</i>	47639547	47639704	MSH2
<i>chr2</i>	47641402	47641562	MSH2
<i>chr2</i>	47643429	47643573	MSH2
<i>chr2</i>	47656875	47657085	MSH2
<i>chr2</i>	47672681	47672801	MSH2
<i>chr2</i>	47690164	47690298	MSH2
<i>chr2</i>	47693791	47693952	MSH2
<i>chr2</i>	47698098	47698206	MSH2
<i>chr2</i>	47702158	47702414	MSH2
<i>chr2</i>	47703500	47703715	MSH2
<i>chr2</i>	47705405	47705663	MSH2
<i>chr2</i>	47707829	47708015	MSH2
<i>chr2</i>	47709912	47710093	MSH2
<i>chr2</i>	47739436	47739578	MSH2
<i>chr2</i>	48010367	48010637	MSH6
<i>chr2</i>	48018060	48018267	MSH6
<i>chr2</i>	48023027	48023207	MSH6
<i>chr2</i>	48025744	48028299	MSH6
<i>chr2</i>	48030553	48030829	MSH6
<i>chr2</i>	48032043	48032171	MSH6
<i>chr2</i>	48032751	48032851	MSH6
<i>chr2</i>	48033337	48033502	MSH6
<i>chr2</i>	48033585	48033795	MSH6

chr2	48033912	48034004	MSH6
chr2	148602716	148602781	ACVR2A
chr2	148653864	148654082	ACVR2A
chr2	148657021	148657141	ACVR2A
chr2	148657307	148657472	ACVR2A
chr2	148672754	148672908	ACVR2A
chr2	148674846	148675000	ACVR2A
chr2	148676010	148676166	ACVR2A
chr2	148677793	148677918	ACVR2A
chr2	148680536	148680685	ACVR2A
chr2	148683594	148683735	ACVR2A
chr2	148684643	148684848	ACVR2A
chr2	203242192	203242278	BMPR2
chr2	203329526	203329707	BMPR2
chr2	203332236	203332417	BMPR2
chr2	203378436	203378557	BMPR2
chr2	203379605	203379707	BMPR2
chr2	203383539	203383780	BMPR2
chr2	203384804	203384929	BMPR2
chr2	203395511	203395682	BMPR2
chr2	203397302	203397460	BMPR2
chr2	203407028	203407175	BMPR2
chr2	203417433	203417616	BMPR2
chr2	203419969	203421259	BMPR2
chr2	203424413	203424674	BMPR2
chr20	57415156	57415946	GNAS
chr20	57428315	57430393	GNAS
chr20	57466776	57466925	GNAS
chr20	57470661	57470744	GNAS
chr20	57473990	57474045	GNAS
chr20	57478577	57478645	GNAS
chr20	57478721	57478851	GNAS
chr20	57480432	57480540	GNAS
chr20	57484211	57484276	GNAS
chr20	57484399	57484483	GNAS
chr20	57484570	57484639	GNAS
chr20	57484733	57484864	GNAS
chr20	57485000	57485141	GNAS
chr20	57485383	57485461	GNAS
chr20	57485732	57485889	GNAS
chr3	37035033	37035159	MLH1
chr3	37038104	37038205	MLH1
chr3	37042440	37042549	MLH1
chr3	37045886	37045970	MLH1
chr3	37048476	37048559	MLH1
chr3	37050299	37050401	MLH1
chr3	37053305	37053358	MLH1
chr3	37053496	37053595	MLH1
chr3	37055917	37056040	MLH1
chr3	37058991	37059095	MLH1

<i>chr3</i>	37061795	37061959	MLH1
<i>chr3</i>	37067122	37067503	MLH1
<i>chr3</i>	37070269	37070428	MLH1
<i>chr3</i>	37081671	37081790	MLH1
<i>chr3</i>	37083753	37083827	MLH1
<i>chr3</i>	37089004	37089179	MLH1
<i>chr3</i>	37090002	37090105	MLH1
<i>chr3</i>	37090389	37090513	MLH1
<i>chr3</i>	37091971	37092149	MLH1
<i>chr3</i>	41265554	41265577	CTNNB1
<i>chr3</i>	41266011	41266249	CTNNB1
<i>chr3</i>	41266439	41266703	CTNNB1
<i>chr3</i>	41266819	41267068	CTNNB1
<i>chr3</i>	41267145	41267357	CTNNB1
<i>chr3</i>	41268693	41268848	CTNNB1
<i>chr3</i>	41274826	41274940	CTNNB1
<i>chr3</i>	41275014	41275363	CTNNB1
<i>chr3</i>	41275624	41275793	CTNNB1
<i>chr3</i>	41277209	41277339	CTNNB1
<i>chr3</i>	41277834	41277995	CTNNB1
<i>chr3</i>	41278073	41278205	CTNNB1
<i>chr3</i>	41279501	41279572	CTNNB1
<i>chr3</i>	41280619	41280838	CTNNB1
<i>chr3</i>	178916608	178916970	PIK3CA
<i>chr3</i>	178917472	178917692	PIK3CA
<i>chr3</i>	178919072	178919333	PIK3CA
<i>chr3</i>	178921326	178921582	PIK3CA
<i>chr3</i>	178922285	178922381	PIK3CA
<i>chr3</i>	178927377	178927493	PIK3CA
<i>chr3</i>	178927968	178928131	PIK3CA
<i>chr3</i>	178928213	178928358	PIK3CA
<i>chr3</i>	178935992	178936127	PIK3CA
<i>chr3</i>	178936978	178937070	PIK3CA
<i>chr3</i>	178937353	178937528	PIK3CA
<i>chr3</i>	178937731	178937845	PIK3CA
<i>chr3</i>	178938768	178938950	PIK3CA
<i>chr3</i>	178941863	178941980	PIK3CA
<i>chr3</i>	178942482	178942614	PIK3CA
<i>chr3</i>	178943744	178943833	PIK3CA
<i>chr3</i>	178947054	178947235	PIK3CA
<i>chr3</i>	178947786	178947914	PIK3CA
<i>chr3</i>	178948007	178948169	PIK3CA
<i>chr3</i>	178951876	178952157	PIK3CA
<i>chr4</i>	153244027	153244306	FBXW7
<i>chr4</i>	153245330	153245551	FBXW7
<i>chr4</i>	153247152	153247388	FBXW7
<i>chr4</i>	153249354	153249546	FBXW7
<i>chr4</i>	153250818	153250942	FBXW7
<i>chr4</i>	153251878	153252025	FBXW7
<i>chr4</i>	153253742	153253876	FBXW7

<i>chr4</i>	153258948	153259093	<i>FBXW7</i>
<i>chr4</i>	153268076	153268228	<i>FBXW7</i>
<i>chr4</i>	153269820	153269886	<i>FBXW7</i>
<i>chr4</i>	153271188	153271281	<i>FBXW7</i>
<i>chr4</i>	153273616	153273887	<i>FBXW7</i>
<i>chr4</i>	153303335	153303492	<i>FBXW7</i>
<i>chr4</i>	153332419	153332960	<i>FBXW7</i>
<i>chr5</i>	112043409	112043584	<i>APC</i>
<i>chr5</i>	112090582	112090727	<i>APC</i>
<i>chr5</i>	112102017	112102112	<i>APC</i>
<i>chr5</i>	112102880	112103092	<i>APC</i>
<i>chr5</i>	112111320	112111439	<i>APC</i>
<i>chr5</i>	112116481	112116605	<i>APC</i>
<i>chr5</i>	112128137	112128231	<i>APC</i>
<i>chr5</i>	112136970	112137085	<i>APC</i>
<i>chr5</i>	112151186	112151295	<i>APC</i>
<i>chr5</i>	112154657	112155046	<i>APC</i>
<i>chr5</i>	112157587	112157693	<i>APC</i>
<i>chr5</i>	112162799	112162949	<i>APC</i>
<i>chr5</i>	112163620	112163708	<i>APC</i>
<i>chr5</i>	112164547	112164674	<i>APC</i>
<i>chr5</i>	112170642	112170867	<i>APC</i>
<i>chr5</i>	112173244	112179828	<i>APC</i>
<i>chr7</i>	140415822	140415841	<i>BRAF</i>
<i>chr7</i>	140426161	140426321	<i>BRAF</i>
<i>chr7</i>	140434391	140434575	<i>BRAF</i>
<i>chr7</i>	140439606	140439751	<i>BRAF</i>
<i>chr7</i>	140449081	140449223	<i>BRAF</i>
<i>chr7</i>	140453069	140453198	<i>BRAF</i>
<i>chr7</i>	140453981	140454038	<i>BRAF</i>
<i>chr7</i>	140476706	140476893	<i>BRAF</i>
<i>chr7</i>	140477785	140477880	<i>BRAF</i>
<i>chr7</i>	140481370	140481498	<i>BRAF</i>
<i>chr7</i>	140482815	140482962	<i>BRAF</i>
<i>chr7</i>	140487342	140487389	<i>BRAF</i>
<i>chr7</i>	140494102	140494272	<i>BRAF</i>
<i>chr7</i>	140500156	140500286	<i>BRAF</i>
<i>chr7</i>	140501206	140501365	<i>BRAF</i>
<i>chr7</i>	140507754	140507867	<i>BRAF</i>
<i>chr7</i>	140508686	140508800	<i>BRAF</i>
<i>chr7</i>	140534403	140534677	<i>BRAF</i>
<i>chr7</i>	140549905	140550017	<i>BRAF</i>
<i>chr7</i>	140624360	140624508	<i>BRAF</i>

D) Parameters used within the Lexogen QuantSeq data analysis pipeline on Partek Flow®

First trim adapter step settings:

Option	Value
Adapters from file	(Default: false)
Trim adapters from	Both (Default: 3' end)
Adapter sequences	AAAAAAAAAAAAA,TTTTTTTTTTTTT
Maximum error rate	0.1
Match times	1
No indels	(Default: false)
Min overlap length	3
Ns in adapter	(Default: false)
N not as wildcards	(Default: false)
Min read length	25
qualityCutoff	0
qualityBase	auto-detect
Read names prefix	
Read names suffix	
zeroCap	true

Second trim adapter step settings:

Option	Value
Adapters from file	true (Default: false)
Trim adapters from	3' end
Maximum error rate	0.1
Match times	1
No indels	(Default: false)
Min overlap length	5 (Default: 3)
Ns in adapter	(Default: false)
N not as wildcards	(Default: false)
Min read length	25
qualityCutoff	0
qualityBase	auto-detect
Read names prefix	
Read names suffix	
zeroCap	true

Trim bases stage settings:

Option	Value
Trim based on	Quality score
End min quality level (Phred)	10 (Default: 20)
Trim from end	3-prime (right end)
Min read length	20 (Default: 25)
Max N	
Quality encoding	Auto detect

STAR stage settings:

Input parameters

Option	Value
Generate unaligned reads	(Default: false)
Max junctions	1000000
Type of filtering	BySJout (Default: Normal)
Multimap score range	1

Option	Value
Max read mapping	20 (Default: 10)
Max mismatches	999 (Default: 10)
Mismatch mapped ratio	0.6 (Default: 0.3)
Mismatch read ratio	1.0
Min score	0
Normalized min score	0.66
Min matched bases	0
Normalized min matched bases	0.66
Filter alignment using their motifs	None
Collapsed splice junctions reads	All
Max junction gap	50000 100000 200000
Non-canonical motifs	true
Min overhang length for splice junctions	30
Min unique map read count per junction	3
Min total read count per junction	3
Min distance to other junctions' donor/acceptor	10
GT/AG motif	true
Min overhang length for splice junctions	12
Min unique map read count per junction	1
Min total read count per junction	1
Min distance to other junctions' donor/acceptor	0
GC/AG motif	true
Min overhang length for splice junctions	12
Min unique map read count per junction	1
Min total read count per junction	1
Min distance to other junctions' donor/acceptor	5
AT/AC motif	true
Min overhang length for splice junctions	12
Min unique map read count per junction	1
Min total read count per junction	1
Min distance to other junctions' donor/acceptor	10
Extra alignment score	2
Gap open penalty	0
Non-canonical gap open penalty	-8

Option	Value
GC/AG gap open penalty	-4
AT/AC gap open penalty	-8
Extra score	-0.25
Deletion open penalty	-2
Deletion extension penalty per base	-2
Insertion open penalty	-2
Insertion extension penalty per base	-2
Max score reduction	1
Search start point	50
Normalized search start point	1.0
Max seed length	
Max mapping for stitching	10000
Max seeds per read	1000
Max seeds per window	50
Max one seed loci per window	10
Min intron size	20 (Default: 21)
Max intron size	1000000
Min spliced alignment overhang	8 (Default: 5)
Min annotated spliced alignment overhang	1 (Default: 3)
Max windows per read	10000
Max transcripts per window	100
Max hits	10000
Read ends alignment type	Local
Soft-clip past reference end	Yes
Max loci anchors	50
Bin size for windows/clustering	16
Max bins between two anchors	9
Left and right flanking region size	4
Chimeric alignment	(Default: false)
Two pass mapping	None
Cufflinks-like strand field flag	intronMotif
SAM attributes	All
Add to quality score	0

Quantify to annotation model settings

Option	Value
require_proper_pair	true
Require junction reads to match introns	true
Strand specificity	No
Minimum read overlap with feature	100%
Report unexplained regions	(Default: false)
Min reads	10

E) Parameters used within the Illumina® Total RNA Sequencing data analysis pipeline on Partek Flow®

STAR alignment:

Option	Value
Generate unaligned reads	(Default: false)
Name, sequence, and quality lengths	NotEqual
Max junctions	1000000
Type of filtering	Normal
Multimap score range	1
Max read mapping	10
Max mismatches	10
Mismatch mapped ratio	0.3
Mismatch read ratio	1.0
Min score	0
Normalized min score	0.66
Min matched bases	0
Normalized min matched bases	0.66
Filter alignment using their motifs	None
Collapsed splice junctions reads	All
Max junction gap	50000 100000 200000
Non-canonical motifs	true
Min overhang length for splice junctions	30
Min unique map read count per junction	3
Min total read count per junction	3
Min distance to other junctions' donor/acceptor	10
GT/AG motif	true
Min overhang length for splice junctions	12
Min unique map read count per junction	1
Min total read count per junction	1
Min distance to other junctions' donor/acceptor	0
GC/AG motif	true
Min overhang length for splice junctions	12
Min unique map read count per junction	1

Option	Value
Min total read count per junction	1
Min distance to other junctions' donor/acceptor	5
AT/AC motif	true
Min overhang length for splice junctions	12
Min unique map read count per junction	1
Min total read count per junction	1
Min distance to other junctions' donor/acceptor	10
Extra alignment score	2
Gap open penalty	0
Non-canonical gap open penalty	-8
GC/AG gap open penalty	-4
AT/AC gap open penalty	-8
Extra score	-0.25
Deletion open penalty	-2
Deletion extension penalty per base	-2
Insertion open penalty	-2
Insertion extension penalty per base	-2
Max score reduction	1
Search start point	50
Normalized search start point	1.0
Max seed length	
Max mapping for stitching	10000
Max seeds per read	1000
Max seeds per window	50
Max one seed loci per window	10
Min intron size	21
Max intron size	
Max gap between two mates	
Min spliced alignment overhang	5
Min annotated spliced alignment overhang	3
Spliced mate min read length	0
Normalized spliced mate min read length	0.66
Max windows per read	10000
Max transcripts per window	100

Option	Value
Max hits	10000
Read ends alignment type	Local
Soft-clip past reference end	Yes
Max loci anchors	50
Bin size for windows/clustering	16
Max bins between two anchors	9
Left and right flanking region size	4
Chimeric alignment	(Default: false)
Two pass mapping	None
Cufflinks-like strand field flag	intronMotif
SAM attributes	All
Add to quality score	0

Quantify to annotation model

Option	Value
Strict paired-end compatibility	true
Require junction reads to match introns	true
Strand specificity	Reverse - Forward (Default: No)
Minimum read overlap with feature	100%
Report unexplained regions	(Default: false)
Min reads	10

F) R Script: GSEA using cluster profiler and DESeq2

Reproduced with permission from Dr Joao D. Barros-Silva,
University of Birmingham

```
if (!requireNamespace("BiocManager", quietly = TRUE))
  install.packages("BiocManager")

BiocManager::install("DESeq2")
install.packages("tidyverse")

library(tidyverse)
library(DESeq2)

library(tidyverse)
library(DESeq2)

setwd("~/Desktop/Organoids RNA-seq analysis/R script & raw gene counts genes by row")

# import data

library(readr)

raw_gene_counts <- read_csv("Desktop/Organoids RNA-seq analysis/R script & raw gene counts
genes by
row/Partek_Ollie_Total_RNA_Seq_PDO_Quantify_to_annotation_model_(Partek_E_M)_Gene_counts.c
sv",
                           col_types = cols(Chromosome = col_skip(),
                                             Start = col_skip(), Stop = col_skip(),
                                             Strand = col_skip(), S2_080 = col_skip(),
                                             S4_376 = col_skip(), S3_157 = col_skip(),
                                             S8_647 = col_skip(), S12_964 = col_skip(),
                                             S10_658 = col_skip(), COL0312_S15 =
col_skip(),
                                             COL0155_S14 = col_skip(), COL0151_S13 =
col_skip()))
View(raw_gene_counts)

write_csv(raw_gene_counts, "raw_gene_counts.csv")

raw_gene_counts <- read_csv("raw_gene_counts.csv")

# remove rows with duplicate Gene Symbol
raw_genecounts <- raw_gene_counts[!duplicated(raw_gene_counts$`Gene Symbol`),]

# Move colum "Transcript" containing the gene IDs to row names
raw_genecounts <- column_to_rownames(raw_genecounts, "Gene Symbol")

# create metadata

org_metadata <- data.frame(condition = c(rep("non.responder",2),rep("responder",4)))
org_metadata$condition <- as.factor(org_metadata$condition)

row.names(org_metadata) <- c("S7_557","S9_653","S6_411","S1_064","S5_389","S11_884")
org_metadata

# order dataframe according to match with metadata rownames
raw_genecounts <- raw_genecounts[,row.names(org_metadata)]
```

```

# add ENSEMBL id, chr number and gene description (optional)

install.packages("devtools")
devtools::install_github("stephenturner/annotables")

library(annotables)

grch38

# this bit is not having the desired result
raw_gene_counts %>%
  dplyr::inner_join(grch38, by = c("Gene Symbol" = "symbol"))

# convert gene counts dataframe to matrix

raw_genecounts <- as.matrix(raw_gene_counts)

# set up DESeqDataSet object and run DESeq pipeline ----

dds <- DESeqDataSetFromMatrix(countData = round(raw_genecounts, digits = 0),
                              colData = org_metadata,
                              design = ~ condition)

dds <- DESeq(dds)
dds

res <- results(dds, contrast = c("condition", "non.responder", "responder"))
res <- res[order(res$pvalue),]
res

# save R objects
save(org_metadata, raw_genecounts, dds, res, file = "data_10_2020.RData")

# load R objects
load("data_10_2020.RData")

summary(res)

library("AnnotationDbi")

if (!requireNamespace("BiocManager", quietly = TRUE))
  install.packages("BiocManager")

BiocManager::install("org.Hs.eg.db")

library("org.Hs.eg.db")
columns(org.Hs.eg.db)

# add ENSEMBL, gene name and EntrezID to results ----

res$ensembl <- mapIds(org.Hs.eg.db,
                     keys=row.names(res),
                     column="ENSEMBL",
                     keytype="SYMBOL",
                     multiVals="first")

res$entrez <- mapIds(org.Hs.eg.db,
                    keys=row.names(res),
                    column="ENTREZID",
                    keytype="SYMBOL",
                    multiVals="first")

res$name <- mapIds(org.Hs.eg.db,
                  keys=row.names(res),
                  column="GENENAME",
                  keytype="SYMBOL",

```

```

        multiVals="first")

res

# save R objects
save(org_metadata, raw_genecounts, dds, res, file = "data_11_2020.RData")

# load R objects ----
load("data_11_2020.RData")

# install pathview

if (!requireNamespace("BiocManager", quietly = TRUE))
  install.packages("BiocManager")

BiocManager::install("pathview")
BiocManager::install("gage")
BiocManager::install("gageData")
BiocManager::install("DOSE")
BiocManager::install("ReactomePA")

# Get files with images of altered pathways using pathview package ----

# For experimentally derived gene sets, GO term groups, etc, coregulation is commonly the
# case,
# hence same.dir = TRUE (default); In KEGG, BioCarta pathways, genes frequently are not
# co-regulated,
# hence it could be informative to let same.dir = FALSE. Although same.dir = TRUE could
# also be interesting for pathways.

library(pathview)
library(gage)
library(gageData)
library(ReactomePA)

data(kegg.sets.hs)
data(sigmet.idx.hs)
kegg.sets.hs <- kegg.sets.hs[sigmet.idx.hs]

foldchanges <- res$log2FoldChange
names(foldchanges) <- res$entrez

# Get the results
keggres <- gage(foldchanges, gsets=kegg.sets.hs, same.dir=TRUE)

keggres_f <- gage(foldchanges, gsets=kegg.sets.hs, same.dir=FALSE)

# Look at both up (greater), down (less), and statistics.
lapply(keggres, head)
lapply(keggres_f, head)

# Get the pathways
keggrespathways <- data.frame(id=rownames(keggres$greater), keggres$greater) %>%
  tbl_df() %>%
  filter(row_number()<=10) %>%
  .$id %>%
  as.character()
keggrespathways

# Get the IDs.
keggresids <- substr(keggrespathways, start=1, stop=8)
keggresids

# Define plotting function for applying later

```



```

plot_pathway <- function(pid) pathview(gene.data=foldchanges, pathway.id=pid,
species="hsa", new.signature=FALSE)

# plot multiple pathways (plots saved to disk and returns a throwaway list object)
tmp <- sapply(keggresids, function(pid) pathview(gene.data=foldchanges, pathway.id=pid,
species="hsa"))

# Log fold change shrinkage ----

resultsNames(dds)

resLFC <- lfcShrink(dds, coef = "condition_responder_vs_non.responder", type = "apeglm")
resLFC

save(resLFC, file = "resLFC.16.11.20.RData")

# prepare input data for gene ontology and pathway enrichment (geneList) ----

library(msigdb)
library(clusterProfiler)

geneList <- data.frame(lfc = res$log2FoldChange, padj = res$padj, gene_id = res$entrez)
rownames(geneList) <- rownames(res)
geneList

# filter out genes with padj values higher than 0.05
geneList <- geneList %>%
  filter(padj<=0.05)

dim(geneList)

is.na(geneList$gene_id)

# remove rows with NA
geneList %>% drop_na() %>% dim() # with NA: 1088 rows
# no NA:945 rows

geneList <- geneList %>% drop_na()

# prepare vector of upregulated genes on non-responders (DE_up)
# subset geneList to include only up-regulated genes (threshold: lfc>=1.5)
gene_up <- geneList %>%
  filter(lfc>=1.5)

# gene id list of significant upregulated DE genes with fold change > or = 1.5

DE_up <- gene_up[,1]

names(DE_up) <- as.character(gene_up[, "gene_id"])

DE_up <- sort(DE_up, decreasing = TRUE)
length(DE_up)

DE_up <- names(DE_up)[DE_up>1.5]
length(DE_up)

head(DE_up)

# prepare vector of upregulated genes on responders DE_dn)
# subset geneList to include only up-regulated genes (threshold: lfc<= -1) [it was lfc <=
-1.5 but it generated a low number of genes]
gene_dn <- geneList %>%
  filter(lfc<=-1)

```

```

# gene id list of significant upregulated DE genes with fold change > or = 1.5
DE_dn <- gene_dn[,1]
names(DE_dn) <- as.character(gene_dn["gene_id"])
DE_dn <- sort(DE_dn, decreasing = TRUE)
length(DE_dn)
DE_dn <- names(DE_dn)
length(DE_dn)
head(DE_dn)
# set up gene TERM2GENE object for enricher()
library("stringi")
colnames(msigdbr(species = "Homo sapiens", category = "C5", subcategory = "GO:MF"))
m_t2g <- msigdbr(species = "Homo sapiens", category = "C5", subcategory = "GO:MF") %>%
  dplyr::select(gs_name, entrez_gene)
C6_t2g <- msigdbr(species = "Homo sapiens", category = "C6") %>%
  dplyr::select(gs_name, entrez_gene)
H_t2g <- msigdbr(species = "Homo sapiens", category = "H") %>%
  dplyr::select(gs_name, entrez_gene)
H_t2g$gs_name <- gsub("_", " ", H_t2g$gs_name, fixed = TRUE)
H_t2g$gs_name <- stri_trans_totitle(H_t2g$gs_name)
C2_t2g <- msigdbr(species = "Homo sapiens", category = "C2", subcategory = "CP") %>%
  dplyr::select(gs_name, entrez_gene)
C1_t2g <- msigdbr(species = "Homo sapiens", category = "C1") %>%
  dplyr::select(gs_name, entrez_gene)
# enrich DE gene lists ----
en_C2_up <- enricher(DE)
en_H <- enricher(DE_up, TERM2GENE = H_t2g)
dotplot(en_H, showCategory = 20)+
  ggtitle("Hallmark pathways up-regulated on non-responders")
en_GO_MF <- enricher(DE_up, TERM2GENE = m_t2g)
dotplot(en_GO_MF)
kegg_enrich <- enrichKEGG(gene = DE_up, organism = "hsa")
dotplot(kegg_enrich)
en_MF <- enrichGO(gene = DE_up, 'org.Hs.eg.db', ont = "MF")
dotplot(en_MF)
en_up_C6 <- enricher(DE_up, TERM2GENE = C6_t2g)
dotplot(en_up_C6, showCategory = 20)+
  ggtitle("Oncogenic pathways (C6) on non-responders")
enKegg_DE_up <- enrichKEGG(gene = DE_up, organism = "hsa")
dotplot(enKegg_DE_up, showCategory = 10)+
  ggtitle("KEGG - Up-regulated genes non-responders")
enKegg_DE_dn <- enrichKEGG(gene = DE_dn, organism = "hsa")
dotplot(enKegg_DE_dn)+
  ggtitle("KEGG - Up-regulated genes responders")

```

```

en_H_DE_dn <- enricher(DE_dn, TERM2GENE = H_t2g)
dotplot(en_H_DE_dn)+
  ggtitle("Hallmark pathways up-regulated on responders")

en_dn_C6 <- enricher(DE_dn, TERM2GENE = C6_t2g, )

# prepare data for pathway comparison of up- vs downregulated

mydf <- data.frame(Entrez = geneList$gene_id,
                  FC = geneList$lfc)
mydf <- mydf[abs(mydf$FC)>1,]
mydf$group <- "upregulated NR"
mydf$group[mydf$FC<0] <- "upregulated R"
dim(mydf)

glimpse(mydf)
mydf %>% filter(group=="upregulated R") %>% dim()
mydf %>% filter(group=="upregulated NR") %>% dim()

# perform enrichment comparing the two groups ----

ck <- compareCluster(Entrez~group, data = mydf, fun = "enricher", TERM2GENE = H_t2g)
dotplot(ck, showCategory = 10)+
  ggtitle("Hallmark pathways")

ck_C2 <- compareCluster(Entrez~group, data = mydf, fun = "enricher", TERM2GENE = C2_t2g)
dotplot(ck_C2)

ck_C1 <- compareCluster(Entrez~group, data = mydf, fun = "enricher", TERM2GENE = C1_t2g)
dotplot(ck_C1)

ck_path <- compareCluster(Entrez~group, data = mydf, fun = "enrichPathway")
dotplot(ck_path)

ck_kegg <- compareCluster(Entrez~group, data = mydf, fun = "enrichKEGG", organism = "hsa")
dotplot(ck_kegg, showCategory = 15)

ck_C6 <- compareCluster(Entrez~group, data = mydf, fun = "enricher", TERM2GENE = C6_t2g)
dotplot(ck_C6)

# create figure with combined enrichment charts ----

library(ggpubr)

dotplot(ck, showCategory = 10)+
  ggtitle("Comparison of Hallmark pathways")

c <- dotplot(en_H, showCategory = 10)+
  ggtitle("Hallmark pathways")+
  scale_y_discrete(labels=function(x) str_wrap(x, width=35)) # to adjust the width of y
axis legend text

a <- dotplot(en_up_C6, showCategory = 10)+
  ggtitle("Oncogenic pathways")

b <- dotplot(enKegg_DE_up, showCategory = 10)+
  ggtitle("KEGG pathways")

ggarrange(a, b, c,
          labels = c("A", "B", "C"),
          ncol = 2,
          nrow = 2)

```

```

# save R objects ----
save(geneList, DE_up, DE_dn, m_t2g, C6_t2g, H_t2g, C2_t2g, C1_t2g, mydf, ck, ck_C2, ck_C1,
ck_path, ck_kegg, ck_C6, file = "pathway enrichment.RData")

# load R objects
load("pathway enrichment.RData")

load("data_11_2020.RData")

# Create gene enrichment tables (and save RData and csv files)

table_enH <- head(en_H, n=10)
table_enH <- as.data.frame(table_enH)

table_enC6 <- head(en_up_C6, n=10)
table_enC6 <- as.data.frame(table_enC6)

table_enKegg <- head(enKegg_DE_up, n=10)
table_enKegg <- as.data.frame(table_enKegg)

save(table_enH, table_enC6, table_enKegg, file = "tables path enrichment graphs.RData")

write.csv(table_enC6, file = "table C6 enrichment.csv")
write.csv(table_enH, file = "table Hallmark enrichment.csv")
write.csv(table_enKegg, file = "table KEGG enrichment.csv")

```

G) R Script: EnhancedVolcano

Reproduced with permission from Dr Joao D. Barros-Silva, University of Birmingham

```
# Install EnhancedVolcano package

if (!requireNamespace('BiocManager', quietly = TRUE))
  install.packages('BiocManager')
BiocManager::install('EnhancedVolcano')

# import data

org_data <- read.csv(file.choose())

org_data

# set genes as row name
# created a new data.frame (org_data2) with the genes as rownames

library(tidyverse)

org_data2 <- column_to_rownames(org_data, var="gene")

# draw Volcano plot highlighting the hypoxia genes

EnhancedVolcano(org_data2,
  lab = rownames(org_data2),
  x = 'log2FoldChange',
  y = 'pvalue',
  selectLab =
c('ECE1', 'PGAM1', 'FAM129B', 'ENO2', 'ARHGAP5', 'GAPDH', 'DDR1', 'FLNA', 'SOX9', 'FAM107B',
'MET', 'HK1', 'TIPARP', 'SAT1', 'FAM57A', 'RIMKLA', 'SRD5A3', 'ASPH', 'GPC5A', 'CDCP1', 'TFF3',
'IDS', 'IGFBP3', 'ELP5', 'BACE2', 'GADD45A', 'ITGA3', 'EFNA3', 'PLAC8', 'CCND1', 'PAM', 'GLRX', 'S100A6',
'MRPS6', 'BNIP3L', 'EGFR', 'IFI27', 'ATP7A', 'SDC4', 'FGFRL1', 'EGR1', 'RASA4', 'TNFRSF10D',
'KRT19',
'ANXA5', 'DST', 'CD59', 'IER5', 'ITGB5', 'HCFC1R1', 'QSOX1', 'MT1E', 'GSN', 'CDKN1A', 'LSR', 'ARL4C',
'ELL2',
'SLC2A1', 'IGFBP2', 'NT5E', 'ARRDC3', 'ANXA2', 'MXRA7', 'KRT15', 'OSBPL10', 'PDGFRL', 'NHS', 'RAB3B',
'EPHA2', 'F3',
'FSCN1', 'PLAUR', 'SDC3', 'CDKN1C', 'CD44', 'TUBB3', 'PADI1', 'PMEPA1', 'S100A2', 'AHNAK2'),
  pCutoff = 0.05,
  labFace = 'bold',
  FCcutoff = 2,
  colAlpha = 0.7,
  xlim = c(-10,10),
  ylim = c(0,5),
  title = "RT resistant vs sensitive",
  subtitle = NULL,
  legendPosition = "right")
```

```

)

# draw Volcano plot highlighting the PIK/AKT/MTOR

EnhancedVolcano(org_data2,
  lab = rownames(org_data2),
  x = 'log2FoldChange',
  y = 'pvalue',
  selectLab = c('PIK3CB', 'PIK3CC', 'PIK3CD',
                'CD55', 'CDKN2B', 'GPD2', 'LGMN', 'PACIN3',
                'PLK2', 'PON2', 'PYGL', 'SEC14L2',
                'TESC', 'TNFRSF12A'),
  pCutoff = 0.06,
  labFace = 'bold',
  legendLabSize = 14,
  legendIconSize = 4.0,
  drawConnectors = TRUE,
  widthConnectors = 1.0,
  FCcutoff = 2,
  colAlpha = 0.4,
  xlim = c(-10,10),
  ylim = c(0,5),
  title = "RT resistant vs sensitive",
  subtitle = NULL,
  legendPosition = "right"
)

# export plot image file

dev.print(tiff, "RT resistant vs sensitive", res=300, height=10, width=15.07, units="cm")

if (!requireNamespace("BiocManager", quietly = TRUE))
  install.packages("BiocManager")

BiocManager::install("EnhancedVolcano")
install.packages("tidyverse")
BiocManager::install("DESeq2")

library(EnhancedVolcano)
library(tidyverse)
library(DESeq2)

# set work directory

setwd("~/Desktop/Paper RT on CRC organoids/R script & raw gene counts genes by row")

# import data ----
# raw counts filtered on DEBrowser (R package)
# filtering method CPM<0.01 at least in 5 samples

raw_filtered <- read.csv("raw_counts_filtered.csv")
raw_filtered <- column_to_rownames(raw_filtered, var = "gene")

# create metadata

metadata <- data.frame(condition = c(rep("responder",4), rep("non.responder",2)))
metadata$condition <- as.factor(metadata$condition)
row.names(metadata) <- c("S1_064", "S6_411", "S5_389", "S11_884", "S7_557", "S9_653")
metadata

# set up DESeqDataSet object and run DESeq pipeline ----

dds <- DESeqDataSetFromMatrix(countData = round(raw_filtered, digits = 0),

```

```

colData = metadata,
design = ~ condition)

dds <- DESeq(dds)
dds

res <- results(dds, contrast = c("condition", "non.responder", "responder"))
res <- res[order(res$pvalue),]
res

# create a list of -log10P >15 & log2 fold change > |5|

top_list <- res
top_list$minus.log10P <- log10(top_list$padj)*-1

top_list <- as.data.frame(top_list)

top_up <- top_list %>%
  filter(minus.log10P>=15 & log2FoldChange >= 5)

top_down <- top_list %>%
  filter(minus.log10P>=15 & log2FoldChange <= -5)

row.names(top_up)
row.names(top_down)

# Create volcano plot ----

EnhancedVolcano(res,
  lab = rownames(res),
  x = "log2FoldChange",
  y = "pvalue",
  pCutoff = 0.01,
  labFace = 'bold',
  labSize = 3,
  FCcutoff = 2,
  colAlpha = 0.6,
  xlim = c(-14,14),
  ylim = c(0,30),
  title = "RT resistant vs sensitive",
  subtitle = NULL,
  legendPosition = "right",
  gridlines.minor = FALSE,
  gridlines.major = FALSE,
  selectLab =
c("SCARA3", "CAV1", "NTN1", "UBASH3B", "EHD2", "GPER1", "PLK2", "SLC39A5", "ABCB1", "OLFM4", "TDGF1")
,
  legendIconSize = 4.0
)

# export plot to .tiff file

dev.print(tiff, "VolcanoPlot organoids non-resp vs resp RT.tiff", res=300, height=14,
width=20, units="cm")
dev.off()

dev.print(tiff, "New VolcanoPlot organoids non-resp vs resp RT.tiff", res=300, height=14,
width=20, units="cm")
dev.off()

```

H) Hierarchical clustering settings on Partek Flow®

Cluster samples - Yes

Cluster features - Yes

Filtering None

Samples:

Cluster distance metric: Average Linkage

Point distance metric: Euclidean

Features:

Cluster distance metric: Average Linkage

Point distance metric: Euclidean

Ordering:

Sample order: Default order

Normalization:

Normalization mode: Standardize

Advanced options:

Option set

-- Default --


```
rownames(pdo_mut$stop_gained)= c("MSH6", "BRAF", "TCF7L2", "BCL9L", "TP53", "B2M", "TGIF1",
"NRAS", "PIK3CA", "GNAS", "SMAD4", "BMP2R", "PTEN", "RPL22", "SMAD2", "ATM", "POLE",
"ARID1A", "FBXW7", "RNF43", "MLH1", "MSH2", "KRAS", "ELF3", "POLD1", "CTNNB1", "ZFP36L2",
"APC", "SOX9", "ACVR2A")
```

```
rownames(pdo_mut$inframe_del)= c("MSH6", "BRAF", "TCF7L2", "BCL9L", "TP53", "B2M", "TGIF1",
"NRAS", "PIK3CA", "GNAS", "SMAD4", "BMP2R", "PTEN", "RPL22", "SMAD2", "ATM", "POLE",
"ARID1A", "FBXW7", "RNF43", "MLH1", "MSH2", "KRAS", "ELF3", "POLD1", "CTNNB1", "ZFP36L2",
"APC", "SOX9", "ACVR2A")
```

```
colnames(pdo_mut$frameshift)= c("PDO_884", "PDO_411", "PDO_653" , "PDO_389" , "PDO_064",
"PDO_557", "PDO_080", "PDO_964", "PDO_157")
```

```
colnames(pdo_mut$missense)= c("PDO_884", "PDO_411", "PDO_653" , "PDO_389" , "PDO_064",
"PDO_557", "PDO_080", "PDO_964", "PDO_157")m
```

```
colnames(pdo_mut$stop_gained)= c("PDO_884", "PDO_411", "PDO_653" , "PDO_389" , "PDO_064",
"PDO_557", "PDO_080", "PDO_964", "PDO_157")
```

```
colnames(pdo_mut$inframe_del)= c("PDO_884", "PDO_411", "PDO_653" , "PDO_389" , "PDO_064",
"PDO_557", "PDO_080", "PDO_964", "PDO_157")
```

```
pdo_mut
```

```
# set colours to each mutation
```

```
col <- c(frameshift="blue", missense="green", stop_gained="red", inframe_del="orange")
```

```
# draw oncoprint chart
```

```
oncoPrint(pdo_mut,
```

```
  alter_fun = list(
```

```
    frameshift = function(x,y,w,h) grid.rect(x,y,w*0.9, h*0.9,
```

```
      gp =
```

```
gpar(fill=col["frameshift"],col=NA)),
```

```
    missense = function(x,y,w,h) grid.rect(x,y,w*0.9,h*0.9,
```

```

gp = gpar(fill=col["missesig
nse"],col=NA)),

stop_gained = function(x,y,w,h) grid.rect(x,y,w*0.9, h*0.9,
gp =
gpar(fill=col["stop_gained"],col=NA)),

inframe_del = function(x,y,w,h) grid.rect(x,y,w*0.9, h*0.9,
gp =
gpar(fill=col["inframe_del"],col=NA)),

background = function(x,y,w,h) grid.rect(x,y,w*0.9,h*0.9,
gp = gpar(fill= "#CCCCCC", col=NA))
), col = col,
row_names_side = "left",
pct_side = "right",
pct_digits = 2,
show_column_names = TRUE,
column_names_rot=45,
remove_empty_rows = TRUE)

```

J) Western blots: protein quantification and normalisation calculations, an example and formulas used

	B	C	D	E	F	G	H	I	J
8	HCT116	Cont - No RT	RT Only	5FU	5FURT	API	API+RT	DACTO	DACTO +RT
9	Samples	0.807	1.09	0.695	0.783	0.541	0.522	0.656	0.57
10	minus 0	=C9-\$J\$4	=D9-\$J\$4	=E9-\$J\$4	=F9-\$J\$4	=G9-\$J\$4	=H9-\$J\$4	=I9-\$J\$4	=J9-\$J\$4
11	Concentrations	=(2761.1*C10)-71.673	=(2761.1*D10)-71.673	=(2761.1*E10)-71.673	=(2761.1*F10)-71.673	=(2761.1*G10)-71.673	=(2761.1*H10)-71.673	=(2761.1*I10)-71.673	=(2761.1*J10)-71.673
12	ul for 20ug	=(20/C11)*1000	=(20/D11)*1000	=(20/E11)*1000	=(20/F11)*1000	=(20/G11)*1000	=(20/H11)*1000	=(20/I11)*1000	=(20/J11)*1000
13	(1in 5) Loading buffer	=\$C\$16/5	=\$C\$16/5	=\$C\$16/5	=\$C\$16/5	=\$C\$16/5	=\$C\$16/5	=\$C\$16/5	=\$C\$16/5
14	H2O	=\$C\$16-(C12+C13)	=\$C\$16-(D12+D13)	=\$C\$16-(E12+E13)	=\$C\$16-(F12+F13)	=\$C\$16-(G12+G13)	=\$C\$16-(H12+H13)	=\$C\$16-(I12+I13)	=\$C\$16-(J12+J13)
15									
16	Vol	23							
17									
18									
19									
20									
21									
22									
23									
24									
25									
26									
27									
28									
29									
30									
31									
32									
33									

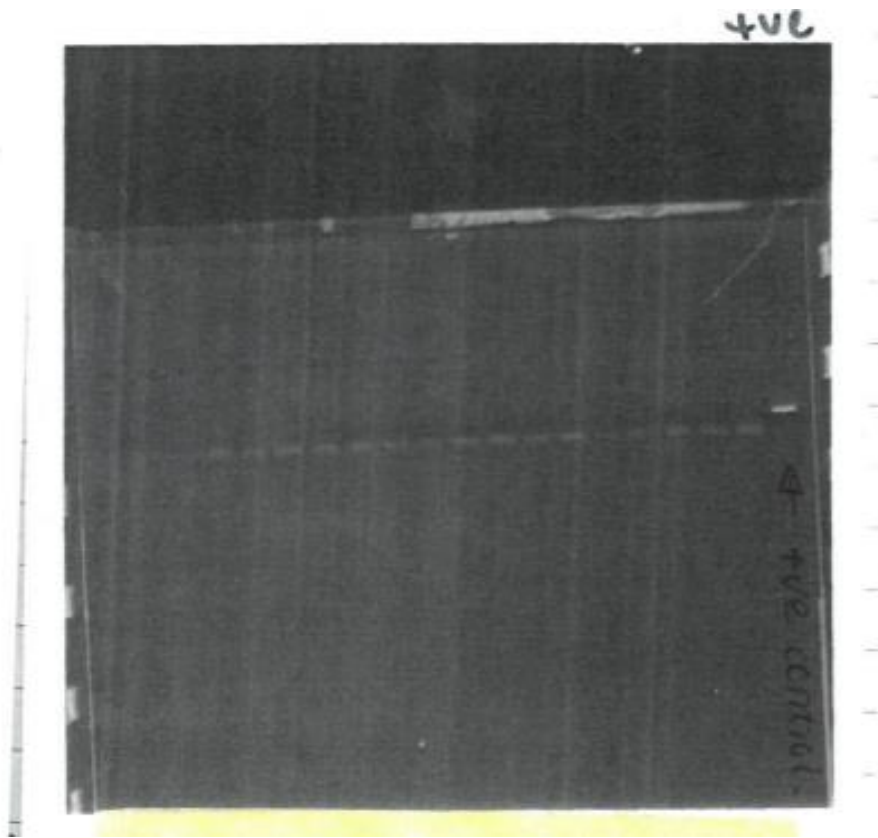
Chart Title

K)KEGG enrichment: All upregulated gene sets in
non-responder post-NCRT surgical resection FFPE
specimens

Gene set	Size	ES	FDR q-value	Rank at max
KEGG_VIRAL_MYOCARDITIS	61	0.51	0.046	6695
KEGG_SNARE_INTERACTIONS_ IN_VESICULAR_TRANSPORT	38	0.5	0.046	6658
KEGG_ARRHYTHMOGENIC_RIGHT_ VENTRICULAR_CARDIOMYOPATHY_ARVC	65	0.49	0.006	6883
KEGG_P53_SIGNALING_PATHWAY	63	0.48	0.051	3551
KEGG_ANTIGEN_PROCESSING_AND_ PRESENTATION	58	0.48	0.126	6451
KEGG_ECM_RECEPTOR_INTERACTION	81	0.46	0.008	2691
KEGG_AUTOIMMUNE_THYROID_DISEASE	32	0.46	0.072	6451
KEGG_ENDOMETRIAL_CANCER	52	0.46	0.13	7327
KEGG_HYPERTROPHIC_CARDIOMYOPATHY_HCM	73	0.45	0.006	7901
KEGG_FOCAL_ADHESION	189	0.45	0.038	7952
KEGG_ADHERENS_JUNCTION	66	0.45	0.176	10639
KEGG_DILATED_CARDIOMYOPATHY	78	0.44	0.008	7901
KEGG_PRION_DISEASES	34	0.44	0.07	2662
<i>KEGG_COLORECTAL_CANCER</i>	60	0.43	0.121	7479
KEGG_VASCULAR_SMOOTH_ MUSCLE_CONTRACTION	101	0.42	0.001	3927

KEGG_REGULATION_OF_ACTIN_CYTOSKELETON	194	0.42	0.053	8142
KEGG_MELANOMA	64	0.4	0.043	7394
KEGG_TIGHT_JUNCTION	117	0.39	0.127	7906
KEGG_LEUKOCYTE_TRANSENDOTHELIAL_MIGRATION	105	0.39	0.132	7778
KEGG_AXON_GUIDANCE	120	0.38	0.047	4198
KEGG_N_GLYCAN_BIOSYNTHESIS	44	0.38	0.249	2322
KEGG_WNT_SIGNALING_PATHWAY	136	0.37	0.128	4866
KEGG_GRAFT_VERSUS_HOST_DISEASE	30	0.37	0.209	5641
KEGG_ACUTE_MYELOID_LEUKEMIA	55	0.37	0.21	7465
KEGG_CHRONIC_MYELOID_LEUKEMIA	73	0.37	0.247	9430
KEGG_CELL_ADHESION_MOLECULES_CAMS	120	0.35	0.118	7626
KEGG_CARDIAC_MUSCLE_CONTRACTION	65	0.35	0.198	9200
KEGG_GLIOMA	64	0.35	0.205	7394
KEGG_PROSTATE_CANCER	87	0.35	0.214	3127
KEGG_BASAL_TRANSCRIPTION_FACTORS	32	0.35	0.216	6939
KEGG_MAPK_SIGNALING_PATHWAY	238	0.34	0.051	7612
KEGG_ERBB_SIGNALING_PATHWAY	84	0.34	0.2	7952
KEGG_LEISHMANIA_INFECTON	66	0.34	0.204	3341
KEGG_RENAL_CELL_CARCINOMA	66	0.34	0.221	9402
KEGG_LONG_TERM_POTENTIATION	64	0.31	0.242	7612
KEGG_PATHWAYS_IN_CANCER	299	0.3	0.208	7479
KEGG_TGF_BETA_SIGNALING_PATHWAY	79	0.3	0.243	4443
KEGG_CALCIIUM_SIGNALING_PATHWAY	143	0.28	0.076	7423
KEGG_CHEMOKINE_SIGNALING_PATHWAY	168	0.28	0.181	9127
KEGG_GNRH_SIGNALING_PATHWAY	90	0.28	0.205	7603
KEGG_MELANOGENESIS	88	0.26	0.239	3803

L) Sample mycoplasma test result



Mycoplasma testing was performed regularly of live cultures (cell lines and PDOs). Example of a mycoplasma test conducted in the laboratory showing only the positive control as positive and remaining lines all negative for mycoplasma DNA.

M) List of mutations identified on PDO lines – QIASeq Targeted DNA Panel1

	PDO 411	PDO 884	PDO 389	PDO 653	PDO 064	PDO 557
<i>APC</i>	stop gained p.Gln1378* Q1378	stop gained p.Tyr1376* Y1376	frameshift p.Gln1338fs Q1338fs	frameshift p.Val1479fs V1479fs	stop gained p.Arg876* R876	missense p.Ala921Ser A921S
<i>TP53</i>	missense p.Arg248Gln R248Q	missense p.Arg175His R175H	missense p.Gly245Asp G245D	in frame deletion p.Pro191del P191del	missense p.Arg282Trp R282W	-
<i>MSH6</i>	frameshift p.Leu1330fs L1330fs	frameshift p.Phe1088fs F1088fs	-	-	-	frameshift p.Phe1104fs F1104fs
<i>SOX9</i>	-	frameshift p.Tyr297fs Y297fs	frameshift p.Ser323fs S323fs	stop gained p.Gln1378* Q1378*	-	-

<i>TCF7L2</i>	frameshift p.Lys485fs K485fs	-	frameshift p.Lys485fs K485fs	-	-	-
<i>PIK3CA</i>	missense p.Glu545Lys E545K	-	-	-	-	missense p.Arg88Gln R88Q
<i>GNAS</i>	missense p.Thr225Pro T225P	missense p.Thr225Pro T225P	-	-	-	-
<i>SMAD4</i>	-	-	missense p.Arg496His R496H	frameshift p.Trp302fs W320fs	-	-
<i>BMPR2</i>	stop gained p.Arg147* R147	-	-	-	-	frameshift p.Asn583fs N583fs

<i>FBXW7</i>	-	-	-	missense p.Arg465His R465H	missense p.Ser582Leu S582L	-
<i>MSH2</i>	missense p.Asp167Val D167V	-	frameshift p.Leu458fs L458fs	-	-	-
<i>KRAS</i>	-	-	-	missense p.Gly12Asp G12D	-	missense p.Gly13Arg G13R
<i>BRAF</i>	missense p.Val600Glu V600E	-	-	-	-	-
<i>BCL9L</i>	-	-	-	-	-	frameshift p.Pro449fs P449fs
<i>TGIF1</i>	-	-	-	-	frameshift p.Phe337fs	-

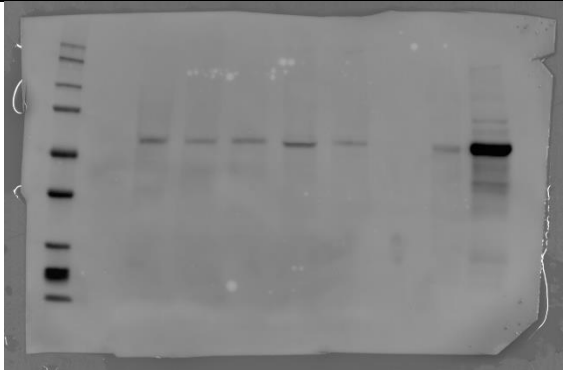
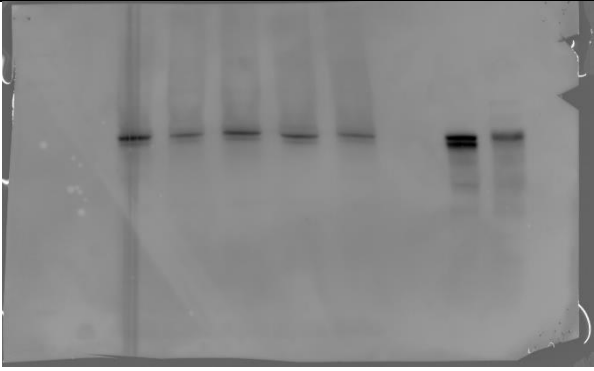
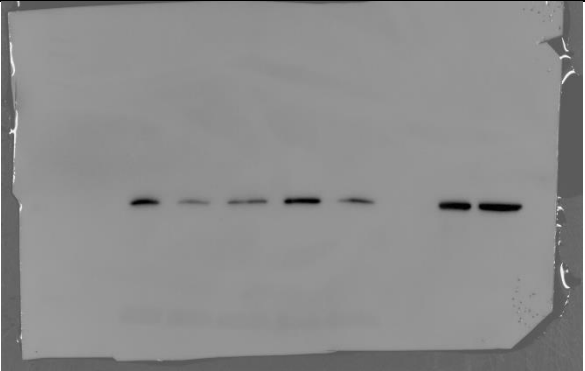
					F337fs	
<i>NRAS</i>	-	missense p.Gly13Arg G13R	-	-	-	-
<i>PTEN</i>	-	-	-	-	-	missense p.Cys136Tyr C136Y
<i>RPL22</i>	-	-	-	-	-	frameshift p.Lys15fs K15fs
<i>POLE</i>	frameshift p.Val1446fs V1446fs	-	-	-	-	-
<i>ACVR2A</i>	-	-	-	-	-	frameshift p.Lys437fs K437fs

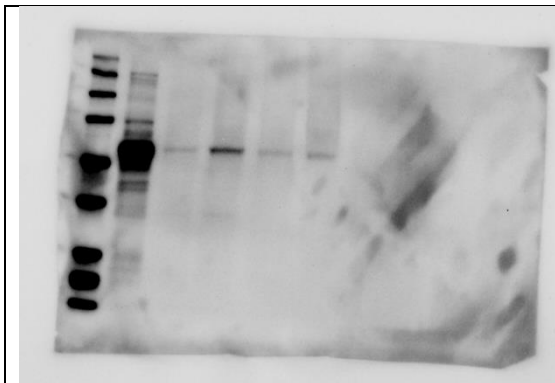
N) HCT116 drug only versus drug and radiotherapy: Welch's two sample t-test

Analysis performed by Mr Mohammed Elsaray, University of Birmingham. Reproduced and used in thesis with permission.

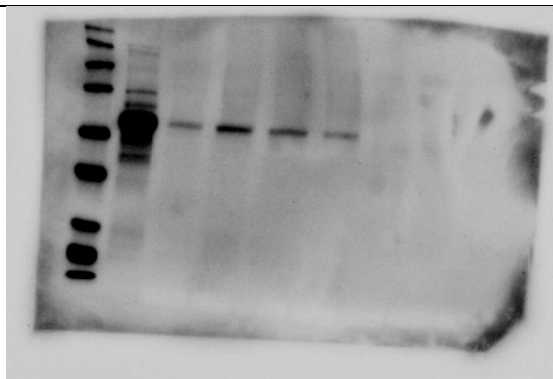
	A	B	C	D	E	F	G	H	I	J	K	L	M	N	O	P	Q	R	S	T	U	V	W	X	Y	Z	AA	AB	AC	AD	AE				
1	5FU Dose (log)																																		
2	2	0.0774	0.0756	0.0668	0.0723	0.066	0.0665	0.066	0.0703	0.0621	0.0639	0.0636	0.065	0.068		0.0702	0.066	0.0649	0.0708	0.0711	0.0709	0.0698	0.0775	0.0687	0.0644	0.0657	0.0679	0.068995				5FU vs 5FU + RT			
3	1.7	0.0969	0.0967	0.0842	0.0874	0.0837	0.094	0.0925	0.0961	0.0965	0.0966	0.1035	0.0967	0.0937 SD		0.1018	0.0994	0.0889	0.1009	0.0923	0.0931	0.092	0.088	0.0926	0.0911	0.0958	0.0906	0.093871				Welch Two Sample t-test			
4	1.4	0.1388	0.1335	0.121	0.1445	0.1456	0.1366	0.1453	0.1408	0.1396	0.1349	0.1409	0.149	0.1392	0.448266	0.1432	0.144	0.1344	0.1453	0.1339	0.1276	0.1373	0.1325	0.1211	0.1105	0.1302	0.1459	0.133819 SD				p-value = 0.399430775953485			
5	1	0.3511	0.3467	0.3344	0.3577	0.3198	0.3259	0.3425	0.3558	0.3348	0.3314	0.3486	0.3478	0.3414		0.2777	0.2667	0.273	0.2836	0.2667	0.2727	0.2791	0.2784	0.2665	0.2883	0.2885	0.2947	0.278006	0.418275				Paired Two-Samples T-test		
6	0.7	0.6115	0.6004	0.6121	0.5815	0.5867	0.596	0.6089	0.5953	0.6417	0.6572	0.6503	0.6563	0.6165		0.5022	0.4869	0.4538	0.4791	0.4476	0.4692	0.4573	0.479	0.4201	0.4114	0.4179	0.4218	0.453869				p-value = 0.0181589580009667			
7	0	1.0597	1.0177	1.041	1.0565	0.9624	1.0278	0.9836	0.9959	1.0243	1.0912	1.0597	1.0866	1.0339		0.9016	0.9118	0.8623	0.8717	0.8288	0.8595	0.8966	0.8663	0.9565	0.9391	0.9842	0.943	0.901778							
8	-1	1.0778	1.06	1.0584	1.0839	1.0302	0.9829	1.0092	1.0163	1.02	1.0908	1.0918	1.0866	1.0507		0.9782	0.9612	0.9745	1.0338	0.9474	0.9739	0.9425	0.9874	1.0832	1.0999	1.0816	1.1176	1.015111							
9	-2	1.0613	1.0414	1.0307	1.1018	1.015	1.0227	1.0288	1.0705	1.05	1.1098	1.1198	1.1206	1.0644		1.0068	0.9919	1.0202	1.0379	0.923	0.9337	0.9516	0.9885	1.0892	1.0534	1.0701	1.0753	1.011799							
10																																			
11																																			
12																																			
13																																			
14																																			
15	API_Dose																																		
16	0.7	0.2118	0.2094	0.2128	0.2039	0.1865	0.1831	0.1862	0.1982	0.1997	0.1884	0.1972	0.2115	0.1991		0.1322	0.1272	0.136	0.1486	0.1222	0.1139	0.1195	0.1264	0.1377	0.1425	0.1374	0.1503	0.132832							
17	0	0.444	0.4174	0.4431	0.4383	0.4255	0.4214	0.4142	0.4819	0.3868	0.4013	0.4243	0.3749	0.4228		0.2574	0.2404	0.2671	0.2512	0.2369	0.2531	0.2201	0.2523	0.2391	0.2236	0.2523	0.2516	0.245408							
18	-0.3	0.6742	0.6468	0.6824	0.6709	0.708	0.72	0.7064	0.7258	0.6912	0.7566	0.7294	0.7443	0.7047 SD		0.3811	0.3784	0.4054	0.3843	0.3815	0.3608	0.3778	0.4391	0.4131	0.4153	0.4257	0.427	0.399144							
19	-1	1.1193	1.1124	1.1235	1.1209	1.1098	1.1299	1.1492	1.1444	1.18	1.2137	1.2156	1.1899	1.1507	0.390517	0.9358	0.9199	0.9561	0.9423	0.9366	0.9267	0.9549	0.9527	0.9201	0.9302	0.9441	0.9444	0.938661 SD							
20	-1.3	1.1404	1.1519	1.1026	1.1301	1.1296	1.1965	1.2276	1.1888	1.2367	1.2535	1.2757	1.2551	1.1907		0.9342	0.9913	1.0031	1.0355	1.0213	1.0484	1.0502	1.0904	1.0102	1.0291	1.0082	0.9939	1.017969	0.39871				Paired Two-Samples T-test		
21	-2	1.0783	1.1276	1.1233	1.0978	1.0726	1.1004	1.1309	1.1165	1.2211	1.2559	1.253	1.2764	1.1545		1.0212	1.0351	1.0368	0.9994	1.0012	1.0605	1.0971	1.0698	1.0503	1.0724	1.0749	1.094	1.051057				p-value = 0.000517920951432003			
22	-2.3	1.0446	1.1015	1.0794	1.0952	1.0163	1.1058	1.1314	1.131	1.1843	1.1993	1.2238	1.1835	1.1247		0.9769	1.0098	0.9735	0.9935	0.9563	1.0002	1.046	1.068	1.0716	1.0832	1.1079	1.109	1.032989							
23	-3	1.096	1.0881	1.0938	1.0754	1.0715	1.1114	1.1104	1.0897	1.1406	1.1914	1.1834	1.2261	1.1231		1.008	0.9429	1.0123	0.995	1.0104	1.0134	1.038	1.0566	1.0734	1.0625	1.0699	1.0887	1.030914							
24																																			
25																																			
26																																			
27																																			
28																																			
29	DACTO_Dose																																		
30	0.7	0.0847	0.0839	0.0757	0.0844	0.0884	0.0835	0.1001	0.1057	0.0891	0.0864	0.0915	0.091	0.0887		0.0642	0.0604	0.065	0.0664	0.0917	0.0845	0.0782	0.0824	0.0754	0.0685	0.0745	0.074	0.073752							
31	0	0.0958	0.0942	0.0984	0.1036	0.0699	0.0837	0.0833	0.0808	0.0734	0.0837	0.0795	0.0781	0.0854		0.0756	0.0793	0.0789	0.0838	0.0635	0.0595	0.0645	0.0674	0.0558	0.0663	0.0658	0.0633	0.068647							
32	-0.3	0.163	0.1485	0.1396	0.1669	0.1545	0.1609	0.1669	0.1779	0.1577	0.1501	0.1424	0.1511	0.1566 SD		0.1069	0.0996	0.0954	0.1007	0.0949	0.1017	0.0989	0.1045	0.085	0.079	0.0881	0.0979	0.096055							
33	-1	0.5848	0.5837	0.5702	0.5644	0.5636	0.5653	0.5338	0.6013	0.5976	0.5867	0.6041	0.6003	0.5797	0.427654	0.2953	0.2783	0.2896	0.2921	0.2749	0.2757	0.2828	0.2932	0.256	0.2561	0.275	0.2761	0.278756 SD							
34	-1.3	0.7014	0.697	0.6533	0.6789	0.7011	0.7401	0.7403	0.7689	0.7097	0.7097	0.7115	0.7069	0.7097		0.3828	0.3772	0.354	0.3743	0.381	0.3825	0.3764	0.4312	0.256	0.2561	0.275	0.2761	0.343553	0.395934				Paired Two-Samples T-test		
35	-2	0.9733	0.986	0.9783	0.9835	0.9292	1.0311	1.0447	1.007	1.0413	1.0598	1.0576	1.0714	1.0136		0.858	0.8308	0.8311	0.8917	0.8087	0.8316	0.8115	0.8394				0.837856								
36	-2.3	0.9911	0.9979	0.993	0.9818	1.0132	1.0084	1.0461	1.0423	1.0775	1.0738	1.0546	1.0564	1.028		0.8792	0.9806	0.9678	0.9792	0.8588	0.9086	0.9144	0.9071	0.9504	0.9355	0.9508	0.9908	0.935263							
37	-3	1.0537	0.9724	0.9442	1.0011	0.9968	1.0594	1.1015	1.1072	1.0234	1.0572	1.0388	1.1013	1.0381		0.8758	1.0036	0.9303	1.0302	0.9252	0.9371	0.9297	0.9555	0.9509	0.9566	1.0018	1.0045	0.958445							
38																																			

O) Western blots: Raw images

HCT-116 irradiation and protein extraction at different time points – Sixty second exposure time on all blots		
pAKT	AKT	GAPDH
		
Drug treatment experiments - Three minute exposure time on all blots		
pAKT – RUN 1	pAKT – RUN 2	pAKT – RUN 3



AKT - RUN 1



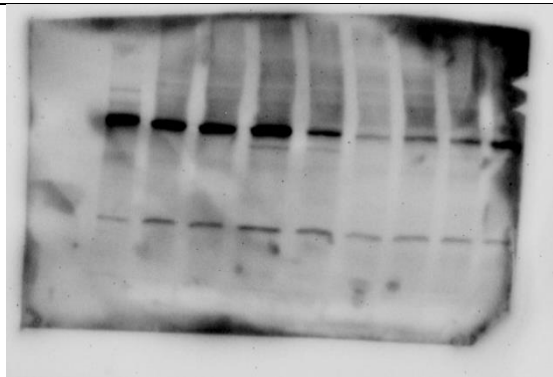
AKT - RUN 2



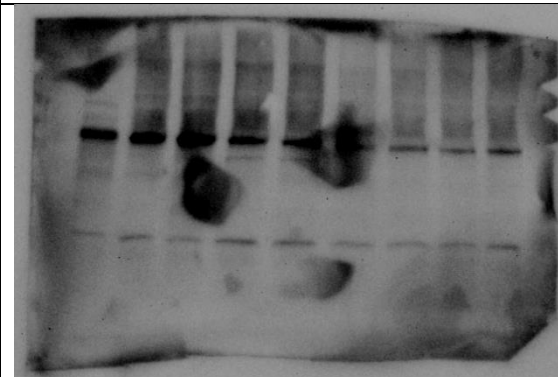
AKT - RUN 3



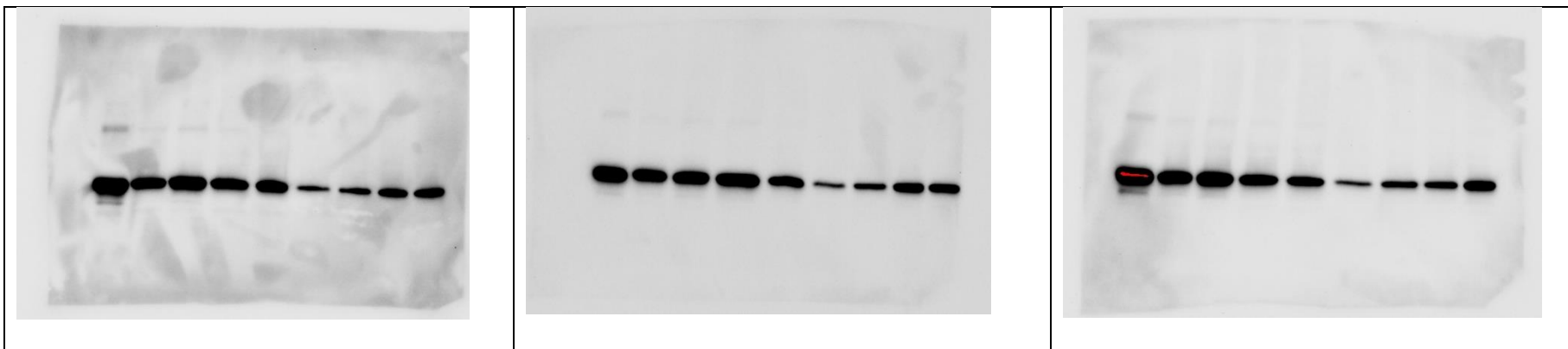
GAPDH - RUN1



GAPDH - RUN2



GAPDH - RUN3



P) Western blots: Image densitometry analysis

	A	B	C	D	E	F	G	H	I
1			AKT		Average		pAKT		Average
2	CONTROL	13061.948	16131.844	13627.856	=AVERAGE(B2:D2)	4456.782	6748.409	5126.974	=AVERAGE(F2:H2)
3	RT ONLY	23402.952	17454.966	10924.401		11600.137	16035.108	12616.501	
4	5FU	13452.806	22488.765	12232.685		3494.104	9822.329	1907.083	
5	5FU_RT	8187.392	9451.279	8995.045		2392.589	4350.974	3232.054	
6	API	5283.773	2364.296	2167.782		97.607	81.364	28.364	
7	API_RT	7371.38	4071.903	4740.388		0	76.95	0	
8	DACTO	7000.43	5533.439	3856.853		0	0	44.78	
9	DACTO_RT	7657.007	2591.125	6101.43		24.536	0	21.536	
10									
11									
12	Normalised				Average				
13	CONTROL	1	1	1	=AVERAGE(B13:D13)				
14	RT ONLY	=F3/\$I\$2	=G3/\$I\$2	=H3/\$I\$2	=AVERAGE(B14:D14)		=TTEST(\$B\$13:\$D\$1:	=TTEST(\$B\$13:\$D\$1:	
15	5FU	=F4/\$I\$2	=G4/\$I\$2	=H4/\$I\$2	=AVERAGE(B15:D15)		=TTEST(\$B\$13:\$D\$1:	=TTEST(\$B\$13:\$D\$1:	
16	5FU_RT	=F5/\$I\$2	=G5/\$I\$2	=H5/\$I\$2	=AVERAGE(B16:D16)		=TTEST(\$B\$13:\$D\$1:	=TTEST(\$B\$13:\$D\$1:	
17	API	=F6/\$I\$2	=G6/\$I\$2	=H6/\$I\$2	=AVERAGE(B17:D17)		=TTEST(\$B\$13:\$D\$1:	=TTEST(\$B\$13:\$D\$1:	
18	API_RT	=F7/\$I\$2	=G7/\$I\$2	=H7/\$I\$2	0.014		=TTEST(\$B\$13:\$D\$1:	=TTEST(\$B\$13:\$D\$1:	
19	DACTO	=F8/\$I\$2	=G8/\$I\$2	=H8/\$I\$2	0.008		=TTEST(\$B\$13:\$D\$1:	=TTEST(\$B\$13:\$D\$1:	
20	DACTO_RT	=F9/\$I\$2	=G9/\$I\$2	=H9/\$I\$2	=AVERAGE(B20,D20)		=TTEST(\$B\$13:\$D\$1:	=TTEST(\$B\$13:\$D\$1:	
21									

Normalised				Average		
CONTROL	100.0%	100.0%	100.0%	100.0%		
RT ONLY	213.1%	294.5%	231.7%	246.5%		0.027157
5FU	64.2%	180.4%	35.0%	93.2%		0.892544
5FU_RT	43.9%	79.9%	59.4%	61.1%		0.064785
API	1.8%	1.5%	0.5%	1.3%		1.51E-05
API_RT	0.0%	1.4%	0.0%	1.4%		2.24E-05
DACTO	0.0%	0.0%	0.8%	0.8%		7.56E-06
DACTO_RT	0.5%	0.0%	0.4%	0.4%		2.03E-06

----- End of thesis -----